Integrodifference models for neutral genetic patterns and trade-offs in ecology

by

Nathan G. Marculis

A thesis submitted in partial fulfillment of the requirements for the degree of

Doctor of Philosophy

in

Applied Mathematics

Department of Mathematical and Statistical Sciences

University of Alberta

Abstract

Integrodifference equations are a common tool used in ecology to model the spread of populations. In this thesis, I explore the neutral genetic patterns formed by range expansions and how dispersal-reproduction trade-offs impact the spread of populations. In Chapter 2, we investigate the inside dynamics of integrodifference equations to understand the genetic consequences of a population with nonoverlapping generations undergoing range expansion. We consider thin-tailed dispersal kernels and a variety of per capita growth rate functions to classify the traveling wave solutions as either pushed or pulled fronts. We find that pulled fronts are synonymous with the founder effect in population genetics. Adding overcompensation to the dynamics of these fronts has no impact on genetic diversity in the expanding population. However, growth functions with a strong Allee effect cause the traveling wave solution to be a pushed front preserving the genetic variation in the population. In Chapter 3, a stage-structured model of integrodifference equations is used to study the asymptotic neutral genetic structure of populations undergoing range expansion. We show that, under some mild assumptions on the dispersal kernels and population projection matrix, the spread is dominated by individuals at the leading edge of the expansion. This result is consistent with the founder effect. In the case where there are multiple neutral fractions at the leading edge, we are able to explicitly calculate the asymptotic proportion of these fractions found in the long-term population spread that depends only on the right and left eigenvectors of the population projection matrix

evaluated at zero and the initial proportion of each neutral fraction at the leading edge. In the absence of a strong Allee effect, multiple neutral fractions can drive the long-term population spread, a situation not possible with the scalar model. In Chapter 4, we develop a neutral genetic mutation model by extending the previously established scalar inside dynamics model. We show that the spread of neutral genetic fractions is dependent on individuals at the leading edge of population as well as the structure of the mutation matrix. Specifically, we find that the neutral fractions that contribute to the spread of the population are those that belong to the same mutation class as the neutral fraction found at the leading edge of the population. We prove that the asymptotic proportion of individuals at the leading edge of the population spread is determined by the dominant right eigenvector of the associated mutation matrix, independent from growth and dispersal parameters. In Chapter 5, we construct a model that incorporates a dispersal-reproduction trade-off effect that allows for a variety of different shaped trade-off curves. We show there is a unique reproductive-dispersal allocation that gives the largest value for the spreading speed and calculate the sensitivities of the reproduction, dispersal, and trade-off shape parameters. Uncertainty in the model parameters affects the expected spread of the population and we calculate the optimal allocation of resources to dispersal that maximizes the expected spreading speed. Higher allocation to dispersal arises from uncertainty in the reproduction parameter or the shape of the reproduction trade-off curve. Lower allocation to dispersal arises form uncertainty in the shape of the dispersal trade-off curve, but does not come from uncertainty in the dispersal parameter. Our findings give insight into how parameter sensitivity and uncertainty influence the spreading speed of a population with a dispersal-reproduction trade-off.

Preface

This thesis has been structured as paper based where Chapters 2-5 are the four main components of original work. Chapter 2 of this thesis in an original work that has been published as Marculis, N.G., Lui, R., & Lewis, M.A. (2017) "Neutral genetic patterns for expanding populations with nonoverlapping generations." *Bulletin of Mathematical Biology*, 79.4, pp. 828-852. https://doi.org/10.1007/s11538-017-0256-7 N.G. Marculis was responsible for the model development, analysis, and manuscript composition. R. Lui assisted in the model analysis and contributed to manuscript edits. M.A. Lewis was the supervisory author and assisted in the model analysis and contributed to manuscript edits.

Chapter 3 of this thesis is an original work that has been published as Marculis, N.G., Garnier, J., Lui, R., & Lewis, M.A. (2019) "Inside dynamics for stage-structured integrodifference equations." *Journal of Mathematical Biology*, pp. 1-31. https://doi.org/10.1007/s00285-019-01378-9 N.G. Marculis was responsible for the model development, analysis, and manuscript composition. J. Garnier and R. Lui assisted in the model analysis and contributed to manuscript edits. M.A. Lewis was the supervisory author and assisted in the model analysis and contributed to manuscript edits.

Chapter 4 of this thesis is an original work that is currently under review as Marculis, N.G. & Lewis, M.A. (2019) "Inside dynamics of integrodifference equations with mutations." *Bulletin of Mathematical Biology.* N.G. Marculis was responsible for the model development, analysis, and manuscript com-

position. M.A. Lewis was the supervisory author and assisted in the model development, analysis, and contributed to manuscript edits.

Chapter 5 of this thesis is an original work that is currently under review as Marculis, N.G., Evenden, M.L., & Lewis, M.A. (2019) "Modeling the dispersal-reproduction trade-off in an expanding population." *Theoretical Population Biology*. N.G. Marculis was responsible for the model development, analysis, and manuscript composition. M.L. Evenden assisted in model development and manuscript edits. M.A. Lewis was the supervisory author and assisted in the model development, analysis, and contributed to manuscript edits.

Acknowledgements

I want to start by thanking my supervisor for providing me the privilege to work with him. Over the five years, Mark has opened up many opportunities for myself and has always looked out for my best interest. Thanks to the other members on my supervisory committee: Roger for introducing me into the world of integrodifference equations and continuing to encourage my growth in the area, and Maya for being available to answer my biological questions. I would also like to thank Jimmy Garnier for inviting me to visit France and collaborate with him. A big shout out to the Lewis Lab is also necessary, without fail they have always been supportive of my research and have provided a countless amount of constructive feedback over the years.

I would like to acknowledge financial support from a Joesphine M. Mitchell Scholarship, a PIMS Student Training Acceleration Award, and TRIA-Net.

Finally, I would like to thank my friends and family for all of their support through what seemed like endless years of research and studying, and to Wafa for believing in me and keeping me in good spirits.

Table of Contents

List of Figures

Chapter 1

Introduction

1.1 Integrodifference equations

Integrodifference equations are mathematical tools that are commonly used for studying problems in spatial ecology. These equations model two primary processes; the reproduction and the dispersal of the population. What separates integrodifference equations from other common mathematical models such as reaction-diffusion equations and integro-differential equations is that integrodifference equations are discrete-time continuous-space models. These discrete-time continuous-space models are particularly useful for modeling populations with synchronous, nonoverlapping generations. To apply the integrodifference equation as a reasonable model, we must assume that dispersal occurs during a distinct phase of the life cycle and the population is sedentary for the remainder of the time. This allows the user to consider the processes of dispersal and reproduction separately. Let $u_t(y)$ be the population density at location y and time t. During the sedentary stage reproduction occurs according to the density-dependent map $f(u_t(y))$. Once the sedentary stage is over, the probability that an individual disperses from the interval $(y, y + dy]$ to the point x is given by $k(x - y)\, dy$ where k is the dispersal kernel function. To account for all possible intervals, we then integrate over the real line to obtain

the classical integrodifference equation

$$u_{t+1}(x) = \int_{-\infty}^{\infty} k(x-y) f(u_t(y))\, dy \tag{1.1}$$

which gives the population density at location x and time $t+1$.

In the literature, these models gained traction in the early to mid 1980's. The theoretical work by Hans Weinberger paved the way for future analyses of these models. In his seminal work, Weinberger studied the long-time behavior of an abstract operator where time was assumed to be discrete and space may or may not be discrete (Weinberger, 1982). While the word itself "integrodifference" is never mentioned in this work, a particular case of the abstract operator studied gives rise to the classical integrodifference equation. The significance of the work from Weinberger (1982) was that Weinberger was able to prove many important results pertaining to the existence, persistence, and asymptotic speed for traveling wave solutions of integrodifference equations. Throughout this thesis, I will regularly use the results from this important study.

The first reference of integrodifference equations in the literature dates back to the work by Mark Kot and William Schaffer on modeling discrete-time growth dispersal processes (Kot and Schaffer, 1986). In their work, they present and discuss a number of simple integrodifference equations to study problems such as determining the minimum habitat size for population persistence and understanding how diffusive processes can cause instability in a model and create complex spatial patterns. Throughout their study they emphasize how integrodifference equations are related to their continuous-time counterparts and emphasize the differences between modeling techniques. In their conclusion, they state that there are simply too many avenues that need to be pursued in regard to studying integrodifference equations. To this day, this comment remains true while the field of integrodifference equations has

continued to grow over the years.

One important concept that I will use throughout this thesis is the idea of the spreading speed for the population typically denoted by c^*. The spreading speed can be thought of in the following way: If an observer is in a moving frame with speed $c > c^*$, then eventually the observer sees the population level at zero, but if the observer is in a frame that moves with speed $c < c^*$, then eventually the observer sees the population at its carrying capacity K. Formally, this can be written in mathematical terms as

$$\lim_{t\to\infty} \sup_{|x|\geq t(c^*+\varepsilon)} u_t(x) = 0 \text{ and } \lim_{t\to\infty} \sup_{|x|\leq t(c^*-\varepsilon)} (K - u_t(x)) = 0 \tag{1.2}$$

where ε is a positive constant and $u_t(x)$ is the population density at time t and location x (Weinberger, 1982). Under some mild assumptions on the growth function and the dispersal kernel, see Weinberger (1982) for the details, there is a simple formula for the asymptotic spreading speed. This result has been extended for structured population models (Lui, 1989a) and growth functions with overcompensation (Li et al., 2009). However, in the case of the strong Allee effect, there is no general formula for the spreading speed and this still remains as an area for future research.

Since their debut, integrodifference equations have been applied to study many different problems in spatial ecology. In particular, these models have been used to study range expansions (Krkošek et al., 2007; Zhou and Kot, 2011), the spread and control of invasive species (Bateman et al., 2017; Kot et al., 1996; Lewis et al., 2016), and determining the critical domain size for population persistence (Lutscher et al., 2005; Reimer et al., 2016; Van Kirk and Lewis, 1997a). In these applications the modeling efforts focus on the population level dynamics and ignore the genetic consequences. The first part of this thesis is devoted to understanding the neutral genetic structure of expanding populations.

1.2 Inside dynamics

Neutral genetic patterns formed by expanding populations have been a recent topic of interest (Hallatschek and Nelson, 2008). One of the main drivers said to reduce the genetic diversity of a population is the founder effect. The founder effect occurs when the establishment of a new population is achieved by a small number of original founders who carry only a small fraction of the total genetic variation of the parental population (Mayr, 1940). During range expansion consecutive founder effects result in the process known as gene surfing (Excoffier and Ray, 2008). This is the spatial analog of genetic drift and occurs when certain alleles reach higher than expected frequencies at the front of a range expansion (Slatkin and Excoffier, 2012). In a theoretical context, I will attempt to determine how and when these processes occur by using an integrodifference equation model.

The term "inside dynamics" was coined by Garnier et al. (2012) where they studied the inside structure of a scalar reaction-diffusion equation. The vital assumption made in their analysis was that the population is composed of several groups with identical diffusion and growth rates. Then the analysis is performed by studying the spatio-temporal development of the distinct subgroups. A theoretical illustration of this decomposition is provided in Figure 1.1(b). One direct application to this work is studying the structure of neutral genetic components in an expanding population. The key word here is neutral, without this assumption of the different components dispersing and growing in the same manner, the analysis becomes substantially more challenging. Even though these neutral genes do not tell us anything about the adaptive or evolutionary potential of a population, neutral genes can be used to understand processes such as gene flow, genetic drift, migration, or dispersal (Holderegger et al., 2006).

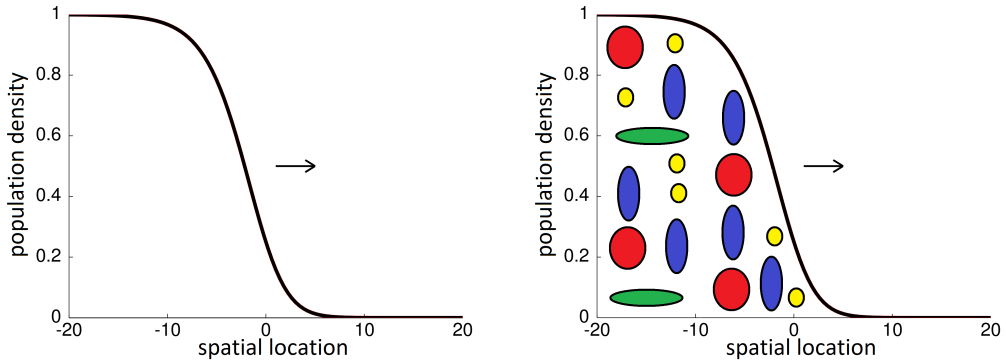

(a) (b)

Figure 1.1: Here I provide a theoretical example for the decomposition of a population into neutral genetic components. In (a), we see a traveling wave solution for an expanding population where the curve is the population destiny. In (b), I illustrate the decomposition of the entire population density into distinct subgroups that can be classified by neutral genetic components denoted by the different shapes.

The inside dynamics analysis was quickly applied to a variety of different continuous-time models. In particular, the inside dynamics of reaction-diffusion equations (Garnier et al., 2012; Garnier and Lewis, 2016; Roques et al., 2012, 2015), delay reaction-diffusion equations (Bonnefon et al., 2013), and integro-differential equations (Bonnefon et al., 2014) were studied. In this thesis, I aim to extend the previous work from continuous-time models to the discrete-time models by applying the inside dynamics analysis to integrodifference equations. Our results pertaining to the inside dynamics of the population are provided in Chapters 2-4. In Chapter 2 we study the inside dynamics of a scalar integrodifference equation, in Chapter 3, we analyze the inside dynamics for a stage-structured integrodifference equation, and in Chapter 4 we incorporate neutral mutations into the scalar inside dynamics model.

In Chapter 2, we study the neutral genetic patterns formed by an expanding population with nonoverlapping generations using a scalar integrodiffer-

ence equation. In particular, the study focuses on the effect that different kinds of growth functions have on the neutral genetic patterns formed by expanding populations. For this study, we compare and contrast the long-term dynamics for three common growth functions with different features. In particular, we look at a monotone growth function with maximal growth rate at zero, a growth function with a strong Allee effect, and a growth function with overcompensation. Previous studies have looked at this same question in the continuous-time framework for the first two growth functions mentioned (Garnier et al., 2012; Roques et al., 2012). In this study, we am able to consider growth functions with overcompensation, because integrodifference equations are discrete-time models. Previous studies were not able to achieve this because this phenomena is not possible to model with a continuous-time scalar equation. Moreover, we can classify our results in terms of pushed and pulled fronts. In particular, we show how a strong Allee effect can promote genetic diversity in an expanding population while monotone growth functions with maximal growth rate at zero and those with overcompensation are prone to extreme founder effects where individuals initially located at the leading edge of the population have an advantage.

In Chapter 3, we then expand the inside dynamics analysis to understand the effects that stage-structure has on the neutral genetic diversity of expanding populations. Previous work has shown that the inclusion of a juvenile class into the population dynamics for the model has shown to decrease the founder effect (Austerlitz et al., 2000). In this chapter, we construct a general stage-structured model and analyze the inside dynamics to see how the genetic diversity would change for an expanding population. Since our focus is on the interactions between stages in the model, we do not consider a variety of dispersal kernels and growth functions as done in Chapter 2, but focus on the structure of the population. In particular, we show how the initial spatial

orientation and the structure of the population influences the neutral genetic patterns of spatial spread.

By performing experiments in the laboratory on two florescently labeled strains of *Escherichia coli*, Hallatschek et al. (2007) reported on how an initially well mixed population can spread in well defined sector-like regions. Moreover, they claim that the formation of these regions is driven by random fluctuations in the pioneers at the leading edge of the population spread. More generally, the experiments by Hallatschek et al. (2007) demonstrate how it is possible for mutations at the leading edge of the population to dominate population spread without any selective advantage illustrating the importance of neutral genetic diversity. In Chapter 4, we consider this complexity by constructing a model that includes neutral genetic mutations. We focus the analysis in Chapter 4 on the mutation structure of the population and its implication on the long term dynamics of neutral genetic structure of the expanding population.

1.3 Dispersal-reproduction trade-offs

In Chapter 5, we shift the interest from the neutral genetic structure of expanding population and focus on how resource allocation to reproduction and dispersal affect population spread. The idea for this is motivated by the principle of allocation which states that if an organism has limited resources, then energy allocation to one function reduces the amount of energy available to all other functions (Cody, 1966). Thus, under resource limitation, there is an inherent trade-off between the different processes. While there are a variety of different trade-offs in natural systems, we limit the scope of the research to the life-history trade-off between dispersal and reproduction that arises from limited resource allocation. That is, the assumption is made that if an individual disperses a long distance, then there will be few resources left over to

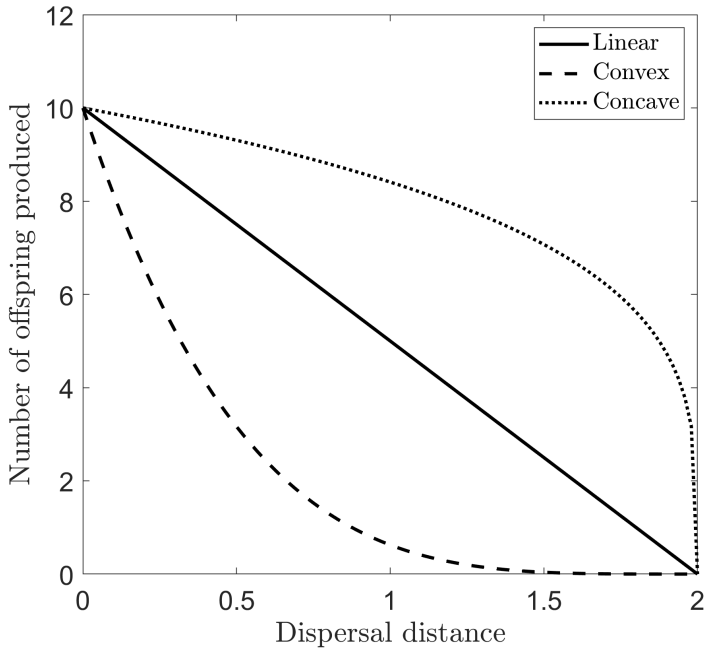

Figure 1.2: Here I provide a theoretical example for the dispersal-reproduction trade-off. The solid lines represents linear trade-off between the dispersal distance and number of offspring produced. The dashed (dotted) line represents a nonlinear trade-off curve that is convex (concave).

be dedicated to producing offspring. A theoretical example of this trade-off is presented in Figure 1.2.

The primary conclusion to draw from Figure 1.2 is that the shape, in particular the curvature, of the trade-off influences the parameter values in the model. For example, by inspecting the trade-off curves in Figure 1.2 we can see that if the dispersal distance is one kilometer, then according to the convex, linear, and concave trade-off curves, the number of offspring produced is less than one, five, and greater than eight, respectively. Thus, even though all these trade-off curves are decreasing and starting and ending at the same value, the curvature can greatly influence the population dynamics. Therefore, when developing our model for the dispersal-reproduction trade-off we attempt to make the model relatively general by including parameters to obtain these different shapes in the dispersal-reproduction trade-off curve.

The understanding of the trade-off curve is commonly described in terms of how much we know about the biological system. First-order understanding of the trade-off curve refers to knowing the slope, second-order understanding is knowing the curvature of the trade-off curve, and third-order refers to knowing all details including interactions terms (Stearns, 1989). While the information for first-order understanding is known in many cases, theoretical studies have argued that the second-order understanding is of vital important for understanding life-history evolution (Schaffer, 1974). Measurement of the third-order understanding is the ultimate goal, but outside of a theoretical or lab study, this may be too complicated to determine.

The inclusion of resource allocation is not typically considered in mathematical models of spread, but are known to produce rich dynamics. By incorporating a trade-off between reproduction and dispersal ability in a population of non-pollinating fig wasps Duthie et al. (2014) constructed a theoretical model that showed coexistence between these different strategies can occur. At first glance, this result appears to be paradoxical to the competitive exclusion principle because non-pollinator species are often closely related, share similar life histories, and compete for similar resources. However, the trade-off in the model influenced individuals to specialize to different degrees on dispersal and reproductive abilities and create individual niches.

Theoretical models have been developed to study the evolution of dispersal in populations with multiple phenotypes. One of the important results from these studies is that there is an evolutionary force causing the phenotype with the lowest diffusion rate to be selected in a competitive environment (Dockery et al., 1998; Hastings, 1983). However, in this thesis we are not interested in what is happening in a competitive environment, but rather during colonization. During colonization, the spreading speed of the population is the primary driving force not high level density-dependence or intraspecific com-

petition unlike in stationary competitive systems. Thus, our analysis aims to address a complementary area that the evolution of dispersal models have not considered. That is, we are interested in understanding how dispersal should be selected for in a colonizing population.

To understand the effect that the dispersal-reproduction trade-off has on population spread, we analyze how the spreading speed for the population is altered by different resource allocations in Chapter 5. To determine how the spreading speed changes with model parameter values, we perform a sensitivity analysis on the demographic, dispersal, and trade-off parameters. Using sensitivity analysis, we then determine the optimal resource allocation to dispersal that maximizes the spreading speed for the population. We also explore how parameter uncertainty affects the population spread and resource allocation. To achieve this, we assume that the model parameters of interest are random variables with a given probability distribution, and then compute the expected value for the spreading speed.

The organization of this thesis is laid out as paper-based where Chapters 2-5 are the four main original works. Chapters 2-5 can be read independently on their own because they each contain their own introduction and discussion sections. The outline for the four original works is given as follows: In Chapter 2, we study the inside dynamics of a scalar integrodifference equations, in Chapter 3, we study the inside dynamics of a stage-structured integrodifference equations, in Chapter 4, we study the inside dynamics of a scalar integrodifference equation with neutral genetic mutations, and in Chapter 5, we study the dispersal-reproduction trade-off effect in an expanding population. I finish with a conclusion of the work in Chapter 6.

Chapter 2

Neutral genetic patterns for expanding populations with nonoverlapping generations

2.1 Introduction

The topic of populations undergoing range expansions in spatial ecology is well studied (Holmes et al., 1994; Ibrahim et al., 1996; Thomas et al., 2001). However, many of the previous mathematical studies focus on the spread of entire populations and ignore the neutral genetic consequences of the expansion (Kot, 1992; Lutscher, 2008; Wang et al., 2002). The aim of this work is to connect the range expansion of a population to the genetic consequences for populations with nonoverlapping generations. To achieve this goal, we develop and analyze a mathematical model of integrodifference equations to connect the fundamental ecological and genetic concepts with mathematical structure.

A recent interest in ecological literature is focused around the neutral genetic consequences of range expansions (Hallatschek and Nelson, 2008). A founder effect is said to occur when the establishment of a new population is performed by a few original founders who carry only a small fraction of the total genetic variation of the parental population (Mayr, 1942). It is a widely accepted notion that range expansions often lead to a loss of genetic

diversity because of the founder effect (Dlugosch and Parker, 2008; Ibrahim et al., 1996). Serial founder events that occur when a population undergoes a range expansion result in the phenomena known as gene surfing (Excoffier and Ray, 2008). This is the spatial analogue of genetic drift and occurs when alleles reach higher than expected frequencies at the front of a range expansion (Slatkin and Excoffier, 2012). By understanding the effect that spatial assortment plays in expanding populations, we can begin to understand the effect that dispersal has on genetic diversity, independent of selection.

It has been shown that, in some scenarios, genetic drift in edge populations can be a stronger driver than selection during range expansion because of the spatial structure of the population (Müller et al., 2014). A simple theoretical experiment was conducted to demonstrate that mutations at expanding frontiers can sweep through a population, even without any selective advantage (Hallatschek et al., 2007). This experiment provides support for theoretical arguments and genetic evidence that common genes in a population may not necessarily reflect positive selection but, instead, may be due to recent range expansions (Hewitt, 2000). This evidence motivates the work conducted in this paper to understand the effect that growth and dispersal have on the neutral genetic composition of a population.

Often, large scale genomic surveys are motivated, in part, by the idea that the neutral genetic variation observed in a population may be used to reconstruct the history of its range expansion (Hewitt, 1996). However, the ability to trace back the colonization pathways of a species from their genetic footprints is limited by our understanding of the genetic consequences of a range expansion (Excoffier, 2004; Hallatschek and Nelson, 2008). The model considered in this work provides a framework for understanding the genetic consequences that in turn can assist the inverse problem of understanding where the species originated.

Mathematically, the concept of modeling the evolution of the neutral genetic diversity of an expanding population is known as the "inside dynamics" of the population. The term comes from the idea that we break the population into subpopulations that can be identified by a neutral genetic marker used to study the underlying structure of the population. A recent series of papers focused on understanding the inside dynamics for a variety of different types of continuous-time models(Bonnefon et al., 2014, 2013; Garnier et al., 2012; Roques et al., 2012). Early work on inside dynamics focused on the study of the classical reaction diffusion equations with monostable, bistable, or ignition type reaction dynamics. The authors were able to classify the inside dynamics of the deterministic population structure in terms of pulled and pushed traveling wave solutions (Garnier et al., 2012). The theory was quickly extended by incorporating biological insight to the original work by showing that Allee effects preserve genetic diversity (Roques et al., 2012). The inside dynamics analysis has also been extended to other kinds of one-dimensional equations such as delayed traveling waves (Bonnefon et al., 2013) and integro-differential equations (Bonnefon et al., 2014).

As was done for the previous studies on continuous time models, this work aims to classify the inside dynamics of solutions to integrodifference equations as pushed or pulled fronts. The classical integrodifference equation is a discrete-time continuous space equation that describes a populations growth and spread. The discrete-time aspect coincides with the assumption that the population has nonoverlapping generations. This provides a widely used biological model for population dynamics (Lewis et al., 2016).

2.2 Mathematical preliminaries and model

In this section we provide necessary background material for the reader. We first discuss the basic model structure with the types of growth functions and

dispersal kernels considered in this work. A few integral transforms are then defined for use in the long time analysis of the model. Next, the concept of inside dynamics is then introduced and the model is formulated. To complete this section we discuss some classical results for traveling wave solutions and define pushed and pulled traveling wave solutions in terms of the inside dynamics.

2.2.1 Model structure

The classical integrodifference equation, describing the growth and dispersal of a population density u, is given by

$$u_{t+1}(x) = \int_{-\infty}^{\infty} k(x-y)g(u_t(y))u_t(y)\,dy. \tag{2.1}$$

In Equation (2.1) g is the density-dependent per capita growth rate function describing the local growth of the population at location y and time t. We assume that g is a nonnegative continuous function where $g(u)u$ has a trivial steady state and a steady state at 1. The function k is a probability density function that describes the probability of movement of individuals from location y to location x. That is, k is a nonnegative function that integrates to one. The recursion in Equation (2.1) describes the reproduction and dispersal of a population with nonoverlapping generations. That is, all individuals first undergo reproduction and then the offspring are redistributed before reproduction occurs in the next generation. Given an initial condition $u_0(x)$, $u_t(x)$ is the solution to Equation (2.1) defined recursively.

For the population growth we consider three different types of functions that include different kinds of effects. In particular, we look at Beverton-Holt, Ricker, and Sigmoid Beverton-Holt type growth functions; see Figure 2.1. The classical Beverton-Holt growth is the discrete analog of logistic growth and the

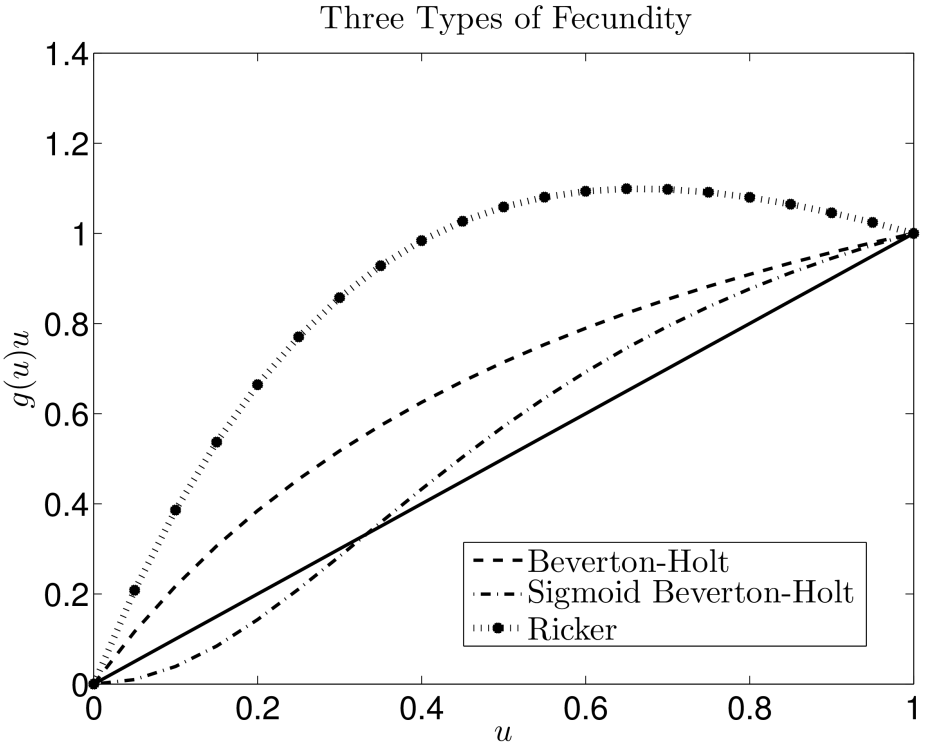

Figure 2.1: The fecundity functions, $g(u)u$, used in the numerical simulations. The intrinsic growth rate, R, for the Beverton-Holt, Sigmoid Beverton-Holt, and Ricker type growth functions are $2.5, 4$, and 1.5 respectively. The positive sigmoid scaling parameter, δ, for the Sigmoid Beverton-Holt function is chosen to be 2. The solid line is the reference line $g(u)u = u$ dictating when there is no change in population density.

per capita growth is defined by

$$g_{bh}(u) = \frac{R}{1 + (R-1)u}, \tag{2.2}$$

where R is the geometric growth rate. A model introduced by Grant Thompson for fisheries, called the Sigmoid Beverton-Holt model, has per capita growth rate

$$g_s(u) = \frac{Ru^{\delta-1}}{1 + (R-1)u^{\delta}}, \tag{2.3}$$

where R is the intrinsic growth rate and δ is a positive sigmoid scaling parameter (Thompson, 1993). It is known that when $\delta > 1$ this growth function exhibits a strong Allee effect.

Since we have scalar discrete time equations we can consider growth functions with overcompensation. This is not possible for a scalar first order continuous time model. Ricker type growth is commonly used when overcompensation is present. The Ricker model has the form

$$g_r(u) = e^{R(1-u)}, \tag{2.4}$$

where R is the intrinsic growth rate (Ricker, 1954). Note that $g_{bh}(u)u$ and $g_s(u)u$ are monotone where $g_r(u)u$ is not, see Figure 2.1.

Definition 2.2.1 (Thin-tailed dispersal kernel)**.** *A dispersal kernel $k(x)$ is called thin-tailed if there exists a real valued $\xi > 0$, such that*

$$\int_{-\infty}^{\infty} k(x)e^{\xi|x|}\,dx < \infty. \tag{2.5}$$

If a dispersal kernel is not thin-tailed, then we say the dispersal kernel is *fat-tailed*. For simplicity, we only consider thin-tailed dispersal kernels in this work. Many of the classical mathematical results for the dynamics of Equation (2.1) focus on thin-tailed dispersal kernels. The thin-tailed assumption implies that $k(x)$ decays at least as fast as an exponential function as $|x| \to \infty$. A consequence of the thin-tailed assumption is that k has a moment generating function. A common dispersal kernel that we consider throughout our work is the Gaussian probability distribution function. That is:

$$k(x;\mu,\sigma) = \frac{1}{\sqrt{2\pi\sigma^2}} e^{-\frac{(x-\mu)^2}{2\sigma^2}}, \tag{2.6}$$

where μ is the mean shift in location and σ^2 is the variance in dispersal distance. In the following sections we use the shorthand notation k is $N(\mu,\sigma^2)$.

2.2.2 Integral transforms

The two integral transforms that are particularly useful in our work are the Fourier transform and the reflected bilateral Laplace transform (Zemanian,

1968). These transformations and their inverses are given in Definitions 2.2.2 and 2.2.3.

Definition 2.2.2 (Fourier transform)**.** *Let* $f : \mathbb{R} \to \mathbb{R}$ *where* $f \in L^1(\mathbb{R})$*. Then, the Fourier transform and its inverse are respectively defined to be*

$$\hat{f}(\omega) = \mathcal{F}[f(x)] = \int_{-\infty}^{\infty} f(x)e^{-i\omega x}\,dx, \text{ and} \tag{2.7}$$

$$f(x) = \mathcal{F}^{-1}[\hat{f}(\omega)] = \frac{1}{2\pi}\int_{-\infty}^{\infty} \hat{f}(\omega)e^{i\omega x}\,d\omega. \tag{2.8}$$

Definition 2.2.3 (reflected bilateral Laplace transform)**.** *Let* $f : \mathbb{R} \to \mathbb{R}$ *where* f *is piecewise continuous on every finite interval in* $\mathbb{R}$ *satisfying* $|f(x)| \leq Me^{-sx}$ *for all* $x \in \mathbb{R}$ *and* $0 < s < s_{max}$*. Then, the reflected bilateral Laplace transform and its inverse are respectively defined to be*

$$F(s) = \mathcal{M}[f(x)] = \int_{-\infty}^{\infty} f(x)e^{sx}\,dx, \text{ and} \tag{2.9}$$

$$f(x) = \mathcal{M}^{-1}[F(s)] = \frac{1}{2\pi i}\lim_{R\to\infty}\int_{\gamma-iR}^{\gamma+iR} F(s)e^{-sx}\,ds \tag{2.10}$$

for $0 < s < s_{max}$*, where the integration in Equation* (2.10) *is over the vertical line,* $Re(s) = \gamma$ *in the complex plane and* γ *is greater than the real parts of all singularities of* $F(s)$*.*

The reflected bilateral Laplace transform can be used to write the solution to our model in terms of its initial condition by using the convolution theorem. This theorem states that the reflected bilateral Laplace transform of a convolution is the product of the reflected bilateral Laplace transforms. That is,

$$\mathcal{M}[f(x) * h(x)](s) = F(s)H(s). \tag{2.11}$$

Note that the reflected bilateral Laplace transform of a probability density function is also referred to as its moment generating function (Casella and Berger, 2002).

2.2.3 Inside dynamics

To include neutral genetic diversity we assume that the population density is composed of either haploid individuals or genes. To analyze the inside dynamics we separate the population into different neutral fractions $v_t^i(x)$. The initial population is defined to be

$$u_0(x) := \sum_{i=1}^{N} v_0^i(x), \tag{2.12}$$

where $v_0^i(x) \geq 0$ is the initial population density for neutral fraction i and N is the finite number of distinct neutral fractions. We assume that the individuals (or genes) in each fraction have the same dispersal and growth capabilities as the entire population u and only differ by position and their label (or their alleles). In short, we assume that individuals in each neutral fraction have no genetic advantage over any other neutral fraction. Then, by decomposing the population density into the neutral fractions gives the following system of N equations:

$$v_{t+1}^i(x) = \int_{-\infty}^{\infty} k(x-y)g(u_t(y))v_t^i(y)\,dy, \tag{2.13}$$

where g is the common per capita growth rate for all neutral fractions. That is, the per capita growth rate of each neutral fraction is the same as the per capita growth rate of the total population giving no genetic advantage of one fraction over another. A key feature of System (2.13) is that the sum of the neutral fraction densities, $v_t^i(x)$, is equal to the entire population density $u_t(x)$. When we add together the N equations in System (2.13), we obtain the integrodifference equation for the entire population density given by Equation (2.1). Using System (2.13) we are now able to track how individual neutral fractions spread.

2.2.4 Traveling wave solutions

We focus our study on classifying the traveling wave solutions of Equation (2.1). A traveling wave solution $U(x - ct)$ is a solution that connects the trivial steady state, 0, to the stable nontrivial steady state, 1, and propagates at a constant speed c. That is $u_t(x) = U(x - ct)$ solves Equation (2.1) with constant density profile U. The traveling wave equation is given by

$$U(x - c) = \int_{-\infty}^{\infty} k(x - y)g(U(y))U(y)\, dy. \tag{2.14}$$

Weinberger was a pioneer in this area and created the seminal work that analyzed traveling wave solutions for scalar discrete time operators (Weinberger, 1982). The main result in his work shows that for thin-tailed dispersal kernels, if $g(u)u$ is nondecreasing, then Equation (2.1) has a family of monotone traveling wave solutions parameterized by the speed c where $c \geq c^*$. The asymptotic spreading speed, c^*, is defined to be the asymptotic speed that a wave with compact initial conditions spreads. It was later shown that the asymptotic spreading speed is the minimum speed for which traveling wave solutions exist. In addition, if the per capita growth rate is maximal at zero, $g(u) \leq g(0)$, then the asymptotic spreading speed can be determined by a simple formula involving $g(0)$ and the dispersal kernel $k(x)$ given below

$$c^* = \inf_{z>0} \frac{1}{z} \ln \left(g(0) \int_{-\infty}^{\infty} k(x)e^{zx}\, dx \right). \tag{2.15}$$

For Gaussian dispersal kernels, we can write down an explicit formula for the asymptotic spreading speed

$$c^* = \sqrt{2\sigma^2 \ln(g(0))} + \mu. \tag{2.16}$$

Many of the fundamental techniques and concepts presented by Weinberger such as the comparison principle, asymptotic spreading speed, and integral transforms will be used in our analysis.

Weinberger's results were extended to include growth functions that have overcompensatory dynamics (Li et al., 2009). The extended theory requires some additional assumptions on the growth function, but commonly used functions such as the Ricker or logistic growth functions satisfy the required assumptions. In this scenario, it is not guaranteed that the traveling wave profile is monotone. The effect of overcompensation allows for complicated or even chaotic dynamics. Existence of traveling wave solutions with a strong Allee effect has been proven for a unique speed $c = c^*$ (Lui, 1983). The decay of the wave profile is given by $U(x) \sim Ce^{-s^*x}$ as $x \to \infty$ where s^* is the unique positive root of

$$\frac{1}{s} \ln \left(g(0) \int_{-\infty}^{\infty} e^{sx} k(x)\, dx \right) = c, \tag{2.17}$$

see Proposition 5 of (Lui, 1983). In the case where k is $N(\mu, \sigma^2)$ we can explicitly calculate s^* to be

$$s^* = \frac{c - \mu + \sqrt{(\mu - c)^2 - 2\sigma^2 \ln(g(0))}}{\sigma^2}. \tag{2.18}$$

Thus, we can conclude that $e^{\frac{c-\mu}{\sigma^2}x} U(x) \in L^1(\mathbb{R})$. When Equation (2.1) has a strong Allee effect there are still many open questions. In our work, we conjecture about the decay rate of pushed fronts that comes from the proof for growth functions with a strong Allee effect.

The techniques used to prove results for strong Allee are based on functional analysis arguments for superpositive operators. A linear operator is called *superpositive* (Krasnosel'skii and Zabreiko, 1984) if it has a simple positive dominant eigenvalue with positive eigenfunction where no other eigenfunction is positive. In particular, Jentsch's theorem provides sufficient conditions for a linear integral operator to be superpositive (Vladimirov, 1971).

In this paper, we focus on pulled and pushed fronts; see Definitions 2.2.4 and 2.2.5 for details. Instead of using the classical definitions of pulled and pushed fronts, see (Rothe, 1981; Stokes, 1976), we classify the waves using the

asymptotic dynamics of the neutral fractions. The following definitions come from the previous work on inside dynamics (Bonnefon et al., 2014).

Definition 2.2.4 (Pulled front)**.** *A traveling wave solution* $u_t(x) = U(x - ct)$ *is said to be a pulled front if, for any neutral fraction* $v_t^i(x)$ *satisfying* (2.13)*,* $0 \leq v_0^i \leq U$ *and* $v_0^i(x) = 0$ *for large* x*, the statement*

$$v_t^i(x + ct) \to 0 \text{ as } t \to \infty,$$

holds uniformly on any compact subset of $\mathbb{R}$*.*

Next, we define what it means for a traveling wave solution to be a pushed front in terms of the neutral fractions.

Definition 2.2.5 (Pushed front)**.** *A traveling wave solution* $u_t(x) = U(x - ct)$ *is said to be a pushed front if, for any neutral fraction* $v_t^i(x)$ *satisfying* (2.13)*,* $0 \leq v_0^i \leq U$ *and* $v_0^i \not\equiv 0$*, there exists* $M > 0$ *such that*

$$\limsup_{t\to\infty} \sup_{x\in[-M,M]} v_t^i(x + ct) > 0.$$

To recap, the preliminary definitions, theory, techniques, and the mathematical model have been laid out. Now that we have all the required knowledge we move into the next section where we classify the asymptotic dynamics of System (2.13).

2.3 Large time neutral genetic variation

In this section, we provide the theoretical results about the neutral genetic composition for System (2.13). In Theorems 2.3.1 and 2.3.2 we assume that the dispersal kernel is Gaussian, see Equation (2.6). This allows us to exploit the fact that the moment generating function for a Gaussian has the following form:

$$M(s) = e^{\mu s + \sigma^2 s^2/2}. \tag{2.19}$$

After the proof of Theorem 2.3.1 we provide two corollaries that provide a better interpretation for the results of Theorem 2.3.1. We then extend the results of Theorem 2.3.1 to the general class of thin-tailed dispersal kernels given by Theorem 2.3.3.

Theorem 2.3.1 (Gaussian kernel with maximum per capita growth at zero)**.** *Consider the solution of System* (2.12)-(2.13) *where* k *is* $N(\mu, \sigma^2)$ *and* $0 < g(u) \leq g(0)$ *for all* $u \in (0, 1)$*. Let* c *be the speed of a moving half-frame. If* $c \geq c^*$ *and* $\int_{-\infty}^{\infty} e^{\frac{c-\mu}{\sigma^2} y} v_0^i(y)\, dy < \infty$*, then for any* $A \in \mathbb{R}$*, the density of the neutral fraction* i*,* $v_t^i(x)$*, converges to* 0 *uniformly as* $t \to \infty$ *in the moving half-frame* $[A + ct, \infty)$*.*

Proof. For simplicity in notation we focus on a single neutral fraction and drop the superscript i notation. Using the fact that $0 < g(u) \leq g(0)$ for all $u \in (0, 1)$ we can use a comparison principle to show that a new sequence $w_t(x)$ defined by

$$w_{t+1}(x) = g(0) \int_{-\infty}^{\infty} k(x - y) w_t(y)\, dy \tag{2.20}$$

is always greater than the solution to any neutral fraction $v_t(x)$ with the same initial condition $w_0(x) = v_0(x)$. The solution of Equation (2.20) is given by the t-fold convolution

$$w_t(x) = (g(0))^t k^{*t} * w_0(x) \tag{2.21}$$

where k^{*t} is k convolved with itself t times. Applying the reflected bilateral Laplace transform to Equation (2.21) and using the convolution theorem, we

obtain

$$\mathcal{M}[w_t(x)](s) = [g(0)]^t \left[\mathcal{M}\left[k(x)\right](s)\right]^t \mathcal{M}\left[w_0(x)\right](s) \tag{2.22}$$

$$= [g(0)]^t \left[e^{\frac{\sigma^2 s^2}{2}+\mu s}\right]^t \mathcal{M}\left[w_0(x)\right](s) \tag{2.23}$$

$$= [g(0)]^t e^{\frac{\sigma^2 t s^2}{2}+\mu t s} \mathcal{M}\left[w_0(x)\right](s) \tag{2.24}$$

$$= [g(0)]^t \mathcal{M}\left[\frac{1}{\sqrt{2\pi\sigma^2 t}} e^{-\frac{(x-\mu t)^2}{2\sigma^2 t}}\right](s) \mathcal{M}\left[w_0(x)\right](s) \tag{2.25}$$

$$= [g(0)]^t \mathcal{M}\left[k_t * w_0)(x)\right](s), \tag{2.26}$$

where k_t is $N(\mu t, \sigma^2 t)$. Then applying the inverse transform yields

$$w_t(x) = [g(0)]^t (k_t * w_0)(x) \tag{2.27}$$

$$= [g(0)]^t \int_{-\infty}^{\infty} \frac{1}{\sqrt{2\pi\sigma^2 t}} e^{-\frac{(x-y-\mu t)^2}{2\sigma^2 t}} w_0(y)\, dy. \tag{2.28}$$

In the moving half-frame $[A + ct, \infty)$ with fixed $A \in \mathbb{R}$, consider the element $x_0 + ct$ with $c \geq c^* = \sqrt{2\sigma^2 \ln(g(0))} + \mu$. When we rewrite $w_t(x)$ in this moving half-frame we have

$$w_t(x_0 + ct) = [g(0)]^t \int_{-\infty}^{\infty} \frac{1}{\sqrt{2\pi\sigma^2 t}} e^{-\frac{(x_0+ct-y-\mu t)^2}{2\sigma^2 t}} w_0(y)\, dy. \tag{2.29}$$

Expanding the exponent, yields

$$\frac{(x_0 + ct - y - \mu t)^2}{2\sigma^2 t} = \frac{(x_0 - y)^2}{2\sigma^2 t} + \frac{2(c-\mu)t(x_0 - y) + (c-\mu)^2 t^2}{2\sigma^2 t} \tag{2.30}$$

$$\geq \frac{(x_0 - y)^2}{2\sigma^2 t} + \frac{c-\mu}{\sigma^2}(x_0 - y) + \ln(g(0))t. \tag{2.31}$$

Thus,

$$w_t(x_0 + ct) \leq \frac{e^{\ln(g(0))t}}{\sqrt{2\pi\sigma^2 t}} \int_{-\infty}^{\infty} e^{-\frac{(x_0-y)^2}{2\sigma^2 t}} e^{-\frac{c-\mu}{\sigma^2}(x_0-y)} e^{-\ln(g(0))t} w_0(y)\, dy \tag{2.32}$$

$$= \frac{1}{\sqrt{2\pi\sigma^2 t}} \int_{-\infty}^{\infty} e^{-\frac{(x_0-y)^2}{2\sigma^2 t}} e^{-\frac{c-\mu}{\sigma^2}(x_0-y)} w_0(y)\, dy \tag{2.33}$$

$$= \frac{e^{-\frac{c-\mu}{\sigma^2}x_0}}{\sqrt{2\pi\sigma^2 t}} \int_{-\infty}^{\infty} e^{-\frac{(x_0-y)^2}{2\sigma^2 t}} e^{\frac{c-\mu}{\sigma^2}y} w_0(y)\, dy. \tag{2.34}$$

Since $x_0 \geq A$ we have

$$w_t(x_0 + ct) \leq \frac{e^{-\frac{A(c-\mu)}{\sigma^2}}}{\sqrt{2\pi\sigma^2 t}} \int_{-\infty}^{\infty} e^{\frac{c-\mu}{\sigma^2}y} w_0(y)\, dy. \tag{2.35}$$

Thus since $\int_{-\infty}^{\infty} e^{\frac{c-\mu}{\sigma^2}y} w_0(y)\,dy < \infty$ we have $w_t(x_0 + ct) \to 0$ uniformly as $t \to \infty$ in $[A, \infty)$. Recall that $w_t(x)$ was constructed so that $0 \leq v_t(x) \leq w_t(x)$. This implies the uniform convergence of $v_t(x) \to 0$ as $t \to \infty$ in the moving half-frame $[A + ct, \infty)$. □

Corollary 2.3.1 (Compact initial conditions)**.** *Consider the solution of System* (2.12)-(2.13) *where k is $N(\mu, \sigma^2)$ and $0 < g(u) \leq g(0)$ for all $u \in (0, 1)$ with compactly supported initial conditions $v_0^i(x)$ for $i = 1, \ldots N$. Then each neutral fraction converges to zero uniformly to zero as $t \to \infty$ in the moving half-frame $[A + ct, \infty)$ where $c \geq c^*$.*

This result is clear from the condition that any compact initial conditions will satisfy the assumption of Theorem 2.3.1 that $\int_{-\infty}^{\infty} e^{\frac{c-\mu}{\sigma^2}y} v_0^i(y)\,dy < \infty$. This result is relevant because when we perform numerical simulations we must use compact initial conditions. Thus, it takes time for the traveling wave solution to spread at the asymptotic spreading speed c^*. Therefore, we will always outrun the solution by looking in the moving half-frame $[A + c^*t, \infty)$.

For the next corollary, we consider initial conditions were $u_0(x) = \sum_{i=1}^{N} v_0^i(x) = U(x)$ and $v_0^1(x) = \mathbb{1}_{x \geq a} U(x)$ where a is a constant. Here we call $v_0^1(x)$ the neutral fraction at the leading edge of the traveling wave.

Corollary 2.3.2 (Traveling wave initial conditions)**.** *Consider the solution of System* (2.12)-(2.13) *where k is $N(\mu, \sigma^2)$ and $0 < g(u) \leq g(0)$ for all $u \in (0, 1)$ with initial condition $\sum_{i=1}^{N} v_0^i(x) = U(x)$ with speed $c \geq c^*$. Then the neutral fraction at the leading edge of the traveling wave converges to $U(x)$ uniformly as $t \to \infty$ in the moving half-frame $[A + ct, \infty)$ and all other neutral fractions converges to zero uniformly to zero as $t \to \infty$ in the moving half-frame $[A + ct, \infty)$.*

In Corollary 2.3.2, the initial conditions for System (2.13) sum to be the traveling wave solution with speed greater than or equal to the minimum

asymptotic spreading speed c^*. In this case we know that traveling wave solutions exist for all $c \geq c^*$ (Weinberger, 1982). The key question is what happens to the neutral fraction at the front of the spread. We see that all other neutral fractions vanish when the moving half-frame is sufficiently far to the right. Thus, each one of these neutral fractions satisfy the assumption $\int_{-\infty}^{\infty} e^{\frac{c-\mu}{\sigma^2}y} v_0^i(y)\, dy < \infty$ required for Theorem 2.3.1. However, the neutral fraction at the leading edge decays no faster than $e^{-\frac{c-\mu}{\sigma^2}y}$. Thus, $\int_{-\infty}^{\infty} e^{\frac{c-\mu}{\sigma^2}y} v_0^i(y)\, dy$ is not finite, and hence one cannot apply Theorem 2.3.1 to this neutral fraction. However, if all other neutral fractions approach zero then it must be the case that the neutral fraction at the leading edge of the traveling wave converges to U uniformly as $t \to \infty$ in the moving half-frame $[A + ct, \infty)$. From Definition 2.2.4, it is clear that the results from Corollary 2.3.2 show that the solution to System (2.12)-(2.13) where k is $N(\mu, \sigma^2)$, $0 < g(u) \leq g(0)$ for all $u \in (0, 1)$, and $\sum_{i=1}^{N} v_0^i(x) = U(x)$ is a pulled front.

Next, we extend the theory to consider growth functions with a strong Allee effect. The idea of proof is different from Theorem 2.3.1 because we can no longer construct a super solution by using the linearization. Instead, we use Hilbert Schmidt theory to obtain the asymptotic dynamics.

Theorem 2.3.2 (Gaussian kernel with strong Allee type growth)**.** *Consider the solution of System* (2.12)-(2.13) *where k is $N(\mu, \sigma^2)$, g has a strong Allee effect, and $\sum_{i=1}^{N} v_0^i(x) = U(x)$. Then for any $A \in \mathbb{R}$, the density of neutral fraction i, $v_t^i(x)$, converges to a proportion $p^i[v_0^i]$ of the total population $U(x - ct)$ uniformly as $t \to \infty$ in the moving half-frame $[A + ct, \infty)$. That is, $|v_t^i(x) - p^i[v_0^i]U(x - ct)| \to 0$ uniformly as $t \to \infty$ in the moving half-frame $[A + ct, \infty)$. Moreover, if $e^{\frac{c-\mu}{\sigma^2}x} U(x) \in L^2(\mathbb{R})$, then the proportion $p^i[v_0^i]$ can be computed explicitly:*

$$p^i[v_0^i] = \frac{\int_{-\infty}^{\infty} v_0^i(x) U(x) e^{\frac{c-\mu}{\sigma^2/2}x}\, dx}{\int_{-\infty}^{\infty} U^2(x) e^{\frac{c-\mu}{\sigma^2/2}x}\, dx}. \tag{2.36}$$

Proof. Consider System (2.13) where k is $N(\mu, \sigma^2)$ and g has a strong Allee effect. For simplicity in notation we focus on a single neutral fraction and drop the superscript i notation. Define $\tilde{v}_t(x) = v_t(x + ct)$, then

$$\tilde{v}_{t+1}(x) = \int_{-\infty}^{\infty} k(x + c - y)g(U(y))\tilde{v}_t(y)\, dy. \tag{2.37}$$

Since k is $N(\mu, \sigma^2)$,

$$k(x + c - y) = \frac{1}{\sqrt{2\pi\sigma^2}} e^{-\frac{(x+c-y-\mu)^2}{2\sigma^2}} \tag{2.38}$$

$$= \frac{1}{\sqrt{2\pi\sigma^2}} e^{-\frac{(x-y)^2}{2\sigma^2}} e^{-\frac{(c-\mu)^2}{2\sigma^2}} e^{-\frac{c-\mu}{\sigma^2}x} e^{\frac{c-\mu}{\sigma^2}y} \tag{2.39}$$

$$= \tilde{k}(x - y) e^{-\frac{(c-\mu)^2}{2\sigma^2}} e^{-\frac{c-\mu}{\sigma^2}x} e^{\frac{(c-\mu)}{\sigma^2}y} \tag{2.40}$$

where $\tilde{k}$ is $N(0, \sigma^2)$. Define $v_t^*(x) = e^{\frac{c-\mu}{\sigma^2}x}\tilde{v}_t(x)$. Then Equation (2.37) becomes

$$v_{t+1}^*(x) = \int_{-\infty}^{\infty} e^{-\frac{(c-\mu)^2}{2\sigma^2}} \tilde{k}(x - y)g(U(y))v_t^*(y)\, dy. \tag{2.41}$$

We know that the weight function $\rho(y) = e^{-\frac{(c-\mu)^2}{2\sigma^2}} g(U(y))$ is a positive and continuous function and $\rho(y)\tilde{k}(x - y) \in L^2(\mathbb{R})$. Then we consider

$$\phi(x) = \int_{-\infty}^{\infty} e^{-\frac{c-\mu}{2\sigma^2}} \tilde{k}(x - y)g(U(y))\phi(y)\, dy. \tag{2.42}$$

Multiplying Equation (2.42) on both sides by $\sqrt{\rho(x)}$, we have

$$\sqrt{\rho(x)}\phi(x) = \int_{-\infty}^{\infty} \sqrt{\rho(x)}\tilde{k}(x - y)\sqrt{\rho(y)}\sqrt{\rho(y)}\phi(y)\, dy. \tag{2.43}$$

Since $\tilde{k}$ is $N(0, \sigma^2)$, the function $\overline{k}(x, y) := \sqrt{\rho(x)}\tilde{k}(x-y)\sqrt{\rho(y)}$ is symmetric; $\overline{k}(x, y) = \overline{k}(y, x)$. Therefore, the Hilbert-Schmidt theory can still be applied with a non-symmetric kernel. Also $\phi(x) = e^{\frac{c-\mu}{\sigma^2}x}U(x)$ is a positive eigenfunction of Equation (2.42) with eigenvalue 1. Thus, by Jentsch's theorem (Vladimirov, 1971), since our eigenfunction is positive, this eigenfunction is associated with the eigenvalue with the largest modulus. Therefore, we know that all other eigenvalues have modulus strictly less than one. We can write the solution by eigenfunction expansion as

$$v_t^*(x) = p\phi(x) + z_t(x) \tag{2.44}$$

where p is a scalar and $z_t(x)$ is composed of elements that are orthogonal to $\phi(x)$ for each $t \in \mathbb{N}$ and $|z_t(x)| \leq K|\lambda|^t$ for some constants $K > 0$ and $|\lambda| < 1$. Hence,

$$|v_t^*(x) - p\phi(x)| \leq K|\lambda|^t. \tag{2.45}$$

Converting back to the moving frame coordinates,

$$\left|e^{\frac{c-\mu}{\sigma^2}x}\tilde{v}_t(x) - pe^{\frac{c-\mu}{\sigma^2}x}U(x)\right| \leq K|\lambda|^t. \tag{2.46}$$

Thus,

$$|\tilde{v}_t(x) - pU(x)| \leq Ke^{-\frac{c-\mu}{\sigma^2}x}|\lambda|^t. \tag{2.47}$$

From this, we can conclude that $|\tilde{v}_t(x) - pU(x)| \to 0$ uniformly as $t \to \infty$ in the interval $[A, \infty)$. Therefore, $|v_t(x) - pU(x - ct)| \to 0$ uniformly as $t \to \infty$ in the moving half-frame $[A + ct, \infty)$.

To obtain the proportion p we multiply Equation (2.44) evaluated at $t = 0$ by $\phi(x)$ and integrate to obtain

$$\int_{-\infty}^{\infty} v_0^*(x)\phi(x)\,dx = \int_{-\infty}^{\infty} p\phi^2(x)\,dx + \int_{-\infty}^{\infty} z_0(x)\phi(x)\,dx \tag{2.48}$$

$$= p\int_{-\infty}^{\infty} \phi^2(x)\,dx \tag{2.49}$$

by the orthogonality of z to ϕ. Solving for p we find

$$p = \frac{\int_{-\infty}^{\infty} v_0^*(x)\phi(x)\,dx}{\int_{-\infty}^{\infty} \phi^2(x)\,dx} \tag{2.50}$$

$$= \frac{\int_{-\infty}^{\infty} e^{\frac{c-\mu}{\sigma^2}x}\tilde{v}_0(x)e^{\frac{c-\mu}{\sigma^2}x}U(x)\,dx}{\int_{-\infty}^{\infty}\left(e^{\frac{c-\mu}{\sigma^2}x}U(x)\right)^2 dx} \tag{2.51}$$

$$= \frac{\int_{-\infty}^{\infty} v_0(x)U(x)e^{\frac{c-\mu}{\sigma^2/2}x}\,dx}{\int_{-\infty}^{\infty} U^2(x)e^{\frac{c-\mu}{\sigma^2/2}x}\,dx}. \tag{2.52}$$

The proof of Theorem 2.3.2 is complete. □

From Definition 2.2.5, it is clear that the results from Theorem 2.3.2 show that the solution to System (2.12)-(2.13) where k is $N(\mu, \sigma^2)$, g has a strong Allee effect, and $u_0(x) = U(x)$ is a pushed front.

The next step in our work is to extend the result of Theorem 2.3.1 to a general class of thin-tailed dispersal kernels. To accomplish this goal we must place some extra constraints on the initial conditions for the neutral fractions. That is, we define the set $B_s := \{v_0^i : x^2 v_0^i(x) e^{sx} \in L^1(\mathbb{R}) \cap L^\infty(\mathbb{R})\}$. This condition is given as the assumption of Lemma 2.3.1.

Lemma 2.3.1. *Let $v_0^i(x) \in B_s$ for all $s > 0$, then there exists a positive constant C such that*

$$w_0^i(x) := \frac{Ce^{-sx}}{1+x^2} \tag{2.53}$$

bounds $v_0^i(x)$ for all $x \in \mathbb{R}$. Moreover, the Fourier transform of $w_0^i(x)e^{sx}$ with respect to x is in $L^1(\mathbb{R})$ and is given by

$$C\pi e^{-|\omega|}. \tag{2.54}$$

The proof of Lemma 2.3.1 is provided in Appendix 2.6.1. Lemma 2.3.1 provides important assumptions to guarantee that the initial conditions can be bounded by a function that has a Fourier transform in $L^1(\mathbb{R})$. This result allows us to extend the result of Theorem 2.3.1 to a general class of thin-tailed dispersal kernels.

Theorem 2.3.3 (Thin-tailed kernel with maximum per capita growth at zero)**.** *Consider the solution of System* (2.12)-(2.13) *where k is a thin-tailed dispersal kernel and g is the per-capita growth rate that satisfies $0 < g(u) \leq g(0)$ for all $u \in (0,1)$. Let c be the speed of a moving half-frame. If $c \geq c^*$ and $v_0^i(x) \in B_{s_0(c)}$ where $s_0(c)$ is the smallest positive root of $\ln(g(0)K(s)) = sc$, then for any $A \in \mathbb{R}$, the density of the neutral fraction i, $v_t^i(x)$, converges to 0 uniformly as $t \to \infty$ in the moving half-frame $[A + ct, \infty)$.*

Proof. Consider the neutral fraction model given by System (2.13). For simplicity, we consider a single neutral fraction $v_t^i(x)$ and drop the superscript i

notation. That is,

$$v_t(x) = \int_{-\infty}^{\infty} k(x-y)g(u_{t-1}(y))v_{t-1}(y)\,dy. \tag{2.55}$$

Equation (2.1) produces traveling wave solutions $u_t(x) = U(x-ct)$. In the case where k, is **a** thin-tailed dispersal kernel and $0 < g(u) \leq g(0)$ for all $u \in (0,1)$ we know that the asymptotic spreading speed c^* can be calculated by

$$c^* = \inf_{s>0} \frac{1}{s} \ln\left(g(0)K(s)\right) \tag{2.56}$$

where $K(s) = \int_{-\infty}^{\infty} k(x)e^{sx}\,dx$ is the moment generating function for the dispersal kernel k. The function $\ln(g(0)K(s))/s$ is positive and convex where $K(s)$ is finite. Thus, there is a unique minimum for c^* obtained at some s^*. That is, $\ln\left(g(0)K(s^*)\right) = s^*c^*$. For all $c > c^*$ the equation $\ln\left(g(0)K(s)\right) = sc$ has at most two positive roots. We define the smallest positive root by $s_0(c) < s^*$. Using the fact that the per-capita growth rate is the largest at zero, we obtain a super-solution $w_t(x)$ to System (2.55) . That is, $w_t(x)$ satisfies the Cauchy problem

$$\begin{cases} w_t(x) = g(0)\int_{-\infty}^{\infty} k(x-y)w_{t-1}(y)\,dy, & t \in \mathbb{N},\, x \in \mathbb{R} \\ w_0(x) = \frac{Ce^{-s_0(c)x}}{1+x^2} \geq v_0(x), & x \in \mathbb{R} \end{cases} \tag{2.57}$$

where $v_t(x) \leq w_t(x)$ for all $t \geq 0$. The solution of Equation (2.57) is given by the t-fold convolution

$$w_t(x) = (g(0))^t k^{*t} * w_0(x). \tag{2.58}$$

Next, we introduce the reflected bilateral Laplace transform defined in Equation (2.9) for all $0 < s < s_{max}$. It is clear that we can apply this transform to $w_t(x)$ because k is thin-tailed and $w_0(x)$ is defined by Equation (2.53). Applying this transform to Equation (2.58) and using the convolution property we obtain

$$\mathcal{M}[w_t(x)](s) = (g(0))^t(\mathcal{M}[k(x)](s))^t\mathcal{M}[w_0(x)](s) \tag{2.59}$$

$$= (g(0))^t(K(s))^t W_0(s). \tag{2.60}$$

To obtain our solution for $w_t(x)$ we must use the inverse transform, as defined in Equation (2.10), given by

$$w_t(x) = \frac{1}{2\pi i} \lim_{R\to\infty} \int_{s_0(c)-iR}^{s_0(c)+iR} (g(0))^t (K(s))^t W_0(s) e^{-sx}\, ds \tag{2.61}$$

where $0 < \mathrm{Re}(s) < s_{max}$ is the region of convergence for $(K(s))^t W_0(s)e^{-sx}$. By performing a change of variables to integrate over the real line by letting $s = s_0(c) + i\omega$ we obtain

$$w_t(x) = \frac{1}{2\pi} \int_{-\infty}^{\infty} (g(0))^t (K(s_0(c)+i\omega))^t W_0(s_0(c)+i\omega) e^{-(s_0(c)+i\omega)x}\, d\omega \tag{2.62}$$

$$= \frac{1}{2\pi} \int_{-\infty}^{\infty} e^{(\mathrm{Log}(g(0))+\mathrm{Log}(K(s_0(c)+i\omega))t} W_0(s_0(c)+i\omega) e^{-(s_0(c)+i\omega)x}\, d\omega, \tag{2.63}$$

where Log is the principal value of the complex logarithm. In the moving frame, $x = x_0 + ct$ choose $x_0 \in \mathbb{R}$, the solution satisfies

$$w_t(x_0+ct) = \frac{1}{2\pi} \int_{-\infty}^{\infty} e^{J(s_0(c)+i\omega)t} W_0(s_0(c)+i\omega) e^{-(s_0(c)+i\omega)x_0}\, d\omega, \tag{2.64}$$

where J is a complex-valued function defined as follows

$$J(s_0(c)+i\omega) := \mathrm{Log}(g(0)) + \mathrm{Log}(K(s_0(c)+i\omega)) - c(s_0(c)+i\omega). \tag{2.65}$$

Although we expect that $w_t(x)$ as a solution to Equation (2.58) is real, this fact is not immediately evident from Equation (2.64). Therefore, we treat $w_t(x)$ as if it were a complex-valued function. The modulus of the supersolution is

$$|w_t(x_0+ct)| = \left| \frac{1}{2\pi} \int_{-\infty}^{\infty} e^{J(s_0(c)+i\omega)t} W_0(s_0(c)+i\omega) e^{-(s_0(c)+i\omega)x_0}\, d\omega \right| \tag{2.66}$$

$$\leq \frac{1}{2\pi} \int_{-\infty}^{\infty} e^{\mathrm{Re}(J(s_0(c)+i\omega))t} \left| W_0(s_0(c)+i\omega) \right| e^{-s_0(c)x_0}\, d\omega. \tag{2.67}$$

Using the results from Lemma 2.3.1 we have that

$$W_0(s_0(c)+i\omega) = \int_{-\infty}^{\infty} w_0(x) e^{(s_0(c)+i\omega)x}\, dx \tag{2.68}$$

$$= \int_{-\infty}^{\infty} w_0(x) e^{s_0(c)x} e^{i\omega x}\, dx \tag{2.69}$$

$$= \mathcal{F}\left[w_0(x) e^{s_0(c)x} \right](-\omega) \tag{2.70}$$

$$= C\pi e^{-|\omega|} \tag{2.71}$$

for all $\omega \in \mathbb{R}$. Then using Equation (2.67) and the previous result we have

$$|w_t(x_0 + ct)| \leq \frac{1}{2\pi} \int_{-\infty}^{\infty} e^{\mathrm{Re}(J(s_0(c)+i\omega))t} C\pi e^{-|\omega|} e^{-s_0(c)x_0}\, d\omega. \tag{2.72}$$

Notice that

$$\mathrm{Re}(J(s_0(c) + i\omega)) = \ln(g(0)) + \mathrm{Re}(\mathrm{Log}(K(s_0(c) + i\omega))) - cs_0(c) \tag{2.73}$$

$$= \ln(g(0)) + \mathrm{Re}\left(\mathrm{Log}\left(\int_{-\infty}^{\infty} k(x) e^{s_0(c)x} e^{i\omega x}\, dx\right)\right) - cs_0(c). \tag{2.74}$$

Let us define

$$I := \mathrm{Re}\left(\mathrm{Log}\left(\int_{-\infty}^{\infty} k(x) e^{s_0(c)x} e^{i\omega x}\, dx\right)\right). \tag{2.75}$$

Using Euler's formula we find that

$$I = \mathrm{Re}\left(\mathrm{Log}\left(\int_{-\infty}^{\infty} k(x) e^{s_0(c)} (\cos(\omega x) + i \sin(\omega x))\, dx\right)\right) \tag{2.76}$$

$$= \ln\left(\sqrt{\left(\int_{-\infty}^{\infty} k(x) e^{s_0(c)x} \cos(\omega x)\, dx\right)^2 + \left(\int_{-\infty}^{\infty} k(x) e^{s_0(c)x} \sin(\omega x)\, dx\right)^2}\right). \tag{2.77}$$

Define $II := \left(\int_{-\infty}^{\infty} k(x) e^{s_0(c)x} \cos(\omega x)\, dx\right)^2 + \left(\int_{-\infty}^{\infty} k(x) e^{s_0(c)x} \sin(\omega x)\, dx\right)^2$. Using Cauchy-Schwarz inequality we find that

$$II < \int_{-\infty}^{\infty} k(x) e^{s_0(c)x}\, dx \int_{-\infty}^{\infty} k(x) e^{s_0(c)x} \cos^2(\omega x)\, dx + \ldots$$

$$\int_{-\infty}^{\infty} k(x) e^{s_0(c)x}\, dx \int_{-\infty}^{\infty} k(x) e^{s_0(c)x} \sin^2(\omega x)\, dx \tag{2.78}$$

$$= \int_{-\infty}^{\infty} k(x) e^{s_0(c)x}\, dx \int_{-\infty}^{\infty} k(x) e^{s_0(c)x} \left(\cos^2(\omega x) + \sin^2(\omega x)\right)\, dx \tag{2.79}$$

$$= \left(\int_{-\infty}^{\infty} k(x) e^{s_0(c)x}\, dx\right)^2. \tag{2.80}$$

Thus,

$$\mathrm{Re}(J(s_0(c)+i\omega)) < \ln(g(0)) + \ln\left(\sqrt{\left(\int_{-\infty}^{\infty} k(x)e^{s_0(c)x}\,dx\right)^2}\right) - cs_0(c) \tag{2.81}$$

$$= \ln(g(0)) + \ln\left(\int_{-\infty}^{\infty} k(x)e^{s_0(c)x}\,dx\right) - cs_0(c) \tag{2.82}$$

$$= \ln(g(0)) + \ln\left(K(s_0(c))\right) - cs_0(c) \tag{2.83}$$

$$= 0 \tag{2.84}$$

for $\omega \neq 0$. When $\omega = 0$, we have that $\mathrm{Re}(J(s_0(c)+i\omega)) = 0$. Returning to Inequality (2.72), by the Dominated Convergence theorem, we have

$$\lim_{t\to\infty} |w_t(x_0+ct)| \leq \lim_{t\to\infty} \frac{1}{2\pi}\int_{-\infty}^{\infty} e^{\mathrm{Re}(J(s_0(c)+i\omega))t} C\pi e^{-|\omega|} e^{-s_0(c)x_0}\,d\omega \tag{2.85}$$

$$= \frac{Ce^{-s_0(c)x_0}}{2}\int_{-\infty}^{\infty} \lim_{t\to\infty} e^{\mathrm{Re}(J(s_0(c)+i\omega))t} e^{-|\omega|}\,d\omega \tag{2.86}$$

$$= 0. \tag{2.87}$$

Thus, for any $A \in \mathbb{R}$

$$\lim_{t\to\infty} \max_{[A,\infty)} w_t(x+ct) = 0. \tag{2.88}$$

Since w was chosen to be a super-solution of v, we can conclude that

$$\lim_{t\to\infty} \max_{[A,\infty)} v_t(x+ct) = 0. \tag{2.89}$$

Therefore, we obtain the desired result that for any $A \in \mathbb{R}$, the density $v_t(x)$ of the neutral fraction converges to 0 uniformly as $t \to \infty$ in the moving half-frame $[A+ct, \infty)$. □

From Definition 2.2.4, it is clear that the results from Theorem 2.3.3 show that the solution to System (2.12)-(2.13) where k is thin-tailed, $0 < g(u) \leq g(0)$ for all $u \in (0,1)$, and $\sum_{i=1}^{N} v_0^i(x) = U(x)$ is a pulled front.

This section contains the main mathematical results of our work. We showed that when the dispersal kernel is assumed to be Gaussian we showed

two main results. When the per capita growth is maximal at zero we see that all neutral fractions converge to zero uniformly in the moving frame. If the growth function has a strong Allee effect then all neutral fractions contribute to the spread. Moreover, the proportion of each neutral fraction in the spread is given by Equation (2.36). We then extended the first result to thin-tailed dispersal kernels showing that when the per capita growth is maximal at zero we see that all neutral fractions converge to zero uniformly in the moving frame.

2.4 Numerical Simulations

The numerical simulations were performed using MATLAB. To calculate the convolution

$$\int_{-\infty}^{\infty} k(x-y)g(u_t(y))v_t^i(y)\,dy \tag{2.90}$$

we use a numerical "fast Fourier transform" `(fft)` with inverse (`ifft`). Solving the problem by using the convolution theorem, changes the numerical scheme to become $O(n\log n)$ instead of $O(n^2)$. Numerically, we implement the following strategy

$$k * (g\cdot v^i) = \texttt{ifft}(\texttt{fft}(k)\cdot\texttt{fft}(g\cdot v^i)). \tag{2.91}$$

For simplicity, in all the numerical simulations we start with the same initial condition and use the same dispersal kernel. We assume that there are eight neutral fractions in the population and assume that they satisfy $v_0^i(x) = \mathbb{1}_{(-0.5i,-0.5(i-1)]}$ where $\mathbb{1}_S$ is the indicator function on a set S. This assumes that we have the strongest initial spatial heterogeneity between the neutral fractions, see Figure 2.2(a) for a plot of the initial conditions. The dispersal kernel is assumed to be Gaussian with $\mu = 0$ and $\sigma^2 = 0.002$. That is,

$$k(x-y) = \frac{1}{\sqrt{0.004\pi}}e^{-\frac{(x-y)^2}{0.004}}. \tag{2.92}$$

Simulations for System (2.13) with the different types of growth functions are provided in Figure 2.2.

The interpretation of the simulations provided in Figure 2.2 must be made carefully because, without proper explanation, they may be misunderstood. In Figure 2.2 the light gray component is the sum all eight neutral fractions. The red component is plotted in front of the light gray and is given by the sum of all neutral fractions except the first one. The same process continues for the rest of the six colors yellow, green, light blue, blue, and dark gray respectively. The easiest way to interpret the numerical results presented in Figure 2.2 is by looking at a vertical strip of the solution for a particular value of x. From this perspective the amount of color showing for each neutral fraction dictates the proportion of that fraction to the entire population density at a particular location x. For example, we can see from the initial condition in Figure 2.2(a) that each neutral fraction has complete spatial segregation from other neutral fractions.

In Figure 2.2(b) we observe that only the rightmost fraction drives the propagation of the total population where as the trailing populations will be left behind in the moving frame. In Figure 2.2(c) we observe that the leading neutral fraction dominates the spread but in this case the traveling wave is nonmonotone. In 2.2(d) the inclusion of a strong Allee effect promotes genetic diversity in the colonization front. The numerical results suggest that the classification of pulled and pushed fronts should be able to be extended for initial conditions other than the traveling wave profile $U(x)$. The complexity in extending the results lie in understanding how to choose the correct speed for the moving half-frame.

It should be noted that the simulations are numerical approximations to System (2.13) because the domain where we can compute the numerics is finite. The results seen in Figure 2.2 provide numerical support for the extension

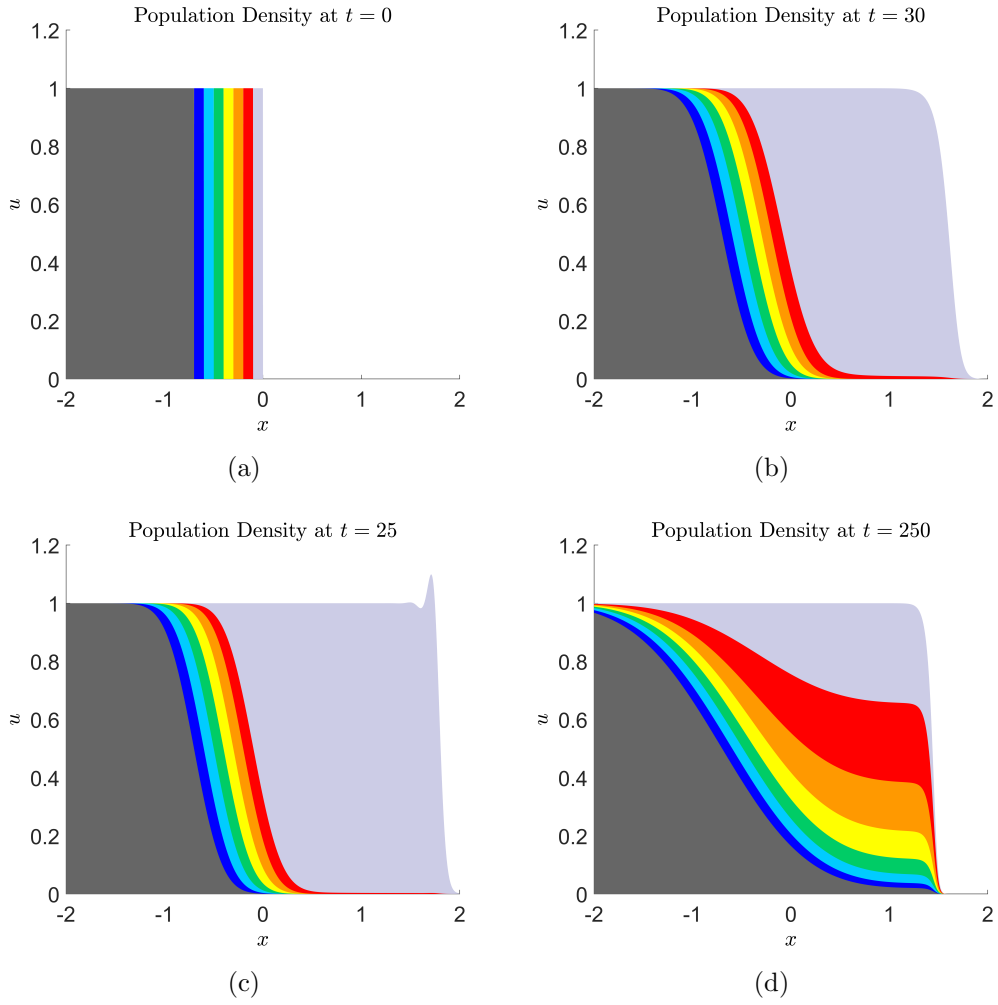

Figure 2.2: Numerical realization for the solution $u_t(x)$ of System (2.13) for three different per capita growth functions
(a) The initial condition for the simulations
(b) Beverton-Holt growth with parameter values $R = 2.5$ at time $t = 30$
(c) Ricker growth with parameter values $R = 1.5$ at time $t = 25$
(d) Sigmoid Beverton-Holt growth with parameter values $R = 4$ and $\delta = 2$ at time $t = 250$

of the results presented in the previous section to compact initial conditions. For Theorem 2.3.2 and Corollary 2.3.2 the results require that the initial conditions are in the form of the traveling wave solution $U(x)$. However, since the computational domain is finite, we know that all the initial conditions will have finite support. This means that we obtain the results from Corollary 2.3.1 when the per capita growth rate is maximal at zero which states that if we move the frame at speed c^* then asymptotically all neutral fractions approach zero. This is because compact initial conditions that converges to a front moving at speed c^* would have fallen behind the moving half-frame that travels at speed c^* for all time.

2.5 Discussion

The work presented in this paper develops a mathematical model to understand the role that dispersal into new territory has on the neutral genetic composition of a population with discrete nonoverlapping generations. We construct our model using the integrodifference framework where space is continuous but time is discrete.

This work extends the previous results on the mathematical analysis of inside dynamics to include discrete time dynamics. All previous analyses of inside dynamics have assumed continuous-time dynamics. By working with discrete time models we explore how overcompensation affects the neutral genetic diversity. Since this phenomena is not possible for a scalar continuous time model, the analysis of the overcompensatory growth is fundamentally new.

We were able to prove asymptotic results about the genetic structure of the expanding population. First, we considered Gaussian dispersal with two different kinds of growth functions. The first having maximum per capita growth at zero, and the second having a strong Allee effect. The results are given by

Theorems 2.3.1 and 2.3.2. The theorems provide very different asymptotic behavior for solutions whose initial conditions are in the shape of the traveling wave solution.

For growth functions whose per capita growth is maximal at zero we see that the spread of the population is dominated by the leading neutral fraction and all other neutral fractions approach zero, see Corollary 2.3.2. However, we are only able to conclude this result when the initial population density is in the shape of the traveling wave solution. Mathematically, this is analogous with the concept of a pulled front where the dynamics of the spread are governed solely by what happens at the leading edge of the wave. From a biological perspective this is an extreme case of the founder effect where the uninhabited area is settled by only one of the neutral fractions. Numerical results suggest that for compact initial conditions the spread is still dominated by the leading neutral fraction. The setback is that we do not know exactly how fast compact initial conditions converge to the traveling wave solution, but the proof of Theorem 2.3.1 suggests that solutions starting with initial conditions spread at most like $c^*t - 1/2\ln(t)$. Hence, we are only able to show that for compact initial conditions that spread at c^*, all neutral fractions will be outrun by the moving half-frame, see Corollary 2.3.1.

When the growth function has a strong Allee effect, we are able to show that asymptotically each neutral fraction converges to a proportion of the traveling wave solution given by Equation (2.36). The proportion of individuals is dependent on the initial condition of the neutral fractions, the traveling wave solution, and the asymptotic spreading speed of the population. It is also clear from Equation (2.36) that the neutral fractions at the wave front contribute a larger proportion of the total population density than those at the rear. This is analogous with the concept of a pushed front, where the genetic variation at the front of the wave comes from the spill over effect from the strong Allee

effect. Generally, the Allee effect is thought to have a negative connotation on expanding populations because of the ability of the population to die out for low density levels. Our results show that the strong Allee effect preserves the neutral genetic variation in an expanding population. Thus, the strong Allee effect has a positive effect on the neutral genetic variation of an expanding population. We did not generalize this result for the general class of thin-tailed dispersal kernels as done in the case where the per capita growth was maximal at zero.

The results proven in this paper can be connected to those for partial differential equations. When the dispersal kernel is Gaussian with mean zero, we are able to compare the results of Theorems 2.3.1 and 2.3.2 to the previous results for reaction diffusion equations, see (Garnier et al., 2012; Roques et al., 2012). The conclusions from Theorem 2.3.1 are the same as for reaction diffusion equations where the growth function is of KPP type. When the growth function has a strong Allee effect, Theorem 2.3.2 predicts that each neutral fraction converges to a proportion of the traveling wave solution given by Equation 2.36. This proportion is the same as the one calculated for the bistable reaction diffusion equation when k is $N(0, 2)$.

We were able to extend the results of Theorem 2.3.1 to thin-tailed dispersal kernels. This result is given by Theorem 2.3.3. Here we see the same results as seen in the previous result for Gaussian kernels that the traveling wave solution is a pulled front and the spread is dominated by the leading neutral fraction. The proofs for Theorems 2.3.1 and 2.3.3 are very different because in the thin-tailed case we were not able to exploit the form of the moment generating function for Gaussian dispersal kernels. Thus, when inverting the bilateral Laplace transform we could not use the convolution theorem to simplify the calculations and were left to compute the complex integral. The extension was not direct because we were forced to place an assumption allowing for our

initial condition to be bounded by a function whose Fourier transform is in $L^1(\mathbb{R})$.

This theory provided by Theorems 2.3.1 and 2.3.3 require that the per capita growth rate is maximal at zero. Thus, we are able to apply these results to growth functions with overcompensation such as the Ricker and logistic type growth. Growth functions with overcompensation can produce nonmonotone traveling wave solutions as seen in Figure 2.2(c). We conjecture that in this scenario the shape of the nonmonotone shape of the traveling wave does not change the inside dynamics results for pulled fronts. The ability to analyze how overcompensation affects the neutral genetic patterns of spread is a unique feature that differentiates our work from previous studies. These types of dynamics were not possible in the previous works due to the fact that the entire population spread was governed by a scalar continuous time model. We see that the sole effect of overcompensation does not promote neutral genetic variation in an expanding population. Thus, the traveling wave solution for the population density is still classified as a pulled front because the spread is dominated by the leading neutral fraction.

The collective results provide a way of classifying traveling wave solutions of integrodifference equations in terms of pulled and pushed fronts. That is, if the spread is dominated by the leading neutral fraction, then the traveling wave solution is a pulled front. If the leading edge of the spread includes components from many neutral fractions, then the traveling wave solution is a pushed front. In the case where we have a Gaussian dispersal kernel, we conjecture that a traveling wave solution can be determined simply by how fast the wave decays at the leading edge. This was stated in Conjecture 2.5.1 where the critical decay depends on the spreading speed and dispersal parameters.

Even though this work answers some of the interesting questions about neutral genetic patterns in populations undergoing a range expansion in dis-

crete time, it is clear that there is still more work to be done. There is still room to extend the result of Theorem 2.3.2 to a general class of thin-tailed dispersal kernels. The inclusion of a fat-tailed dispersal kernel is known to produce accelerating traveling waves. Whether this occurs when the growth function has an Allee effect is still unknown. Another direction of future work is to consider what happens to solutions with fat-tailed dispersal. In this case we have accelerating traveling waves meaning that the speed that the wave travels increases with time.

The convergence rate for compact initial conditions to traveling wave solution is not known for integrodifference equations. If such a result was known then we would be able to alter the speed of the moving half-frame to extend this result as to never outrun the solution of System (2.13). This points toward the need for convergence theory about the speed of the solution approaching the traveling wave solution for integrodifference equations. For example, with partial differential equations, a well-known result by Bramson shows that in the frame of reference moving at $2t - \frac{3}{2}\ln(t) + x_\infty$, where x_∞ is dependent on the initial condition, the solution of the Fisher KPP equation converges as $t \to \infty$ to a translation of the traveling wave solution corresponding to the minimal asymptotic spreading speed $c^* = 2$ (Bramson, 1983). This result gives us the exact speed needed for the moving frame to capture the solution for compact initial conditions in the reaction diffusion equation framework with KPP type growth.

Based on the assumption made on the decay of the initial condition in Theorem 2.3.1 and the decay traveling wave solution made in Theorem 2.3.2, we make the following conjecture for the classification of traveling wave solutions to Equation (2.1).

Conjecture 2.5.1 (Decay properties of Gaussian traveling waves)**.** *Consider*

a traveling wave solution $U(x-ct)$, to Equation (2.1) *with a Gaussian dispersal kernel. If we have that $\int_{-\infty}^{\infty} e^{\frac{c-\mu}{\sigma^2}y} U(y)\,dy < \infty$ (U decays faster than $e^{\frac{c-\mu}{\sigma^2}y}$) then $U(x-ct)$ is a pushed front. If we have that $U(x-ct)$ decays exactly at the exponential rate $e^{\frac{c-\mu}{\sigma^2}y}$, then $U(x-ct)$ is a pulled front solution corresponding to the minimum asymptotic spreading speed $c^* = \sqrt{2\sigma^2 \ln(g(0))} + \mu$. If $U(x-ct)$ decays slower than $e^{\frac{c-\mu}{\sigma^2}y}$, then $U(x-ct)$ is a pulled front with speed $c > c^*$.*

If Conjecture 2.5.1 is true, then it could give insight to the issue of pushed versus pulled fronts for growth functions with a weak Allee effect. Moreover, Conjecture 2.5.1 provides the critical decay rate for differentiating traveling wave solutions as pulled or pushed fronts.

Outside of the realm of the inside dynamics analysis, this work also motivates future work for many general questions about traveling wave solutions for integrodifference equations. The open questions that we encountered for integrodifference equations when completing this work were as follows:

1. What are the asymptotic decay properties for traveling wave solutions?

2. How fast do pulled front solutions with compact initial conditions approach the traveling wave solution?

3. What is the asymptotic spreading speed for growth functions with a strong Allee effect?

In summary, our work presents a framework for understanding the neutral genetic consequences of a population with nonoverlapping generations undergoing a range expansion. By connecting the ecological concepts with a mathematical model we encounter many interesting mathematical problems. The results shown in Section 2.3 provide an excellent start to understanding the question of interest; however, there are many questions that we were not able to answer due to limited mathematical theory. Therefore, with improved

mathematical theory we can provide better insight to understanding the neutral genetic diversity of expanding populations.

2.6 Appendix

2.6.1 Proof of Lemma 2.3.1

Proof. For simplicity in notation we focus on a single neutral fraction and drop the superscript i notation. By assumption, $x^2 v_0(x) e^{sx} \in L^1(\mathbb{R}) \cap L^\infty(\mathbb{R})$. Thus, we have

$$x^2 v_0(x) e^{sx} \leq (1 + x^2) v_0(x) e^{sx} \leq C \tag{2.93}$$

for all $x \in \mathbb{R}$ where C is a positive constant. Rearranging the previous inequality,

$$v_0(x) \leq \frac{C e^{-sx}}{1 + x^2} \tag{2.94}$$

for all $x \in \mathbb{R}$. Thus, there exists a positive constant C such that the function $w_0(x)$ defined by

$$w_0(x) := \frac{C e^{-sx}}{1 + x^2} \tag{2.95}$$

satisfies $v_0(x) \leq w_0(x)$ for all $x \in \mathbb{R}$. It is easy to see that $w_0(x) e^{sx} \in L^1(\mathbb{R}) \cap L^\infty(\mathbb{R})$. Hence, the Fourier transform of $w_0(x) e^{sx} \in L^1(\mathbb{R})$. To calculate the Fourier Transform of $w_0(x) e^{sx}$, note that

$$\begin{aligned}
\mathcal{F}\left[e^{-|x|}\right](\omega) &= \int_{-\infty}^{\infty} e^{-|x|} e^{-i\omega x}\, dx && (2.96)\\
&= \int_{-\infty}^{0} e^{(1-i\omega)x}\, dx + \int_{0}^{\infty} e^{-(1+i\omega)x}\, dx && (2.97)\\
&= \lim_{b\to\infty} \left[\frac{e^{(1-i\omega)x}}{(1-i\omega)}\bigg|_{-b}^{0} - \frac{e^{-(1+i\omega)x}}{(1+i\omega)}\bigg|_{0}^{b} \right] && (2.98)\\
&= \lim_{b\to\infty} \left[\frac{1}{(1-i\omega)} - \frac{e^{-(1-i\omega)b}}{(1-i\omega)} - \frac{e^{-(1+i\omega)b}}{(1+i\omega)} + \frac{1}{(1+i\omega)} \right] && (2.99)\\
&= \left[\frac{1}{(1-i\omega)} + \frac{1}{(1+i\omega)} \right] && (2.100)\\
&= \frac{2}{1+\omega^2}. && (2.101)
\end{aligned}$$

From the inverse Fourier Transform,

$$\pi e^{-|x|} = \frac{\pi}{2\pi} \int_{-\infty}^{\infty} \frac{2}{1+\omega^2} e^{i\omega x}\, d\omega \tag{2.102}$$

$$= \int_{-\infty}^{\infty} \frac{1}{1+\omega^2} e^{i\omega x}\, d\omega. \tag{2.103}$$

Using the above result,

$$\mathcal{F}\left[\frac{C}{1+x^2}\right](\omega) = \mathcal{F}\left[\frac{C}{1+(-x)^2}\right](\omega) \tag{2.104}$$

$$= C \int_{-\infty}^{\infty} \frac{1}{1+(-x)^2} e^{-i\omega(-x)}\, dx \tag{2.105}$$

$$= C \int_{-\infty}^{\infty} \frac{1}{1+x^2} e^{i\omega x}\, dx \tag{2.106}$$

$$= C\pi e^{-|\omega|}. \tag{2.107}$$

The proof of the lemma is complete. □

References

Bonnefon, Olivier, Jérôme Coville, Jimmy Garnier, and Lionel Roques (2014). "Inside dynamics of solutions of integro-differential equations." *Discrete and Continuous Dynamical Systems-Series B* 19.10, pp. 3057–3085.

Bonnefon, Olivier, Jimmy Garnier, François Hamel, and Lionel Roques (2013). "Inside dynamics of delayed traveling waves." *Mathematical Modelling of Natural Phenomena* 8.3, pp. 42–59.

Bramson, Maury (1983). *Convergence of solutions of the Kolmogorov equation to travelling waves*. Vol. 285. American Mathematical Society.

Casella, George and Roger L Berger (2002). *Statistical inference*. Vol. 2. Duxbury Pacific Grove, CA.

Dlugosch, Katrina M and Ingrid M Parker (2008). "Founding events in species invasions: genetic variation, adaptive evolution, and the role of multiple introductions." *Molecular Ecology* 17.1, pp. 431–449.

Excoffier, Laurent (2004). "Patterns of DNA sequence diversity and genetic structure after a range expansion: lessons from the infinite-island model." *Molecular Ecology* 13.4, pp. 853–864.

Excoffier, Laurent and Nicolas Ray (2008). "Surfing during population expansions promotes genetic revolutions and structuration." *Trends in Ecology & Evolution* 23.7, pp. 347–351.

Garnier, Jimmy, Thomas Giletti, François Hamel, and Lionel Roques (2012). "Inside dynamics of pulled and pushed fronts." *Journal de Mathématiques Pures et Appliquées* 98.4, pp. 428–449.

Hallatschek, Oskar, Pascal Hersen, Sharad Ramanathan, and David R Nelson (2007). "Genetic drift at expanding frontiers promotes gene segregation." *Proceedings of the National Academy of Sciences* 104.50, pp. 19926–19930.

Hallatschek, Oskar and David R Nelson (2008). "Gene surfing in expanding populations." *Theoretical Population Biology* 73.1, pp. 158–170.

Hewitt, Godfrey M (1996). "Some genetic consequences of ice ages, and their role in divergence and speciation." *Biological Journal of the Linnean Society* 58.3, pp. 247–276.

— (2000). "The genetic legacy of the Quaternary ice ages." *Nature* 405.6789, pp. 907–913.

Holmes, Elizabeth E, Mark A Lewis, John E Banks, and Richard R Veit (1994). "Partial differential equations in ecology: spatial interactions and population dynamics." *Ecology* 75.1, pp. 17–29.

Ibrahim, Kamal M, Richard A Nichols, and Godfrey M Hewitt (1996). "Spatial patterns of genetic variation generated by different forms of dispersal." *Heredity* 77, pp. 282–291.

Kot, Mark (1992). "Discrete-time travelling waves: ecological examples." *Journal of Mathematical Biology* 30.4, pp. 413–436.

Krasnosel'skii, Mark A and Petr P Zabreiko (1984). *Geometrical methods of nonlinear analysis*.

Lewis, Mark A, Sergei V Petrovskii, and Jonathan R Potts (2016). *The Mathematics Behind Biological Invasions*. Vol. 44. Springer.

Li, Bingtuan, Mark A Lewis, and Hans F Weinberger (2009). "Existence of traveling waves for integral recursions with nonmonotone growth functions." *Journal of Mathematical Biology* 58.3, pp. 323–338.

Lui, Roger (1983). "Existence and stability of travelling wave solutions of a nonlinear integral operator." *Journal of Mathematical Biology* 16.3, pp. 199–220.

Lutscher, Frithjof (2008). "Density-dependent dispersal in integrodifference equations." *Journal of Mathematical Biology* 56.4, pp. 499–524.

Mayr, Ernst (1942). *Systematics and the origin of species, from the viewpoint of a zoologist*. Harvard University Press.

Müller, Melanie JI, Beverly I Neugeboren, David R Nelson, and Andrew W Murray (2014). "Genetic drift opposes mutualism during spatial population expansion." *Proceedings of the National Academy of Sciences* 111.3, pp. 1037–1042.

Ricker, William E (1954). "Stock and recruitment." *Journal of the Fisheries Board of Canada* 11.5, pp. 559–623.

Roques, Lionel, Jimmy Garnier, François Hamel, and Etienne K Klein (2012). "Allee effect promotes diversity in traveling waves of colonization." *Proceedings of the National Academy of Sciences* 109.23, pp. 8828–8833.

Rothe, Franz (1981). "Convergence to pushed fronts." *Rocky Mountain Journal of Mathematics* 11.4.

Slatkin, Montgomery and Laurent Excoffier (2012). "Serial founder effects during range expansion: a spatial analog of genetic drift." *Genetics* 191.1, pp. 171–181.

Stokes, AN (1976). "On two types of moving front in quasilinear diffusion." *Mathematical Biosciences* 31.3-4, pp. 307–315.

Thomas, Chris D, EJ Bodsworth, Robert J Wilson, Adam D Simmons, Zoe G Davies, Martin Musche, and Larissa Conradt (2001). "Ecological and evolutionary processes at expanding range margins." *Nature* 411.6837, pp. 577–581.

Thompson, Grant G (1993). "A proposal for a threshold stock size and maximum fishing mortality rate." *Canadian Special Publication of Fisheries and Aquatic Sciences*, pp. 303–320.

Vladimirov, Vasilij Sergeevič (1971). *Equations of mathematical physics (Uravneniia matematicheskoĭ fiziki)*. Marcel Dekker, New York.

Wang, Mei-Hui, Mark Kot, and Michael G Neubert (2002). "Integrodifference equations, Allee effects, and invasions." *Journal of Mathematical Biology* 44.2, pp. 150–168.

Weinberger, Hans F (1982). "Long-time behavior of a class of biological models." *SIAM Journal on Mathematical Analysis* 13.3, pp. 353–396.

Zemanian, Armen H (1968). *Generalized integral transformations*. Vol. 140. Interscience Publishers New York.

Chapter 3

Inside dynamics for stage-structured integrodifference equations

3.1 Introduction

There are a wide array of observational (Cullingham et al., 2011), empirical (Liebhold et al., 1992; Lubina and S. A. Levin, 1988), and theoretical studies (Li et al., 2009; Lui, 1989a; Weinberger, 1982) for the spatial spread of populations by range expansion. Over the last decades, theoretical studies about range expansion mainly focused on the asymptotic speed of propagation of the expanding population or the profile of invasion (Hastings et al., 2005). Spatial models in population genetics have also been developed for studying the spread of an advantageous gene in a population (Lui, 1982a,b, 1983; Weinberger, 1978, 1982). Recently, much effort have been invested to understand the genetic consequences of range expansion (Hallatschek and Nelson, 2008; Roques et al., 2012). Indeed, range expansions are known to have significant effects on genetic diversity (Davis and Shaw, 2001; Hewitt, 2000). For instance, if range expansion occurs through successive founder effects, genetic diversity is likely to decrease. However, empirical and theoretical studies have shown that many mechanisms may reduce or reverse the loss of diversity

in an expanding population (Pluess, 2011). In particular, the presence of an Allee effect (Roques et al., 2012) which reduces the per-capita growth rate at low density, the occurrence of long distance dispersal events (Bonnefon et al., 2014; Ibrahim et al., 1996), or the existence of a juvenile stage (Austerlitz and Garnier-Géré, 2003) may promote neutral genetic diversity in traveling waves of colonization. In this work, we are interested in the neutral genetic dynamics of a stage-structured population undergoing range expansion.

It is well known that the structure of the population is important for understanding the asymptotic dynamics. For example, individuals often must undergo a maturation period before they can produce offspring. For discrete population models, the dynamics of the life history traits have typically been structured according to age, Leslie matrix (Leslie, 1945), or developmental stage, Lefkovitch matrix (Lefkovitch, 1965), but matrix models can be easily generalized to include other physiological characteristics. It is also common for sessile species to typically have a motile stage in their development, such as seed dispersal in plant populations (Howe and Smallwood, 1982) and larval dispersal in marine environments (L. A. Levin, 2006).

Our study considers a stage-structured integrodifference equation describing range expansion for a population of the form:

$$\mathbf{u}_{t+1}(x) = \int_{-\infty}^{\infty} \left[\mathbf{K}(x-y) \circ \mathbf{B}(\mathbf{u}_t(y))\right] \mathbf{u}_t(y)\, dy, \tag{3.1}$$

where $\mathbf{u}_t(x)$ corresponds to the population density at time t and location x. The population is structured into m stages, whose densities are given by $\mathbf{u}_t(x) = [u_{1,t}(x), \ldots, u_{m,t}(x)]$. Each stage distribution changes in time and space through the successive effects of dispersal, described by the dispersal matrix $\mathbf{K} = [k_{jl}]$, and the demography, embodied in the population projection matrix $\mathbf{B}(\mathbf{u}) = [b_{jl}(\mathbf{u})]$ which takes into account density-dependence. The succession of the reproduction stage and dispersal stage is described by the

Hadamard product $\circ$ (element-wise multiplication of matrix). This model allows the different stages to spread, reproduce, and interact in a variety of ways that cannot be captured by scalar models (Neubert and Caswell, 2000). More precisely, if we consider stage j, where $j = 1, \ldots, m$, then its density, $u_{j,t}(x)$, satisfies the following equation

$$u_{j,t+1} = \int_{-\infty}^{\infty} \sum_{l=1}^{m} k_{jl}(x-y) b_{jl}(u_{1,t}(y), \ldots, u_{m,t}(y)) u_{l,t}(y)\, dy \tag{3.2}$$

where $k_{jl}(x-y)\, dy$ is the probability that an individual transitioning from stage l to stage j disperses from the interval $(y, y+dy]$ to location x, and the function b_{jl} is the per-capita production of stage j individuals from stage l individuals. Such a model has been used to describe epidemic spread (Lui, 1989b), biological invasions (Bateman et al., 2017; Veit and Lewis, 1996), and critical domain size (Lutscher and Lewis, 2004).

The model (3.1) is biologically valid if the stages are chosen in a way such that the life history and dispersal parameters vary within stages as little as possible. In some cases this is easy; for example, a division between juvenile and adult individuals is normally determined by the ability to reproduce. In other cases, the division may not be so clear, and partitions may be difficult to decide. Fortunately, there are algorithms that can be used to minimize errors associated with partitioning a population into distinct stages (Moloney, 1986; Vandermeer, 1978). If the division of population structure is modeled using a continuous variable such as size or mass, and there is no natural break point to structure the population into distinct stages then an integral projection model may be more appropriate (Easterling et al., 2000).

The goal of this work is to understand the neutral genetic patterns of structured populations. Neutral genetic markers are genes that have no direct effect on individual fitness. Even though this type of gene tells us nothing about the adaptive or evolutionary potential of a population, neutral genetic markers can

be used to understand processes such as gene flow, genetic drift, migration, or dispersal (Holderegger et al., 2006). It has also been shown by simulations that high levels of neutral genetic diversity can be correlated with increased allelic richness at loci under selection (Bataillon et al., 1996). Our analysis will be focused on the inside dynamics of stage-structured integrodifference equations.

This paper is organized as follows. Section 3.2 is dedicated to providing necessary background material for understanding the main results. Within this section, we break it into two subsections: Section 3.2.1 provides background to the analysis of inside dynamics and the stage-structured integrodifference equation used in our analysis and Section 3.2.2 lays out four of the major assumptions made about the demographic and dispersal processes. In Section 3.3, we provide asymptotic results regarding population structure. This section is broken into three parts. Section 3.3.1 covers the inside dynamics of neutral fractions not present at the leading edge, Section 3.3.2 discusses the inside dynamics of neutral fractions that are located at the leading edge, and Section 3.3.3 contains proofs for our main theorems. To complement the analytical results, numerical simulations are given in Section 3.4. Finally, in Section 3.5, we discuss the modeling technique, results, numerical simulations, and implications of our work.

3.2 Materials and methods

3.2.1 Inside dynamics

To study the neutral genetic distribution of a population, we consider the inside dynamics of the population. The term inside dynamics refers to the inside structure of the population rather than the total density. The key assumption in the analysis of inside dynamics is that all individuals grow and

disperse in the same manner, differing only with respect to neutral genetic markers. In other words, all individuals in the population have the same fitness. This allows us to split up the population into distinct subgroups called neutral fractions with which we track the spatiotemporal evolution of these subgroups.

Inside dynamics have been studied for reaction-diffusion equations (Garnier et al., 2012; Garnier and Lewis, 2016; Roques et al., 2012), delay reaction-diffusion equations (Bonnefon et al., 2013), integro-differential equations (Bonnefon et al., 2014), and integrodifference equations (Lewis et al., 2018; Marculis et al., 2017). In these works, the subject for analysis was a scalar population model. Indeed, to date, there is only one study of the inside dynamics of systems of equations. This study concentrated on the analysis on a diffusive Lotka-Volterra competition system (Roques et al., 2015). Our mathematical contribution to this area of research is to extend the analysis of inside dynamics to stage-structured integrodifference equations.

Recall the stage-structured population model in (3.1). Separating the initial population up into distinct neutral fractions, we obtain the initial condition

$$\mathbf{u}_0(x) = \sum_{i=1}^{n} \mathbf{v}_0^i(x), \tag{3.3}$$

where $\mathbf{v}_0^i(x) \geq 0$ is the initial population density for neutral fraction i and n is the finite number of neutral fractions. An illustration of this decomposition can be seen in Figures 3.1(a) and 3.2(a). By assuming that individuals in each neutral fraction grow and disperse similarly, we obtain the following system of equations:

$$\mathbf{v}_{t+1}^i(x) = \int_{-\infty}^{\infty} \left[\mathbf{K}(x-y) \circ \mathbf{B}(\mathbf{u}_t(y))\right] \mathbf{v}_t^i(y)\, dy, \quad i = 1, \ldots, n, \tag{3.4}$$

where $\mathbf{u}_t(y) = \sum_{i=1}^{n} \mathbf{v}_t^i(y)$. Throughout the remaining sections, we use the superscript i to denote the neutral fraction and, when not written in vector

form, subscript j to denotes the stage. Note that the number of neutral fractions, n, and the number of stages in the population, m, need not be the same ($n \neq m$). Also, observe the model given in Equation (3.4) is natural extension of the scalar model to a system of recursions (Marculis et al., 2017). Thus, it can be expected that many of the results proven for the scalar equation can be extended to systems of cooperative equations. This is the approach we take in what follows.

3.2.2 Demographic and dispersal assumptions

For each of our main theorems, we make five assumptions regarding Equations (3.3)-(3.4). The first three assumptions are related to the population projection matrix, the fourth assumption is related to the dispersal kernel, and the fifth and final assumption is related to the decay of the initial conditions. In this section, we outline the first four assumptions related to the demography and dispersal of the population.

Population projection matrix

We begin with looking at the population projection matrix $\mathbf{B}(\mathbf{u})$. Here, we outline three assumptions about the population projection matrix. The population projection matrix describes reproduction, survival, and interactions between stages. As a projection matrix, its entries should be nonnegative:

$A1:$ *The matrix* $\mathbf{B}(\mathbf{u})$ *is nonnegative for any* $\mathbf{u} \in (0, \infty)^m$.

Moreover, we can see from (3.1) that $\mathbf{0}$ is a steady state of the problem. Define

$$\mathbf{B_0} := \mathbf{B}(\mathbf{u})\big|_{\mathbf{u}=\mathbf{0}}. \tag{3.5}$$

Notice that $\mathbf{B_0}$ is the population projection matrix evaluated at $\mathbf{u} = \mathbf{0}$. We will assume that this steady state is unstable. More precisely, we assume:

$A2:$ $\mathbf{B_0}$ *is a primitive matrix, that is there exists* $k > 0$ *such that* $\mathbf{B_0^k}$ *is positive, and its dominant eigenvalue,* λ_1*, is greater than* 1*,* $\lambda_1 > 1$*.*

Finally, we assume that there are no Allee effects. That is:

$A3:$ $\mathbf{B}(\mathbf{u})$ *is bounded by its linearization at the steady state* $\mathbf{0}$*,* $\mathbf{B}(\mathbf{u})\mathbf{v} \leq \mathbf{B_0}\mathbf{v}$ *for all* $\mathbf{v} \in (0, \infty)^m$*.*

Dispersal kernel

In our model, we assume that individuals in the population may disperse at long distance but those events are rare in the following sense:

Definition 3.2.1. *A dispersal kernel,* $k(x)$*, is called thin-tailed if there exists a* $\xi > 0$*, such that*

$$\int_{-\infty}^{\infty} k(x)e^{\xi|x|}\,dx < \infty. \tag{3.6}$$

A dispersal kernel that is not thin-tailed is called a fat-tailed dispersal kernel, and in this case, the long distance dispersal events become frequent, which leads to different behaviors for some solutions, such as accelerating waves. Many of the classical mathematical results for (3.1), such as traveling wave solutions and the asymptotic speed of propagation, rely on the assumption that the dispersal kernel is thin-tailed. A common dispersal kernel that we consider throughout our work is the Gaussian probability density function:

$$k(x;\mu,\sigma) = \frac{1}{\sqrt{2\pi\sigma^2}}e^{-\frac{(x-\mu)^2}{2\sigma^2}}, \tag{3.7}$$

where μ is the mean shift in location and σ^2 is the variance in dispersal distance. In the following sections, we use the following shorthand notation to denote that the dispersal kernel is Gaussian by k is $N(\mu, \sigma^2)$. In what follows, we will make one of two assumptions about the dispersal kernels.

$A4:$ *Each kernel,* $k_{jl}(x-y)$*, is thin-tailed.*

$A4'$: *Each kernel,* $k_{jl}(x-y)$*, is* $N(\mu, \sigma^2)$.

From above, we see that our fourth assumption provides a condition on the dispersal kernels. In both cases, we assume, at a minimum, that every dispersal kernel is thin-tailed in order to calculate the asymptotic speed of propagation. The above assumption implies that we are not considering a population with accelerating waves (Kot et al., 1996).

Asymptotic speed of propagation

Under the previous assumptions $A1$-$A4$ we can deduce from the work of Lui (1989a) that solutions of (3.1) will spread to the right with an asymptotic spreading speed c greater than or equal to a critical spreading speed $c^* > 0$ for appropriately chosen initial conditions. Moreover, the critical spreading speed c^* can be computed explicitly by the following formula

$$c^* := \min_{0<s<s^+} \frac{1}{s} \ln \rho(s), \tag{3.8}$$

where $\rho(s) := \rho(\mathbf{H}(s)) > 1$ is the dominant eigenvalue of $\mathbf{H}(s)$ defined by

$$\mathbf{H}(s) := \mathbf{M}(s) \circ \mathbf{B_0}. \tag{3.9}$$

The moment generating function matrix $\mathbf{M}(s)$ is calculated by applying the reflected bilateral Laplace transform to the dispersal kernel matrix $\mathbf{K}$ and is defined by

$$\mathbf{M}(s) := \int_{-\infty}^{\infty} \mathbf{K}(x) e^{sx}\, dx. \tag{3.10}$$

Since the entries of the dispersal kernel matrix, k_{jl}, are thin-tailed by Assumption $A5$, this matrix is well defined over $(0, s^+)$ where $s^+ \in (0, \infty]$. Throughout our analysis, we let $s_0(c)$ be the smallest positive root of the equation

$$cs = \ln(\rho(s)) \text{ for } c \geq c^*. \tag{3.11}$$

We know that $s_0(c)$ exists because $\rho(s)$ is log convex; see Lemma 6.4 by Lui (1989a). In particular, when each kernel is Gaussian, k_{jl} is $N(\mu, \sigma^2)$, then we have an explicit formula for the asymptotic speed of propagation given by

$$c^* = \sqrt{2\sigma^2 \ln(\lambda_1)} + \mu, \tag{3.12}$$

where λ_1 is the dominant eigenvalue of $\mathbf{B_0}$ and we can explicitly compute $s_0(c)$ to be

$$s_0(c) = \frac{c - \mu + \sqrt{(c-\mu)^2 - 2\sigma^2 \ln(\lambda_1)}}{\sigma^2}. \tag{3.13}$$

The technical details for the asymptotic speed of propagation are provided in Appendix 3.6.1.

3.3 Main results

Henceforth, we assume that the structured population, $\mathbf{u}_t(x)$, satisfies (3.1) with an initial condition $\mathbf{u}_0(x)$. With such initial condition, the population is spreading to the right with an asymptotic speed of propagation, c, greater than or equal to c^*, given by formula (3.8). We first consider neutral fractions that are not present at the leading edge of the solution and then afterwards consider neutral fractions that are at the leading edge of the expanding population.

Our fifth and final assumption places a requirement on the initial conditions for the neutral fractions. This requirement is closely connected to the decay rate of the solution for the population and determines whether or not an individual is at the leading edge of the population spread. In particular, we know that the traveling wave solution for the linearized equation is given by an exponential function and the decay rate defines the leading edge of the population. The technical details of whether or not a neutral fraction is located at the leading edge is defined in the statement of our main theorems. We do not explicitly write these out here, but rather save them for the statement of our theorems because this assumption takes different forms based on our

assumptions. We are now ready to present our first two theorems, that provides sufficient conditions for when the density of neutral fractions converges to zero in the moving half-frame.

3.3.1 Inside dynamics not at the leading edge

Theorem 3.3.1. *Let us assume that A1-A4 hold true. Let* $\mathbf{v}_t^i(x)$ *be a neutral fraction satisfying* (3.4) *with initial condition* $\mathbf{v}_0^i(x)$ *satisfying* (3.3) *that is not present at the leading edge of the expanding population, in the sense that*

$A5:\ x^2\mathbf{v}_0^i(x)e^{s_0(c)x} \in L^1(\mathbb{R}) \cap L^\infty(\mathbb{R})$ *for a given* $c \geq c^*$.

Then, for any $A \in \mathbb{R}$, *the density of neutral fraction* i, $\mathbf{v}_t^i(x)$, *converges to* $\mathbf{0}$ *uniformly as* $t \to \infty$ *in the moving half-frame* $[A + ct, \infty)$.

In summary, Theorem 3.3.1 provides sufficient conditions for neutral fractions in the population to approach zero asymptotically. This result implies that the only neutral fractions that will contribute to the spread of the population are those that are initially at the leading edge. In this scenario, we observe an extreme founder effect for the population spread. For this proof, see Section 3.3.3.

By making a stronger assumption on the dispersal kernels, we are able to relax Assumption $A5$ on the initial conditions in Theorem 3.3.1. In particular, for the next theorem we assume that all dispersal kernels are Gaussian with the same mean and variance as given by Assumption $A4'$ and the assumption on the initial condition becomes a simple integrability condition.

Theorem 3.3.2. *Let us assume that A1-A3 and* $A4'$ *hold true. Let* $\mathbf{v}_t^i(x)$ *be a neutral fraction satisfying* (3.4) *with initial condition* $\mathbf{v}_0^i(x)$ *satisfying* (3.3) *that is not present at the leading edge of the expanding population, in the sense that*

$A5'$: $\int_{-\infty}^{\infty} e^{\frac{c-\mu}{\sigma^2}y} \mathbf{v}_0^i(y)\, dy < \infty$ *for a given* $c \geq c^*$.

Then, for any $A \in \mathbb{R}$*, the density of neutral fraction* i*,* $\mathbf{v}_t^i(x)$*, converges to* $\mathbf{0}$ *uniformly as* $t \to \infty$ *in the moving half-frame* $[A + ct, \infty)$.

In summary, Theorem 3.3.2 provides the same result as Theorem 3.3.1 but with different assumptions on the dispersal kernels and initial conditions. That is, Theorem 3.3.2 provides sufficient conditions for when the neutral fractions do not contribute to the population spread. Under Assumption $A5'$, we see that the leading edge is determined by the decaying exponential $e^{-\frac{c-\mu}{\sigma^2}x}$. This condition is much different than those given by Assumption $A5$ in Theorem 3.3.1. As in the previous theorem, we also observe here that the only neutral fractions that will contribute to the spread of the population are those that are initially at the leading edge. For this proof, see Section 3.3.3.

The proof of Theorem 3.3.1 is more complicated than that of Theorem 3.3.2, even though the method of proof and conclusions are the same. The difference is due to the assumptions made about the dispersal kernels. In Theorem 3.3.1 we assume the dispersal kernels are thin-tailed and must use the definition of the inverse reflected bilateral Laplace transform. In Theorem 3.3.2 we assume all dispersal kernels are Gaussian with the same mean and variance. This assumption simplifies the proof because convolving Gaussian distributions results in another Gaussian.

If the initial conditions are all compactly supported, then all neutral fractions will satisfy Assumption $A5$ and $A5'$ respectively in Theorems 3.3.1 and 3.3.2. If the initial conditions decay according to the traveling wave solution, then all neutral fractions except those at the leading edge will satisfy Assumption $A5$ and $A5'$ in Theorems 3.3.1 and 3.3.2 respectively. This means that the only neutral fractions that we will see in the moving half-frame are those that were initially at the leading edge. However, Theorems 3.3.1 and 3.3.2 do

not tell us anything about these neutral fractions.

3.3.2 Inside dynamics at the leading edge

In the next theorem, we look at initial data that decay slower than Assumption $A5'$ in Theorem 3.3.2. Here we are able to calculate the asymptotic proportion of each neutral fraction provided we move at the slowest speed c^*.

Theorem 3.3.3. *Let us assume that A1-A3 and A4′ hold true. Let* $\mathbf{v}_t^i(x)$ *be a neutral fraction satisfying* (3.4) *with initial condition* $\mathbf{v}_0^i(x)$ *satisfying* (3.3) *that is present at the leading edge of the expanding population, in the sense that for* $c = c^*$

$A5''$: $\mathbf{v}_0^i(x) = (\mathbf{p}_0^i \circ \mathbf{r})\, e^{-\frac{c-\mu}{\sigma^2}x}$, *where* $\mathbf{p}_0^i$ *is the initial proportion for neutral fraction* i *in each stage,* $\mathbf{r}$ *is the right eigenvector of* $\mathbf{B_0}$ *corresponding to* λ_1.

Then, for any $A \in \mathbb{R}$, *the density of neutral fraction* i, $\mathbf{v}_t^i(x)$, *asymptotically approaches a proportion,* p^i, *of the traveling wave for the linear equation as* $t \to \infty$ *in the moving half-frame* $[A + ct, \infty)$. *That is,*

$$\lim_{t\to\infty} \mathbf{v}_t^i(x_0 + ct) = e^{-\frac{c-\mu}{\sigma^2}x_0}\mathbf{r}p^i \tag{3.14}$$

for $x_0 \geq A$. *Moreover, the proportion can be calculated to be the scalar*

$$p^i = \boldsymbol{\ell}\left(\mathbf{p}_0^i \circ \mathbf{r}\right) \tag{3.15}$$

where $\boldsymbol{\ell}$ *is the left eigenvector of* $\mathbf{B_0}$ *corresponding to* λ_1 *with* $\boldsymbol{\ell}$ *normalized by* $\left\langle \boldsymbol{\ell}^T, \mathbf{r} \right\rangle$.

Theorem 3.3.3 provides a formula for the asymptotic proportion of neutral fractions based on the initial distribution at the leading edge of the population. The formula is simple because it depends only on the right and left eigenvectors of $\mathbf{B_0}$ and the initial proportion of neutral fractions. This theorem

characterizes the fate of neutral fractions at the leading edge. One drawback to this theorem is that it is only valid for initial conditions that decay at a specific rate, $e^{-\frac{c-\mu}{\sigma^2}x}$, with a solution that moves at a specific speed, $c = c^*$. The reason why we cannot prove this theorem for $c > c^*$ and a slower decay rate for the initial condition is because we do not have an explicit formula for the spreading speed $c > c^*$. For this proof, see Section 3.3.3.

It is also important to note that $A5''$ in Theorem 3.3.3 is not completely biologically realistic since the population grows without bound as $x \to -\infty$. However, this type of initial condition is needed based on the construction of our sub-solution and super-solutions. It may be possible to relax this assumption by studying the nonlinear operator and considering a more biologically realistic class of initial conditions. Next, we present the proofs of Theorems 3.3.1-3.3.3 in Section 3.3.3. For a comprehensive review of the necessary mathematical material needed in the proofs of the theorems, we direct the reader to Appendix 3.6.2.

3.3.3 Proofs of the main theorems

Proof of Theorem 3.3.1

Proof. For simplicity, we drop the superscript i in (3.4) and focus on a single neutral fraction. Our equation of interest is

$$\mathbf{v}_{t+1}(x) = \int_{-\infty}^{\infty} \left[\mathbf{K}(x-y) \circ \mathbf{B}(\mathbf{u}_t(y))\right] \mathbf{v}_t(y)\, dy. \tag{3.16}$$

Let

$$\mathbf{w}_0(x) = \frac{\mathbf{C}e^{-s_0(c)x}}{1+x^2} \tag{3.17}$$

where $\mathbf{C} = \kappa\boldsymbol{\phi}$ and $\boldsymbol{\phi}$ is the eigenvector of $\mathbf{H}(s_0(c))$ with dominant eigenvalue $\rho(s_0(c))$. From Lemma 3.6.1, we know that $\mathbf{w}_0(x)$ is an upper bound for $\mathbf{v}_0(x)$. By Assumption $A3$, we know that $\mathbf{B}(\mathbf{u}_t(y))\mathbf{v} \leq \mathbf{B_0}\mathbf{v}$ for all $\mathbf{v} \geq 0$. Hence, we

can construct a super-solution $\mathbf{w}_t(x)$ that satisfies the following equation

$$\mathbf{w}_{t+1}(x) = \int_{-\infty}^{\infty} [\mathbf{K}(x-y) \circ \mathbf{B_0}]\, \mathbf{w}_t(y)\, dy \tag{3.18}$$

with initial condition given by (3.17). By iterating we can write the solution to the above system as the t-fold convolution

$$\mathbf{w}_t(x) = [\mathbf{K}(x-y) \circ \mathbf{B_0}]^{*t}\, \mathbf{w}_0(y). \tag{3.19}$$

Applying the bilateral Laplace transform

$$\mathbf{W}_t(s) = [\mathbf{M}(s) \circ \mathbf{B_0}]^t\, \mathbf{W}_0(s) \tag{3.20}$$

$$= [\mathbf{H}(s)]^t\, \mathbf{W}_0(s). \tag{3.21}$$

Recall that $s_0(c)$ is the smallest positive root of $sc = \ln(\rho(s))$ for $c \geq c^*$. Then, the inverse transform as defined in Appendix 3.6.2, see (3.130), yields

$$\mathbf{w}_t(x) = \frac{1}{2\pi i} \lim_{R\to\infty} \int_{s_0(c)-iR}^{s_0(c)+iR} [\mathbf{H}(s)]^t\, \mathbf{W}_0(s) e^{-sx}\, ds \tag{3.22}$$

$$= \frac{1}{2\pi} \int_{-\infty}^{\infty} [\mathbf{H}(s_0(c)+i\omega)]^t\, \mathbf{W}_0(s_0(c)+i\omega) e^{-(s_0(c)+i\omega)x}\, d\omega \tag{3.23}$$

for $c \geq c^*$. In the moving frame we have

$$\mathbf{w}_t(x_0+ct) = \frac{1}{2\pi} \int_{-\infty}^{\infty} [\mathbf{H}(s_0(c)+i\omega)]^t\, \mathbf{W}_0(s_0(c)+i\omega) e^{-(s_0(c)+i\omega)x_0} e^{-(s_0(c)+i\omega)ct}\, d\omega. \tag{3.24}$$

Using the results from Lemma 3.6.1, see Appendix 3.6.2 for details, we are able to write the initial condition in terms of a Fourier transform that is known. This is seen as follows,

$$\mathbf{W}_0(s_0(c)+i\omega) = \int_{-\infty}^{\infty} \mathbf{w}_0(x) e^{(s_0(c)+i\omega)x}\, dx \tag{3.25}$$

$$= \int_{-\infty}^{\infty} \mathbf{w}_0(x) e^{s_0(c)x} e^{i\omega x}\, dx \tag{3.26}$$

$$= \mathcal{F}\left[\mathbf{w}_0(x) e^{s_0(c)x}\right](-\omega) \tag{3.27}$$

$$= \mathbf{C}\pi e^{-|\omega|} \tag{3.28}$$

for all $\omega \in \mathbb{R}$. Recall that $\mathbf{C} = \kappa\boldsymbol{\phi}$. This gives

$$\mathbf{w}_t(x_0 + ct) = \frac{1}{2\pi}\int_{-\infty}^{\infty} [\mathbf{H}(s_0(c) + i\omega)]^t \, \mathbf{C}\pi e^{-|\omega|} e^{-(s_0(c)+i\omega)x_0} e^{-(s_0(c)+i\omega)ct}\, d\omega \tag{3.29}$$

$$= \frac{1}{2}\int_{-\infty}^{\infty} [\mathbf{H}(s_0(c) + i\omega)]^t \, \kappa e^{-s_0(c)ct}\boldsymbol{\phi} e^{-|\omega|} e^{-(s_0(c)+i\omega)x_0} e^{-i\omega ct}\, d\omega. \tag{3.30}$$

Since $s_0(c)c = \ln(\rho(s_0(c)))$, we have

$$\mathbf{w}_t(x_0 + ct) = \frac{\kappa e^{-s_0(c)x_0}}{2}\int_{-\infty}^{\infty} [\mathbf{H}(s_0(c) + i\omega)]^t \, e^{-\ln(\rho(s_0(c)))t}\boldsymbol{\phi} e^{-|\omega|} e^{-i\omega x_0} e^{-i\omega ct}\, d\omega \tag{3.31}$$

$$= \frac{\kappa e^{-s_0(c)x_0}}{2}\int_{-\infty}^{\infty} [\mathbf{H}(s_0(c) + i\omega)]^t \, (\rho(s_0(c))^{-t}\boldsymbol{\phi} e^{-|\omega|} e^{-i\omega x_0} e^{-i\omega ct}\, d\omega. \tag{3.32}$$

Since $\rho(s_0(c))$ is the dominant eigenvalue of $\mathbf{H}(s_0(c))$ with eigenvector $\boldsymbol{\phi}$,

$$\mathbf{w}_t(x_0 + ct) = \frac{\kappa e^{-s_0(c)x_0}}{2}\int_{-\infty}^{\infty} [\mathbf{H}(s_0(c) + i\omega)]^t \, [\mathbf{H}(s_0(c))]^{-t}\boldsymbol{\phi} e^{-|\omega|} e^{-i\omega x_0} e^{-i\omega ct}\, d\omega. \tag{3.33}$$

Applying the matrix norm and using the sub-additive property, we find that

$$\|\mathbf{w}_t(x_0 + ct)\| \leq \frac{\kappa e^{-s_0(c)x_0}}{2}\int_{-\infty}^{\infty} \left\|\left|[\mathbf{H}(s_0(c) + i\omega)]^t\right|\right\| \left\|[\mathbf{H}(s_0(c))]^{-t}\right\| \|\boldsymbol{\phi}\| e^{-|\omega|} \left|e^{-i\omega x_0}\right| \left|e^{-i\omega ct}\right| \, d\omega \tag{3.34}$$

$$= \frac{\kappa e^{-s_0(c)x_0}}{2}\int_{-\infty}^{\infty} \left\|\left|[\mathbf{H}(s_0(c) + i\omega)]^t\right|\right\| \left\|[\mathbf{H}(s_0(c))]^{-t}\right\| \|\boldsymbol{\phi}\| e^{-|\omega|}\, d\omega. \tag{3.35}$$

We can also see that

$$|\mathbf{H}(s_0(c) + i\omega)| = |\mathbf{M}(s_0(c) + i\omega) \circ \mathbf{B_0})| \tag{3.36}$$

$$= \left|\int_{-\infty}^{\infty} [\mathbf{K}(x) \circ \mathbf{B_0}] e^{(s_0(c)+i\omega)x}\, dx\right| \tag{3.37}$$

$$= \left|\int_{-\infty}^{\infty} [\mathbf{K}(x) \circ \mathbf{B_0}] e^{s_0(c)x} \left(\cos(\omega x) + i\sin(\omega x)\right)\, dx\right| \tag{3.38}$$

$$= I, \tag{3.39}$$

where I is defined to be

$$I := \sqrt{\left(\int_{-\infty}^{\infty} [\mathbf{K}(x) \circ \mathbf{B_0}] e^{s_0(c)x}\cos(\omega x)\, dx\right)^2 + \left(\int_{-\infty}^{\infty} [\mathbf{K}(x) \circ \mathbf{B_0}] e^{s_0(c)x}\sin(\omega x)\, dx\right)^2}. \tag{3.40}$$

By the Cauchy-Schwarz inequality, using a similar technique as in Theorem 3 of (Marculis et al., 2017),

$$I < \int_{-\infty}^{\infty} [\mathbf{K}(x) \circ \mathbf{B_0}] e^{s_0(c)x}\, dx \tag{3.41}$$

$$= \mathbf{M}(s_0(c)) \circ \mathbf{B_0} \tag{3.42}$$

$$= \mathbf{H}(s_0(c)) \tag{3.43}$$

for $\omega \neq 0$. From the above calculation we can conclude that $|\mathbf{H}(s_0(c) + i\omega)| < \mathbf{H}(s_0(c))$ for $\omega \neq 0$. Consequently, $\rho\left(|\mathbf{H}(s_0(c) + i\omega)|\right) < \rho(s_0(c))$ for $\omega \neq 0$. By Gelfand's formula,

$$\lim_{t\to\infty} \left\| \left| [\mathbf{H}(s_0(c) + i\omega)]^t \right| \right\|^{\frac{1}{t}} = \rho(|\mathbf{H}(s_0(c) + i\omega)|) \quad \text{and} \tag{3.44}$$

$$\lim_{t\to\infty} \left\| [\mathbf{H}(s_0(c))]^{-t} \right\|^{\frac{1}{t}} = \frac{1}{\rho(s_0(c))}. \tag{3.45}$$

Thus, for $\omega \neq 0$, we can choose $\varepsilon > 0$ such that $(\rho(|\mathbf{H}(s_0(c) + i\omega)|) + \varepsilon)\left(\frac{1}{\rho(s_0(c))} + \varepsilon\right) < 1$. Therefore,

$$\left\| \left| [\mathbf{H}(s_0(c) + i\omega)]^t \right| \right\| \left\| [\mathbf{H}(s_0(c))]^{-t} \right\| < 1 \tag{3.46}$$

for large t and

$$\lim_{t\to\infty} \left\| \left| [\mathbf{H}(s_0(c) + i\omega)]^t \right| \right\| \left\| [\mathbf{H}(s_0(c))]^{-t} \right\| = 0. \tag{3.47}$$

From (3.35) and the dominated convergence theorem,

$$\lim_{t\to\infty} \|\mathbf{w}_t(x_0 + ct)\| \leq \frac{\kappa e^{-s_0(c)x_0}}{2} \int_{-\infty}^{\infty} \lim_{t\to\infty} \left\| \left| [\mathbf{H}(s_0(c) + i\omega)]^t \right| \right\| \left\| [\mathbf{H}(s_0(c))]^{-t} \right\| \|\boldsymbol{\phi}\| e^{-|\omega|}\, d\omega \tag{3.48}$$

$$= \mathbf{0}. \tag{3.49}$$

Therefore, for any $A \in \mathbb{R}$ and $c \geq c^*$,

$$\lim_{t\to\infty} \max_{[A,\infty)} \mathbf{w}_t(x + ct) = \mathbf{0}. \tag{3.50}$$

Since $\mathbf{w}$ was constructed as a super-solution, we can conclude that

$$\lim_{t\to\infty} \max_{[A,\infty)} \mathbf{v}_t(x + ct) = \mathbf{0}. \tag{3.51}$$

The proof of Theorem 3.3.1 is complete. □

Proof of Theorem 3.3.2

Proof. For simplicity, we focus on a single neutral fraction and drop the superscript i. By Assumption $A3$, $\mathbf{B}(\mathbf{u}_t(y))\mathbf{v} \leq \mathbf{B_0}\mathbf{v}$ for all $\mathbf{v} \geq 0$, we can use a comparison principle to show that a new sequence $\mathbf{w}_t(x)$ defined by

$$\mathbf{w}_{t+1}(x) = \int_{-\infty}^{\infty} \left[\mathbf{K}(x-y) \circ \mathbf{B_0}\right] \mathbf{w}_t(y)\, dy \tag{3.52}$$

is always greater than the solution to any neutral fraction $\mathbf{v}_t(x)$ with the same initial condition, $\mathbf{w}_0(x) = \mathbf{v}_0(x)$. By iterating we can write the solution to Equation (3.52) as the t-fold convolution

$$\mathbf{w}_t(x) = \left[\mathbf{K}(x-y) \circ \mathbf{B_0}\right]^{*t} \mathbf{w}_0(y). \tag{3.53}$$

Taking the bilateral Laplace transform

$$\mathcal{M}[\mathbf{w}_t(x)](s) = \left[\mathcal{M}[\mathbf{K}(x)](s) \circ \mathbf{B_0}\right]^t \mathcal{M}[\mathbf{w}_0(x)](s). \tag{3.54}$$

Since all of the dispersal kernels are Gaussian, we know that $\mathcal{M}[\mathbf{K}(x)](s) = e^{\frac{\sigma^2 s^2}{2} + \mu s}\mathbf{1}$ where $\mathbf{1}$ is a matrix of all ones. Then,

$$\begin{aligned}
\left[\mathcal{M}[\mathbf{K}(x)](s) \circ \mathbf{B_0}\right]^t \mathcal{M}[\mathbf{w}_0(x)](s) &= \left[e^{\frac{\sigma^2 s^2}{2} + \mu s}\mathbf{1} \circ \mathbf{B_0}\right]^t \mathcal{M}[\mathbf{w}_0(x)](s) && (3.55)\\
&= \left[e^{\frac{\sigma^2 s^2}{2} + \mu s}\mathbf{B_0}\right]^t \mathcal{M}[\mathbf{w}_0(x)](s) && (3.56)\\
&= e^{\frac{\sigma^2 t s^2}{2} + \mu t s} \left[\mathbf{B_0}\right]^t \mathcal{M}[\mathbf{w}_0(x)](s) && (3.57)\\
&= \left[\mathbf{B_0}\right]^t \mathcal{M}\left[\frac{1}{\sqrt{2\pi\sigma^2 t}} e^{-\frac{(x-\mu t)^2}{2\sigma^2 t}}\right](s) \mathcal{M}[\mathbf{w}_0(x)](s) && (3.58)\\
&= \left[\mathbf{B_0}\right]^t \mathcal{M}\left[(K_t * \mathbf{w}_0)(x)\right](s) && (3.59)
\end{aligned}$$

where K_t is $N(\mu t, \sigma^2 t)$. From (3.54)

$$\mathcal{M}[\mathbf{w}_t(x)](s) = \left[\mathbf{B_0}\right]^t \mathcal{M}\left[(K_t * \mathbf{w}_0)(x)\right](s). \tag{3.60}$$

Applying the inverse bilateral Laplace transform,

$$\begin{aligned}
\mathbf{w}_t(x) &= \left[\mathbf{B_0}\right]^t (K_t * \mathbf{w}_0)(x) && (3.61)\\
&= \left[\mathbf{B_0}\right]^t \int_{-\infty}^{\infty} \frac{1}{\sqrt{2\pi\sigma^2 t}} e^{-\frac{(x-y-\mu t)^2}{2\sigma^2 t}} \mathbf{w}_0(y)\, dy && (3.62)
\end{aligned}$$

In the moving half-frame $[A + ct, \infty)$ with $c \geq c^*$ we have

$$\mathbf{w}_t(x_0 + ct) = [\mathbf{B_0}]^t \int_{-\infty}^{\infty} \frac{1}{\sqrt{2\pi\sigma^2 t}} e^{-\frac{(x_0+ct-y-\mu t)^2}{2\sigma^2 t}} \mathbf{w}_0(y)\, dy. \tag{3.63}$$

From (3.12), we know that $c^* = \sqrt{2\sigma^2 \ln(\lambda_1)} + \mu$, expanding the exponent, yields

$$\frac{(x_0 + ct - y - \mu t)^2}{2\sigma^2 t} = \frac{(x_0 - y)^2}{2\sigma^2 t} + \frac{2(c-\mu)t(x_0 - y) + (c-\mu)^2 t^2}{2\sigma^2 t} \tag{3.64}$$

$$\geq \frac{(x_0 - y)^2}{2\sigma^2 t} + \frac{c-\mu}{\sigma^2}(x_0 - y) + \ln(\lambda_1) t. \tag{3.65}$$

Thus,

$$\mathbf{w}_t(x_0 + ct) \leq \frac{[\mathbf{B_0}]^t}{\sqrt{2\pi\sigma^2 t}} \int_{-\infty}^{\infty} e^{-\frac{(x_0-y)^2}{2\sigma^2 t}} e^{-\frac{c-\mu}{\sigma^2}(x_0-y)} e^{-\ln(\lambda_1)t} \mathbf{w}_0(y)\, dy \tag{3.66}$$

$$= \left[\frac{\mathbf{B_0}}{\lambda_1}\right]^t \frac{1}{\sqrt{2\pi\sigma^2 t}} \int_{-\infty}^{\infty} e^{-\frac{(x_0-y)^2}{2\sigma^2 t}} e^{-\frac{c-\mu}{\sigma^2}(x_0-y)} \mathbf{w}_0(y)\, dy. \tag{3.67}$$

Since $x_0 \geq A$ and $e^{-\frac{(x_0-y)^2}{2\sigma^2 t}} \leq 1$, we have

$$\mathbf{w}_t(x_0 + ct) \leq \left[\frac{\mathbf{B_0}}{\lambda_1}\right]^t \frac{e^{-\frac{A(c-\mu)}{\sigma^2}}}{\sqrt{2\pi\sigma^2 t}} \int_{-\infty}^{\infty} e^{\frac{c-\mu}{\sigma^2} y} \mathbf{w}_0(y)\, dy. \tag{3.68}$$

From Lemma 3.6.2, see Appendix 3.6.2 for details, we know that

$$\lim_{t\to\infty} \left[\frac{\mathbf{B_0}}{\lambda_1}\right]^t = \mathbf{r}\boldsymbol{\ell}, \tag{3.69}$$

where $\mathbf{r}$ and $\boldsymbol{\ell}$ are the right and left eigenvectors of $\mathbf{B_0}$ corresponding to λ_1 respectively with $\boldsymbol{\ell}$ normalized by $\langle \boldsymbol{\ell}^T, \mathbf{r} \rangle$ to account for the scaling in $\mathbf{r}$. Note that $\mathbf{r}\boldsymbol{\ell}$ is a $m \times m$ matrix since $\mathbf{r}$ is $m \times 1$ and $\boldsymbol{\ell}$ is $1 \times m$. Thus since $\int_{-\infty}^{\infty} e^{\frac{c-\mu}{\sigma^2} y} \mathbf{w}_0(y)\, dy < \infty$ by Assumption $A5'$ and (3.69) we have $\mathbf{w}_t(x_0+ct) \to \mathbf{0}$ uniformly as $t \to \infty$ in $[A, \infty)$. Recall that $\mathbf{w}_t(x)$ was a constructed as a super-solution, $\mathbf{0} \leq \mathbf{v}_t(x) \leq \mathbf{w}_t(x)$. This implies the uniform convergence of $\mathbf{v}_t(x) \to \mathbf{0}$ as $t \to \infty$ in the moving half-frame $[A + ct, \infty)$. The proof of Theorem 3.3.2 is complete. □

Proof of Theorem 3.3.3

Proof. For simplicity, we focus on a single neutral fraction and drop the superscript i. Using the fact that $\mathbf{B}(\mathbf{u}_t(y))\mathbf{v} \leq \mathbf{B_0}\mathbf{v}$ for all $\mathbf{v} \geq 0$ we can use a comparison principle to show that a new sequence $\mathbf{w}_t(x)$ defined by

$$\mathbf{w}_{t+1}(x) = \int_{-\infty}^{\infty} \left[\mathbf{K}(x-y) \circ \mathbf{B_0}\right] \mathbf{w}_t(y)\, dy \tag{3.70}$$

is a super-solution to any neutral fraction $\mathbf{v}_t(x)$ with the same initial condition $\mathbf{w}_0(x) = \mathbf{v}_0(x)$. By iterating we can write the solution to Equation (3.70) as the t-fold convolution

$$\mathbf{w}_t(x) = \left[\mathbf{K}(x-y) \circ \mathbf{B_0}\right]^{*t} \mathbf{w}_0(y). \tag{3.71}$$

Taking the bilateral Laplace transform

$$\mathcal{M}[\mathbf{w}_t(x)](s) = \left[\mathcal{M}[\mathbf{K}(x)](s) \circ \mathbf{B_0}\right]^t \mathcal{M}[\mathbf{w}_0(x)](s). \tag{3.72}$$

Since all of the dispersal kernels are Gaussian, we know that $\mathcal{M}[\mathbf{K}(x)](s) = e^{\frac{\sigma^2 s^2}{2} + \mu s}\mathbf{1}$ where $\mathbf{1}$ is a matrix of all ones. Then, we can see that

$$\begin{aligned}
\left[\mathcal{M}[\mathbf{K}(x)](s) \circ \mathbf{B_0}\right]^t \mathcal{M}[\mathbf{w}_0(x)](s) &= \left[e^{\frac{\sigma^2 s^2}{2} + \mu s}\mathbf{1} \circ \mathbf{B_0}\right]^t \mathcal{M}[\mathbf{w}_0(x)](s) && (3.73)\\
&= \left[e^{\frac{\sigma^2 s^2}{2} + \mu s}\mathbf{B_0}\right]^t \mathcal{M}[\mathbf{w}_0(x)](s) && (3.74)\\
&= e^{\frac{\sigma^2 t s^2}{2} + \mu t s}\mathbf{I}\left[\mathbf{B_0}\right]^t \mathcal{M}[\mathbf{w}_0(x)](s) && (3.75)\\
&= \left[\mathbf{B_0}\right]^t \mathcal{M}\left[\frac{1}{\sqrt{2\pi\sigma^2 t}} e^{-\frac{(x-\mu t)^2}{2\sigma^2 t}}\mathbf{I}\right](s)\mathcal{M}[\mathbf{w}_0(x)](s) && (3.76)\\
&= \left[\mathbf{B_0}\right]^t \mathcal{M}\left[(\mathbf{K}_t * \mathbf{w}_0)(x)\right](s) && (3.77)
\end{aligned}$$

where $\mathbf{K}_t$ is a diagonal matrix with $N(\mu t, \sigma^2 t)$ entries and $\mathbf{I}$ is the identity matrix. Thus, we have

$$\mathcal{M}[\mathbf{w}_t(x)](s) = \left[\mathbf{B_0}\right]^t \mathcal{M}\left[(\mathbf{K}_t * \mathbf{w}_0)(x)\right](s). \tag{3.78}$$

Then applying the inverse transform yields

$$\mathbf{w}_t(x) = [\mathbf{B_0}]^t(\mathbf{K}_t * \mathbf{w}_0)(x) \tag{3.79}$$

$$= [\mathbf{B_0}]^t \int_{-\infty}^{\infty} \frac{1}{\sqrt{2\pi\sigma^2 t}} e^{-\frac{(x-y-\mu t)^2}{2\sigma^2 t}} \mathbf{w}_0(y)\, dy \tag{3.80}$$

In the moving half-frame $[A + ct, \infty)$ with fixed $A \in \mathbb{R}$, consider the element $x_0 + ct$ with $c = c^* = \sqrt{2\sigma^2 \ln(\lambda_1)} + \mu$ where λ_1 is the dominant eigenvalue of $\mathbf{B_0}$ as given by (3.12). By rewriting $\mathbf{w}_t(x)$ in this moving half-frame we have

$$\mathbf{w}_t(x_0 + ct) = [\mathbf{B_0}]^t \int_{-\infty}^{\infty} \frac{1}{\sqrt{2\pi\sigma^2 t}} e^{-\frac{(x_0+ct-y-\mu t)^2}{2\sigma^2 t}} \mathbf{w}_0(y)\, dy. \tag{3.81}$$

Expanding the exponent, yields

$$\frac{(x_0 + ct - y - \mu t)^2}{2\sigma^2 t} = \frac{(y - x_0)^2}{2\sigma^2 t} + \frac{(c-\mu)(x_0 - y)}{\sigma^2} + \frac{(c-\mu)^2}{2\sigma^2} t. \tag{3.82}$$

Thus,

$$\mathbf{w}_t(x_0 + ct) = \frac{[\mathbf{B_0}]^t}{\sqrt{2\pi\sigma^2 t}} \int_{-\infty}^{\infty} e^{-\frac{(y-x_0)^2}{2\sigma^2 t}} e^{-\frac{(c-\mu)(x_0-y)}{\sigma^2}} e^{-\frac{(c-\mu)^2}{2\sigma^2} t} \mathbf{w}_0(y)\, dy \tag{3.83}$$

$$= \left[\frac{\mathbf{B_0}}{\lambda_1}\right]^t \frac{1}{\sqrt{2\pi\sigma^2 t}} \int_{-\infty}^{\infty} e^{-\frac{(y-x_0)^2}{2\sigma^2 t}} e^{-\frac{(c-\mu)(x_0-y)}{\sigma^2}} e^{\left[-\frac{(c-\mu)^2}{2\sigma^2} + \ln(\lambda_1)\right] t} \mathbf{w}_0(y)\, dy. \tag{3.84}$$

Since $c = c^* = \sqrt{2\sigma^2 \ln(\lambda_1)} + \mu$, we have that

$$\mathbf{w}_t(x_0 + ct) = \left[\frac{\mathbf{B_0}}{\lambda_1}\right]^t \frac{1}{\sqrt{2\pi\sigma^2 t}} \int_{-\infty}^{\infty} e^{-\frac{(y-x_0)^2}{2\sigma^2 t}} e^{-\frac{(c-\mu)(x_0-y)}{\sigma^2}} \mathbf{w}_0(y)\, dy. \tag{3.85}$$

From Assumption $A5''$, $\mathbf{w}_0(y) = (\mathbf{p}_0 \circ \mathbf{r})\, e^{-\frac{c-\mu}{\sigma^2} y}$. Thus,

$$\mathbf{w}_t(x_0 + ct) = \left[\frac{\mathbf{B_0}}{\lambda_1}\right]^t (\mathbf{p}_0 \circ \mathbf{r})\, e^{-\frac{(c-\mu)}{\sigma^2} x_0} \frac{1}{\sqrt{2\pi\sigma^2 t}} \int_{-\infty}^{\infty} e^{-\frac{(y-x_0)^2}{2\sigma^2 t}}\, dy \tag{3.86}$$

$$= \left[\frac{\mathbf{B_0}}{\lambda_1}\right]^t (\mathbf{p}_0 \circ \mathbf{r})\, e^{-\frac{(c-\mu)}{\sigma^2} x_0}. \tag{3.87}$$

From Lemma 3.6.2, see Appendix 3.6.2 for details, we know that

$$\lim_{t\to\infty} \left[\frac{\mathbf{B_0}}{\lambda_1}\right]^t = \mathbf{r}\boldsymbol{\ell} \tag{3.88}$$

where $\mathbf{r}$ and $\boldsymbol{\ell}$ are the right and left eigenvectors of $\mathbf{B_0}$ corresponding to λ_1 respectively where $\boldsymbol{\ell}$ is normalized by $\langle \boldsymbol{\ell}^T, \mathbf{r} \rangle$. Thus,

$$\lim_{t\to\infty} \mathbf{w}_t(x_0 + ct) = \lim_{t\to\infty} \left[\frac{\mathbf{B_0}}{\lambda_1}\right]^t (\mathbf{p}_0 \circ \mathbf{r})\, e^{-\frac{(c-\mu)}{\sigma^2}x_0} \tag{3.89}$$

$$= \mathbf{r}\boldsymbol{\ell}\,(\mathbf{p}_0 \circ \mathbf{r})\, e^{-\frac{(c-\mu)}{\sigma^2}x_0} \tag{3.90}$$

$$= e^{-\frac{(c-\mu)}{\sigma^2}x_0}\mathbf{r}p. \tag{3.91}$$

From the above calculations, we find that the super-solution approaches a proportion, p, of the traveling wave for the linear equation where $p = \boldsymbol{\ell}\,(\mathbf{p}_0 \circ \mathbf{r})$. We now move onto our sub-solution. For any $0 < \varepsilon \ll 1$, $\boldsymbol{\delta}$ is chosen such that $(1-\varepsilon)\mathbf{B_0}\boldsymbol{\delta} = \mathbf{B}(\boldsymbol{\delta})\boldsymbol{\delta}$ and we define

$$\left(\mathbf{B}_{sub}(\mathbf{u};\varepsilon)\right)_{jl} := \begin{cases} (1-\varepsilon)\left(\mathbf{B}(\mathbf{u})\right)_{jl} & \text{if } \left(\mathbf{B}(\mathbf{u})\right)_{jl} \text{ is constant} \\ \beta_{jl}(\mathbf{u};\varepsilon) & \text{if } \left(\mathbf{B}(\mathbf{u})\right)_{jl} \text{ is non-constant,} \end{cases} \tag{3.92}$$

where

$$\beta_{jl}(\mathbf{u};\varepsilon) := \begin{cases} (1-\varepsilon)\left(\mathbf{B_0}\right)_{jl} & \text{for } 0 \le \mathbf{u} < \boldsymbol{\delta} \\ \left(\mathbf{B}(\mathbf{u})\right)_{jl} & \text{for } \mathbf{u} \ge \boldsymbol{\delta}. \end{cases} \tag{3.93}$$

Then,

$$\mathbf{z}_{t+1}(x) = \int_{-\infty}^{\infty} \left[\mathbf{K}(x-y) \circ \mathbf{B}_{sub}(\mathbf{u}_t(y);\varepsilon)\right] \mathbf{z}_t(y)\, dy \tag{3.94}$$

with $\mathbf{z}_0(x) = \mathbf{v}_0(x)$ is a sub-solution of $\mathbf{v}_t(x)$ by the comparison principle since $\mathbf{B}_{sub}(\mathbf{u};\varepsilon)\mathbf{v} \le \mathbf{B}(\mathbf{u})\mathbf{v}$ for all $\mathbf{v} \ge 0$. Define $c(\varepsilon) := \sqrt{2\sigma^2 \ln((1-\varepsilon)\lambda_1)} + \mu$ where $(1-\varepsilon)\lambda_1$ is the dominant eigenvalue of the constant matrix $(1-\varepsilon)\mathbf{B_0}$. In the moving half-frame $[A + c(\varepsilon)t, \infty)$ with fixed $A \in \mathbb{R}$, choose x_0 large such that $\mathbf{u}_t(y)$ in (3.94) satisfies $\mathbf{u}_t(y) < \boldsymbol{\delta}$ for all t where $y \in [x_0 + c(\varepsilon)t, \infty)$. Then by the definition of $\mathbf{B}_{sub}(\mathbf{u};\varepsilon)$

$$\mathbf{z}_{t+1}(x_0 + c(\varepsilon)t) = \int_{-\infty}^{\infty} \left[\mathbf{K}(x_0 + c(\varepsilon)t - y) \circ (1-\varepsilon)\mathbf{B_0}\right] \mathbf{z}_t(y)\, dy. \tag{3.95}$$

By iterating we can write the solution to (4.61) as the t-fold convolution

$$\mathbf{z}_t(x_0 + c(\varepsilon)t) = \left[\mathbf{K}(x_0 + c(\varepsilon)t - y) \circ (1-\varepsilon)\mathbf{B_0}\right]^{*t} \mathbf{z}_0(y). \tag{3.96}$$

Since we assumed that all of the dispersal kernels are Gaussian, by repeating calculations done previously we find that

$$\mathbf{z}_t(x_0 + c(\varepsilon)t) = [(1-\varepsilon)\mathbf{B_0}]^t \int_{-\infty}^{\infty} \frac{1}{\sqrt{2\pi\sigma^2 t}} e^{-\frac{(x_0+c(\varepsilon)t-y-\mu t)^2}{2\sigma^2 t}} \mathbf{z}_0(y)\, dy \tag{3.97}$$

$$= \frac{[(1-\varepsilon)\mathbf{B_0}]^t}{\sqrt{2\pi\sigma^2 t}} \int_{-\infty}^{\infty} e^{-\frac{(x_0-y)^2}{2\sigma^2 t}} e^{-\frac{(c(\varepsilon)-\mu)(x_0-y)}{\sigma^2}} e^{-\frac{(c(\varepsilon)-\mu)^2}{2\sigma^2}t} \mathbf{z}_0(y)\, dy \tag{3.98}$$

$$= \left[\frac{(1-\varepsilon)\mathbf{B_0}}{(1-\varepsilon)\lambda_1}\right]^t \frac{1}{\sqrt{2\pi\sigma^2 t}} \int_{-\infty}^{\infty} e^{-\frac{(x_0-y)^2}{2\sigma^2 t}} e^{-\frac{(c(\varepsilon)-\mu)(x_0-y)}{\sigma^2}} e^{\left[-\frac{(c(\varepsilon)-\mu)^2}{2\sigma^2}+\ln((1-\varepsilon)\lambda_1)\right]t} \mathbf{z}_0(y)\, dy \tag{3.99}$$

$$= \left[\frac{\mathbf{B_0}}{\lambda_1}\right]^t \frac{1}{\sqrt{2\pi\sigma^2 t}} \int_{-\infty}^{\infty} e^{-\frac{(x_0-y)^2}{2\sigma^2 t}} e^{-\frac{(c(\varepsilon)-\mu)(x_0-y)}{\sigma^2}} e^{\left[-\frac{(c(\varepsilon)-\mu)^2}{2\sigma^2}+\ln((1-\varepsilon)\lambda_1)\right]t} \mathbf{z}_0(y)\, dy. \tag{3.100}$$

Since $c(\varepsilon) = \sqrt{2\sigma^2 \ln((1-\varepsilon)\lambda_1)} + \mu$,

$$\mathbf{z}_t(x_0 + c(\varepsilon)t) = \left[\frac{\mathbf{B_0}}{\lambda_1}\right]^t \frac{1}{\sqrt{2\pi\sigma^2 t}} \int_{-\infty}^{\infty} e^{-\frac{(x_0-y)^2}{2\sigma^2 t}} e^{-\frac{(c(\varepsilon)-\mu)(x_0-y)}{\sigma^2}} \mathbf{z}_0(y)\, dy. \tag{3.101}$$

Note that the integrand in (3.101) is nonnegative and integrable. Using Fatou's lemma we fix t and let $\varepsilon \to 0$, giving

$$\mathbf{z}_t(x_0 + ct) = \liminf_{\varepsilon\to 0} \mathbf{z}_t(x_0 + c(\varepsilon)t) \tag{3.102}$$

$$= \liminf_{\varepsilon\to 0} \left[\frac{\mathbf{B_0}}{\lambda_1}\right]^t \frac{1}{\sqrt{2\pi\sigma^2 t}} \int_{-\infty}^{\infty} e^{-\frac{(x_0-y)^2}{2\sigma^2 t}} e^{-\frac{(c(\varepsilon)-\mu)(x_0-y)}{\sigma^2}} \mathbf{z}_0(y)\, dy \tag{3.103}$$

$$\geq \left[\frac{\mathbf{B_0}}{\lambda_1}\right]^t \frac{1}{\sqrt{2\pi\sigma^2 t}} \int_{-\infty}^{\infty} \liminf_{\varepsilon\to 0} e^{-\frac{(x_0-y)^2}{2\sigma^2 t}} e^{-\frac{(c(\varepsilon)-\mu)(x_0-y)}{\sigma^2}} \mathbf{z}_0(y)\, dy \tag{3.104}$$

$$= \left[\frac{\mathbf{B_0}}{\lambda_1}\right]^t \frac{1}{\sqrt{2\pi\sigma^2 t}} \int_{-\infty}^{\infty} e^{-\frac{(x_0-y)^2}{2\sigma^2 t}} e^{-\frac{(c-\mu)(x_0-y)}{\sigma^2}} \mathbf{z}_0(y)\, dy. \tag{3.105}$$

From Assumption $A5''$, $\mathbf{z}_0(y) = (\mathbf{p}_0 \circ \mathbf{r})\, e^{-\frac{(c-\mu)}{\sigma^2}y}$. Thus, by the same calculations used in (3.86)-(3.87) for the super-solution

$$\mathbf{z}_t(x_0 + ct) \geq \left[\frac{\mathbf{B_0}}{\lambda_1}\right]^t (\mathbf{p}_0 \circ \mathbf{r})\, e^{-\frac{(c-\mu)}{\sigma^2}x_0}. \tag{3.106}$$

From Lemma 3.6.2, see Appendix 3.6.2 for details, we see that

$$\lim_{t\to\infty} \left[\frac{\mathbf{B_0}}{\lambda_1}\right]^t = \mathbf{r}\boldsymbol{\ell}, \tag{3.107}$$

where $\mathbf{r}$ and $\boldsymbol{\ell}$ are the right and left eigenvectors corresponding to λ_1 respectively where the $\boldsymbol{\ell}$ is normalized by $\langle \boldsymbol{\ell}^T, \mathbf{r} \rangle$. Thus,

$$\lim_{t\to\infty} \mathbf{z}_t(x_0 + ct) \geq \lim_{t\to\infty} \left[\frac{\mathbf{B_0}}{\lambda_1}\right]^t (\mathbf{p}_0 \circ \mathbf{r})\, e^{-\frac{(c-\mu)}{\sigma^2}x_0} \tag{3.108}$$

$$= \mathbf{r}\boldsymbol{\ell}\,(\mathbf{p}_0 \circ \mathbf{r})\, e^{-\frac{(c-\mu)}{\sigma^2}x_0} \tag{3.109}$$

$$= e^{-\frac{(c-\mu)}{\sigma^2}x_0}\mathbf{r}p. \tag{3.110}$$

Asymptotically, our sub-solution is bounded below by a proportion of the traveling wave for the linear equation where $p = \boldsymbol{\ell}\,(\mathbf{p}_0 \circ \mathbf{r})$. Since our super-solution satisfies

$$\lim_{t\to\infty} \mathbf{w}_t(x_0 + ct) \leq e^{-\frac{(c-\mu)}{\sigma^2}x_0}\mathbf{r}p, \tag{3.111}$$

and our sub-solution satisfies

$$\lim_{t\to\infty} \mathbf{z}_t(x_0 + ct) \geq e^{-\frac{(c-\mu)}{\sigma^2}x_0}\mathbf{r}p \tag{3.112}$$

it follows that

$$\lim_{t\to\infty} \mathbf{v}_t(x_0 + ct) = e^{-\frac{(c-\mu)}{\sigma^2}x_0}\mathbf{r}p. \tag{3.113}$$

The proof of Theorem 3.3.3 is complete. □

3.4 Numerical simulations

In this section, we illustrate the theory of Section 3.3 with a numerical example. All simulations were done using the fast Fourier transform technique (Cooley and Tukey, 1965). This method is better than classical quadrature because it speeds up the numerical process from $O(n^2)$ to $O(n\log(n))$.

We begin with a two-stage population model of juveniles, J, and adults, A. The equations in this model are given below,

$$\begin{aligned} J^i_{t+1}(x) &= \int_{-\infty}^{\infty} k(x-y)\zeta(1-m)J^i_t(y)\,dy + \int_{-\infty}^{\infty} k(x-y) f_0 e^{-\sum_{i=1}^{n}\left(J^i_t(y)+A^i_t(y)\right)} A^i_t(y)\,dy, \\ A^i_{t+1}(x) &= \int_{-\infty}^{\infty} k(x-y)\zeta m J^i_t(y)\,dy + \int_{-\infty}^{\infty} k(x-y)\zeta A^i_t(y)\,dy, \end{aligned} \tag{3.114}$$

where

$$k(x-y) = \frac{1}{\sqrt{2\pi\sigma^2}} e^{-\frac{(x-y)^2}{2\sigma^2}}. \tag{3.115}$$

The demography in (3.114) follows a classical model for biological invasions (Neubert and Caswell, 2000), but we assume Gaussian dispersal to align with the assumptions in our theorems. In (3.114), ζ is the probability of survival to the next generation, m is the probability of maturation from a juvenile to an adult, f_0 is the number of juveniles produced by an adult in the absence of density-dependent effects. All individuals are assumed to disperse according to a Gaussian dispersal kernel. The growth function for adults producing juveniles is assumed to be a Ricker type growth function where the nonlinearity depends on the density of both juveniles and adults. In the juvenile equation of (3.114), juveniles can remain juveniles if they survive and do not mature and adults from location y can produce juveniles that disperse to location x. In the adult equation of (3.114), juveniles become adults if they survive and mature, and adults remain adults if they survive from the previous year.

Let

$$\mathbf{v}_t^i(x) = \begin{bmatrix} J_t^i(x) \\ A_t^i(x) \end{bmatrix}, \tag{3.116}$$

$$\mathbf{K}(x-y) = \begin{bmatrix} \frac{1}{\sqrt{2\pi\sigma^2}} e^{-\frac{(x-y)^2}{2\sigma^2}} & \frac{1}{\sqrt{2\pi\sigma^2}} e^{-\frac{(x-y)^2}{2\sigma^2}} \\ \frac{1}{\sqrt{2\pi\sigma^2}} e^{-\frac{(x-y)^2}{2\sigma^2}} & \frac{1}{\sqrt{2\pi\sigma^2}} e^{-\frac{(x-y)^2}{2\sigma^2}} \end{bmatrix}, \text{ and} \tag{3.117}$$

$$\mathbf{B}(\mathbf{u}_t(y)) = \begin{bmatrix} \zeta(1-m) & f_0 e^{-\sum_{i=1}^n \left(J_t^i(y) + A_t^i(y)\right)} \\ \zeta m & \zeta \end{bmatrix}. \tag{3.118}$$

Then we can write (3.114) in the matrix and vector notation provided in (3.4).

First, let us verify that the assumptions of Theorems 3.3.2 and 3.3.3 are satisfied. Recall that Assumptions $A1$-$A3$ and $A4'$ are the same for these two theorems. For Assumption $A1$, it is clear that our population projection matrix, $\mathbf{B}(\mathbf{u}_t(y))$, is nonnegative from (3.118) since $\zeta, m, f_0 > 0$. We can

calculate $\mathbf{B_0}$ to be

$$\mathbf{B_0} = \begin{bmatrix} \zeta(1-m) & f_0 \\ \zeta m & \zeta \end{bmatrix}. \tag{3.119}$$

Thus, $\mathbf{B_0}$ is primitive. For Assumption $A2$, the dominant eigenvalue of $\mathbf{B_0}$ is greater than one if

$$f_0 > \frac{(1-\zeta)(1-\zeta(1-m))}{\zeta m}. \tag{3.120}$$

For details of this calculation see Proposition 3.1 of Marculis and Lui (2016). Since $e^{-\sum_{i=1}^{n}\left(J_t^i(y)+A_t^i(y)\right)} \leq 1$ we have $\mathbf{B}(\mathbf{u}_t(y))\mathbf{v} \leq \mathbf{B_0}\mathbf{v}$ for all $\mathbf{v} \geq 0$ and Assumption $A3$ is satisfied. Even though our operator is not order preserving because of the overcompensation in the Ricker function, Proposition 3.1 in Li et al. (2009) suggests that the calculation for the spreading speed should still hold true. Assumption $A4'$ is clear from the definition of (3.117). Finally, if we assume our initial condition to decay faster than $e^{-\frac{c-\mu}{\sigma^2}x}$, then the neutral fractions will satisfy Assumption $A5'$ of Theorem 3.3.2 and we can see that (3.114) has a unique positive steady state given by

$$J^* = \frac{1-\zeta}{\zeta m}A^* \text{ and } A^* = -\ln\left(\frac{(1-\zeta)(1-\zeta(1-m))}{f_0\zeta m}\right), \tag{3.121}$$

see again Proposition 3.1 of Marculis and Lui (2016). In our numerical simulations the only neutral fraction that does not decay faster than $e^{-\frac{c-\mu}{\sigma^2}x}$ is the one at the leading edge because it was chosen to have an initial form of the traveling wave solution with $c = c^*$. It should be mentioned here that since we are solving this problem numerically it is solved on a finite domain and this is only an approximation to the solution. Therefore, in the moving half-frame, the only neutral fractions that we see are the ones initially at the leading edge. The neutral fractions at the leading edge do not satisfy the exact Assumption $A5''$ of Theorem 3.3.3, but asymptotically they decay like $e^{-\frac{c-\mu}{\sigma^2}x}$. However, the asymptotic proportion calculated from Theorem 3.3.3 agrees with the numerical simulation suggesting that this result should be able to extend to a wider array of initial conditions.

We provide some numerical simulations to see the neutral genetic patterns produced by (3.114). We begin by running a simulation where the juvenile and adult populations have the same initial distribution as seen in Figure 3.1(a). This simulation shows that the spread of both juveniles and adults is dominated by the neutral fraction at the leading edge as seen in Figure 3.1(b). Switching the ordering of the neutral fractions behind the leading edge does not affect the asymptotic behavior in the moving frame. This observation is consistent with the founder effect. The simulations seen in Figure 3.1 agree with the results of Theorems 3.3.2 and 3.3.3.

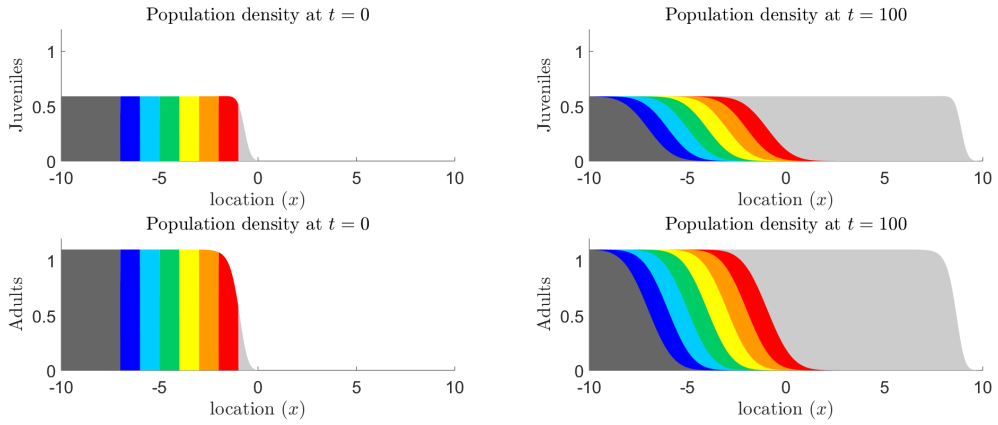

(a) (b)

Figure 3.1: Numerical realization of (3.114) for the parameter values $\sigma^2 = 0.01$, $\mu = 0$, $\zeta = 0.7$, $m = 0.8$, and $f_0 = 2.5$ for $n = 8$ neutral fractions. In (a) the plots are the initial conditions for the juvenile and adult populations. Notice that the distribution of neutral fractions for juvenile and adult populations have the same order. In (b) we plot the densities of the juvenile and adult neutral fractions at $t = 100$.

For our next simulation, we consider the case where the distribution of the neutral fractions of juveniles and adults do not appear in the same order. This is seen in Figure 3.2(a). Here we keep the same initial distribution of juvenile individuals as in Figure 3.1(a), but the initial distribution of adult neutral fractions is assorted differently. In Figure 3.2(a) we can see that initially the

neutral fractions at the leading edge of the juvenile and adult populations are light gray and red respectively. Figure 3.2(b) shows the distribution of neutral fractions at $t = 100$. At the leading edge the spread is dominated by the light gray and red neutral fractions. This simulation agrees with our theoretical results because Theorem 3.3.2 and 3.3.3 suggest that the spread should be dominated by the neutral fractions that are initially at the leading edge of the population. Again we see that the neutral fractions behind the leading edge do not contribute to the asymptotic spread.

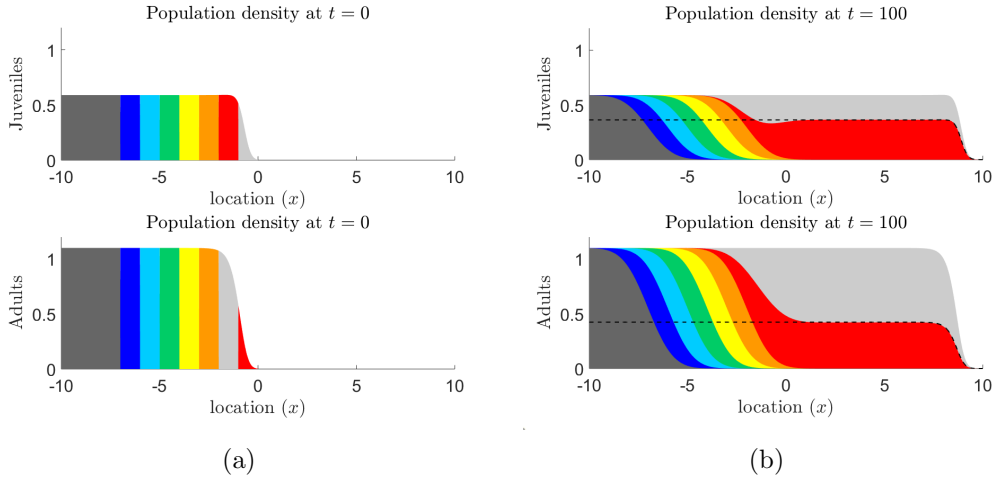

(a) (b)

Figure 3.2: Numerical realization of (3.114) for the parameter values $\sigma^2 = 0.01$, $\mu = 0$, $\zeta = 0.7$, $m = 0.8$, and $f_0 = 2.5$ for $n = 8$ neutral fractions. For these parameters $\mathbf{u}^* = (J^*, A^*) = (0.5900, 1.1013)$. In (a) the plots are the initial conditions for the juvenile and adult population. Notice that the distribution of the first two neutral fractions is different for juveniles and adults. The plots in (b) are the densities of the juvenile and adult neutral fractions at $t = 100$. The neutral genetic pattern produced here is due to the difference in the initial distribution of neutral fractions for juveniles and adults. The dashed lines in (b) are calculated from Theorem 3.3.3, they represent the proportions of red juveniles and adults. Behind the leading edge the proportions are $p^2 J^* = 0.3629$ for juveniles and $p^1 A^* = 0.4238$ for adults.

3.5 Discussion

The main objective of this work is to understand the effect that stage-structure has on the neutral genetic composition of expanding populations as outlined in Section 3.1. We derived the model for the inside dynamics of a stage-structured integrodifference equation in Section 3.2.1. Section 3.2.2 describes five of our main assumptions related to demography and dispersal. Four of these assumptions are related to the population projection matrix and the fifth is related to the form of the dispersal kernel.

The three main results of the paper are provided in Section 3.3, with their respective proofs in Section 3.3.3. Theorem 3.3.1 is our first main result, which provides sufficient conditions for a neutral fraction to converge uniformly to zero in the moving half-frame. The five assumptions that must be satisfied are as follows: the population projection matrix must be nonnegative, the population projection matrix evaluated at zero must be primitive and its dominant eigenvalue must be greater than one, the population projection matrix must be maximal at the trivial steady state, all dispersal kernels must be thin-tailed, and the initial condition must satisfy the decay assumption given in Lemma 3.6.1. It should be noted that the Dirac delta function is a thin-tailed dispersal kernel and thus we can consider cases where there is no dispersal between some transitions making this theorem very general in terms of the dispersal assumptions.

The second main result is Theorem 3.3.2. Similar to Theorem 3.3.1, this theorem also shows conditions under which each neutral fraction converges uniformly to zero in the moving half-frame. The difference with this theorem is that we make a stronger assumption on the dispersal kernels in exchange for a weaker condition on the initial condition. In particular, we assume that all dispersal kernels are Gaussian with identical means and variances. Due this

this assumption, we are then able to relax the decay condition on the initial condition of the population to be slightly weaker than is required for Theorem 3.3.1. The proof for Theorem 3.3.2 is more elegant than the proof for Theorem 3.3.1. However, this comes at some cost in the biological realism of the model since it is not common for all stages and transitions to disperse exactly via a Gaussian distribution.

The final result is given in Theorem 3.3.3. The first four assumptions of this theorem are the same as Theorem 3.3.2. The fifth assumption assumes that the initial condition decays according to the traveling wave ansatz for the linear equation. Under these assumptions, we are able to asymptotically calculate the proportion that each neutral fraction approaches in the moving frame. This proportion is dependent on the right and left eigenvectors of the population projection matrix evaluated at zero and the initial proportion of each neutral fraction at the leading edge. The proof relies on the construction of super- and sub-solutions to the system. The super-solution, as expected, is chosen to be the linearization of our operator while the sub-solution is defined in a piecewise manner to lie below the nonlinearities. Since all dispersal kernels were assumed to be identical Gaussian distributions, the proportion calculated by Theorem 3.3.3 does not apply when some stages and transitions do not disperse in the same way.

After completion of the mathematical results, we performed some numerical simulations in Section 3.4 to compare our analytical results to a reasonable biological model. We chose to look at a classical two-stage juvenile adult model where dispersal occurs between all stages and transitions. The first simulation, in Figure 3.1, shows that the spread is dominated by the neutral fraction at the leading edge which is an extreme version of the founder effect. However, since we are working with a system of equations, it is possible for the initial distribution of neutral fractions in the juvenile and adult stages to be

different. This is seen in Figure 3.2(a). As predicted from Theorem 3.3.2, in Figure 3.2(b), we see that all neutral fractions, except the ones at the leading edge of the juvenile and adult populations, converge uniformly to zero in the moving half-frame. The asymptotic proportions for the two neutral fractions that were initially at the leading edge of the juvenile and adult populations are given by the formula in Theorem 3.3.3 and plotted as the dashed line in Figure 3.2(b).

As expected, some of the same results obtained here are similar to those for the scalar population model. That is, Theorem 3.3.1 and Theorem 3.3.2 are equivalent to their scalar counterparts, Theorem 3 and Theorem 1 respectively, given in Marculis et al. (2017). However, Theorem 3.3.3 provides a new result for a special case of interacting neutral fractions at the leading edge. This is not possible in the scalar population model. From this theorem, we see the ability for multiple neutral fractions to contribute to the spread of the population. Contributions from multiple neutral fractions to the population spread are only possible in the scalar model when there is a strong Allee effect (Marculis et al., 2017). Although we would expect similar behavior from our stage-structured model, we are not able to analyze the inside dynamics of a stage-structured model with a strong Allee effect. This is due to the requirement that our results for the strong Allee effect in scalar systems rely on the operator being compact. For a system of equations the necessary theory is more complicated and we were unable to perform this analysis. In the special case where all dispersal kernels are Gaussian with the same mean and variance and all entries of the population projection matrix have the same strong Allee effect type per-capita growth function, then Theorem 2 given in Marculis et al. (2017) can be applied. However, such stringent assumptions would defeat the purpose for considering a stage-structured population model because all stages and transitions would grow and disperse in the same way, essentially reducing

the stage-structured model to a scalar equation.

The interesting additional feature that the stage-structured population model offers over scalar models is the ability to have a different initial distribution of neutral fractions for each stage. This difference can lead to multiple neutral fractions driving the spread of the population. Here, we see these dynamics solely for the reason that the initial spatial distribution of neutral fractions is different for each stage.

Several assumptions about the integrodifference dynamics and dispersal kernels limit the applicability of the results in this paper. One limitation to the applicability of our work is seen in Assumption $A3$. Here we require that our population projection matrix is maximal at zero. This means that we are not considering any kind of demography with Allee effects. In order to prove the asymptotic proportion result seen in Theorem 3.3.3 we make some restrictive assumptions on the dispersal kernels and initial conditions in the model. Assumption $A4'$ in Theorem 3.3.3 states that all dispersal kernels are Gaussian with the same mean and variance. This assumption may be unrealistic for many populations because the reason to use a stage-structured population model over a scalar population model is to include differences in demography and dispersal between stages. Assumption $A5''$ in Theorem 3.3.3 makes the assumption that the initial conditions are in the form of the traveling wave ansatz for the linear equation. It would be beneficial to generalize Theorem 3.3.3 for initial conditions that are in the form of the traveling wave solution. The numerical simulations show that we should be able to relax our sixth assumption in our in theorems to a more general class of initial conditions. These simulations are not only useful for verifying our mathematical results, but they also provide some insight into opportunities for further mathematical analysis.

3.6 Appendix

3.6.1 Asymptotic speed of propagation for a system

The following Proposition is taken from (Lui, 1989a). Let $\boldsymbol{\beta} \in \mathbb{R}^n$ be a positive vector. We define

$$\mathcal{C} = \{\mathbf{u} = (u^1, ..., u^n) \mid \mathbf{0} \leq \mathbf{u}(x) \leq \boldsymbol{\beta},\ u^i(x) : \mathbb{R} \to [0, \boldsymbol{\beta}^i]$$
$$\text{is piecewise continuous for } i = 1, ..., n\}.$$

The operator $\mathbf{Q}$ used in our analytical results is given by

$$\mathbf{Q}[\mathbf{u}] = \int_{-\infty}^{\infty} [\mathbf{K}(x-y) \circ \mathbf{B}(\mathbf{u}(y))]\, \mathbf{u}(y)\, dy. \tag{3.122}$$

Proposition 3.6.1. *Let $\mathbf{Q} = (Q^1, ..., Q^n) : \mathcal{C} \to \mathcal{C}$ satisfy the following conditions:*

(1) $\mathbf{Q}[\mathbf{0}] = \mathbf{0}\,,\ \mathbf{Q}[\boldsymbol{\beta}] = \boldsymbol{\beta}$, $\mathbf{0}$ *is unstable and* $\boldsymbol{\beta}$ *is stable with respect to* $\mathbf{Q}$.

(2) $\mathbf{Q}$ *is translation invariant and has no other fixed-point besides* $\mathbf{0}$ *and* $\boldsymbol{\beta}$ *in* $\mathcal{C}$.

(3) $\mathbf{Q}$ *is monotone or order-preserving in* $\mathcal{C}$*; that is, if* $\mathbf{u} \leq \mathbf{v}$ *in* $\mathcal{C}$*, then* $\mathbf{Q}[\mathbf{u}] \leq \mathbf{Q}[\mathbf{v}]$.

(4) $\mathbf{Q}$ *is continuous in the topology of uniform convergence on bounded subsets of* $\mathbb{R}$.

(5) Let

$$(\mathbf{M}[\mathbf{u}](x))_i = \sum_{j=1}^{n} \int_{-\infty}^{\infty} \mathbf{u}_j(x-y) m^{ij}(y)\, dy\,. \tag{3.123}$$

be the linearization of $\mathbf{Q}$ *at* $\mathbf{0}$*, where* $m^{ij}(y) \geq 0$ *is an integrable function. We assume that*

$$\mathbf{Q}[\mathbf{u}] \leq \mathbf{M}[\mathbf{u}] \quad \textit{for all } \mathbf{u} \in \mathcal{C}\,. \tag{3.124}$$

(6) The matrix $\mathbf{B}(s) = (b^{ij}(s))$*, where*

$$b^{ij}(s) = \int_{-\infty}^{\infty} e^{sy}\, m^{ij}(y)\, dy \tag{3.125}$$

is irreducible for $0 < s < s^+$*.*

Let $\rho(s)$ *be the dominant eigenvalue of* $\mathbf{B}(s)$ *and let*

$$c^* = \min_{0<s<s^+} \frac{1}{s} \ln \rho(s)\,. \tag{3.126}$$

Then c^* *is the asymptotic speed of propagation of the operator* $\mathbf{Q}$ *in the positive direction in the following sense. Let* $\mathbf{u}_0 \in \mathcal{C}$*,* $\mathbf{u}_0$ *is non-trivial and vanishes outside of a bounded interval in* $\mathbb{R}$*. Let* $\mathbf{u}_t$ *be defined by* $\mathbf{u}_{t+1} = \mathbf{Q}[\mathbf{u}_t]$ *for* $t = 0, 1, 2....$ *Then for any small* $\varepsilon > 0$*,*

$$\lim_{t\to\infty} \min_{x \le t(c^*-\varepsilon)} |\mathbf{u}_t(x) - \boldsymbol{\beta}| = 0 \tag{3.127}$$

and

$$\lim_{t\to\infty} \max_{x \ge t(c^*+\varepsilon)} |\mathbf{u}_t(x)| = 0\,. \tag{3.128}$$

3.6.2 Mathematical details

The purpose of this section is to provide the mathematical background needed to prove the theorems in Section 3.3. One tool that is used throughout all of our theorems is the reflected Bilateral Laplace transform.

Definition 3.6.1. *Let* $f : \mathbb{R} \to \mathbb{R}$ *where* f *is piecewise continuous on every finite interval in* $\mathbb{R}$ *and there exists a* $M \in \mathbb{R}^+$ *such that* $|f(x)| \le Me^{-sx}$ *for all* $x \in \mathbb{R}$ *and* $0 < s < s^+$*. Then, the reflected bilateral Laplace transform and its inverse are defined to be*

$$F(s) = \mathcal{M}[f(x)] := \int_{-\infty}^{\infty} f(x) e^{sx}\, dx, \text{ and} \tag{3.129}$$

$$f(x) = \mathcal{M}^{-1}[F(s)] := \frac{1}{2\pi i} \lim_{R\to\infty} \int_{\gamma-iR}^{\gamma+iR} F(s) e^{-sx}\, ds \tag{3.130}$$

for $0 < s < s^+$*, where the integration in Equation* (3.130) *is over the vertical line,* $Re(s) = \gamma$ *in the complex plane and* γ *is greater than the real parts of all singularities of* $F(s)$*.*

By using the convolution theorem, the reflected bilateral Laplace transform can be used to write the solution to our model in terms of the initial condition. This theorem states that the reflected bilateral Laplace transform of a convolution is the product of the reflected bilateral Laplace transforms. That is,

$$\mathcal{M}[f(x) * h(x)](s) = F(s)H(s). \tag{3.131}$$

Note that the reflected bilateral Laplace transform of a probability density function is also referred to as its moment generating function.

Next, we provide results regarding vector and matrix analysis that are relevant to our subsequent analysis. First, it should be noted that when we write $\mathbf{x} \geq \mathbf{y}$, the inequality is element-wise. That is, $x_i \geq y_i$ for each i. In a similar manner, $\mathbf{x} > \mathbf{y}$ means that $x_i > y_i$ for each i. For the matrix analysis, the following definitions and proposition are needed:

Definition 3.6.2. *Let $\lambda_1, \ldots, \lambda_m$ be the eigenvalues of a matrix $\mathbf{A}$. Then its spectral radius $\rho(\mathbf{A})$ is defined as:*

$$\rho(\mathbf{A}) := \max_{i=1,\ldots,m} |\lambda_i| . \tag{3.132}$$

In other words, the spectral radius of a matrix $\mathbf{A}$ is the modulus of the largest eigenvalue.

Definition 3.6.3. *A matrix $\mathbf{A}$ is called nonnegative, $\mathbf{A} \geq \mathbf{0}$, if $a_{ij} \geq 0$ for all i, j .*

Definition 3.6.3 states that a matrix is nonnegative if all elements of the matrix are greater than or equal to zero. Next, we consider primitive matrices.

Definition 3.6.4. *A nonnegative matrix $\mathbf{A}$ is primitive if there is a positive integer k such that $\mathbf{A}^k > \mathbf{0}$.*

Another important concept is that of the dominant eigenvalue of a matrix.

Definition 3.6.5. *Let $\lambda_1, \ldots, \lambda_m$ be the eigenvalues of an $m \times m$ matrix $\mathbf{A}$. If $|\lambda_1| > |\lambda_j|$ for $j = 2, \ldots m$, then λ_1 is called the dominant eigenvalue of $\mathbf{A}$.*

Next, we discuss the Perron-Frobenius theorem for nonnegative primitive matrices (Bapat and Raghavan, 1997).

Proposition 3.6.2 (Perron-Frobenius theorem)**.** *Let $\mathbf{A} \geq \mathbf{0}$ be an $m \times m$ primitive matrix. Then $\mathbf{A}\mathbf{y} = \lambda_1 \mathbf{y}$ for some $\lambda_1 > 0$, $\mathbf{y} > \mathbf{0}$ where*

(i) The eigenvalue λ_1 is algebraically simple.

(ii) The eigenvalue λ_1 is dominant. That is, for any other eigenvalue μ of $\mathbf{A}$, $|\mu| < \lambda_1$.

(iii) The only nonnegative eigenvectors of $\mathbf{A}$ are positive scalar multiples of $\mathbf{y}$.

By the Perron-Frobenius theorem we know that the spectral radius of a nonnegative primitive matrix is equal to the dominant eigenvalue of that matrix; $\rho(\mathbf{A}) = \lambda_1$. In our analysis we also make use of the Jordan canonical form for square matrices. We use this decomposition because while a nonnegative primitive matrix is not necessarily diagonalizable, every square matrix can none-the-less be written in its Jordan canonical form.

Definition 3.6.6. *For any square matrix $\mathbf{A}$, there exists a matrix $\mathbf{J}$ such that*

$$\mathbf{A} = \mathbf{P}\mathbf{J}\mathbf{P}^{-1}, \tag{3.133}$$

where $\mathbf{J}$ is the Jordan canonical form of $\mathbf{A}$. The Jordan canonical form is a block diagonal matrix

$$\mathbf{J} = \begin{bmatrix} \mathbf{J}_1 & \ldots & \mathbf{0} \\ \vdots & \ddots & \vdots \\ \mathbf{0} & \ldots & \mathbf{J}_b \end{bmatrix}, \tag{3.134}$$

where each $\mathbf{J_i}$ is called a Jordan block of $\mathbf{A}$. For Jordan block i, the diagonal entries are λ_i, the superdiagonal entries are one, and all other entries are zero.

Next, we present two lemmas that were used in the proofs of the main theorems. The first lemma was used in Theorem 3.3.1 and bounds our initial condition for each neutral fraction i for each stage j, $v^i_{j,0}(x)$, sufficiently to establish the uniform convergence results for the neutral fractions.

Lemma 3.6.1. *Let $x \to v^i_{j,0}(x)$ satisfy $x^2 v^i_{j,0}(x) e^{sx} \in L^1(\mathbb{R}) \cap L^\infty(\mathbb{R})$, then for each $s > 0$ there exists a positive constant C_j such that*

$$w^i_{j,0}(x) = \frac{C_j e^{-sx}}{1 + x^2} \tag{3.135}$$

bounds $v^i_{j,0}(x)$ for all $x \in \mathbb{R}$. Moreover, the Fourier transform of $w^i_{j,0}(x)e^{sx}$ with respect to x is in $L^1(\mathbb{R})$ and is given by

$$C_j \pi e^{-|\omega|}. \tag{3.136}$$

For the proof of Lemma 3.6.1, we refer the reader to Lemma 1 by Marculis et al. (2017).

We next provide a lemma that will be used in the proofs of the Theorems 3.3.2 and 3.3.3. In particular, we make use of the Jordan canonical form and the Perron-Frobenius theorem outlined above.

Lemma 3.6.2. *Assume that the matrix $\mathbf{B_0}$ is nonnegative and primitive. Let λ_1 be the dominant eigenvalue of $\mathbf{B_0}$, then*

$$\lim_{t\to\infty} \left[\frac{\mathbf{B_0}}{\lambda_1}\right]^t = \mathbf{r}\boldsymbol{\ell} \tag{3.137}$$

where $\mathbf{r}$ and $\boldsymbol{\ell}$ are the right and left eigenvectors corresponding to λ_1 respectively with $\boldsymbol{\ell}$ normalized by $\left\langle \boldsymbol{\ell}^T, \mathbf{r} \right\rangle$ to account for the scaling in $\mathbf{r}$.

Proof. Writing $\mathbf{B_0}$ in terms of its Jordan canonical form, we have

$$\lim_{t\to\infty} \left[\frac{\mathbf{B_0}}{\lambda_1}\right]^t = \lim_{t\to\infty} \left[\frac{\mathbf{P}\mathbf{J}\mathbf{P}^{-1}}{\lambda_1}\right]^t \tag{3.138}$$

$$= \lim_{t\to\infty} \frac{\mathbf{P}\mathbf{J}^t\mathbf{P}^{-1}}{\lambda_1^t}. \tag{3.139}$$

Since $\mathbf{J}$ is block diagonal,

$$\mathbf{J}^t = \begin{bmatrix} \mathbf{J}_1^t & \dots & \mathbf{0} \\ \vdots & \ddots & \vdots \\ \mathbf{0} & \dots & \mathbf{J}_b^t \end{bmatrix}. \tag{3.140}$$

By the Perron-Frobenius theorem there exists a dominant eigenvalue λ_1 of $\mathbf{B_0}$ because $\mathbf{B_0}$ is nonnegative and primitive . The first Jordan block is $\mathbf{J}_1 = \begin{bmatrix}\lambda_1\end{bmatrix}$ and $\mathbf{J}_1^t = \begin{bmatrix}\lambda_1^t\end{bmatrix}$. For Jordan block j of size $b_j \times b_j$ we have

$$\mathbf{J}_j^t = \begin{bmatrix} \lambda_j^t & \binom{t}{1}\lambda_j^{t-1} & \dots & \binom{t}{b_j-2}\lambda_j^{t-b_j+2} & \binom{t}{b_j-1}\lambda_j^{t-b_j+1} \\ 0 & \lambda_j^t & \dots & \binom{t}{b_j-3}\lambda_j^{t-b_j+3} & \binom{t}{b_j-2}\lambda_j^{t-b_j+2} \\ \vdots & \vdots & \ddots & \vdots & \vdots \\ 0 & 0 & \dots & \lambda_j^t & \binom{t}{1}\lambda_j^{t-1} \\ 0 & 0 & \dots & 0 & \lambda_j^t \end{bmatrix} \tag{3.141}$$

for $t \geq b_j - 1$. Since $|\lambda_j| < \lambda_1$, using L'Hôpital's rule, we have

$$\lim_{t\to\infty} \frac{\mathbf{J}_j^t}{\lambda_1^t} = \mathbf{0} \tag{3.142}$$

for $j = 2, \dots, b$. Returning to the Jordan canonical form,

$$\lim_{t\to\infty} \frac{\mathbf{J}^t}{\lambda_1^t} = \begin{bmatrix} 1 & \dots & 0 \\ \vdots & \ddots & \vdots \\ 0 & \dots & 0 \end{bmatrix}. \tag{3.143}$$

Hence from (3.139),

$$\lim_{t\to\infty} \frac{\mathbf{P}\mathbf{J}^t\mathbf{P}^{-1}}{\lambda_1^t} = \mathbf{P} \lim_{t\to\infty} \frac{\mathbf{J}^t}{\lambda_1^t}\mathbf{P}^{-1} \tag{3.144}$$

$$= \mathbf{P} \begin{bmatrix} 1 & \dots & 0 \\ \vdots & \ddots & \vdots \\ 0 & \dots & 0 \end{bmatrix} \mathbf{P}^{-1} \tag{3.145}$$

$$= \mathbf{r}\boldsymbol{\ell} \tag{3.146}$$

because $\mathbf{r}$ is the first column vector of $\mathbf{P}$ and $\boldsymbol{\ell}$ is the first row vector of $\mathbf{P}^{-1}$. Therefore, from (3.139) and (3.146),

$$\lim_{t\to\infty} \left[\frac{\mathbf{B_0}}{\lambda_1}\right]^t = \mathbf{r}\boldsymbol{\ell}. \tag{3.147}$$

The proof of Lemma 3.6.2 is complete. □

References

Austerlitz, Frédéric and Pauline Hélène Garnier-Géré (2003). "Modelling the impact of colonisation on genetic diversity and differentiation of forest trees: interaction of life cycle, pollen flow and seed long-distance dispersal." *Heredity* 90.4, p. 282.

Bapat, Ravi B and Tirukkannamangai ES Raghavan (1997). *Nonnegative matrices and applications*. Vol. 64. Cambridge university press.

Bataillon, Thomas M, Jacques L David, and Daniel J Schoen (1996). "Neutral genetic markers and conservation genetics: simulated germplasm collections." *Genetics* 144.1, pp. 409–417.

Bateman, Andrew W, Andreas Buttenschön, Kelley D Erickson, and Nathan G Marculis (2017). "Barnacles vs bullies: modelling biocontrol of the invasive European green crab using a castrating barnacle parasite." *Theoretical Ecology* 10.3, pp. 305–318.

Bonnefon, Olivier, Jérôme Coville, Jimmy Garnier, and Lionel Roques (2014). "Inside dynamics of solutions of integro-differential equations." *Discrete and Continuous Dynamical Systems-Series B* 19.10, pp. 3057–3085.

Bonnefon, Olivier, Jimmy Garnier, François Hamel, and Lionel Roques (2013). "Inside dynamics of delayed traveling waves." *Mathematical Modelling of Natural Phenomena* 8.3, pp. 42–59.

Cooley, James W and John W Tukey (1965). "An algorithm for the machine calculation of complex Fourier series." *Mathematics of Computation* 19.90, pp. 297–301.

Cullingham, Catherine I, Janice EK Cooke, Sophie Dang, Corey S Davis, Barry J Cooke, and David W Coltman (2011). "Mountain pine beetle host-range expansion threatens the boreal forest." *Molecular Ecology* 20.10, pp. 2157–2171.

Davis, Margaret B and Ruth G Shaw (2001). "Range shifts and adaptive responses to Quaternary climate change." *Science* 292.5517, pp. 673–679.

Easterling, Michael R, Stephen P Ellner, and Philip M Dixon (2000). "Size-specific sensitivity: applying a new structured population model." *Ecology* 81.3, pp. 694–708.

Garnier, Jimmy, Thomas Giletti, François Hamel, and Lionel Roques (2012). "Inside dynamics of pulled and pushed fronts." *Journal de Mathématiques Pures et Appliquées* 98.4, pp. 428–449.

Garnier, Jimmy and Mark A Lewis (2016). "Expansion under climate change: the genetic consequences." *Bulletin of Mathematical Biology* 78.11, pp. 2165–2185.

Hallatschek, Oskar and David R Nelson (2008). "Gene surfing in expanding populations." *Theoretical Population Biology* 73.1, pp. 158–170.

Hastings, Alan, Kim Cuddington, Kendi F Davies, Christopher J Dugaw, Sarah Elmendorf, Amy Freestone, Susan Harrison, Matthew Holland, John Lambrinos, Urmila Malvadkar, Brett A Melbourne, Kara Moore, Caz Taylor, and Diane Thomson (2005). "The spatial spread of invasions: new developments in theory and evidence." *Ecology Letters* 8.1, pp. 91–101.

Hewitt, Godfrey M (2000). "The genetic legacy of the Quaternary ice ages." *Nature* 405.6789, pp. 907–913.

Holderegger, Rolf, Urs Kamm, and Felix Gugerli (2006). "Adaptive vs. neutral genetic diversity: implications for landscape genetics." *Landscape Ecology* 21.6, pp. 797–807.

Howe, Henry F and Judith Smallwood (1982). "Ecology of seed dispersal." *Annual Review of Ecology and Systematics* 13.1, pp. 201–228.

Ibrahim, Kamal M, Richard A Nichols, and Godfrey M Hewitt (1996). "Spatial patterns of genetic variation generated by different forms of dispersal." *Heredity* 77, pp. 282–291.

Kot, Mark, Mark A Lewis, and Pauline van den Driessche (1996). "Dispersal data and the spread of invading organisms." *Ecology* 77.7, pp. 2027–2042.

Lefkovitch, LP (1965). "The study of population growth in organisms grouped by stages." *Biometrics*, pp. 1–18.

Leslie, Patrick H (1945). "On the use of matrices in certain population mathematics." *Biometrika* 33.3, pp. 183–212.

Levin, Lisa A (2006). "Recent progress in understanding larval dispersal: new directions and digressions." *Integrative and Comparative Biology* 46.3, pp. 282–297.

Lewis, Mark A, Nathan G Marculis, and Zhongwei Shen (2018). "Integrodifference equations in the presence of climate change: persistence criterion, travelling waves and inside dynamics." *Journal of Mathematical Biology* 77.6-7, pp. 1649–1687.

Li, Bingtuan, Mark A Lewis, and Hans F Weinberger (2009). "Existence of traveling waves for integral recursions with nonmonotone growth functions." *Journal of Mathematical Biology* 58.3, pp. 323–338.

Liebhold, Andrew M, Joel A Halverson, and Gregory A Elmes (1992). "Gypsy moth invasion in North America: a quantitative analysis." *Journal of Biogeography*, pp. 513–520.

Lubina, John A and Simon A Levin (1988). "The spread of a reinvading species: range expansion in the California sea otter." *The American Naturalist* 131.4, pp. 526–543.

Lui, Roger (1982a). "A nonlinear integral operator arising from a model in population genetics I. Monotone initial data." *SIAM Journal of Mathematical Analysis* 13.6, pp. 913–937.

— (1982b). "A nonlinear integral operator arising from a model in population genetics II. Initial data with compact support." *SIAM Journal of Mathematical Analysis* 13.6, pp. 938–953.

— (1983). "Existence and stability of travelling wave solutions of a nonlinear integral operator." *Journal of Mathematical Biology* 16.3, pp. 199–220.

— (1989a). "Biological growth and spread modeled by systems of recursions. I. Mathematical theory." *Mathematical Biosciences* 93.2, pp. 269–295.

— (1989b). "Biological growth and spread modeled by systems of recursions. II. Biological theory." *Mathematical Biosciences* 93.2, pp. 297–311.

Lutscher, Frithjof and Mark A Lewis (2004). "Spatially-explicit matrix models." *Journal of Mathematical Biology* 48.3, pp. 293–324.

Marculis, Nathan G and Roger Lui (2016). "Modelling the biological invasion of Carcinus maenas (the European green crab)." *Journal of Biological Dynamics* 10.1, pp. 140–163.

Marculis, Nathan G, Roger Lui, and Mark A Lewis (2017). "Neutral Genetic Patterns for Expanding Populations with Nonoverlapping Generations." *Bulletin of Mathematical Biology* 79.4, pp. 828–852.

Moloney, Kirk A (1986). "A generalized algorithm for determining category size." *Oecologia* 69.2, pp. 176–180.

Neubert, Michael G and Hal Caswell (2000). "Demography and dispersal: calculation and sensitivity analysis of invasion speed for structured populations." *Ecology* 81.6, pp. 1613–1628.

Pluess, Andrea R (2011). "Pursuing glacier retreat: genetic structure of a rapidly expanding Larix decidua population." *Molecular Ecology* 20.3, pp. 473–485.

Roques, Lionel, Jimmy Garnier, François Hamel, and Etienne K Klein (2012). "Allee effect promotes diversity in traveling waves of colonization." *Proceedings of the National Academy of Sciences* 109.23, pp. 8828–8833.

Roques, Lionel, Yuzo Hosono, Olivier Bonnefon, and Thomas Boivin (2015). "The effect of competition on the neutral intraspecific diversity of invasive species." *Journal of Mathematical Biology* 71.2, pp. 465–489.

Vandermeer, John (1978). "Choosing category size in a stage projection matrix." *Oecologia* 32.1, pp. 79–84.

Veit, Richard R and Mark A Lewis (1996). "Dispersal, population growth, and the Allee effect: dynamics of the house finch invasion of eastern North America." *The American Naturalist* 148.2, pp. 255–274.

Weinberger, Hans F (1978). "Asymptotic behavior of a model in population genetics." *Nonlinear Partial Differential Equations and Applications*. Springer, pp. 47–96.

— (1982). "Long-time behavior of a class of biological models." *SIAM Journal on Mathematical Analysis* 13.3, pp. 353–396.

Chapter 4

Inside dynamics of integrodifference equations with mutations

4.1 Introduction

The neutral theory of molecular evolution posits that most of the genetic variation in populations is independent of selection and hence is neutral (Duret, 2008). When this theory is true, it suggests that much of the variation in populations is due to events such as mutations or genetic drift, without the influence of selection. This provides support for including neutral mutation dynamics into models of genetic spread. The molecular clock hypothesis states that genes evolve at a relatively constant rate over time (Bromham and Penny, 2003). We use this hypothesis in our model formulation by assuming the probability genes mutating is constant over time. This theory suggests the genetic difference between any two species is proportional to the time since these species last shared a common ancestor. Therefore, if the molecular clock hypothesis is true, this can be used for estimating evolutionary timescales (Ho, 2008).

Neutral genetic patterns caused by range expansions is a topic of recent interest (Hallatschek and Nelson, 2008). The establishment of a new population,

undertaken by a few original founders who carry only a small fraction of the total genetic variation of the parental population is referred to as the founder effect (Mayr, 1940). Range expansions are commonly thought to reduce genetic diversity of a population due to the founder effect. When a population is expanding its range, consecutive founder events result in the phenomena known as gene surfing (Excoffier and Ray, 2008). This is the spatial analog of genetic drift and occurs when certain alleles reach higher than expected frequencies at the front of a range expansion (Slatkin and Excoffier, 2012). However in the presence of neutral mutations, these processes may be altered. We are not the first to model this problem; previous studies have used simulation based models (Edmonds et al., 2004; Klopfstein et al., 2006) and lab experiments (Hallatschek et al., 2007) to understand the effects of neutral mutations on the wave of range expansions.

Integrodifference equations have played a central role in studying problems in theoretical ecology such as range expansions (Krkošek et al., 2007; Zhou and Kot, 2011), the spread of invasive species (Bateman et al., 2017; Kot et al., 1996; Lewis et al., 2016), determining the critical domain size for population persistence (Lutscher et al., 2005; Reimer et al., 2016; Van Kirk and Lewis, 1997), and more recently understanding the neutral genetic structure of populations (Lewis et al., 2018; Marculis et al., 2019, 2017). In this work, we aim to understand role that mutations play in the neutral genetic diversity of a population undergoing range expansion by studying an integrodifference equation model.

Recall that the classical integrodifference equation is

$$u_{t+1}(x) = \int_{-\infty}^{\infty} k(x-y)g(u_t(y))u_t(y)\,dy \tag{4.1}$$

where u is the population density, k is the dispersal kernel, and g is the per-capita growth function. To understand the role that mutations play on the

neutral genetic diversity of a spreading population, we study the inside dynamics of integrodifference equations with neutral mutations. The term inside dynamics refers to changes in the inside structure of the population rather than the total density. The key assumption in the analysis for inside dynamics is that all individuals grow and disperse in the same manner differing only with respect to neutral genetic markers. In other words, all individuals in the population have the same fitness. This allows us to partition the population into distinct subgroups called neutral fractions where we track the spatio-temporal evolution of these subgroups. By making the assumption of neutral fractions, we obtain the following system of equations for the inside dynamics of our scalar integrodifference equation,

$$v_{t+1}^i(x) = \int_{-\infty}^{\infty} k(x-y)g(u_t(y))v_t^i(y)\,dy, \text{ for } i = 1, \ldots, n, \tag{4.2}$$

where n is the finite number of neutral fractions and $u_t(x) = \sum_{i=1}^{n} v_t^i(x)$.

Inside dynamics have been studied for a variety of different spatio-temporal population models, including reaction-diffusion equations (Garnier et al., 2012; Garnier and Lewis, 2016; Roques et al., 2012, 2015), delay reaction-diffusion equations (Bonnefon et al., 2013), integro-differential equations (Bonnefon et al., 2014), and integrodifference equations (Lewis et al., 2018; Marculis et al., 2019, 2017). The three previous studies on integrodifference equations analyzed a scalar model (Marculis et al., 2017), a model with climate change (Lewis et al., 2018), and a stage-structured population model (Marculis et al., 2019). Our extension to these previous works is to analyze the inside dynamics of a scalar integrodifference equation with neutral mutations. By comparing the differences between our model and those previously studied, we can begin to understand what role mutations play in the spread of neutral genetic markers.

Mutations between neutral fractions are called neutral mutations because

there is no direct effect on the fitness of the individual. This process adds a level of biological complexity and increases the biological realism of the model. The addition of neutral mutations to the model is important for realism because it is a natural process that is known to occur and can be used in studying molecular clocks to identify evolutionary events such as speciation and evolutionary radiation. For our analyses, we are interested in how the addition of neutral mutations into the modeling structure can impact the resulting patterns of genetic spread.

The organization of the paper is laid out in the following way. Section 4.2 provides a derivation of our mutation matrix model. That is, we extend (4.2) to include mutations between the neutral fractions. In Section 4.3, we lay out some preliminary material and assumptions that will be useful in the main theorems. Once the preliminary material has been established, we move on to the main results. Here, we state four main theorems about the asymptotic spread of the neutral fractions in Section 5.3. In Section 4.5, we perform some numerical simulations to support our main results and understand how different components affect the asymptotic dynamics. These simulations lead to conjectures regarding which assumptions in the main theorems could be relaxed without changing the results. Finally, in Section 4.6, we provide a discussion of the work including model development, outcomes, limitations, and some future directions.

4.2 Mutation matrix model

Our goal is to extend the system of equations in (4.2) to include neutral mutations that happen during reproduction. To do this, we must determine how to incorporate mutations into the model. A common method that has been previously used to study the mutations of DNA is the substitution model. A substitution model describes the process of genetic variation by which one

variant is replaced by another, with a given constant mutation rate (Arenas, 2015). To model the substitution process, continuous-time Markov chains are a common tool of choice. The first and simplest substitution model was developed by Jukes and Cantor for the mutation of DNA base pairs in amino acids (Jukes and Cantor, 1969) . This model assumes equal base frequencies and equal mutation rates, giving a simplistic one parameter depiction. Others have added complexity to the Jukes Cantor model by distinguishing between types of transitions (Kimura, 1980), and by allowing the base frequencies to vary (Felsenstein, 1981). In all of these models, the dynamics are driven by the rate matrix for the continuous-time Markov chain.

In our work, we are not concerned with modeling DNA sequence evolution in amino acids, but the change of neutral genetic markers in an organism which reproduces at discrete time intervals. To achieve this, we use a modeling framework similar to substitution models, but with a discrete-time Markov chain. Since our neutral fraction model is an integrodifference equation and we are assuming that the mutations are occurring during reproduction, a discrete-time Markov chain is suitable to model the mutation process. Thus, we can construct a mutation matrix where the entries are described by mutation probabilities. Consider a single locus with n different neutral alleles and let m_{jl} be the probability of mutation from a type l to a type j individual and $\mathbf{v} = [v^1, v^2, \ldots, v^n]^T$. Then, we obtain the following equation

$$\mathbf{v}_{t+1}(x) = \int_{-\infty}^{\infty} k(x-y)\mathbf{M}g(u_t(y))\mathbf{v}_t(y)\,dy, \tag{4.3}$$

where $u_t(x) = \sum_{i=1}^{n} v_t^i(x)$, $\mathbf{M}$ is the mutation matrix given by

$$\mathbf{M} = \begin{bmatrix} 1-\sum_{j\neq 1} m_{j1} & m_{12} & \ldots & m_{1(n-1)} & m_{1n} \\ m_{21} & 1-\sum_{j\neq 2} m_{j2} & \ldots & m_{2(n-1)} & m_{2n} \\ \vdots & \vdots & \ddots & \vdots & \vdots \\ m_{(n-1)1} & m_{(n-1)2} & \ldots & 1-\sum_{j\neq n-1} m_{j(n-1)} & m_{(n-1)n} \\ m_{n1} & m_{n2} & \ldots & m_{n(n-1)} & 1-\sum_{j\neq n} m_{jn} \end{bmatrix}, \tag{4.4}$$

and our initial condition, $\mathbf{v}_0(x)$, satisfies

$$\sum_{i=1}^{n} v_0^i(x) = u_0(x). \tag{4.5}$$

It should be noted that the same general form of the mutation matrix, (4.4), can be attained by assuming there are m loci with a different neutral alleles; see Appendix 4.7.1. Thus, our model is quite general and could be applied to commonly studied neutral genetic marks such as microsatellite data (Selkoe and Toonen, 2006) or mutations by single nucleotide polymorphisms (SNPs) (Morin et al., 2004). In particular, to study the effects of SNPs on a single locus the mutation matrix will have dimensions 4×4 to account for the mutation rates between the four nucleotides. Our mutation matrix model given in (4.3) is different from the scalar model in (4.2) because there are interactions between the neutral fractions. Thus, for our analysis we must consider all neutral fractions rather than focusing on a single neutral fraction as done in previous studies for the scalar model.

4.3 Preliminary material

For expanding populations, there is a classical result for the spreading speed of a population introduced over a compact region. When the maximum per-capita growth is at the lowest densities, ($g(u) \leq g(0)$ for all $u \in (0,1)$), k is thin-tailed (i.e., has a moment generating function), and the operator is order preserving, we can compute the rightward spreading speed with the following formula,

$$c^* = \inf_{s>0} \frac{1}{s} \ln \left(g(0) \int_{-\infty}^{\infty} k(x) e^{sx}\, dx \right) \tag{4.6}$$

(Weinberger, 1982). We can find the leftward spreading speed with a calculation similar to (4.6),

$$c_-^* = \inf_{s>0} \frac{1}{s} \ln \left(g(0) \int_{-\infty}^{\infty} k(x) e^{-sx}\, dx \right). \tag{4.7}$$

In particular, when k is a Gaussian dispersal kernel with mean μ and variance σ^2,

$$k(x;\mu,\sigma) = \frac{1}{\sqrt{2\pi\sigma^2}} e^{-\frac{(x-\mu)^2}{2\sigma^2}}, \tag{4.8}$$

the rightward spreading speed is

$$c^* = \sqrt{2\sigma^2 \ln(g(0))} + \mu, \tag{4.9}$$

and the leftward spreading speed is

$$c^*_- = \sqrt{2\sigma^2 \ln(g(0))} - \mu. \tag{4.10}$$

Definition 4.3.1. *A square matrix is called a Markov matrix if all entries are nonnegative and the sum of each column vector is equal to one.*

One consequence of a Markov matrix that we will frequently use throughout our work is that the dominant eigenvalue is equal to one. The mutation matrix given in (4.4) is a Markov matrix. If $\mathbf{M}$ is irreducible then it is possible to mutate from any given genotype to any other genotype in a finite number of steps. A stricter version of irreducibility is primitivity. If $\mathbf{M}$ is primitive then there exists a t such that it is possible to mutate from any given neutral genotype to any other in exactly t steps (i.e., $\mathbf{M}^t > \mathbf{0}$). We assume that this is the case. Recall that a nonnegative matrix is primitive if it is irreducible and all entries on the diagonal are strictly positive. Thus, by assuming primitivity instead of irreducibility for the mutation matrix means that at each time step for each neutral fraction there are some individuals that do not mutate into another type.

In our work we consider Markov matrices that are not necessarily primitive but are block diagonal primitive.

Definition 4.3.2. *A square matrix* $\mathbf{M}$ *is block diagonal primitive if for some* $t > 0$, $\mathbf{M}^t$ *can be written as a block diagonal matrix where each block is prim-*

itive. That is, there exits a t such that

$$\mathbf{M}^t = \begin{bmatrix} \mathbf{M}_1^t & 0 & \dots & 0 \\ 0 & \mathbf{M}_2^t & \dots & 0 \\ \vdots & \vdots & \ddots & \vdots \\ 0 & 0 & \dots & \mathbf{M}_b^t \end{bmatrix} \tag{4.11}$$

where $\mathbf{M}_q^t > 0$ *for* $q = 1, \dots, b$.

Note that each block could be primitive with a different power t_q. This would mean that (4.11) holds true for $t = \prod_{q=1}^{b} t_q$. A consequence of the mutation matrix being a nontrivial block diagonal primitive matrix is that neutral fractions can only mutate into a select subset of the different types. The block primitive assumption is much more general than primitivity and allows us to study models where the mutations of alleles occurs on b different loci. We next define a set that encompasses how the neutral fractions can mutate.

Definition 4.3.3. *Neutral fraction i is in the mutation class q if $m_{ix} \in \mathbf{M}_q$ for some x.*

In the analysis that follows, we make the following assumptions on Equation (4.3):

$A1:$ *The matrix* $\mathbf{M}$ *is Markov and block diagonal primitive,*

$A2:$ $0 < g(u) \leq g(0)$ *for all* $u \in (0, 1)$, *and*

$A3:$ k *is Gaussian with mean* μ *and variance* σ^2.

Assumption $A1$ (Markov and block diagonal primitive matrix) is needed so we can apply the Perron-Frobenius theorem to each block in our analysis. Assumption $A2$ (maximum per-capita growth rate as density approaches zero) is relevant to expanding populations exhibiting "pulled" waves (Stokes, 1976), where the leading edge of the wave determines the spreading speed (4.6).

Assumption $A3$ (a Gaussian dispersal kernel) is made for mathematical convenience. This will allow us to prove rigorous results about the resulting system. However, we relax this assumption when conducting numerical simulations in Section 4.5.

A fourth assumption that will be made in our theorems in the next section is related to the decay rate of the initial condition. This decay assumption is derived from Proposition 5 in Lui (1983). To compute the critical decay rate for the rightward spread we solve for the unique value of s that satisfies (4.6) for the rightward spread. In the case when the dispersal kernel is Gaussian, we can explicitly solve for this value of s and obtain the value $\frac{c-\mu}{\sigma^2}$. Similarly, for the leftward spread, the critical decay rate for the leftward spread is the unique value of s that satisfies (4.7). In the case when the dispersal kernel is Gaussian, we can explicitly solve for this value of s and obtain the value $\frac{c+\mu}{\sigma^2}$. In each of the four theorems, which we present in the next section, the precise form of the fourth assumption differs. Thus, we do not explicitly write out the different assumptions here, but save them for the statement of the theorems. With the definitions, assumptions, and preliminary material in place, we can present the main results of the paper.

4.4 Asymptotic results

In this section, we provide some theoretical results for the asymptotic dynamics of our model given by (4.3)-(4.5). Here, we state the four main theorems about the asymptotic spread of the neutral fractions.

Theorem 4.4.1 provides sufficient conditions for when neutral fractions in a given mutation class are left behind during the population spread and do not contribute to the spread of the population. In other words, Theorem 4.4.1 states that if there are no neutral fractions in a given mutation class at the leading edge, then all members of this mutation class converge to zero

uniformly in the moving half-frame.

Theorem 4.4.1. *Consider* (4.3)-(4.5) *where* $A1$-$A3$ *hold as well as the additional assumption:*

$A4:$ $\int_{-\infty}^{\infty} e^{\frac{c-\mu}{\sigma^2}y} v_0^i(y)\,dy < \infty$ *for every* i *in mutation class* q.

If $c \geq c^*$, *then for any* $A \in \mathbb{R}$, *the density of the neutral fraction* i, $v_t^i(x)$, *converges to* 0 *uniformly as* $t \to \infty$ *in the moving half-frame* $[A + ct, \infty)$.

Theorem 4.4.1 shows when neutral fractions for a rightward spreading population converge to zero in the moving half-frame. We can also consider the case when we have a leftward spreading population in the following theorem.

Theorem 4.4.2. *Consider* (4.3)-(4.5) *where* $A1$-$A3$ *hold as well as the additional assumption:*

$A4^-:$ $\int_{-\infty}^{\infty} e^{-\frac{c+\mu}{\sigma^2}y} v_0^i(y)\,dy < \infty$ *for every* i *in mutation class* q.

If $c \geq c_-^*$, *then for any* $A \in \mathbb{R}$, *the density of the neutral fraction* i, $v_t^i(x)$, *converges to* 0 *uniformly as* $t \to \infty$ *in the moving half-frame* $(-\infty, A - ct]$.

From Theorems 4.4.1 and 4.4.2 we conclude that if each neutral fraction in a given mutation class is not located at the leading edge of the spread, then these neutral fractions will converge to zero in the moving half-frame. The question remains as to what happens to the neutral fractions at the leading edge and to the rest of the neutral fractions in the same mutation class. The next two theorems provide asymptotic results for these neutral fractions for a particular class of initial data where neutral fractions are proportional to the exponentially decaying leading edge of the wave.

Theorem 4.4.3. *Consider* (4.3)-(4.5) *where* $A1$-$A3$ *hold as well as the additional assumption:*

$A4'$: $v_0^i(x) = p_0^i e^{-\frac{c-\mu}{\sigma^2}x}$ *where* p_0^i *is the initial proportion of neutral fraction* i *and belongs to mutation class* q *of size* m_q *such that* $\sum_{j=1}^{m_q} p_{j,0}^i = 1$.

Then, for $c = c^*$ *and any* $A \in \mathbb{R}$, *the density of neutral fractions belonging to mutation class* q, $\mathbf{v}_{q,t}(x)$, *asymptotically approaches a proportion of the traveling wave for the linear equation as* $t \to \infty$ *in the moving half-frame* $[A + ct, \infty)$. *That is,*

$$\lim_{t\to\infty} \mathbf{v}_{q,t}(x_0 + ct) = \mathbf{r}_q e^{-\frac{c-\mu}{\sigma^2}x_0} \tag{4.12}$$

for $x_0 \geq A$ *where* $\mathbf{r}_q$ *is the right eigenvector of* $\mathbf{M}_q$.

Theorem 4.4.3 provides the asymptotic proportion of each neutral fraction in mutation class q for the rightward spread. This proportion is simply the right eigenvector of $\mathbf{M}_q$ corresponding to eigenvalue 1. We can also compute the leftward proportion in the following theorem.

Theorem 4.4.4. *Consider* (4.3)-(4.5) *where* $A1$-$A3$ *hold as well as the additional assumption:*

$A4'^{-}$: $v_0^i(x) = p_0^i e^{\frac{c+\mu}{\sigma^2}x}$ *where* p_0^i *is the initial proportion of neutral fraction* i *and belongs to mutation class* q *of size* m_q *such that* $\sum_{j=1}^{m_q} p_{j,0}^i = 1$.

Then, for $c = c_-^*$ *and any* $A \in \mathbb{R}$, *the density of neutral fractions belonging to mutation class* q, $\mathbf{v}_{q,t}(x)$, *asymptotically approaches a proportion of the traveling wave for the linear equation as* $t \to \infty$ *in the moving half-frame* $(-\infty, A - ct]$. *That is,*

$$\lim_{t\to\infty} \mathbf{v}_{q,t}(x_0 - ct) = \mathbf{r}_q e^{\frac{c+\mu}{\sigma^2}x_0} \tag{4.13}$$

for $x_0 \leq A$ *where* $\mathbf{r}_q$ *is the right eigenvector of* $\mathbf{M}_q$.

The proofs of Theorems 4.4.1-4.4.4 are provided in Appendix 4.7.2.

4.5 Numerical simulations

In this section we illustrate our theory in Section 5.3 by some simple examples. All simulations were done by using the fast Fourier transform technique (Cooley and Tukey, 1965). This method is better than classical quadrature because it speeds up the numerical process from $O(n^2)$ to $O(n\log(n))$.

For our first set of simulations, we consider an example where the Assumptions $A1$, $A2$, and $A3$ are satisfied. Specifically, we assume that k is a Gaussian dispersal kernel and g is the Beverton-Holt growth function. That is, k is given by (4.8) and

$$g(u_t(y)) = \frac{R}{1+\frac{R-1}{K}u_t(y)}. \tag{4.14}$$

The model we simulate is

$$\mathbf{v}_{t+1}(x) = \int_{-\infty}^{\infty} \frac{1}{\sqrt{2\pi\sigma^2}} e^{-\frac{(x-y-\mu)^2}{2\sigma^2}} \frac{R}{1+\frac{R-1}{K}u_t(y)} \mathbf{M}\mathbf{v}_t(y)\, dy \tag{4.15}$$

where $\mathbf{M}$ is the mutation matrix. In this section, we consider a few different mutation matrices. The first mutation matrix is primitive and allows for mutations between all neutral fractions. This matrix is given by

$$\mathbf{M1} = \begin{bmatrix} 0.85 & 0.01 & 0.04 & 0.02 & 0.03 \\ 0.03 & 0.92 & 0.02 & 0.01 & 0.05 \\ 0.07 & 0.05 & 0.86 & 0.02 & 0.03 \\ 0.01 & 0.01 & 0.06 & 0.93 & 0.03 \\ 0.04 & 0.01 & 0.02 & 0.02 & 0.86 \end{bmatrix}. \tag{4.16}$$

The second mutation matrix we consider is block primitive. Here, the parameters are the same as in **M1** except we let $m_{13} = m_{14} = m_{15} = m_{23} = m_{24} = m_{25} = m_{31} = m_{32} = m_{41} = m_{42} = m_{51} = m_{52} = 0$. Then **M2** is given by

$$\mathbf{M2} = \begin{bmatrix} 0.97 & 0.01 & 0 & 0 & 0 \\ 0.03 & 0.99 & 0 & 0 & 0 \\ 0 & 0 & 0.92 & 0.02 & 0.03 \\ 0 & 0 & 0.06 & 0.96 & 0.03 \\ 0 & 0 & 0.02 & 0.02 & 0.94 \end{bmatrix}. \tag{4.17}$$

Notice that **M2** is block primitive because it only allows for mutations between two distinct classes of neutral fractions. The two mutation classes are given

by $\{1, 2\}$ and $\{3, 4, 5\}$. Thus, neutral fractions 1 and 2 can mutate into each other but not into neutral fractions 3, 4, and 5 and vice-versa.

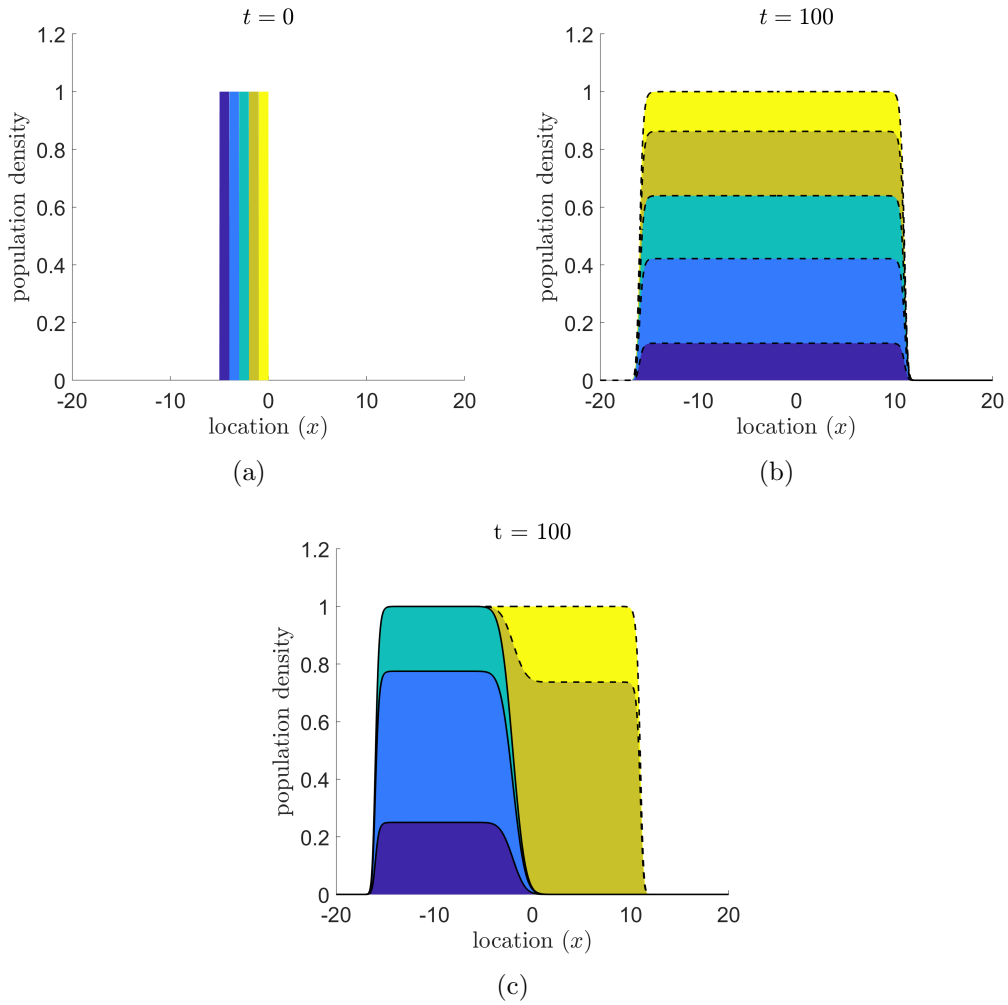

Figure 4.1: Numerical realization of (4.15) for the parameter values $\sigma^2 = 0.01$, $\mu = 0$, $R = 2$, $K = 1$. Figure 4.1(a) is the initial condition for the simulations seen in Figures 4.1(b) and 4.1(c). In 4.1(b) we use the mutation matrix **M1** given by (4.16). The dashed lines in Figure 4.1(b) give the asymptotic proportion of neutral fractions as calculated in Theorem 4.4.3. In 4.1(c) we use the mutation matrix **M2** given by (4.17). The dashed lines in Figure 4.1(c) give the rightward asymptotic proportion of neutral fractions as calculated in Theorem 4.4.3 and the solid lines in Figure 4.1(c) give the leftward asymptotic proportion of neutral fractions as calculated in Theorem 4.4.4.

The simulations for our model are given in Figure 4.1. We chose these initial conditions so as to satisfy Assumptions $A4$ (see Theorem 4.4.1) and

$A4^-$ (see Theorem 4.4.2). However, note that the initial conditions plotted in Figure 4.1(a) are not the same as those assumed by $A4'$ and $A4'^-$ for Theorems 4.4.3 and 4.4.4. These initial data were chosen in an effort to see if the results of the theorems could hold for a more general class of initial data than was assumed in the statement of the theorems. The initial density of each neutral fraction is given by $v_0^i(x) = \mathbb{1}_{-i<x\leq-(i-1)}$ where $\mathbb{1}$ is the indicator function. In Figure 4.1(b), we are using the mutation matrix **M1** given by (4.16) where there is only one mutation class. Thus, the stable distribution of neutral fraction is calculated using Theorems 4.4.3 and 4.4.4 and is given by $\mathbf{r}_1 = [0.1377, 0.2229, 0.2179, 0.2932, 0.1283]^T$. The stable distribution can be seen by the dashed lines in Figure 4.1(b). In Figure 4.1(c), we use the mutation matrix **M2** given by (4.17) and we can see that the spread to the right and left have different neutral fractions because of the initial distribution of neutral fractions and because the structure of the mutation matrix is block diagonal primitive with two blocks. The asymptotic distribution of neutral fractions for the first mutation class $\{1, 2\}$ in the rightward spread is calculated by Theorem 4.4.3 and is given by $\mathbf{r}_1 = [0.25, 0.75]^T$. This is seen by the dashed lines in Figure 4.1(c). The asymptotic distribution of neutral fractions for the second mutation class $\{3, 4, 5\}$ in the leftward spread is calculated by Theorem 4.4.4 and is given by $\mathbf{r}_2 = [0.225, 0.525, 0.25]^T$. This is seen by the solid lines in Figure 4.1(c).

In this section, we also would like to understand dynamics of mutation matrices that do not satisfy Assumptions $A1$ and $A3$ of Theorems 4.4.1-4.4.4. In particular, we want to consider a dispersal kernel that is not Gaussian and matrix structures that do not fit to the block diagonal primitive assumption. We first, consider the Laplace dispersal kernel,

$$k(x-y) = \frac{1}{2b}e^{-|x-\mu|/b} \tag{4.18}$$

again with Beverton-Holt growth given by (4.14). Then the model that we simulate is given by

$$\mathbf{v}_{t+1}(x) = \int_{-\infty}^{\infty} \frac{1}{2b} e^{-|x-\mu|/b} \frac{R}{1 + \frac{R-1}{K} u_t(y)} \mathbf{M}\mathbf{v}_t(y)\, dy. \tag{4.19}$$

For our simulations, we want to compare the effect of the dispersal kernel on the asymptotic proportion of neutral fractions. Thus, we run simulations similar to those in Figure 4.1 by using the same demographic parameters and mutation matrices, but we use a Laplace dispersal kernel.

The simulations for our model are given in Figure 4.2. The initial conditions are plotted in Figure 4.2(a) and are the same initial conditions used for the simulations in Figure 4.1. The initial density of each neutral fraction is given by $v_0^i(x) = \mathbb{1}_{-i<x\leq-(i-1)}$ where $\mathbb{1}$ is the indicator function. In Figure 4.2(b) since we are using the mutation matrix **M1** given by (4.16) there is only one mutation class. We can see that the stable distribution of neutral fraction is given by $\mathbf{r}_1 = [0.1377, 0.2229, 0.2179, 0.2932, 0.1283]^T$ and is the same distribution as calculated using Theorems 4.4.3 and 4.4.4. This suggests that the dispersal kernel does not affect the asymptotic proportion, as expected, since the asymptotic proportion calculated by our main theorems is independent of the dispersal parameters. The stable distribution can be seen by the dashed lines in Figure 4.2(b). In Figure 4.2(c), we can see that the spread to the right and left have different neutral fractions because of the initial distribution of neutral fractions and because the mutation matrix **M2** given by (4.17) is block diagonal primitive with two blocks. The asymptotic distribution of neutral fractions for the first mutation class $\{1, 2\}$ in the rightward spread is $\mathbf{r}_1 = [0.25, 0.75]^T$. This is seen by the dashed lines in Figure 4.2(c). The asymptotic distribution of neutral fractions for the second mutation class $\{3, 4, 5\}$ in the leftward spread is $\mathbf{r}_2 = [0.225, 0.525, 0.25]^T$. This is seen by the solid lines in Figure 4.2(c). Notice that these proportions are again the same

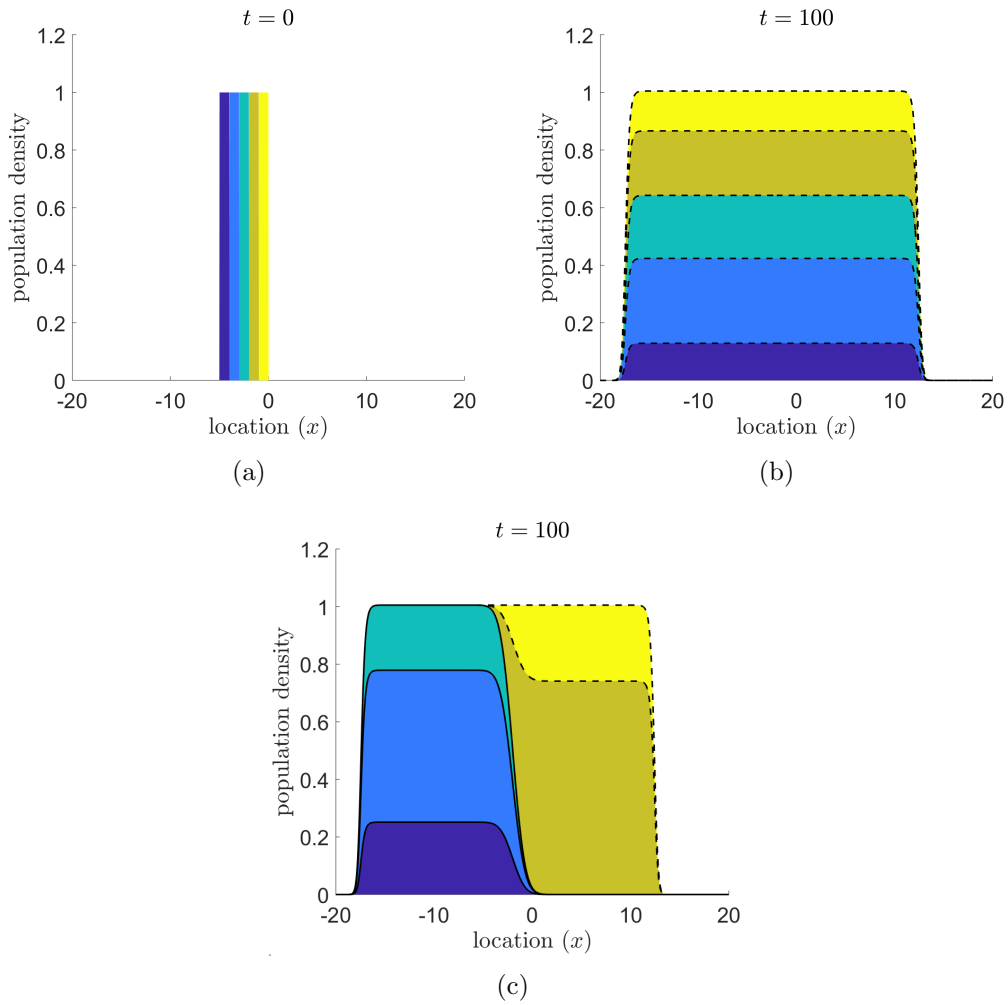

Figure 4.2: Numerical realization of (4.19) for the parameter values $b = \sqrt{0.005}$, $\mu = 0$, $R = 2$, $K = 1$. We chose b and μ this way so that the mean and variance for the Laplace kernel is the same as the Gaussian kernel used for the simulations in Figure 4.1. Figure 4.2(a) is the initial condition for the simulations seen in Figures 4.2(b) and 4.2(c). In 4.2(b) we use the mutation matrix **M1** given by (4.16). The dashed lines in Figure 4.2(b) give the asymptotic proportion of neutral fractions as calculated in Theorem 4.4.3. In 4.2(c) we use the mutation matrix **M2** given by (4.17). The dashed lines in Figure 4.2(c) give the rightward asymptotic proportion of neutral fractions and the solid lines in Figure 4.2(c) give the leftward asymptotic proportion of neutral fractions.

as suggested by Theorems 4.4.3 and 4.4.4.

Next, we consider a mutation matrix where the mutation classes are weakly

linked. An example of this can be seen in the following matrix,

$$\mathbf{M3} = \begin{bmatrix} 0.97 & 0.01 & 0 & 0 & 0 \\ 0.03 & 0.99 & \varepsilon & 0 & 0 \\ 0 & 0 & 0.92 - \varepsilon & 0.02 & 0.03 \\ 0 & 0 & 0.06 & 0.96 & 0.03 \\ 0 & 0 & 0.02 & 0.02 & 0.94 \end{bmatrix} \tag{4.20}$$

where ε is small. In this scenario, we see that there is only one mutation class because of the weak linkage parameter ε. This matrix structure violates Assumption $A2$ because it is not block primitive or irreducible as the bottom left block of the matrix is always zero. The structure of this matrix suggests that eventually all neutral fractions should become one of the first two types. For our simulation with this mutation matrix, we use a Gaussian dispersal kernel and Beverton-Holt growth function as given by (4.15). We can see a simulation of this in Figure 4.3.

For the mutation matrix **M3** we can see that it has one eigenvalue of 1 with eigenvector $\mathbf{r}_1 = [0.25, 0.75, 0, 0, 0]$. Thus, in this scenario, we conjecture that the asymptotic distribution of neutral fractions is given by $\mathbf{r}_1$. To test this conjecture, we simulate the model in Figure 4.3. One thing to note from Figure 4.3 is the amount time it takes to converge to the asymptotic proportion. Here we see that the leftward moving front takes over two thousand generations to reach the steady state. This is due to the fact that there is only one weak linkage, ε, between $\{3, 4, 5\}$ and $\{1, 2\}$.

4.6 Discussion

By incorporating mutations of neutral fractions into a scalar inside dynamics model, we developed a neutral mutation model to study the effect of mutations on the neutral genetic structure of an expanding population. In previous studies concerning the inside dynamics for scalar population models, the analysis concerns a single neutral fraction at a time (Marculis et al., 2017). In

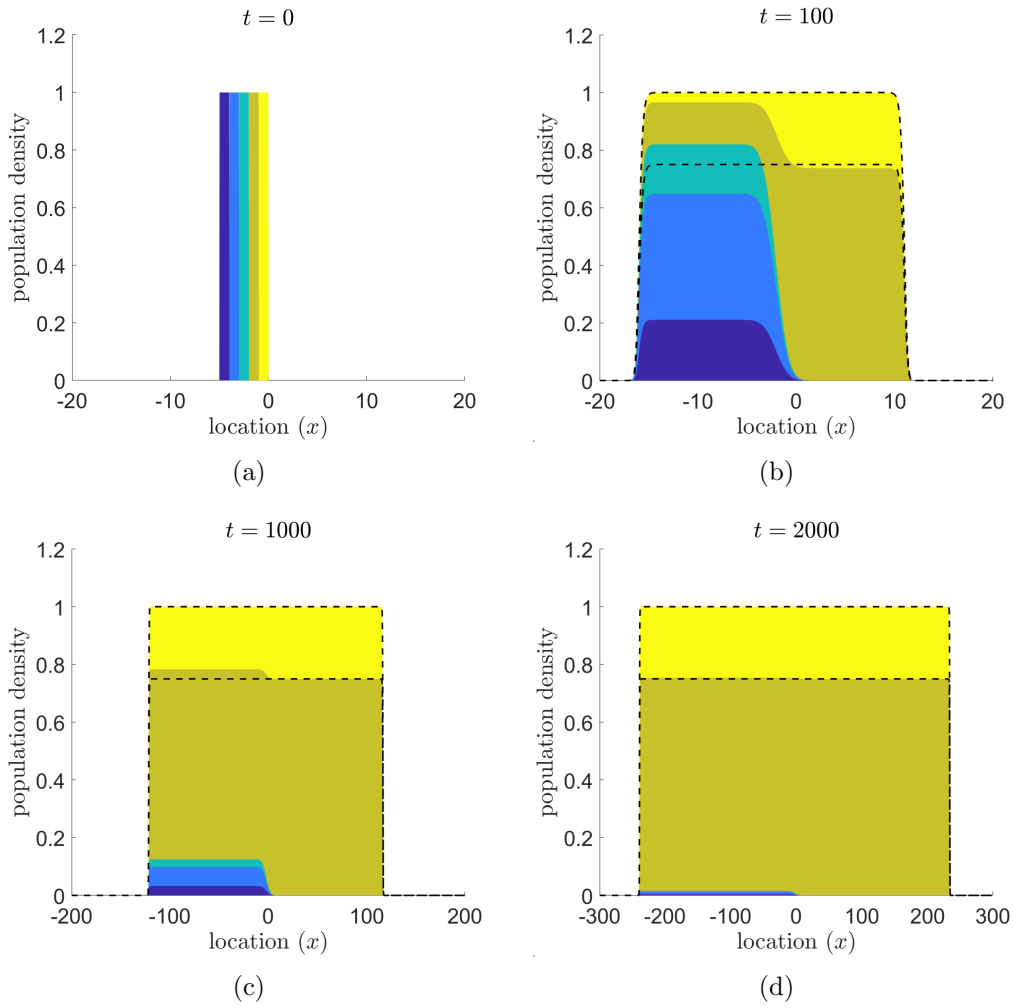

Figure 4.3: Numerical realization of (4.15) for the parameter values $\sigma^2 = 0.01$, $\mu = 0$, $R = 2$, $K = 1$ with the mutation matrix **M3** given by (4.20) where $\varepsilon = 0.01$. Figure 4.1(a) is the initial condition for the simulations seen in Figures 4.3(b), 4.3(c), and 4.3(d). The dashed lines in Figure 4.3(b), 4.3(c), and 4.3(d) are the conjectured asymptotic proportion of neutral fractions.

our model, the interactions between the neutral fractions by mutation require us to analyze a system of equations for the neutral fractions. By studying a system we must include an assumption on the interactions so as to prove the asymptotic results presented in Section 5.3.

We derive our model from the scalar inside dynamics integrodifference equation in Section 4.2. To include the mutations in our model, we allow

for neutral fractions to mutate into one another with a given probability. The molecular clock hypothesis states that genes evolve at a relatively constant rate over time (Ho, 2008). Thus, our model is in line with the molecular clock hypothesis because we assume a constant probability of mutation over time. This modeling framework is commonly referred to in the genetic literature as a substitution model. The addition of mutations changes the model by now having interactions between neutral fractions that are governed by a mutation matrix.

In Section 4.3 we lay out some of the key definitions and assumptions for our model. In particular, we assume that the interactions are simply mutation probabilities and the matrix structure is Markov. We make the additional assumption that the mutation matrix is block diagonal primitive. These assumptions are given in Assumption $A1$. The block diagonal assumption allows for us to have multiple mutation classes and the primitive assumption states that at some point in time, mutations can occur between all neutral fractions in a given block. This assumption is necessary so we can apply the Perron-Frobenius theorem in the proofs of our results. We also must assume that our maximum per-capita growth rate occurs at low density; see Assumption $A2$. This is required so we can compute the asymptotic spreading speed for the expanding population. In Assumption $A3$, we assume that the dispersal behavior is governed by a Gaussian probability density function. This assumption is needed for mathematical convenience. Our final and fourth assumption is related to the decay rate of the traveling wave for the linear equation. This assumption takes a different form in each of our four theorems.

The results in Section 5.3 are divided into four theorems. We first show when neutral fractions converge to zero uniformly in a moving half-frame. These results are provided in Theorems 4.4.1 and 4.4.2. We see that this happens when the neutral fractions in a given mutation class are not initially

present at the leading edge of the expansion. In Theorems 4.4.3 and 4.4.4, we show that the only neutral fractions that matter are those at the leading edge and are in the accompanying mutation class. Moreover, Theorems 4.4.3 and 4.4.4 show that the proportion of neutral fractions is given by the right dominant eigenvector of the mutation matrix for the mutation class that was initially present at the leading edge of the population.

Our results only apply to a certain class of models. While the mutation matrix is quite general, the assumptions on the dispersal and demography in the model are somewhat restrictive. First, we make the assumption that the mutation matrix is block primitive on top of the Markov structure. This assumption is needed to apply the Perron-Frobenius theorem guaranteeing that we have a dominant eigenvalue. We also assume that our growth function is bounded by its value at zero. This assumption does not allow for growth functions with Allee effects which we know from the scalar model to produce interesting asymptotic dynamics (Marculis et al., 2017). In addition we assume that the dispersal kernel is Gaussian. While this is needed for mathematical convenience, we conjecture that this assumption should be able to be weakened to an assumption that the dispersal kernel is thin-tailed since the results for the asymptotic proportion of each neutral fraction is independent of the parameters from the dispersal kernel. We should also mention that our fourth assumption is restrictive in the sense that we require our initial condition to decay exactly like the traveling wave for the linear equation. We also conjecture that it should be possible to relax this assumption.

Our numerical simulations in Section 4.5 provide some examples illustrating the results of our theorems in Section 5.3. In Figure 4.1, we consider two different kinds of mutation matrices. The first mutation matrix is primitive and only contains one mutation class because every neutral fraction can mutate into one another. Thus, we see that all neutral fractions contribute the

spread of the population and each neutral fraction converges to a proportion of the traveling wave solution. The result of the simulation is seen in Figure 4.1(b). In the second example, the mutation matrix has two mutation classes and we see the spread of one mutation class to the right and the spread of the other mutation class to the left in Figure 4.1(c). This is because of the initial positioning of the neutral fractions as seen in Figure 4.1(a). Therefore, we conclude that the spread of the neutral fractions is dependent on the initial positioning of each neutral fraction as well as the structure of the mutation matrix.

We also provided simulations for a Laplace dispersal kernel as seen in Figure 4.2. These simulations show that by only changing the form of the dispersal kernel, we can obtain the same asymptotic proportion of neutral fractions as seen in Figure 4.1. Recall that Assumption $A3$ in our theorems require the dispersal kernel to be Gaussian. Thus, we cannot apply the results of our theorems to this simulation, but since the asymptotic proportion is the same this suggests that we should be able to extend the results of our main theorems to a more general class of thin-tailed dispersal kernels. We were not able to rigorously prove this result and instead leave this conjecture for future analysis.

In addition, we numerically examined a mutation matrix structure that does not satisfy Assumption $A1$ of our main theorems. In particular, we constructed a mutation matrix that is not block diagonal primitive. This matrix is similar to our second example with two mutation classes, but we include a small parameter to introduce a weak linkage between the two mutation classes. This matrix is given by (4.20). We see that the weak linkage only allows for individuals to mutate from the second mutation class $\{3, 4, 5\}$ to the first mutation class $\{1, 2\}$. In particular, we see that the weak linkage is a small mutation probability from neutral fraction 3 to 2. Thus, because of this structure, we expect that eventually all individuals will be in the first muta-

tion class regardless of the initial distribution of individuals. The simulations for this model are given in Figure 4.3. The initial condition for the neutral fractions is seen in Figure 4.3(a). Then, the dynamics of the neutral fractions is seen in Figures 4.3(b)-4.3(d). We see that the asymptotic distribution of neutral fractions is given by the right eigenvector corresponding to eigenvalue 1. However, convergence to the asymptotic distribution takes a long time because of the weak linkage. We conjecture that if the linkage were larger or if there were more linkages then we expect the convergence to the asymptotic proportion would be faster.

By adding the complexity of mutations into the modeling framework, we are able to obtain interesting dynamics that are not seen in scalar models that have no mutations. Unlike the scalar model case, we find that multiple neutral fractions can contribute to the spread of the population in absence of an Allee effect. Thus, we can conclude that these neutral mutations and their structure are an important driver of maintaining genetic diversity in an expanding population. This conclusion agrees with previous studies that have shown range expansions affect the neutral genetic variation of the population (Excoffier et al., 2009; Lehe et al., 2012).

Other spatial models have shown that neutral mutations at the leading edge of a range expansion sometimes surf on the wave (Edmonds et al., 2004; Klopfstein et al., 2006). In particular, one study found that due to the gene surfing, the mutations reach a larger spatial distribution and higher frequency than would be expected in stationary populations (Edmonds et al., 2004). Our results agree with these studies that the neutral mutations at the leading edge are the drivers of the population spread. However, our model predicts that the spatial distribution of neutral fractions at the leading edge is the same as what would be expected in a stationary population. The primary conclusion for another simulation based model found that the final spatial and frequency

distributions depend on the local size of a subdivided population (Klopfstein et al., 2006). We showed that the asymptotic distribution of neutral fractions is dependent on what individuals were at the leading edge, however, our asymptotic proportion we calculate does not depend on on the initial size of the population. We believe that these differences arise because the way we incorporate mutations is deterministic, but gene surfing is an inherently stochastic process. Thus, in some sense our model describes the average behavior as seen from many realizations of the stochastic process of spread.

Overall, our results show how adding neutral mutations to a model can strongly influence the spread of neutral fractions. We find that the mutation matrix structure and the initial distribution of neutral fractions are important drivers in determining the spread of neutral fractions. However, it should be noted that our model structure is restricted to consider mutations between neutral fractions, so there is no selection occurring in the population dynamics. The mutations are incorporated into the model through a matrix where there are constant probabilities of mutations occurs between individuals. Even though this mutation matrix structure is very general, there are still other ways of including mutation dynamics that could be explored such as including stochastic mutation probabilities. The results we were able to prove in our four theorems relied upon somewhat restrictive assumptions. First, we make the assumption throughout every theorem that the dispersal kernel is Gaussian. However, since our numerical simulations find that our asymptotic proportion does not directly depend on the Gaussian kernel parameters, we conjecture that our result should extend to a larger class of thin-tailed dispersal kernels. Second, the assumption of block primitivity placed on the mutation matrix is not always satisfied for biological realistic models. We illustrate this with the weak connectivity example. Finally, the assumptions on the initial conditions for Theorems 4.4.3 and 4.4.4 are not realistic, because they become

unbounded for large x, even though the predictions of the theorems appear to hold when the assumptions are relaxed. The ability to analyze a model where this assumption is relaxed to something that more closely resembles the profile of the traveling wave solution would generalize our result to a more realistic initial condition.

4.7 Appendix

4.7.1 Derivation of a general mutation matrix

Here we show how one can generalize the assumption of a single locus with n different neutral alleles to m loci with two neutral alleles. Let there be m independent loci a_i, $1 \leq i \leq m$, where each loci has one of two possible alleles, $a_i = 0$ or $a_i = 1$. Then we define the transition probabilities as follows:

$$\Pr\{a_i = 0 \to a_i = 1\} = q_i \text{ and } \Pr\{a_i = 1 \to a_i = 0\} = r_i. \tag{4.21}$$

We index this process by $t \in \mathbb{N}$ where t describes the number of possible transitions taken so far. There are 2^m possible states for this system. Let $n = 2^m$ and let the probability of being in state j, $1 \leq j \leq n$, be given by v^j where the state is

$$j = 1 + \sum_{i=1}^{m} a_i 2^{i-1}. \tag{4.22}$$

In the case when $m = 2$, there are four total states. We denote our states in the following form,

$$\begin{pmatrix} a_1 \\ a_2 \end{pmatrix}. \tag{4.23}$$

Our indexing for j gives the following relationship between the state and the index as follows:

Index	$j = 1$	$j = 2$	$j = 3$	$j = 4$
State	$\begin{pmatrix} 0 \\ 0 \end{pmatrix}$	$\begin{pmatrix} 1 \\ 0 \end{pmatrix}$	$\begin{pmatrix} 0 \\ 1 \end{pmatrix}$	$\begin{pmatrix} 1 \\ 1 \end{pmatrix}$

.

By letting $m_{jl} = \Pr\{v^j \to v^l\}$, then the mutation matrix becomes

$$\mathbf{M} = \begin{bmatrix} (1-q_1)(1-q_2) & r_1(1-q_2) & (1-q_1)r_2 & r_1 r_2 \\ q_1(1-q_2) & (1-r_1)(1-q_2) & q_1 r_2 & (1-r_1)r_2 \\ (1-q_1)q_2 & r_1 q_2 & (1-q_1)(1-r_2) & r_1(1-r_2) \\ q_1 q_2 & (1-r_1)q_2 & q_1(1-r_2) & (1-r_1)(1-r_2) \end{bmatrix}. \tag{4.24}$$

From this example, one can deduce how to generalize this process for more than two neutral alleles making the structure of this mutation matrix quite general.

4.7.2 Proofs of the theorems

Proof of Theorem 4.4.1

Proof. Without loss of generality, we can assume that neutral fraction i belongs to the mutation class q. Then, since $\mathbf{M}$ is block diagonal, we only need to consider the following equation

$$\mathbf{v}_{q,t+1}(x) = \mathbf{M}_q \int_{-\infty}^{\infty} k(x-y) g(u_t(y)) \mathbf{v}_{q,t}(y)\, dy. \tag{4.25}$$

Using the fact that $0 < g(u) \leq g(0)$ for all $u \in (0,1)$ we can use a comparison principle to show that a new sequence $\mathbf{w}_{q,t}(x)$ defined by

$$\mathbf{w}_{q,t+1}(x) = g(0)\mathbf{M}_q \int_{-\infty}^{\infty} k(x-y) \mathbf{w}_{q,t}(y)\, dy \tag{4.26}$$

is always greater than the solution to any neutral fraction, $\mathbf{v}_{q,t}(x)$, with the same initial condition $\mathbf{w}_{q,0}(x) = \mathbf{v}_{q,0}(x)$. The solution of (4.26) is given by the t-fold convolution

$$\mathbf{w}_{q,t}(x) = [g(0)\mathbf{M}_q]^t\, k^{*t} \mathbf{w}_{q,0}(x). \tag{4.27}$$

Applying the reflected bilateral Laplace transform to (4.27) and using the

convolution theorem, we obtain

$$\mathcal{M}[\mathbf{w}_{q,t}(x)](s) = [g(0)\mathbf{M}_q]^t \left[\mathcal{M}\left[k(x)\right](s)\right]^t \mathcal{M}\left[\mathbf{w}_{q,0}(x)\right](s) \tag{4.28}$$

$$= [g(0)\mathbf{M}_q]^t \left[e^{\frac{\sigma^2 s^2}{2}+\mu s}\right]^t \mathcal{M}\left[\mathbf{w}_{q,0}(x)\right](s) \tag{4.29}$$

$$= [g(0)\mathbf{M}_q]^t e^{\frac{\sigma^2 t s^2}{2}+\mu t s} \mathcal{M}\left[\mathbf{w}_{q,0}(x)\right](s) \tag{4.30}$$

$$= [g(0)\mathbf{M}_q]^t \mathcal{M}\left[\frac{1}{\sqrt{2\pi\sigma^2 t}} e^{-\frac{(x-\mu t)^2}{2\sigma^2 t}}\right](s) \mathcal{M}\left[\mathbf{w}_{q,0}(x)\right](s) \tag{4.31}$$

$$= [g(0)\mathbf{M}_q]^t \mathcal{M}\left[(k_t * \mathbf{w}_{q,0})(x)\right](s) \tag{4.32}$$

where k_t is Gaussian with mean μt and variance $\sigma^2 t$. Then applying the inverse transform yields

$$\mathbf{w}_{q,t}(x) = [g(0)\mathbf{M}_q]^t (k_t * \mathbf{w}_{q,0})(x) \tag{4.33}$$

$$= [g(0)\mathbf{M}_q]^t \int_{-\infty}^{\infty} \frac{1}{\sqrt{2\pi\sigma^2 t}} e^{-\frac{(x-y-\mu t)^2}{2\sigma^2 t}} \mathbf{w}_{q,0}(y)\, dy. \tag{4.34}$$

In the moving half-frame with fixed $A \in \mathbb{R}$, consider the element $x_0 + ct$ with $c \geq c^* = \sqrt{2\sigma^2 \ln(g(0))} + \mu$. When we rewrite $\mathbf{w}_{q,t}(x)$ in this moving half-frame we have

$$\mathbf{w}_{q,t}(x_0 + ct) = [g(0)\mathbf{M}_q]^t \int_{-\infty}^{\infty} \frac{1}{\sqrt{2\pi\sigma^2 t}} e^{-\frac{(x_0+ct-y-\mu t)^2}{2\sigma^2 t}} \mathbf{w}_{q,0}(y)\, dy. \tag{4.35}$$

Expanding in the exponential, yields

$$\frac{(x_0 + ct - y - \mu t)^2}{2\sigma^2 t} = \frac{(x_0 - y)^2}{2\sigma^2 t} + \frac{2(c-\mu)t(x_0 - y) + (c-\mu)^2 t^2}{2\sigma^2 t} \tag{4.36}$$

$$\geq \frac{(x_0 - y)^2}{2\sigma^2 t} + \frac{c-\mu}{\sigma^2}(x_0 - y) + \ln(g(0))t. \tag{4.37}$$

Thus,

$$\mathbf{w}_{q,t}(x_0 + ct) \leq \mathbf{M}_q^t \frac{e^{\ln(g(0))t}}{\sqrt{2\pi\sigma^2 t}} \int_{-\infty}^{\infty} e^{-\frac{(x_0-y)^2}{2\sigma^2 t}} e^{-\frac{c-\mu}{\sigma^2}(x_0-y)} e^{-\ln(g(0))t} \mathbf{w}_{q,0}(y)\, dy \tag{4.38}$$

$$= \mathbf{M}_q^t \frac{1}{\sqrt{2\pi\sigma^2 t}} \int_{-\infty}^{\infty} e^{-\frac{(x_0-y)^2}{2\sigma^2 t}} e^{-\frac{c-\mu}{\sigma^2}(x_0-y)} \mathbf{w}_{q,0}(y)\, dy \tag{4.39}$$

$$= \mathbf{M}_q^t \frac{e^{-\frac{c-\mu}{\sigma^2}x_0}}{\sqrt{2\pi\sigma^2 t}} \int_{-\infty}^{\infty} e^{-\frac{(x_0-y)^2}{2\sigma^2 t}} e^{\frac{c-\mu}{\sigma^2}y} \mathbf{w}_{q,0}(y)\, dy. \tag{4.40}$$

Since $x_0 \geq A$ we have

$$\mathbf{w}_{q,t}(x_0 + ct) \leq \mathbf{M}_q^t \frac{e^{-\frac{A(c-\mu)}{\sigma^2}}}{\sqrt{2\pi\sigma^2 t}} \int_{-\infty}^{\infty} e^{\frac{c-\mu}{\sigma^2}y} \mathbf{w}_{q,0}(y)\, dy. \tag{4.41}$$

Since $\mathbf{M}_q$ is a Markov matrix, we know that $\lim_{t\to\infty} \mathbf{M}_q^t = [\mathbf{r}_q, \ldots, \mathbf{r}_q]$ where $\mathbf{r}_q$ is the right eigenvector of $\mathbf{M}_q$ corresponding to eigenvalue 1 such that $\sum_{i=1} r_{q,i} = 1$. By Assumption $A4$, $\int_{-\infty}^{\infty} e^{\frac{c-\mu}{\sigma^2}y} w_{q,0}^i(y)\, dy < \infty$ for every i in mutation class q we have $w_{q,t}^i(x_0 + ct) \to 0$ uniformly as $t \to \infty$ in $[A, \infty)$. Recall that w_q^i was constructed so that $0 \leq v_{q,t}^i(x) \leq w_{q,t}^i(x)$. This implies the uniform convergence of $v_t^i(x) \to 0$ as $t \to \infty$ in the moving half-frame $[A + ct, \infty)$ for each i in mutation class q. The proof of Theorem 4.4.1 is complete. □

Proof of Theorem 4.4.2

Proof. Repeat the proof of Theorem 4.4.1 in the left moving half-frame with fixed $A \in \mathbb{R}$ and consider the element $x_0 - ct$ with $c \geq c_-^* = \sqrt{2\sigma^2 \ln(g(0))} - \mu$. From this change, the result follows in the same manner as in Theorem 4.4.1. □

Proof of Theorem 4.4.3

Proof. Without loss of generality we may assume that neutral fraction i belongs to mutation class q. Using the fact that $g(u) \leq g(0)$ for all $u \in (0, 1)$ we can use a comparison principle to show that a new sequence $\mathbf{w}_{q,t}(x)$ defined by

$$\mathbf{w}_{q,t+1}(x) = g(0)\mathbf{M}_q \int_{-\infty}^{\infty} k(x - y)\mathbf{w}_{q,t}(y)\, dy \tag{4.42}$$

is a super-solution to any neutral fraction $\mathbf{v}_{q,t}(x)$ with the same initial condition $\mathbf{w}_{q,0}(x) = \mathbf{v}_{q,0}(x)$. By iterating, we can write the solution to Equation (4.42) as the t-fold convolution

$$\mathbf{w}_{q,t}(x) = [g(0)\mathbf{M}_q]^t\, k^{*t}(x - y)\mathbf{w}_{q,0}(y). \tag{4.43}$$

Taking the bilateral Laplace transform

$$\mathcal{M}[\mathbf{w}_{q,t}(x)](s) = [g(0)\mathbf{M}_q]^t \left[\mathcal{M}[k(x)](s)\right]^t \mathcal{M}[\mathbf{w}_{q,0}(x)](s). \tag{4.44}$$

Since the dispersal kernel is Gaussian, we know that $\mathcal{M}[k(x)](s) = e^{\frac{\sigma^2 s^2}{2} + \mu s}$. Then, we can see that

$$\left[\mathcal{M}[k(x)](s)\right]^t \mathcal{M}[\mathbf{w}_{q,0}(x)](s) = \mathcal{M}\left[(k_t * \mathbf{w}_{q,0})(x)\right](s) \tag{4.45}$$

where k_t is Gaussian with mean μt and variance $\sigma^2 t$. Thus, we have

$$\mathcal{M}[\mathbf{w}_{q,t}(x)](s) = [g(0)\mathbf{M}_q]^t \, \mathcal{M}\left[(k_t * \mathbf{w}_{q,0})(x)\right](s). \tag{4.46}$$

Then applying the inverse transform yields

$$\mathbf{w}_{q,t}(x) = [g(0)\mathbf{M}_q]^t \int_{-\infty}^{\infty} \frac{1}{\sqrt{2\pi\sigma^2 t}} e^{-\frac{(x-y-\mu t)^2}{2\sigma^2 t}} \mathbf{w}_{q,0}(y)\, dy. \tag{4.47}$$

In the moving half-frame $[A + ct, \infty)$ with fixed $A \in \mathbb{R}$, consider the element $x_0 + ct$ with $c = c^* = \sqrt{2\sigma^2 \ln(g(0))} + \mu$. When we rewrite $\mathbf{w}_{q,t}(x)$ in this moving half-frame we have

$$\mathbf{w}_{q,t}(x_0 + ct) = [g(0)\mathbf{M}_q]^t \int_{-\infty}^{\infty} \frac{1}{\sqrt{2\pi\sigma^2 t}} e^{-\frac{(x_0+ct-y-\mu t)^2}{2\sigma^2 t}} \mathbf{w}_{q,0}(y)\, dy. \tag{4.48}$$

Expanding the exponent, yields

$$\begin{aligned} \frac{(x_0 + ct - y - \mu t)^2}{2\sigma^2 t} &= \frac{(y - x_0)^2}{2\sigma^2 t} + \frac{(c-\mu)(x_0 - y)}{\sigma^2} + \frac{(c-\mu)^2}{2\sigma^2} t & (4.49) \\ &= \frac{(y - x_0)^2}{2\sigma^2 t} + \frac{(c-\mu)(x_0 - y)}{\sigma^2} + \ln(g(0))t. & (4.50) \end{aligned}$$

Thus,

$$\begin{aligned} \mathbf{w}_{q,t}(x_0 + ct) &= \frac{[g(0)\mathbf{M}_q]^t}{\sqrt{2\pi\sigma^2 t}} \int_{-\infty}^{\infty} e^{-\frac{(y-x_0)^2}{2\sigma^2 t}} e^{-\frac{(c-\mu)(x_0-y)}{\sigma^2}} e^{-g(0)t} \mathbf{w}_{q,0}(y)\, dy & (4.51) \\ &= \frac{\mathbf{M}_q^t}{\sqrt{2\pi\sigma^2 t}} \int_{-\infty}^{\infty} e^{-\frac{(y-x_0)^2}{2\sigma^2 t}} e^{-\frac{(c-\mu)(x_0-y)}{\sigma^2}} \mathbf{w}_{q,0}(y)\, dy. & (4.52) \end{aligned}$$

By Assumption $A4'$, $\mathbf{w}_{q,0}(y) = \mathbf{p}_{q,0} e^{-\frac{c-\mu}{\sigma^2} y}$. Thus,

$$\begin{aligned} \mathbf{w}_{q,t}(x_0 + ct) &= \mathbf{M}_q^t \mathbf{p}_{q,0} e^{-\frac{(c-\mu)}{\sigma^2} x_0} \frac{1}{\sqrt{2\pi\sigma^2 t}} \int_{-\infty}^{\infty} e^{-\frac{(y-x_0)^2}{2\sigma^2 t}}\, dy & (4.53) \\ &= \mathbf{M}_q^t \mathbf{p}_{q,0} e^{-\frac{(c-\mu)}{\sigma^2} x_0}. & (4.54) \end{aligned}$$

Since $\mathbf{M}_q$ is a Markov matrix, we know that

$$\lim_{t\to\infty} \mathbf{M}_q^t = \begin{bmatrix} \mathbf{r}_q & \mathbf{r}_q & \dots & \mathbf{r}_q \end{bmatrix} \tag{4.55}$$

where $\mathbf{r}_q$ is the right eigenvector of $\mathbf{M}_q$ corresponding to eigenvalue 1 normalized such that $\sum_{j=1}^{m_q} r_{q,j} = 1$. Thus,

$$\lim_{t\to\infty} \mathbf{w}_t(x_0 + ct) = \lim_{t\to\infty} \mathbf{M}_q^t \mathbf{p}_{q,0} e^{-\frac{(c-\mu)}{\sigma^2} x_0} \tag{4.56}$$

$$= \begin{bmatrix} \mathbf{r}_q & \mathbf{r}_q & \dots & \mathbf{r}_q \end{bmatrix} \mathbf{p}_{q,0} e^{-\frac{(c-\mu)}{\sigma^2} x_0} \tag{4.57}$$

$$= \mathbf{r}_q e^{-\frac{(c-\mu)}{\sigma^2} x_0}. \tag{4.58}$$

since $\sum_{j=1}^{m_q} p_{q,0,j} = 1$. From the above calculations, we find that the super-solution approaches a proportion of the traveling wave for the linear equation. Next, we move onto our sub-solution. We define

$$g_{sub}(u;\varepsilon) = \begin{cases} (1-\varepsilon)g(0) & \text{for } 0 \le u < \delta \\ g(u) & \text{for } u \ge \delta \end{cases} \tag{4.59}$$

where for any $0 < \varepsilon \ll 1$, δ is chosen such that $(1-\varepsilon)g(0)\delta = g(\delta)\delta$. Then,

$$\mathbf{z}_{q,t+1}(x) = \int_{-\infty}^{\infty} k(x-y) g_{sub}(u_t(y);\varepsilon) \mathbf{M}_q \mathbf{z}_{q,t}(y)\, dy \tag{4.60}$$

with $\mathbf{z}_{q,0}(x) = \mathbf{v}_{q,0}(x)$ is a sub-solution of $\mathbf{v}_{q,t}(x)$ by the comparison principle since $g_{sub}(u;\varepsilon)\mathbf{v} \le g(u)\mathbf{v}$ for all $\mathbf{v} \ge 0$. In the moving half-frame $[A + c(\varepsilon)t, \infty)$ with fixed $A \in \mathbb{R}$, consider the element $x_0 + c(\varepsilon)t$ large enough such that $u < \delta$ with $c(\varepsilon) = \sqrt{2\sigma^2 \ln((1-\varepsilon)g(0))} + \mu$. Then,

$$\mathbf{z}_{q,t+1}(x_0 + c(\varepsilon)t) = \int_{-\infty}^{\infty} k(x_0 + c(\varepsilon) - y)(1-\varepsilon)g(0)\mathbf{M}_q \mathbf{z}_{q,t}(y)\, dy. \tag{4.61}$$

By iterating, we can write the solution to Equation (4.61) as the t-fold convolution

$$\mathbf{z}_{q,t}(x_0 + c(\varepsilon)t) = \left[(1-\varepsilon)g(0)\mathbf{M}_q\right]^t \left[k(x_0 + c(\varepsilon)t - y)\right]^{*t} \mathbf{z}_{q,0}(y). \tag{4.62}$$

Since we assumed that all of the dispersal kernels are Gaussian, by repeating calculations done previously we find that

$$\mathbf{z}_{q,t}(x_0 + c(\varepsilon)t) = [(1-\varepsilon)g(0)\mathbf{M}_q]^t \int_{-\infty}^{\infty} \frac{1}{\sqrt{2\pi\sigma^2 t}} e^{-\frac{(x_0+c(\varepsilon)t-y-\mu t)^2}{2\sigma^2 t}} \mathbf{z}_{q,0}(y)\, dy \tag{4.63}$$

$$= \frac{[(1-\varepsilon)g(0)\mathbf{M}_q]^t}{\sqrt{2\pi\sigma^2 t}} \int_{-\infty}^{\infty} e^{-\frac{(x_0-y)^2}{2\sigma^2 t}} e^{-\frac{(c(\varepsilon)-\mu)(x_0-y)}{\sigma^2}} e^{-\frac{(c(\varepsilon)-\mu)^2}{2\sigma^2}t} \mathbf{z}_{q,0}(y)\, dy. \tag{4.64}$$

Then,

$$\mathbf{z}_{q,t}(x_0 + c(\varepsilon)t) = \mathbf{M}_q^t \frac{1}{\sqrt{2\pi\sigma^2 t}} \int_{-\infty}^{\infty} e^{-\frac{(x_0-y)^2}{2\sigma^2 t}} e^{-\frac{(c(\varepsilon)-\mu)(x_0-y)}{\sigma^2}} \mathbf{z}_{q,0}(y)\, dy. \tag{4.65}$$

Note that the integrand in (4.65) is nonnegative and integrable. Using Fatou's lemma we fix t and let $\varepsilon \to 0$, giving

$$\mathbf{z}_{q,t}(x_0 + ct) = \liminf_{\varepsilon\to 0} \mathbf{z}_{q,t}(x_0 + c(\varepsilon)t) \tag{4.66}$$

$$= \liminf_{\varepsilon\to 0} \mathbf{M}_q^t \frac{1}{\sqrt{2\pi\sigma^2 t}} \int_{-\infty}^{\infty} e^{-\frac{(x_0-y)^2}{2\sigma^2 t}} e^{-\frac{(c(\varepsilon)-\mu)(x_0-y)}{\sigma^2}} \mathbf{z}_{q,0}(y)\, dy \tag{4.67}$$

$$\geq \mathbf{M}_q^t \frac{1}{\sqrt{2\pi\sigma^2 t}} \int_{-\infty}^{\infty} \liminf_{\varepsilon\to 0} e^{-\frac{(x_0-y)^2}{2\sigma^2 t}} e^{-\frac{(c(\varepsilon)-\mu)(x_0-y)}{\sigma^2}} \mathbf{z}_{q,0}(y)\, dy \tag{4.68}$$

$$= \mathbf{M}_q^t \frac{1}{\sqrt{2\pi\sigma^2 t}} \int_{-\infty}^{\infty} e^{-\frac{(x_0-y)^2}{2\sigma^2 t}} e^{-\frac{(c-\mu)(x_0-y)}{\sigma^2}} \mathbf{z}_{q,0}(y)\, dy. \tag{4.69}$$

By assumption, $\mathbf{z}_{q,0}(y) = \mathbf{p}_{q,0} e^{-\frac{c-\mu}{\sigma^2}y}$. Thus,

$$\mathbf{z}_{q,t}(x_0 + ct) \geq \mathbf{M}_q^t \mathbf{p}_{q,0} e^{-\frac{(c-\mu)}{\sigma^2}x_0} \frac{1}{\sqrt{2\pi\sigma^2 t}} \int_{-\infty}^{\infty} e^{-\frac{(y-x_0)^2}{2\sigma^2 t}}\, dy \tag{4.70}$$

$$= \mathbf{M}_q^t \mathbf{p}_{q,0} e^{-\frac{(c-\mu)}{\sigma^2}x_0}. \tag{4.71}$$

Since $\mathbf{M}_q$ is a Markov matrix, we know that

$$\lim_{t\to\infty} \mathbf{M}_q^t = \begin{bmatrix} \mathbf{r}_q & \mathbf{r}_q & \dots & \mathbf{r}_q \end{bmatrix} \tag{4.72}$$

where $\mathbf{r}_q$ is the right eigenvector of $\mathbf{M}_q$ corresponding to eigenvalue 1 normalized such that $\sum_{j=1}^{m_q} r_{q,j} = 1$. Thus,

$$\lim_{t\to\infty} \mathbf{z}_{q,t}(x_0 + ct) \geq \lim_{t\to\infty} \mathbf{M}_q^t \mathbf{p}_{q,0} e^{-\frac{(c-\mu)}{\sigma^2}x_0} \tag{4.73}$$

$$= \begin{bmatrix} \mathbf{r}_q & \mathbf{r}_q & \dots & \mathbf{r}_q \end{bmatrix} \mathbf{p}_{q,0} e^{-\frac{(c-\mu)}{\sigma^2}x_0} \tag{4.74}$$

$$= \mathbf{r}_q e^{-\frac{(c-\mu)}{\sigma^2}x_0}. \tag{4.75}$$

since $\sum_{j=1}^{m_q} p_{q,0,j} = 1$. From the above calculations, we find that the sub-solution approaches a proportion of the traveling wave for the linear equation. Using our results from our super- and sub-solutions we see that

$$\mathbf{r}_q e^{-\frac{(c-\mu)}{\sigma^2}x_0} \leq \lim_{t\to\infty} \mathbf{z}_{q,t}(x_0+ct) \leq \lim_{t\to\infty} \mathbf{v}_{q,t}(x_0+ct) \leq \lim_{t\to\infty} \mathbf{w}_{q,t}(x_0+ct) = \mathbf{r}_q e^{-\frac{(c-\mu)}{\sigma^2}x_0}. \tag{4.76}$$

Thus,

$$\lim_{t\to\infty} \mathbf{v}_{q,t}(x_0+ct) = \mathbf{r}_q e^{-\frac{(c-\mu)}{\sigma^2}x_0}. \tag{4.77}$$

Therefore, asymptotically, our solution approaches a proportion of the traveling wave for the linear equation. The proof of Theorem 4.4.3 is complete. □

Proof of Theorem 4.4.4

Proof. Repeat the proof of Theorem 4.4.3 in the left moving half-frame with fixed $A \in \mathbb{R}$. For the super-solution, consider the element $x_0 - ct$ with $c = c_-^* = \sqrt{2\sigma^2 \ln(g(0))} - \mu$. For the sub-solution, consider the element $x_0 - c(\varepsilon)t$ with $c(\varepsilon) = \sqrt{2\sigma^2 \ln((1-\varepsilon)g(0))} - \mu$. Then the result follows in the same manner as in Theorem 4.4.3. □

References

Arenas, Miguel (2015). "Trends in substitution models of molecular evolution." *Frontiers in Genetics* 6, p. 319.

Bateman, Andrew W, Andreas Buttenschön, Kelley D Erickson, and Nathan G Marculis (2017). "Barnacles vs bullies: modelling biocontrol of the invasive European green crab using a castrating barnacle parasite." *Theoretical Ecology* 10.3, pp. 305–318.

Bonnefon, Olivier, Jérôme Coville, Jimmy Garnier, and Lionel Roques (2014). "Inside dynamics of solutions of integro-differential equations." *Discrete and Continuous Dynamical Systems-Series B* 19.10, pp. 3057–3085.

Bonnefon, Olivier, Jimmy Garnier, François Hamel, and Lionel Roques (2013). "Inside dynamics of delayed traveling waves." *Mathematical Modelling of Natural Phenomena* 8.3, pp. 42–59.

Bromham, Lindell and David Penny (2003). "The modern molecular clock." *Nature Reviews Genetics* 4.3, p. 216.

Cooley, James W and John W Tukey (1965). "An algorithm for the machine calculation of complex Fourier series." *Mathematics of Computation* 19.90, pp. 297–301.

Duret, Laurent (2008). "Neutral theory: the null hypothesis of molecular evolution." *Nature Education* 1, pp. 803–806.

Edmonds, Christopher A, Anita S Lillie, and L Luca Cavalli-Sforza (2004). "Mutations arising in the wave front of an expanding population." *Proceeds of the National Academy of Sciences* 101.4, pp. 975–979.

Excoffier, Laurent, Matthieu Foll, and Rémy J Petit (2009). "Genetic consequences of range expansions." *Annual Review of Ecology, Evolution, and Systematics* 40, pp. 481–501.

Excoffier, Laurent and Nicolas Ray (2008). "Surfing during population expansions promotes genetic revolutions and structuration." *Trends in Ecology & Evolution* 23.7, pp. 347–351.

Felsenstein, Joseph (1981). "Evolutionary trees from DNA sequences: a maximum likelihood approach." *Journal of Molecular Evolution* 17.6, pp. 368–376.

Garnier, Jimmy, Thomas Giletti, François Hamel, and Lionel Roques (2012). "Inside dynamics of pulled and pushed fronts." *Journal de Mathématiques Pures et Appliquées* 98.4, pp. 428–449.

Garnier, Jimmy and Mark A Lewis (2016). "Expansion under climate change: the genetic consequences." *Bulletin of Mathematical Biology* 78.11, pp. 2165–2185.

Hallatschek, Oskar, Pascal Hersen, Sharad Ramanathan, and David R Nelson (2007). "Genetic drift at expanding frontiers promotes gene segregation." *Proceedings of the National Academy of Sciences* 104.50, pp. 19926–19930.

Hallatschek, Oskar and David R Nelson (2008). "Gene surfing in expanding populations." *Theoretical Population Biology* 73.1, pp. 158–170.

Ho, Simon (2008). "The molecular clock and estimating species divergence." *Nature Education* 1.1, pp. 1–2.

Jukes, Thomas H and Charles R Cantor (1969). *Evolution of protein molecules. In 'Mammalian Protein Metabolism'.(Ed. HN Munro.) pp. 21–132.*

Kimura, Motoo (1980). "A simple method for estimating evolutionary rates of base substitutions through comparative studies of nucleotide sequences." *Journal of Molecular Evolution* 16.2, pp. 111–120.

Klopfstein, Seraina, Mathias Currat, and Laurent Excoffier (2006). "The fate of mutations surfing on the wave of a range expansion." *Molecular Biology and Evolution* 23.3, pp. 482–490.

Kot, Mark, Mark A Lewis, and Pauline van den Driessche (1996). "Dispersal data and the spread of invading organisms." *Ecology* 77.7, pp. 2027–2042.

Krkošek, Martin, Jean-Sébastien Lauzon-Guay, and Mark A Lewis (2007). "Relating dispersal and range expansion of California sea otters." *Theoretical Population Biology* 71.4, pp. 401–407.

Lehe, Rémi, Oskar Hallatschek, and Luca Peliti (2012). "The rate of beneficial mutations surfing on the wave of a range expansion." *PLoS Computational Biology* 8.3, e1002447.

Lewis, Mark A, Nathan G Marculis, and Zhongwei Shen (2018). "Integrodifference equations in the presence of climate change: persistence criterion, travelling waves and inside dynamics." *Journal of Mathematical Biology* 77.6-7, pp. 1649–1687.

Lewis, Mark A, Sergei V Petrovskii, and Jonathan R Potts (2016). *The Mathematics Behind Biological Invasions*. Vol. 44. Springer.

Lui, Roger (1983). "Existence and stability of travelling wave solutions of a nonlinear integral operator." *Journal of Mathematical Biology* 16.3, pp. 199–220.

Lutscher, Frithjof, Elizaveta Pachepsky, and Mark A Lewis (2005). "The effect of dispersal patterns on stream populations." *SIAM Review* 47.4, pp. 749–772.

Marculis, Nathan G, Jimmy Garnier, Roger Lui, and Mark A Lewis (2019). "Inside dynamics for stage-structured integrodifference equations." *Journal of Mathematical Biology* In Press.

Marculis, Nathan G, Roger Lui, and Mark A Lewis (2017). "Neutral Genetic Patterns for Expanding Populations with Nonoverlapping Generations." *Bulletin of Mathematical Biology* 79.4, pp. 828–852.

Mayr, Ernst (1940). "Speciation phenomena in birds." *The American Naturalist* 74.752, pp. 249–278.

Morin, Phillip A, Gordon Luikart, and Robert K Wayne (2004). "SNPs in ecology, evolution and conservation." *Trends in Ecology & Evolution* 19.4, pp. 208–216.

Reimer, Jody R, Michael B Bonsall, and Philip K Maini (2016). "Approximating the critical domain size of integrodifference equations." *Bulletin of Mathematical Biology* 78.1, pp. 72–109.

Roques, Lionel, Jimmy Garnier, François Hamel, and Etienne K Klein (2012). "Allee effect promotes diversity in traveling waves of colonization." *Proceedings of the National Academy of Sciences* 109.23, pp. 8828–8833.

Roques, Lionel, Yuzo Hosono, Olivier Bonnefon, and Thomas Boivin (2015). "The effect of competition on the neutral intraspecific diversity of invasive species." *Journal of Mathematical Biology* 71.2, pp. 465–489.

Selkoe, Kimberly A and Robert J Toonen (2006). "Microsatellites for ecologists: a practical guide to using and evaluating microsatellite markers." *Ecology Letters* 9.5, pp. 615–629.

Slatkin, Montgomery and Laurent Excoffier (2012). "Serial founder effects during range expansion: a spatial analog of genetic drift." *Genetics* 191.1, pp. 171–181.

Stokes, AN (1976). "On two types of moving front in quasilinear diffusion." *Mathematical Biosciences* 31.3-4, pp. 307–315.

Van Kirk, Rob W and Mark A Lewis (1997). "Integrodifference models for persistence in fragmented habitats." *Bulletin of Mathematical Biology* 59.1, p. 107.

Weinberger, Hans F (1982). "Long-time behavior of a class of biological models." *SIAM Journal on Mathematical Analysis* 13.3, pp. 353–396.

Zhou, Ying and Mark Kot (2011). "Discrete-time growth-dispersal models with shifting species ranges." *Theoretical Ecology* 4.1, pp. 13–25.

Chapter 5

Modeling the dispersal-reproduction trade-off in an expanding population

5.1 Introduction

The principle of allocation states that if an organism has limited resources, then energy allocation to one function reduces the amount of energy available to all other functions (Cody, 1966). Under resource limitation, it can be assumed that an inherent trade-off will usually occur between different functions. There are a variety of trade-off effects that occur in populations such as behavioral trade-offs (Cressler et al., 2010; Verdolin, 2006), evolutionary trade-offs (Burton et al., 2010; Hughes et al., 2003; Yoshida et al., 2004), and life history trade-offs (Hanski et al., 2006; Zera and Harshman, 2001). In this work, we are interested in the life history trade-off between dispersal and reproduction. That is, by the principle of allocation we will consider the case in our study in which the further an individual disperses the fewer resources it will have for reproduction and vice versa.

The empirical evidence for the dispersal-reproduction trade-off effect in natural ecosystems occurs in a variety of insect species (Duthie et al., 2014; Elliott and Evenden, 2012; Hanski et al., 2006; Hughes et al., 2003; Stevens

et al., 2000; Tigreros and Davidowitz, 2019; Zhao and Zera, 2002). In extreme cases, some female insects completely lose the ability to fly (Harrison, 1980; Roff, 1984, 1990; Zera and Denno, 1997). This response is commonly interpreted as an evolutionary adaptation to increase fecundity in a specific location. To elaborate on one example of this trade-off, we briefly discuss the results from Elliott and Evenden (2012) on the effect of flight and reproduction in an outbreaking forest lepidopteran, *Choristoneura conflictana*. Here, the population density of the insects limits the post-flight reproductive investment by females. High density levels reduce the amount of resources available to the individuals within the population and an adaptive response would be to disperse in order to access more food. Flight, however, reduces the stores available and in response individuals that disperse further also produce fewer eggs.

The dispersal-reproduction trade-off is not limited to insects, this trade-off has also been examined in diaspores (a seed with additional tissues that assist dispersal). There is a relationship between seed mass and dispersal capacity in wind-dispersed diaspores (Greene and Johnson, 1993; Siggins, 1933; Thompson et al., 2002). This is directly related to reproduction because increases seed mass is proportional to maternal provisioning. Assuming there is only passive wind-dispersal, the trade-off occurs because diaspores with larger seed mass will not spread as far as those with a lighter mass by wind due to the force of gravity causing the larger mass diaspores to settle earlier. There is also evidence for a trade-off between dispersal and reproduction for migrating birds (Gill, 2006; Proctor and Lynch, 1993; Prop et al., 2003; Récapet et al., 2017; Schmidt-Wellenburg et al., 2008). For migratory birds, the reproductive success of an individual correlates with the migration timing, which is determined by the pre-migration body fat stores. A similar trade-off has also been documented in a wild population of lizards (Cotto et al., 2015).

Incorporation of trade-offs into theoretical models has produced rich dynamics that are not present without such effects (Chuang and Peterson, 2016). By incorporating a trade-off between reproduction and dispersal ability in a population of non-pollinating fig wasps Duthie et al. (2014) constructed a theoretical model to explain the coexistence of these different strategies. At first glance, this result appears to be paradoxical to the competitive exclusion principle because non-pollinating fig wasps share similar life histories and compete for similar resources. However, the trade-off in the model influences individuals to specialize to different degrees on dispersal and reproductive abilities and create individual niches.

Theoretical models can also be used to study the evolution of dispersal in populations with multiple phenotypes in a spatially heterogeneous habitat. A primary finding from these studies is that the phenotype with the lowest diffusion rate is selected in a competitive environment (Dockery et al., 1998; Hastings, 1983). However, in our work, we are interested not in what is happening in a competitive environment but during colonization. During colonization, the spreading speed of the population is the primary driving force, not high level density-dependence or intraspecific competition, unlike in stationary competitive systems. Thus, our analysis aims to address a complementary area that evolution of dispersal models do not consider. That is, we are interested in understanding how dispersal is selected in a colonizing population under range expansion.

In this work, we construct a theoretical model for population spread that incorporates a dispersal-reproduction trade-off. For our mathematical model, we use an integrodifference equation for reproduction and dispersal. We chose this particular model type because of its wide applicability in ecological modeling of populations with non-overlapping generations (Kot, 1992). The shape of trade-off curves are critical for predicting population dynamics (Hoyle et al.,

2008). Therefore, in our model, we aim to incorporate a general trade-off effect that can encompass many different scenarios.

Throughout our analysis, we focus on the formula for the spreading speed because we are interested in how the dispersal-reproduction trade-off influences the colonizing population dynamics. Our goal is to understand how the dispersal-reproduction trade-off affects the spreading speed. In particular, we perform a sensitivity analysis to determine parameter sensitivity to the formula. This allows us to understand how the spreading speed would change with parameter variation. We then consider how parameter uncertainty in the trade-off affects the spreading speed formula. To achieve this, we assume that the uncertain parameters in the model are random variables with an underlying probability distribution, and then analyze the impact on optimal resource allocation.

In Section 5.2, we provide a general background for integrodifference equations, describe our assumptions on how the dispersal-reproduction trade-off is incorporated into the model, and present the trade-off model. We begin Section 5.3 with determining the condition for population persistence and calculating the formula for the spreading speed. The remainder of Section 5.3 is broken down into two primary parts; the first concerning the sensitivity of model parameters (Section 5.3.1), and the second for the uncertainty in the model parameters (Section 5.3.2). In Section 5.3.1, our results are divided into two pieces; in the first part we perform a sensitivity analysis on the trade-off parameters (Section 5.3.1.1), and in the second part we perform a sensitivity analysis on the reproduction and dispersal parameters (Section 5.3.1.2). In a similar manner for Section 5.3.2, we partition the results into two parts; the first concerning how the trade-off parameters affect the expected spreading speed (Section 5.3.2.1), and the second understanding how the reproduction and dispersal parameters affect the expected spreading speed (Section 5.3.2.2).

To conclude the results, we provide a discussion of our model, techniques, and analyses in Section 5.4. For those interested in the technical details of our results, we present the proofs of the theorems in the Appendix.

5.2 Mathematical model

Integrodifference equations are a popular tool used in theoretical ecology to model spreading populations (Kot and Schaffer, 1986). Traditionally, the integrodifference equation is written in the following form

$$u_{t+1}(x) = \int_{-\infty}^{\infty} k(x-y) f(u_t(y))\, dy, \qquad t > 0,\, x \in \mathbb{R} \tag{5.1}$$

where u is the population density, f is the density-dependent local population growth function, and $k(x-y)\,dy$ is a probability density function, commonly called the dispersal kernel, describing the movement of individuals from the interval $(y, y+dy]$ to location x.

To incorporate a dispersal-reproduction trade-off into (5.1) we assume that the dispersal capability of an individual and the population growth rate are each given by a single parameter, and that the proportion of resources allocated to dispersal is given by p and the proportion of resources allocated to reproduction is given by $1-p$. Under resource limitation, we assume power functions for the change in reproductive and dispersal ability, so they are proportional to $(1-p)^\alpha$ and p^β, respectively where $\alpha, \beta > 0$. When $\alpha, \beta = 0$ there is no trade-off in the model. Note that since we are modeling the trade-off in terms of resources allocated we obtain two different curves, one for the reproductive value against the allocation of resources, and the second for the dispersal value against the allocation of resources. We can see from Figure 5.1 that if $\alpha, \beta = 1$, then the resource allocation curves are linear. This means that the growth rate per generation (variation in dispersal distance) has a constant rate of decrease (increase) with the proportion of resources allocated

to dispersal. In other words, the change in reproductive and dispersal ability is directly proportional to the proportion of resources invested. If $\alpha, \beta < 1$, then the curves are concave. This means that the growth rate per generation (variation in dispersal distance) has an increasing (decreasing) rate of decrease (increase) with the proportion of resources allocated to dispersal. If $\alpha, \beta > 1$, then the allocation curves are convex. This means that the growth rate per generation (variation in dispersal distance) has a decreasing (increasing) rate of decrease (increase) with the proportion of resources allocated to dispersal. Previous studies have also incorporated trade-off effects using these same types of power functions (Cressler et al., 2010; Jones and Ellner, 2004).

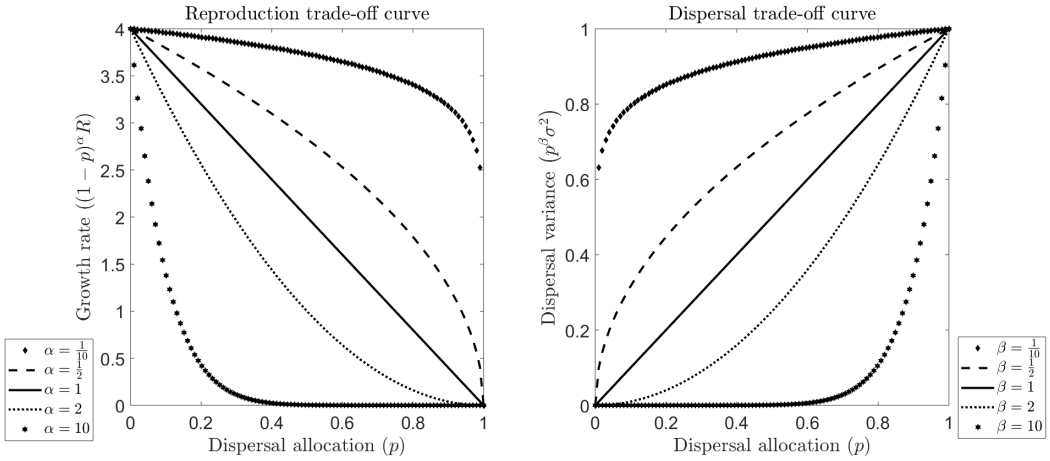

Figure 5.1: Allocation for dispersal and reproduction for different values of α and β with parameter values $R = 4$ and $\sigma^2 = 1$.

For simplicity, we consider a population that spreads by diffusion (Kot et al., 1996) and reproduces according to a Beverton-Holt type growth function (Beverton and Holt, 2012). That is, the dispersal kernel k is a Gaussian probability density function with zero mean and variance σ^2,

$$k(x-y) = \frac{1}{\sqrt{2\pi\sigma^2}} e^{-\frac{(x-y)^2}{2\sigma^2}}, \tag{5.2}$$

and the growth function f is given by the Beverton-Holt dynamics

$$f(u_t(y)) = \frac{Ru_t(y)}{1 + \frac{R-1}{K} u_t(y)} \tag{5.3}$$

where K is the carrying capacity and R is the growth rate per generation. By incorporating the dispersal-reproduction trade-off into the model as described above, the population density is then governed by

$$u_{t+1}(x) = \int_{-\infty}^{\infty} \frac{1}{\sqrt{2\pi p^{\beta}\sigma^2}} e^{-\frac{(x-y)^2}{2p^{\beta}\sigma^2}} \frac{(1-p)^{\alpha} R u_t(y)}{1 + \frac{(1-p)^{\alpha}R-1}{K} u_t(y)}\, dy. \tag{5.4}$$

In the trade-off model, the growth rate per generation is given by $(1 - p)^{\alpha}R$. Thus, was have that R is the scaling parameter and α acts as a shape parameter. The variation in dispersal distance is given by $p^{\beta}\sigma^2$. In a similar manner, we see that σ^2 is the scaling parameter and β is the shape parameter. One interesting consequence of our model is the scaling of how we incorporate the trade-off in the model. For example, if $\beta = 1$, then we are assuming that the variance in dispersal distance is proportional to the proportion of resources invested. When $\beta = 2$, we are assuming that the standard deviation in dispersal distance is proportional to the proportion of resources invested.

5.3 Results

In this section, we provide the theoretical results for our model with the trade-off presented in (5.4). We begin with a brief description of fundamental results related to the existence, persistence, and spread of populations governed by (5.4). Once this preliminary material is established, we move into our primary analyses that are composed of two parts. We begin with performing a sensitivity analysis on the parameters of the model in Section 5.3.1. This section is split into two parts, a sensitivity analysis on the trade-off parameters (Section 5.3.1.1), and a sensitivity analysis on the reproduction and dispersal parameters (Section 5.3.1.2). Then, we move onto the second part where we explore the effects of parameter uncertainty in Section 5.3.2, which is also split into two parts. First, we calculate the expected spreading speed and optimal resource allocation to dispersal when the trade-off parameters are uncertain

(Section 5.3.2.1), and second we perform the same kinds of calculations when the reproduction and dispersal parameters are uncertain (Section 5.3.2.2).

We first deduce when the study population is persistent. When we say the population is persistent, we mean that there exists a traveling wave solution to (5.4) that spreads at some positive speed. This idea is consistent with the concept of weak uniform persistence (Freedman and Moson, 1990; Vasilyeva et al., 2016). The condition for persistence can be calculated directly by applying the seminal work from Weinberger (1982) and is provided in Proposition 5.3.1.

Proposition 5.3.1. *The population modeled by* (5.4) *is persistent if*

$$(1-p)^{\alpha}R > 1. \tag{5.5}$$

Note that this condition does not depend on the dispersal parameter, σ^2, or its shape parameter, β, but it does depend on the proportion of resources allocated to dispersal, p. In Figure 5.2, we can see that there are two areas of interest; above each curve is when $(1-p)^{\alpha}R > 1$ and hence we have population persistence, and the area equal to or below each curve is when $(1-p)^{\alpha}R \leq 1$ and the population becomes extinct. Note that when $(1-p)^{\alpha}R = 1$ our model becomes a purely diffusive process and hence the population cannot persist. Notice that as α increases the (p, R) parameter space where we have population persistence decreases, which is evident from the different curves plotted in Figure 5.2. As α approaches 0, we see that our persistence requirement becomes the standard persistence requirement in absence of the trade-off; that is, $R > 1$.

When the population is persistent, we can also determine the spreading speed for our traveling wave solution. Weinberger (1982) proved that if the population is persistent, then (5.4) emits traveling wave solutions. That is, the population density spreads with fixed spatial profile that is translated by a fixed distance per generation. This translation is called the spreading

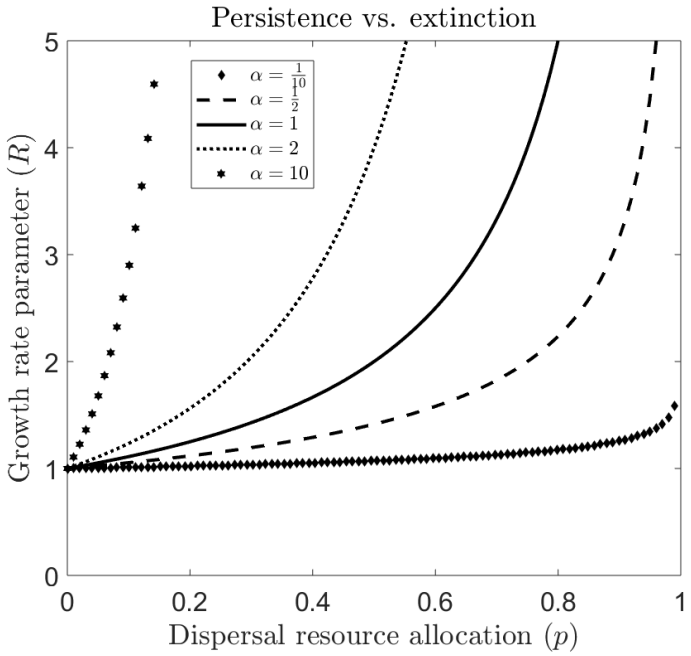

Figure 5.2: The stability regions for the parameters p and R are shown. For each value of α, the area above each respective curve corresponds to population persistence whereas the area below the curve results in population extinction.

speed. For a newly introduced population, the asymptotic spreading speed can be thought of in the following way. The population is said to spread with asymptotic speed c^* if an observer who travels at some speed $c > c^*$ will eventually be ahead of the population and see a density of zero whereas an observer who travels at speed $c < c^*$ will eventually see the population at this carrying capacity.

Proposition 5.3.2. *Assume that the population in* (5.4) *is persistent, then the spreading speed of the population is given by*

$$c^* = \sqrt{2p^\beta \sigma^2 \ln[(1-p)^\alpha R]}. \tag{5.6}$$

Throughout our analysis we use (5.6) frequently. The first thing we notice from the formula for the spreading speed is that it depends on the dispersal and reproduction parameters, the shape of the trade-off curves, and the allocation of resources. Thus, as we continue our analysis, we break down our results in

terms of these individual pieces.

5.3.1 Sensitivity analysis

The technique of parameter sensitivity analysis is used to understand how the model response is altered by perturbations in the parameter values. The sensitivity is defined by the incremental rate of proportional change in the response (output) λ related to an incremental rate of proportional change in parameter values (input) θ (Haefner, 2005). In this paper we use proportional sensitivity

$$\text{Sensitivity}(\lambda, \theta) := \frac{\theta}{\lambda}\frac{\partial \lambda}{\partial \theta}, \tag{5.7}$$

henceforth referred to simply as sensitivity. In some contexts this is called elasticity (Neubert and Caswell, 2000). The proportionality in (5.7) allows us to compare parameters with different scales (Link and Doherty Jr, 2002).

5.3.1.1 Sensitivity of trade-off parameters

In this section, we aim to understand how the trade-off parameters in our model affect the value for the spreading speed of the population. Using (5.7), we compute the sensitivity of c^* with respect to α, β, and p and find that

$$\text{Sensitivity}(c^*, \alpha) = \frac{\alpha \ln(1-p)}{2\ln\left((1-p)^\alpha R\right)}, \tag{5.8}$$

$$\text{Sensitivity}(c^*, \beta) = \frac{\beta \ln(p)}{2}, \text{ and} \tag{5.9}$$

$$\text{Sensitivity}(c^*, p) = \frac{1}{2}\left(\beta - \frac{\alpha p}{(1-p)\ln\left((1-p)^\alpha R\right)}\right). \tag{5.10}$$

Since $0 < p < 1$, we can immediately conclude that $\text{Sensitivity}(c^*, \alpha) < 0$ and $\text{Sensitivity}(c^*, \beta) < 0$. Thus, we find that any increase in α or β will cause the spreading speed of the population to decrease. We also see that when $\text{Sensitivity}(c^*, p) = 0$, we obtain an interesting result that we outline in Theorem 5.3.1. In particular, we can determine the fastest speed at which a species can spread and how it should allocate its resources to do so.

Theorem 5.3.1. *Consider* (5.4) *with the persistence condition* $(1-p)^{\alpha}R > 1$. *Then, the optimal allocation of resources to dispersal* (p^*) *for the fastest spread of the population is given by the unique solution to the transcendental equation*

$$\frac{\beta \ln\left((1-p^*)^{\alpha}R\right)}{p^*} = \frac{\alpha}{(1-p^*)}. \tag{5.11}$$

The proof of Theorem 5.3.1 is provided in the Appendix see Section 5.5.1. It is interesting to note that the optimal allocation of resources does not depend on the diffusivity parameter σ^2. This is because the formula for the asymptotic spreading speed scales linearly with σ. We also see that the optimal resource allocation to dispersal is obtained when Sensitivity$(c^*, p) = 0$. To illustrate the results of Theorem 5.3.1, a plot of the spreading speed for different value of p and R with fixed values for α, β, and σ^2 is provided in Figure 5.3. Here the solid lines are a contour plot for the spreading speed where we vary the values of proportion of resources allocated to dispersal (p), and the growth rate per generation (R). The dashed line in Figure 5.3 is the optimal resource allocation to dispersal as calculated by Theorem 5.3.1. Notice that for each value of $R > 1$, there is a unique value for p that maximizes the spreading speed as predicted by Theorem 5.3.1.

In Figure 5.4 we plot the spreading speed (c^*) against the proportion of resources allocated to dispersal (p). The difference between the three plots is the value of α used. The values for α are $\frac{1}{4}$, 1, and 4 for the left, center, and right plots, respectively. In each of the plots there are three curves where the value for β is $\frac{1}{4}$, 1, and 4 for the dashed, solid, and dotted lines, respectively. The optimal resource allocation to dispersal can be determined from the peak of each curve. From these plots, we can see that, as we increase β, the value for the optimal resource allocation to dispersal increases. We can see from comparing the three plots that as we increase the value of α, the value for the optimal resource allocation to dispersal decreases. This intuitively makes

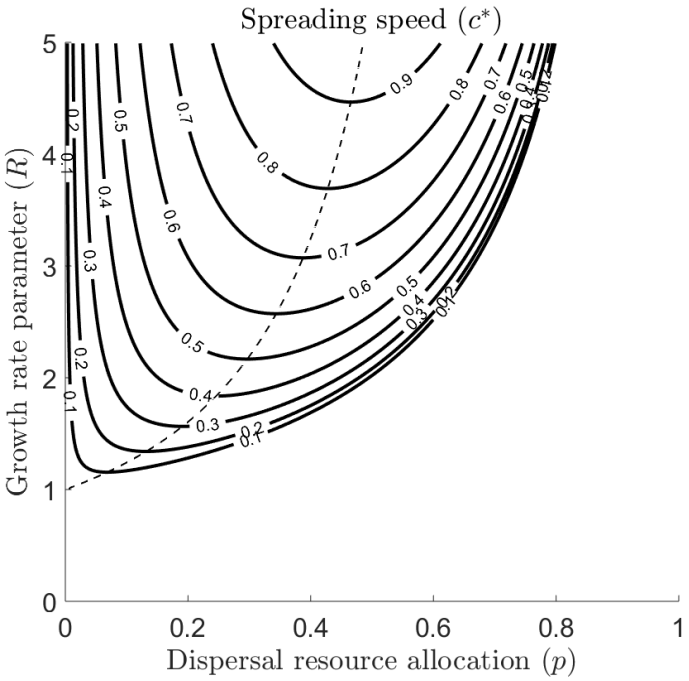

Figure 5.3: A contour plot for the spreading speed, c^*, for $\alpha = 1$, $\beta = 1$, and $\sigma^2 = 1$. In the plot above we vary the values of p and R. The dashed line is the optimal resource allocation to dispersal (p^*) as calculated by Theorem 5.3.1.

sense since p is the proportion of resources allocated to dispersal. Next, we determine whether α or β is more sensitive when the population is at its optimal resource allocation to dispersal.

Theorem 5.3.2. *Let the optimal resource allocation to dispersal be denoted by p^*. Then, for the spreading speed (c^*)*

- *If $p^* < \frac{1}{2}$, then α is less sensitive than β.*
- *If $p^* = \frac{1}{2}$, then α and β are equally sensitive.*
- *If $p^* > \frac{1}{2}$, then α is more sensitive than β.*

The proof of Theorem 5.3.2 is provided in the Appendix see Section 5.5.1. The first result of Theorem 5.3.2 states that if more resources are allocated to reproduction than dispersal, then the shape parameter for the dispersal trade-

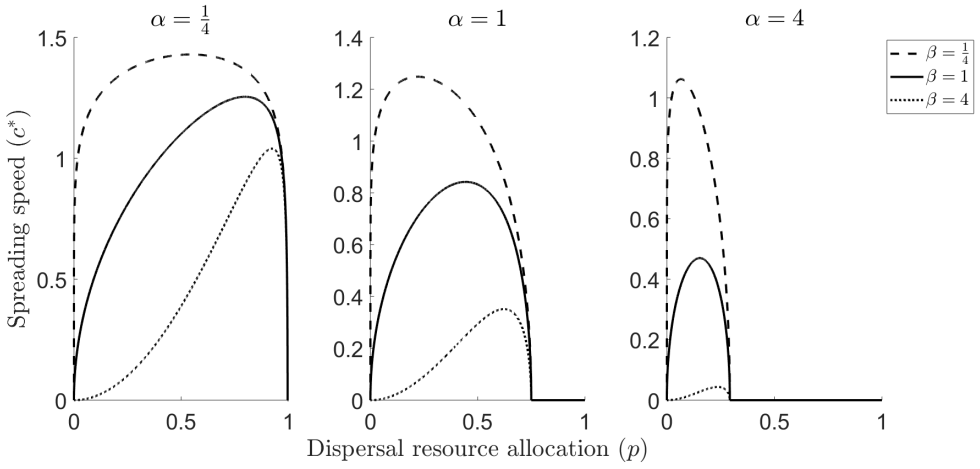

Figure 5.4: Three plots for the spreading speed, c^*, where $R = 4$ and $\sigma^2 = 1$. In the left, center, and right plots the values for α are $\frac{1}{4}$, 1, and 4, respectively. In each plot we vary β as indicated by the legend.

off curve is more sensitive than the shape parameter for the reproduction trade-off curve. The second result of Theorem 5.3.2 states that if the resources are split equally between dispersal and reproduction, then the shape parameters for the dispersal and reproduction trade-off curves are equally sensitive. The third result of Theorem 5.3.2 states that if more resources are allocated to dispersal than reproduction, then the shape parameter for the reproduction trade-off curve is more sensitive than the shape parameter for the dispersal trade-off curve.

We can see the result of Theorem 5.3.2 illustrated in Figure 5.5. In Figure 5.5, we vary R in the three bar plots. Recall that the optimal resource allocation to dispersal can be determined by calculating where $\text{Sensitivity}(c^*, p) = 0$ or by solving (5.11). In the left bar plot of Figure 5.5 the optimal resource allocation to dispersal is approximately 0.3818, in the center plot the optimal resource allocation to dispersal is 0.5, and in the right plot the optimal resource allocation to dispersal is 0.6374. In the left bar plot of Figure 5.5, we can see that since the optimal resource allocation is less than one half, that β is more sensitive than α. In the center bar plot of Figure 5.5 since the optimal

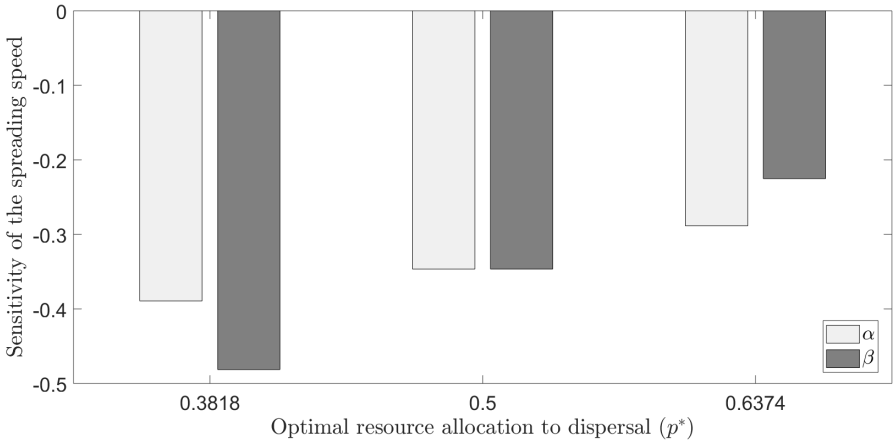

Figure 5.5: In this figure we plot the sensitivity of the spreading speed with respect to the parameter values α and β against different values for the optimal resource allocation to dispersal (p^*). In all three simulations we used the parameter values $\sigma^2 = 1$, $\alpha = 1$, $\beta = 1$ and vary $R = 3, 2e$, and 16, for the left, center, and right bar plots, respectively.

resource allocation is exactly one half, then α and β are both equally sensitive. In the right bar plot of Figure 5.5 since the optimal resource allocation is greater than one half, then α is more sensitive than β.

5.3.1.2 Sensitivity of reproduction and dispersal parameters

In this section, we aim to understand how the growth rate and standard deviation in dispersal distance affect the value for the spreading speed of the population. This idea is not novel; previous studies have used sensitivity analysis to understand the effect that dispersal and demographic parameters have on the spreading speed (Bateman et al., 2017; Gharouni et al., 2015; Neubert and Caswell, 2000). A commonality between all these studies is that the model used was a structured integrodifference equation. We are able to apply a simplified version to the theoretical results from Neubert and Caswell (2000) to perform a sensitivity analysis because we are studying a scalar model.

In our analysis, we consider the sensitivity of the spreading speed with respect to the population growth rate per generation (R) and the standard

deviation in dispersal distance (σ). Using (5.7), we calculate

$$\text{Sensitivity}(c^*, R) = \frac{1}{2\ln\left((1-p)^\alpha R\right)}, \text{ and} \tag{5.12}$$

$$\text{Sensitivity}(c^*, \sigma) = 1. \tag{5.13}$$

The first thing to notice from these sensitivity calculations is that Sensitivity$(c^*, \sigma) = 1$. Since Sensitivity$(c^*, \sigma) = 1$, we can conclude that σ is a scaling parameter in the formula for the spreading speed. This is also evident from looking directly at the formula for the spreading speed in (5.6).

Assuming that the population is persistent, we can conclude that the Sensitivity(c^*, R) is always positive. Since the natural logarithm is a monotone increasing function, we can conclude that when $(1-p)^\alpha R$ is small (but still greater than one) then Sensitivity(c^*, R) is high, but when $(1-p)^\alpha R$ becomes large then Sensitivity(c^*, R) becomes smaller. By a direct comparison between (5.12) and (5.13) we can conclude that if $(1-p)^\alpha R < (>) e^{\frac{1}{2}}$, then R is more (less) sensitive than σ, and if $(1-p)^\alpha R = e^{\frac{1}{2}}$, then R and σ are equally sensitive. This is seen in Figure 5.6. Recall that if population is persistent when $(1-p)^\alpha R > 1$, and notice that $e^{\frac{1}{2}} \approx 1.6487$. Therefore, the region where R is more sensitive than σ is quite small and only occurs when the growth rate per generation of the population is small.

5.3.2 Parameter uncertainty

In this section, we attempt to understand how the spreading speed changes when there is parameter uncertainty in the trade-off shape and scale parameters. To achieve this, we assume throughout that the parameter of interest is a random variable with some underlying probability distribution and then compute the expected value for the spreading speed. We break the results into two sections; the first section covers the case when there is uncertainty in the shape of the trade-off curves (Section 5.3.2.1), and the second section covers

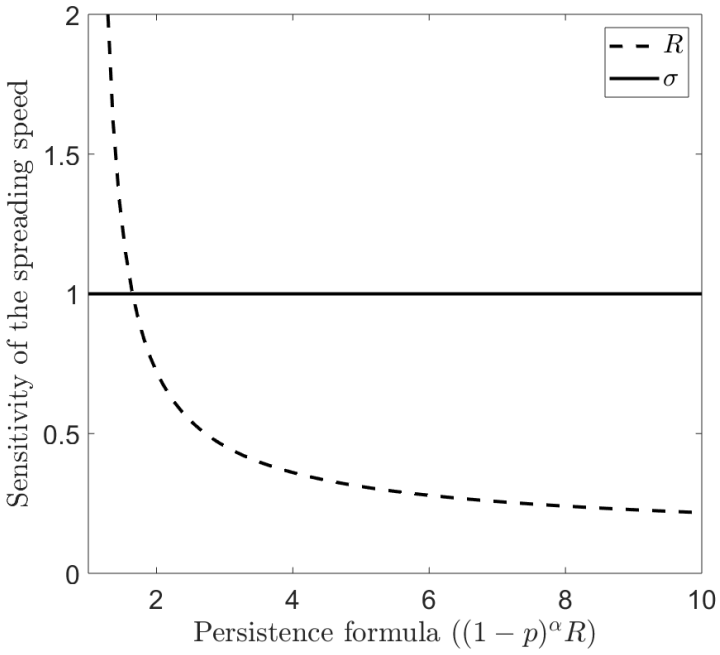

Figure 5.6: In this figure we plot the sensitivity of the spreading speed with respect to the parameter values R and σ against the persistence formula $(1-p)^{\alpha}R$.

the case when there is uncertainty in the reproduction and dispersal parameters or as mentioned earlier the scaling parameters for the trade-off curves (Section 5.3.2.2).

5.3.2.1 Uncertainty in the shape of the trade-off curves

In this section, we study the uncertainty in the shape parameters for the trade-off curves α and β. To model the uncertainty in the parameters for α and β, we assume that these parameters are random variables. Since β can be any nonnegative real number, the probability density function for β must also cover the nonnegative real numbers. For α, we need to place a restriction on the upper bound because we require that the population is persistent. Returning to (5.5) we can see that the upper bound for α should be $-\frac{\ln(R)}{\ln(1-p)}$. Thus, the probability density function for α needs to be defined on $\left(0, -\frac{\ln(R)}{\ln(1-p)}\right)$. With this given uncertainty about the shape parameters for our trade-off curves, we

wish to find the expected value for the spreading speed.

We begin with the case where the reproduction trade-off shape, α, is known and the dispersal trade-off shape, β, is uncertain. In this scenario, the parameter of interest is defined on $(0, \infty)$, and we use the gamma distribution with shape parameter $a > 0$ and scale parameter $b > 0$. This distribution is

$$f_1(\beta) = \frac{1}{\Gamma(a)b^a}\beta^{a-1}e^{-\frac{\beta}{b}} \tag{5.14}$$

with mean ab and variance ab^2. For shorthand notation we denote that β is a gamma distribution with shape parameter a and scale parameter b by $\beta \sim \text{Gamma}(a, b)$. We choose to use this distribution because of its generality due to the fact that special cases of this distribution are the exponential distribution, chi-squared distribution, and Dirac-delta distribution. We calculate the expected spreading speed in Theorem 5.3.3.

Theorem 5.3.3. *Let us assume that β is a random variable distributed on $(0, \infty)$. Then, the expected value for the spreading speed is*

$$E\left[c^*\right] = \sqrt{2\sigma^2 \ln[(1-p)^\alpha R]}M_\beta\left(\frac{\ln(p)}{2}\right) \tag{5.15}$$

where M_β is the moment generating function of β. Moreover, if $\beta \sim Gamma(a, b)$, then

$$E\left[c^*\right] = \frac{\sqrt{2\sigma^2 \ln[(1-p)^\alpha R]}}{\left(1 - b\frac{\ln(p)}{2}\right)^a} \tag{5.16}$$

and the optimal resource allocation to dispersal (p^*) is given by the transcendental equation

$$\frac{E[\beta]}{\alpha}\ln\left[(1-p^*)^\alpha R\right](1-p^*) = p^*\left(1 - \frac{1}{2}\frac{Var[\beta]}{E[\beta]}\ln(p^*)\right). \tag{5.17}$$

The proof of Theorem 5.3.3 is provided in the Appendix see Section 5.5.1. The results from Theorem 5.3.3 can be applied to understand how a population would expect to spread if the shape of the dispersal trade-off curve is uncertain.

Here we provide a general formula for the expected spreading speed for a random variable β defined on $(0, \infty)$ in terms of its moment generating function in (5.15). In the special case when $\beta \sim \text{Gamma}(a, b)$, we calculate the formula for the expected spreading speed in (5.16) and calculate the optimal resource allocation to dispersal by the implicit equation (5.17). When $\text{Var}[\beta] = 0$, we have that $E[\beta] = \beta$ and (5.17) is equivalent to (5.11) in Theorem 5.3.1.

To understand the effects of the variation in the dispersal trade-off shape parameter, β, we provide plots of the optimal resource allocation to dispersal in Figure 5.7. For the plots in Figure 5.7 we illustrate how the optimal resource allocation to dispersal changes with the expected dispersal trade-off shape for three different values for the variance of the dispersal trade-off shape. For the left (right) plot in Figure 5.7, this is when the expected dispersal trade-off shape is convex (concave). In both plots, we see that as the expected dispersal trade-off shape increases, the optimal resource allocation to dispersal also increases. We also see that as the variation in the shape of the dispersal trade-off increases, the optimal resource allocation to dispersal decreases. That is, if there is a lot of uncertainty in the shape of the dispersal trade-off curve, then the best choice for the population is to invest more resources into reproduction.

Next, we consider the case when the reproduction trade-off shape, α, is uncertain and the dispersal trade-off shape, β, is known. To be able to discuss the spreading speed for the population here, we need to guarantee that the population is persistent. That is $(1-p)^{\alpha}R > 1$. Recall that this is satisfied when $\alpha < -\frac{\ln(R)}{\ln(1-p)}$. This provides us with an upper bound on the potential values for α. Hence, our distribution for α must be defined on the bounded interval $\left(0, -\frac{\ln(R)}{\ln(1-p)}\right)$ to guarantee persistence. In our case we will use a scaled

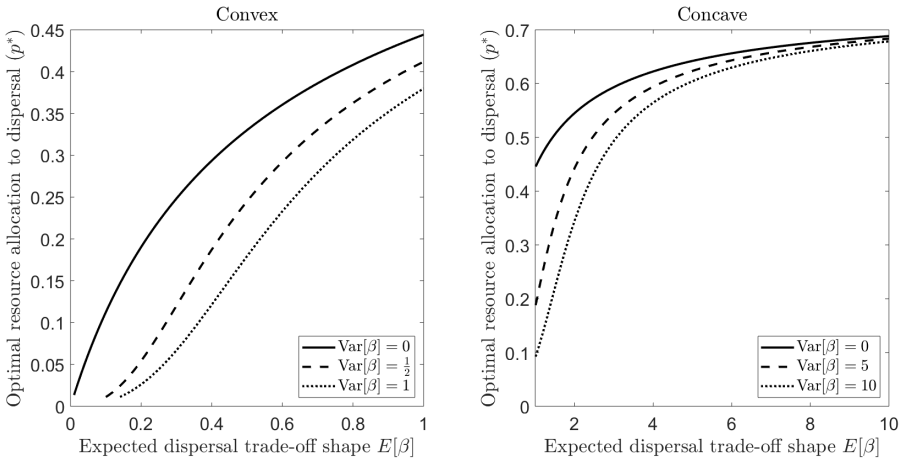

Figure 5.7: The plot in this figure shows the dispersal resource allocation versus the $E[\beta]$ for different values of $\mathrm{Var}[\beta]$ for the parameter values $\alpha = 1$ and $R = 4$.

beta distribution given by

$$f_2(\alpha) = \frac{\alpha^{a-1}\left(-\frac{\ln(R)}{\ln(1-p)} - \alpha\right)^{b-1}}{B(a,b)\left(-\frac{\ln(R)}{\ln(1-p)}\right)^{a+b-1}} \tag{5.18}$$

with shape parameter $a \geq 1$ and scale parameter $b \geq 1$ where B is the beta function. For our shorthand notation we say that $\alpha \sim \mathrm{Beta}(a,b)$ on $\left(0, -\frac{\ln(R)}{\ln(1-p)}\right)$. We choose this distribution because it has a variety of shapes. It is interesting to note that when the shape and scale parameters are one, then the scaled beta distribution becomes the uniform distribution on $\left(0, -\frac{\ln(R)}{\ln(1-p)}\right)$.

Theorem 5.3.4. *Let us assume that α is a random variable distributed on $\left(0, -\frac{\ln(R)}{\ln(1-p)}\right)$. Then, the expected value for the spreading speed is*

$$E\left[c^*\right] = \sqrt{2\sigma^2 p^\beta \ln(R)} \sum_{n=0}^{\infty} \binom{\frac{1}{2}}{n} \left(\frac{\ln(1-p)}{\ln(R)}\right)^n E\left[\alpha^n\right]. \tag{5.19}$$

Moreover, if $\alpha \sim Beta(a,b)$ on $\left(0, -\frac{\ln(R)}{\ln(1-p)}\right)$, then

$$E\left[c^*\right] = \sqrt{2\sigma^2 p^\beta \ln(R)} \frac{\Gamma(a+b)\Gamma\left(b+\frac{1}{2}\right)}{\Gamma(b)\Gamma\left(a+b+\frac{1}{2}\right)} \tag{5.20}$$

and the optimal resource allocation to dispersal (p^*) is the largest value of p that satisfies

$$p < 1 - \frac{1}{\sqrt[\alpha]{R}}. \tag{5.21}$$

The proof of Theorem 5.3.4 is provided in the Appendix see Section 5.5.1. A plot of the optimal resource allocation to dispersal is provided in Figure 5.8. This figure provides insight into how the optimal resource allocation to dispersal changes with the reproduction trade-off curve shape, α, and the growth rate parameter, R. Figure 5.8 is split into two parts for the shape of the reproduction trade-off curve. That is, in the left plot when $0 < \alpha < 1$ the reproduction trade-off curve is convex and in the right plot when $1 < \alpha < 10$ the reproduction trade-off curve is concave. It is clear from the left plot in Figure 5.8 that when α and R are small, the optimal resource allocation to dispersal is highly volatile. We also see that by increasing the growth rate parameter, R, increases the optimal resource allocation to dispersal. This is interesting because it suggests that by increasing the growth rate parameter an individual should invest more resources into dispersal to maximize their spreading speed. We also can conclude from Figure 5.8 that by increasing the reproduction trade-off shape parameter, α, decreases the optimal resource allocation to dispersal.

5.3.2.2 Uncertainty in the reproduction and dispersal parameters

In this section we will study the uncertainty in the reproduction and dispersal parameters R and σ. To model the uncertainty in the parameters for R and σ, we assume that these parameters are random variables. First, we will consider when R is known and σ is uncertain. Since σ is the standard deviation in dispersal distance, this value can be any real valued number so our distribution for σ should be defined over the nonnegative real line. We begin with calculating the expected spreading speed and the optimal resource allocation

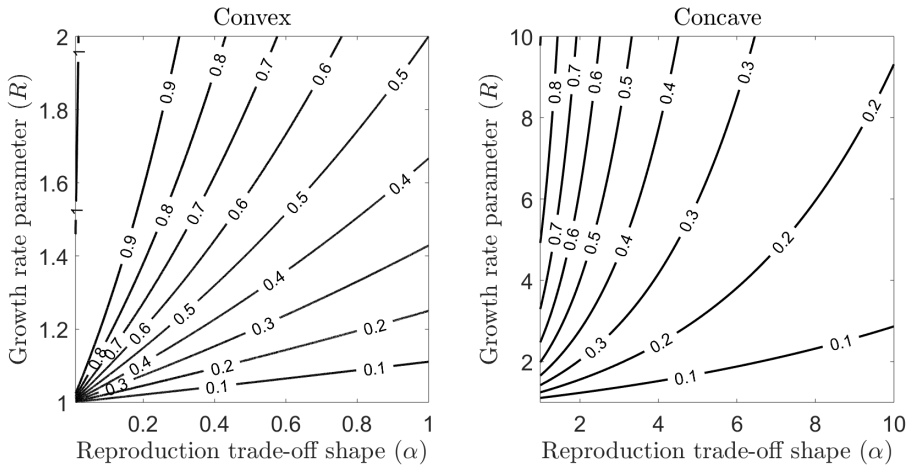

Figure 5.8: The contour plots in this figure show the optimal resource allocation to dispersal for different values of α and R. In the left plot, we have $0 < \alpha < 1$ that means the shape of the reproduction trade-off curve is convex. In the right plot, we have $1 < \alpha < 10$ that means the shape of the reproduction trade-off curve is concave.

to dispersal in Theorem 5.3.5.

Theorem 5.3.5. *Let us assume that σ is a random variable distributed on $[0, \infty)$. Then, the expected value for the spreading speed is*

$$E\left[c^*\right] = \sqrt{2p^\beta \ln[(1-p)^\alpha R]} E\left[\sigma\right]. \tag{5.22}$$

Moreover, the optimal resource allocation to dispersal (p^*) is given by

$$\frac{\beta \ln\left((1-p^*)^\alpha R\right)}{p^*} = \frac{\alpha}{(1-p^*)}. \tag{5.23}$$

The proof of Theorem 5.3.5 is provided in the Appendix see Section 5.5.1. Since σ is a scaling parameter in the formula for the spreading speed, we see that the by simply replacing σ by $E[\sigma]$ in (5.6), we obtain the formula for the expected spreading speed. Notice that (5.23) is the same as (5.11) in Theorem 5.3.1. This means that the optimal resource allocation to dispersal when all parameter values are known is the same for when σ is uncertain. Therefore, the uncertainty in σ does not affect the optimal resource allocation to dispersal.

Next, we will consider when R is uncertain and σ is known. Since R is the population growth rate parameter, this value must be greater than $\frac{1}{(1-p)^\alpha}$ to

guarantee population persistence. For simplicity in our calculations, we look at the distribution of $\ln(R)$ on $(-\alpha\ln(1-p),\infty)$. Thus, we look at a translated random variable that is shifted by $-\alpha\ln(1-p)$. In this scenario, we assume that $\ln(R)$ is a shifted gamma distribution on $(-\alpha\ln(1-p),\infty)$ with shape parameter $a>0$ and scale parameter $b>0$. For shorthand notation, we say that $\ln(R)\sim \text{Gamma}(a,b)$ on $(-\alpha\ln(1-p),\infty)$. This distribution is given by

$$f_4(\ln(R)) = \frac{1}{\Gamma(a)b^a}\left(\ln(R)+\alpha\ln(1-p)\right)^{a-1} e^{-\frac{(\ln(R)+\alpha\ln(1-p))}{b}} \tag{5.24}$$

for $\ln(R)\in(-\alpha\ln(1-p),\infty)$.

Theorem 5.3.6. *Let us assume that* $\ln(R)$ *is a shifted random variable distributed on* $(-\alpha\ln(1-p),\infty)$. *Then, the expected value for the spreading speed is*

$$E\left[c^*\right] = \sqrt{2p^\beta\sigma^2}E\left[\left(\ln(R)+\alpha\ln(1-p)\right)^{\frac{1}{2}}\right]. \tag{5.25}$$

Moreover, if $\ln(R)\sim$ *Gamma*(a,b) *on* $(-\alpha\ln(1-p),\infty)$, *then*

$$E\left[c^*\right] = \sqrt{2p^\beta\sigma^2 b}\frac{\Gamma\left(a+\frac{1}{2}\right)}{\Gamma(a)}, \tag{5.26}$$

and the optimal resource allocation to dispersal (p^*) *is the largest value of* p *that satisfies*

$$p < 1-\frac{1}{\sqrt[\alpha]{R}}. \tag{5.27}$$

The proof of Theorem 5.3.6 is provided in the Appendix see Section 5.5.1. In Theorem 5.3.6, we compute the expected spreading speed for the population for a shifted random variable distributed on $(-\alpha(1-p),\infty)$ in (5.25). Notice that the expected spreading speed is written in terms of the one halfth moment. In (5.26) we provide an example for when $\ln(R)\sim\text{Gamma}(a,b)$ on $(-\alpha\ln(1-p),\infty)$ where the expected spreading speed now depends on the shape and scale parameters of the distribution. After computing the spreading speed, we also determine the optimal resource allocation to dispersal in (5.27). Note

that the optimal resource allocation to dispersal in this theorem is the same as when we assumed that α was uncertain in Theorem 5.3.4. Therefore, a plot of the optimal resource allocation when R is uncertain is also given in Figure 5.8.

5.4 Discussion

The model presented in (5.4) provides a framework to understand the effects of dispersal-reproduction trade-offs on population persistence and the spreading speed of a population. From our analysis, it is evident that resource allocation is an important feature that impacts both the persistence and spread of a population. The influence of the trade-off shows that if an organism allocates too many resources to dispersal there may not be enough resources left for successful reproduction. Alternatively, if an individual spends too many resources on reproduction then it will not be able to spread quickly. We also determined how sensitive the spreading speed is to small changes in the model parameters, and studied how parameter uncertainty impacts the population spread.

We first derived the formula for the population persistence in our model. This formula is given by (5.5) and depends on the proportion of resources allocated to dispersal, p, the shape parameter for the reproduction trade-off curve, α, and the growth rate per generation, R. In the case when there is no trade-off, $\alpha = 0$, the persistence condition reduces to the classical case requiring that the growth rate per generation is greater than one. We were also able to explicitly compute a formula for the spreading speed of the population in (5.6) which depends on the dispersal, reproduction, and all of the trade-off parameters. The case when both shape parameters for the trade-off are zero reduces the formula to the classical spreading speed formula in absence of the trade-off (Weinberger, 1982).

To understand how trade-off parameter values affect the spreading speed of the population we performed a sensitivity analysis in Section 5.3.1 (Haefner, 2005). In Theorem 5.3.1, we were able to prove that there is a unique value for the optimal allocation of resources to dispersal that maximizes the spreading speed for the population. We are not able to explicitly solve for this value of p, but must express it as a transcendental equation in (5.11). This formula does not depend on the variation in dispersal distance σ^2 due to the fact that σ is a scaling parameter in the formula for the spreading speed. The formula for the optimal resource allocation to dispersal can also be found by simply solving for p when the sensitivity of the spreading speed with respect to the resource allocation to dispersal is equal to zero. That is, we set (5.10) equal to zero and solve for p. To illustrate this result, we plot an example in Figure 5.3. This plot illustrates that for each value of the growth rate parameter R, there is a unique value of the resource allocation to dispersal that maximizes the spreading speed. However, this unique value is not always observed in practice for other trade-offs. For a trade-off between seed size and number, Geritz (1995) showed that by assuming asymmetric intraspecific competition in favor of larger seeds that any unique seed size can be unstable and the evolutionary stable strategy becomes polymorphic. Intraspecific competition, determined by a trade-off between egg load and dispersal ability, leads to coexistence of non-pollinating fig wasps that specialize to different degrees on dispersal ability and fecundity (Duthie et al., 2014).

By calculating the sensitivity of the spreading speed with respect to the trade-off shape parameters α and β, we first deduce that these quantities are always negative. This means that the spreading speed always decreases when the trade-off shape parameters increase. In Figure 5.4, we illustrate this result by plotting the spreading speed versus the resource allocation to dispersal for different values of the trade-off shape parameters. It is clear from the three

plots that as α and β increase the value for the spreading speed decreases. This suggests that the value for the fastest spreading speed would be when $\alpha = \beta = 0$ meaning that there is no trade-off in the model. Therefore, the trade-off effect is not beneficial for expanding populations. From Figure 5.4, we also see how the optimal resource allocation to dispersal changes for different values of the trade-off parameters. First, we conclude from looking at the peaks in Figure 5.4 that by increasing α decreases the optimal resource allocation to dispersal. In a similar manner, we can also conclude that increasing the value of β increases the optimal resource allocation to dispersal. Intuitively this makes sense because α is the shape parameter for the reproduction trade-off curve and β is the shape parameter for the dispersal trade-off curve.

We were able to prove in Theorem 5.3.2 that if the population is at its optimal resource allocation and the resources are split equally between dispersal and reproduction, then α and β are equally sensitive. The results from Theorem 5.3.2 also show that if the population is at its optimal resource allocation and more (less) resources are allocated to dispersal than reproduction, then α is more (less) sensitive than β. An example of this result is seen in Figure 5.5. This result is somewhat counter intuitive because α is the shape parameter for the reproduction trade-off curve and β is the shape parameter for the dispersal trade-off curve. This means that if more (less) resources are allocated to dispersal than reproduction, then the shape of the reproduction (dispersal) trade-off curve is more sensitive than the shape of the dispersal (reproduction) trade-off curve.

To conclude our results on the sensitivity analysis for the spreading speed, we calculated the sensitivity of the spreading speed with respect to the population growth rate per generation (R) and the standard deviation in dispersal distance (σ). We find that the sensitivity of the spreading speed with respect to σ is constant because σ is a scaling parameter in the formula for the spread-

ing speed. Assuming that the population is persistent, the sensitivity of the spreading speed with respect to R is always positive. In Figure 5.6, we see that when the persistence formula is small, then R is more sensitive than σ, but when the persistence formula is greater than $e^{\frac{1}{2}}$, then σ is more sensitive than R. This means that R is more sensitive than σ when the population is close to extinction, but if the population is not at risk of extinction, then σ is more sensitive than R.

In Section 5.3.2, we explored how parameter uncertainty influences the expected spreading speed of the population and the optimal resource allocation to dispersal. This problem has been studied before for linear models where the emphasis is on how stochasticity can influence the spreading speed (Mollison, 1991) and more complicated nonlinear models (Lewis and Pacala, 2000). We split our results into two parts: Section 5.3.2.1 considers the case when the trade-off shape parameters are uncertain, and Section 5.3.2.2 considers when the reproduction and dispersal parameters are uncertain. To include the parameter uncertainty, we simply assume the parameter of interest is a random variable distributed on a suitable interval. In all cases, we determine two things; the expected spreading speed for the population and the optimal resource allocation to dispersal.

We begin with the case where the dispersal trade-off shape parameter (β) is uncertain, and provide our result in Theorem 5.3.3. We can express the expected spreading speed for the population in terms of the moment generating function for β as given in (5.15). We then provide the formula for the expected spreading speed when $\beta \sim \text{Gamma}(a, b)$ in (5.16). Moreover, we can determine the optimal resource allocation to dispersal and express this in terms of the expected value and variance of our random variable β as seen by (5.17). We provide two plots for the optimal resource allocation for the convex and concave trade-off curve shapes in Figure 5.7. Here, we plot the optimal

resource allocation to dispersal versus the expected dispersal trade-off shape. Within each plot, we plot different curves for different values of the variance of β. We can see that when the variance of β is zero, there is no uncertainty in β, and the optimal resource allocation to dispersal reduces back to (5.11). We can conclude from the plots that as the variance of β increases, the value for the optimal resource allocation to dispersal decreases. That is, if there is a lot of variation in the shape of the dispersal trade-off curve, then it is a better strategy to invest more resources into reproduction. We can also conclude that as the expected value of β increases, the optimal resource allocation to dispersal increases. This agrees with the our previous results from the sensitivity analysis as seen in Figure 5.4.

Next, we consider the case when α is uncertain. Here we require an upper bound on the value of α in order to guarantee population persistence and hence have a formula for the spreading speed of the population. In Theorem 5.3.4, we are able to derive a formula for the expected spreading speed of the population in (5.19) written in terms of a series of moments for α. In the case when $\alpha \sim \text{Beta}(a, b)$ on $\left(0, -\frac{\ln(R)}{\ln(1-p)}\right)$, the expected value for the spreading speed is given by (5.20). Note that when $a = b = 1$, this is a special case of the beta distribution where α is a uniform random variable on $\left(0, -\frac{\ln(R)}{\ln(1-p)}\right)$. When we attempt to determine the optimal resource allocation to dispersal, we find that this occurs when as many resources as possible are allocated to dispersal while still maintaining the persistence criterion. This is given by (5.21). Thus, due to this uncertainty, the optimal solution is to put as many resources into dispersal while still maintaining population persistence. Two plots for the optimal resource allocation to dispersal are provided in Figure 5.8. In these plots, we vary the reproduction trade-off shape (α) and the growth rate parameter (R). We can see that when α and R are small then the optimal resource allocation to dispersal is highly volatile.

In Section 5.3.2.2, we continue our analysis on the parameter uncertainty by assuming the reproduction and dispersal parameters are uncertain. First, we assume that the standard deviation in the dispersal distance is uncertain. In Theorem 5.3.5, we assume that σ is a random variable distributed on the real line and calculate the expected value for the spreading speed to be given by (5.22). Due to the fact that σ is a scaling variable in the formula for the spreading speed, we see that the only difference in the formula for the expected value for the spreading speed compared to the formula with no parameter uncertainty by replacing σ by the expected value of σ. In Theorem 5.3.5, we also calculate the optimal resource allocation to dispersal in (5.23). The formula in (5.23) is the same as (5.11) in Theorem 5.3.1. Thus, the optimal resource allocation to dispersal when σ is uncertain is the same for when all parameter values are known. We believe that this is an artifact of the dispersal kernel chosen.

To finish our analysis on parameter uncertainty, we consider the case when the population growth rate parameter R is uncertain. For simplicity in our calculation we assume that $\ln(R)$ is our random variable of interest, and we must assume that $\ln(R) > -\alpha \ln(1-p)$ to guarantee population persistence. In Theorem 5.3.6, we assume that $\ln(R)$ is a shifted random variable on $(-\alpha \ln(1-p), \infty)$ and find the expected value for the spreading speed in (5.25). By assuming that $\ln(R)$ is a shifted gamma distribution on $(-\alpha \ln(1-p), \infty)$ with shape parameter a and scale parameter b, we calculated the expected spreading speed in (5.26). Here, we find that the expected spreading speed is slower than if there was no uncertainty which is consistent with previous studies (Clark et al., 2001; Snyder, 2003). In this case, we find that the optimal resource allocation to dispersal happens when as many resources as possible are allocated to dispersal while still maintaining the persistence criterion. Note that this optimal resource allocation is the same in the case when we assumed

that α was uncertain. Thus, if there is uncertainty in the shape of the reproduction trade-off curve or the population growth rate parameter, then the best strategy to optimize the spreading speed is to allocate as many resources as possible to dispersal while still maintaining the persistence criterion.

While dispersal-reproduction trade-offs have been widely accepted in the literature, it should be mentioned that there are numerous examples for which this trade-off does not occur, or if it does, the degree of the trade-off varies greatly (Guerra, 2011; Mole and Zera, 1994; Roff, 1995; Sappington and Showers, 1992; Therry et al., 2015; Tigreros and Davidowitz, 2019). These studies argue for a lack of a trade-off between dispersal and reproduction in some insect species, or even a positive association between dispersal and reproduction. A recent meta-analysis indicates that although trade-offs between dispersal and reproduction likely occur in many insects, the strength and correlation of the trade-off vary significantly across insect orders (Guerra, 2011). Our model suggests that the trade-off occurs due to resource limitation, which is supported by another meta-analysis showing that in 76% of the studies, conditions of resource restriction result in a negative association between dispersal and reproduction (Tigreros and Davidowitz, 2019). Moreover, negative associations between dispersal and reproduction do not necessarily indicate a resource allocation trade-off.

A shortcoming in the model is the assumption that the life history strategies do not evolve over time. This assumption is only biologically reasonable if the time scale of the model is much shorter than the time it takes for the life history to change. In many cases this is not feasible. It has been empirically shown that resource allocation can have seasonal fluctuations (Barbour et al., 1999) or evolve due to genetic mutations in offspring (Burton et al., 2010). Typical annual plants, a plant that completes its life cycle within one year and then dies, devote most resources to growth in the early part of the grow-

ing season with a small amount of resources for maintenance, and late in the growing season nearly all the resources are devoted to reproduction. Whereas stress-tolerant plants such as shrubs in subarctic or dessert regions must allocate most resources to maintenance, and a small amount to growth. Only during good years, when resources are plentiful, can they devote resources to reproduction (Barbour et al., 1999). Thus, the type of resource allocation is highly dependent on the particular population of interest. Time-dependent variation in reproduction and dispersal can accelerate the spread of invading species (Ellner and Schreiber, 2012). In our study, we find variation in reproduction slows the spread, whereas variation in dispersal does not alter the expected spreading speed. This provides motivation to extend the model to include time-dependent trade-offs.

Another drawback of the modeling techniques presented is that there is no spatial heterogeneity in the resource allocation. In other systems, resource allocation is highly dependent on the location of the individuals in the population (Burton et al., 2010). Individuals in the core of the population were found to allocate more resources on reproduction than dispersal while individuals at the front of the population allocated more resources to dispersal than reproduction. Understanding the consequences of populations colonizing new habitats can also be explored by incorporating spatial heterogeneity in the resource allocation. One way to incorporate this into the model would be to consider density-dependent trade-offs.

Habitat fragmentation can affect the dispersal-reproduction trade-off (Ziv and Davidowitz, 2019). Using a common garden experiment, Gibbs and Van Dyck (2010) studied the effects of increased dispersal on the reproduction of speckled wood butterflies from closed continuous woodland populations to open highly fragmented agricultural landscapes. Gibbs and Van Dyck (2010) concluded that butterflies from fragmented landscapes were better able to cope

with the increased dispersal demands relative to those from non-fragmented landscapes suggesting a difference in the strength of trade-off due to the energetic cost of dispersal. Theoretical studies using integrodifference equations have previously investigated the role that landscape heterogeneity plays in predicting population dynamics (Dewhirst and Lutscher, 2009; Kawasaki and Shigesada, 2007; Latore et al., 1999; Van Kirk and Lewis, 1997), but have yet to incorporate dispersal-reproduction trade-offs into the models. A natural extension would be to fuse these two approaches together.

While our model is aimed to be applied to populations with nonoverlapping generations that have distinct dispersal and reproduction phases in their life cycle, these kinds of dispersal-reproduction trade-offs have also been documented in smaller scales of daily dispersal and foraging patterns (Bonte et al., 2012; Van Dyck and Baguette, 2005). Empirical evidence for these small scale dispersal-reproduction trade-offs have been documented in insects (Harrison, 1980), guppies (Ghalambor et al., 2004), lizards (Cox and Calsbeek, 2010; Miles et al., 2000), and snakes (Seigel et al., 1987). Thus, extending this modeling approach beyond integrodifference equations would allow for these types of trade-offs to be considered in a theoretical framework.

5.5 Appendix

5.5.1 Proofs of the theorems

5.5.1.0.1 Proof of Theorem 5.3.1

Proof. To begin, it should be noted that we treat α, β, R, and σ^2 as constants since we are interested in how p affects the asymptotic spreading speed c^*. To find the optimal allocation of resources for a species to spread we first find the first derivative of $(c^*)^2/2\sigma^2$ with respect to p. Using Equation (5.6), we

calculate

$$\frac{d(c^*)^2/2\sigma^2}{dp} = \beta p^{\beta-1}\ln\left((1-p)^\alpha R\right) + p^\beta \frac{-\alpha(1-p)^{\alpha-1}}{(1-p)^\alpha} \tag{5.28}$$

$$= p^\beta\left(\frac{\beta\ln\left((1-p)^\alpha R\right)}{p} - \frac{\alpha}{(1-p)}\right). \tag{5.29}$$

Hence, we have a critical point when

$$\frac{\beta\ln\left((1-p)^\alpha R\right)}{p} = \frac{\alpha}{(1-p)}. \tag{5.30}$$

Next, we show that Equation (5.30) has a unique solution. Define

$$l(p) := \frac{\ln\left((1-p)^\alpha R\right)}{p} \quad \text{and} \tag{5.31}$$

$$r(p) := \frac{1}{1-p}. \tag{5.32}$$

Both $l(p)$ and $r(p)$ are continuous functions on $(0,1)$. Also, $l(p)$ is a monotone decreasing function for $p \in (0,1)$ where $\lim_{p\to 0} l(p) = \infty$ and $\lim_{p\to 1} l(p) = -\infty$. We also have that $r(p)$ is a monotone increasing function for $p \in (0,1)$ where $r(0) = 1$ and $\lim_{p\to 1} r(p) = \infty$. Therefore, for each α, β, and R there exists a unique value $p^* \in (0,1)$ such that p^* solves Equation (5.30). □

5.5.1.0.2 Proof of Theorem 5.3.2

Proof. Recall that the optimal resource allocation is given by (5.11). That is,

$$\beta = \frac{\alpha p}{(1-p)\ln\left((1-p)^\alpha R\right)}. \tag{5.33}$$

To determine which parameter is more sensitive we compare Sensitivity(c^*, α) and Sensitivity(c^*, β). Recall that from (5.8) and (5.9) we know that Sensitivity(c^*, α) and Sensitivity(c^*, β) are both negative. When Sensitivity(c^*, α) = Sensitivity(c^*, β), this means that α and β are equally sensitive, when Sensitivity$(c^*, \alpha) >$ Sensitivity(c^*, β) this means that α is less sensitive than β, and finally when Sensitivity$(c^*, \alpha) <$ Sensitivity(c^*, β), this means that α is more sensitive than

β. We will first compute when α and β are equally sensitive. That is,

$$\text{Sensitivity}(c^*, \alpha) = \text{Sensitivity}(c^*, \beta) \tag{5.34}$$

gives

$$\frac{\alpha \ln(1-p)}{2\ln\left((1-p)^\alpha R\right)} = \frac{\beta \ln(p)}{2}. \tag{5.35}$$

Since we are assuming we are at the optimal resource allocation, substituting (5.33) into the previous equation we have

$$\frac{\alpha \ln(1-p)}{2\ln\left((1-p)^\alpha R\right)} = \frac{\alpha p \ln(p)}{2(1-p)\ln\left((1-p)^\alpha R\right)}. \tag{5.36}$$

Simplifying, we find that

$$(1-p)\ln(1-p) = p\ln(p). \tag{5.37}$$

The only solution to this equation is given by $1-p=p$. Solving for p we find that $p=\frac{1}{2}$. Thus, if the optimal resource allocation is $p=\frac{1}{2}$, then α and β are both equally sensitive parameters. Repeating these same calculations but with $\text{Sensitivity}(c^*, \alpha) > \text{Sensitivity}(c^*, \beta)$, we find that $0 < p < \frac{1}{2}$. Thus, if the optimal resource allocation is less than $\frac{1}{2}$, then β is more sensitive than α. By repeating these same calculations but with $\text{Sensitivity}(c^*, \alpha) < \text{Sensitivity}(c^*, \beta)$, we find that $\frac{1}{2} < p < 1$. Thus, if the optimal resource allocation is greater than $\frac{1}{2}$, then α is more sensitive than β. □

5.5.1.0.3 Proof of Theorem 5.3.3

Proof. Assuming that β is a random variable defined on $(0, \infty)$ with probabil-

ity density function $f_1(\beta)$, the expected spreading speed is given by

$$E\left[c^*\right] = \int_0^\infty \sqrt{2p^\beta \sigma^2 \ln[(1-p)^\alpha R]} f_1(\beta)\, d\beta \tag{5.38}$$

$$= \sqrt{2\sigma^2 \ln[(1-p)^\alpha R]} \int_0^\infty p^{\frac{\beta}{2}} f_1(\beta)\, d\beta \tag{5.39}$$

$$= \sqrt{2\sigma^2 \ln[(1-p)^\alpha R]} \int_0^\infty e^{\beta \frac{\ln(p)}{2}} f_1(\beta)\, d\beta \tag{5.40}$$

$$= \sqrt{2\sigma^2 \ln[(1-p)^\alpha R]} M_\beta\left(\frac{\ln(p)}{2}\right). \tag{5.41}$$

Note that the above integral becomes the moment generating function of $f_2(\beta)$, with parameter $\frac{\ln(p)}{2}$. If $f_1(\beta)$ is a gamma distribution, then

$$M_\beta\left(\frac{\ln(p)}{2}\right) = \int_0^\infty e^{\beta \frac{\ln(p)}{2}} \frac{1}{\Gamma(a) b^a} \beta^{a-1} e^{-\frac{\beta}{b}}\, d\beta \tag{5.42}$$

$$= \frac{1}{\Gamma(a) b^a} \int_0^\infty \beta^{a-1} e^{-\frac{\beta}{b}\left(1 - b\frac{\ln(p)}{2}\right)}\, d\beta \tag{5.43}$$

$$= \frac{1}{\Gamma(a) b^a} \Gamma(a) \left(\frac{b}{\left(1 - b\frac{\ln(p)}{2}\right)}\right)^a \tag{5.44}$$

$$= \frac{1}{\left(1 - b\frac{\ln(p)}{2}\right)^a} \tag{5.45}$$

for $\frac{\ln(p)}{2} < \frac{1}{b}$. Since $0 < p < 1$ and $b > 0$, this condition is always satisfied. Therefore,

$$E\left[c^*\right] = \frac{\sqrt{2\sigma^2 \ln[(1-p)^\alpha R]}}{\left(1 - b\frac{\ln(p)}{2}\right)^a}. \tag{5.46}$$

We can next determine what the optimal resource allocation to dispersal should be in order to maximize the expected value of the spreading speed. To do this, we determine when

$$\frac{d}{dp} E\left[c^*\right] = 0. \tag{5.47}$$

We find that the implicit equation that satisfies this is given by

$$\frac{a}{\alpha} \ln\left[(1-p)^\alpha R\right](1-p) = \frac{p}{b}\left(1 - \frac{1}{2} b \ln(p)\right). \tag{5.48}$$

Recall that the $E[\beta] = ab$ and $\text{Var}[\beta] = ab^2$. We can rewrite our previous condition as

$$\frac{E[\beta]}{\alpha} \ln\left[(1-p^*)^\alpha R\right](1-p^*) = p^*\left(1 - \frac{1}{2}\frac{\text{Var}[\beta]}{E[\beta]}\ln(p^*)\right). \tag{5.49}$$

Therefore, the optimal resource allocation for dispersal is given implicitly by (5.49). □

5.5.1.0.4 Proof of Theorem 5.3.4

Proof. Assuming that α is a random variable defined on $\left(0, -\frac{\ln(R)}{\ln(1-p)}\right)$ with probability density function $f_2(\alpha)$, the expected spreading speed is given by

$$E[c^*] = \int_0^{-\frac{\ln(R)}{\ln(1-p)}} \sqrt{2p^\beta\sigma^2 \ln[(1-p)^\alpha R]} f_2(\alpha)\, d\alpha \tag{5.50}$$

$$= \sqrt{2p^\beta\sigma^2} \int_0^{-\frac{\ln(R)}{\ln(1-p)}} \sqrt{\ln[(1-p)^\alpha R]} f_2(\alpha)\, d\alpha \tag{5.51}$$

$$= \sqrt{2p^\beta\sigma^2} \int_0^{-\frac{\ln(R)}{\ln(1-p)}} \sqrt{\alpha\ln(1-p) + \ln(R)} f_2(\alpha)\, d\alpha. \tag{5.52}$$

Using Newton's Generalized binomial theorem, we have that

$$\sqrt{\alpha\ln(1-p) + \ln(R)} = \sum_{n=0}^{\infty} \binom{\frac{1}{2}}{n} (\ln(R))^{\frac{1}{2}-n} (\alpha\ln(1-p))^n \tag{5.53}$$

$$= \sqrt{\ln(R)} \sum_{n=0}^{\infty} \binom{\frac{1}{2}}{n} \left(\frac{\ln(1-p)}{\ln(R)}\right)^n \alpha^n. \tag{5.54}$$

This series converges when $\ln(R) > |\alpha\ln(1-p)|$ which is equivalent to our persistence criterion $R(1-p)^\alpha > 1$. Using Fubini's theorem,

$$\int_0^{-\frac{\ln(R)}{\ln(1-p)}} \sum_{n=0}^{\infty} \binom{\frac{1}{2}}{n} \left(\frac{\ln(1-p)}{\ln(R)}\right)^n \alpha^n f_2(\alpha)\, d\alpha = \sum_{n=0}^{\infty} \binom{\frac{1}{2}}{n} \left(\frac{\ln(1-p)}{\ln(R)}\right)^n \int_0^{-\frac{\ln(R)}{\ln(1-p)}} \alpha^n f_2(\alpha)\, d\alpha \tag{5.55}$$

$$= \sum_{n=0}^{\infty} \binom{\frac{1}{2}}{n} \left(\frac{\ln(1-p)}{\ln(R)}\right)^n E[\alpha^n]. \tag{5.56}$$

From (5.52), (5.54), and (5.56) we can see that when α is uncertain the expected value for the spreading speed is given by

$$E\left[c^*\right] = \sqrt{2\sigma^2 p^\beta \ln(R)} \sum_{n=0}^{\infty} \binom{\frac{1}{2}}{n} \left(\frac{\ln(1-p)}{\ln(R)}\right)^n E\left[\alpha^n\right]. \tag{5.57}$$

Therefore, we can express the expected value for the spreading speed in terms of a series of the moments of the distribution. In particular, when $\alpha \sim$ Beta(a, b) on $\left(0, -\frac{\ln(R)}{\ln(1-p)}\right)$,

$$E\left[\alpha^n\right] = \int_0^{-\frac{\ln(R)}{\ln(1-p)}} \alpha^n \frac{\alpha^{a-1}\left(-\frac{\ln(R)}{\ln(1-p)} - \alpha\right)^{b-1}}{B(a,b)\left(-\frac{\ln(R)}{\ln(1-p)}\right)^{a+b-1}} d\alpha \tag{5.58}$$

$$= \left(-\frac{\ln(R)}{\ln(1-p)}\right)^n \int_0^{-\frac{\ln(R)}{\ln(1-p)}} \frac{\alpha^{a+n-1}\left(-\frac{\ln(R)}{\ln(1-p)} - \alpha\right)^{b-1}}{B(a,b)\left(-\frac{\ln(R)}{\ln(1-p)}\right)^{a+n+b-1}} d\alpha \tag{5.59}$$

$$= \left(-\frac{\ln(R)}{\ln(1-p)}\right)^n \frac{B(a+n,b)}{B(a+b)} \tag{5.60}$$

$$= \left(-\frac{\ln(R)}{\ln(1-p)}\right)^n \frac{\Gamma(a+b)\Gamma(a+n)}{\Gamma(a)\Gamma(a+b+n)} \tag{5.61}$$

for $n \geq 0$, and the expected value for the spreading speed is

$$E\left[c^*\right] = \sqrt{2\sigma^2 p^\beta \ln(R)} \sum_{n=0}^{\infty} \binom{\frac{1}{2}}{n} \left(\frac{\ln(1-p)}{\ln(R)}\right)^n \left(-\frac{\ln(R)}{\ln(1-p)}\right)^n \frac{\Gamma(a+b)\Gamma(a+n)}{\Gamma(a)\Gamma(a+b+n)} \tag{5.62}$$

$$= \sqrt{2\sigma^2 p^\beta \ln(R)} \frac{\Gamma(a+b)}{\Gamma(a)} \sum_{n=0}^{\infty} \binom{\frac{1}{2}}{n} (-1)^n \frac{\Gamma(a+n)}{\Gamma(a+b+n)} \tag{5.63}$$

Using the fact that

$$\sum_{n=0}^{\infty} \binom{\frac{1}{2}}{n} (-1)^n \frac{\Gamma(a+n)}{\Gamma(a+b+n)} = \frac{\Gamma\left(b+\frac{1}{2}\right)\Gamma(a)}{\Gamma\left(a+b+\frac{1}{2}\right)\Gamma(b)}, \tag{5.64}$$

we can simplify (5.63) to

$$E\left[c^*\right] = \sqrt{2\sigma^2 p^\beta \ln(R)} \frac{\Gamma(a+b)\Gamma\left(b+\frac{1}{2}\right)}{\Gamma(b)\Gamma\left(a+b+\frac{1}{2}\right)}. \tag{5.65}$$

Attempting to determine the optimal resource allocation to dispersal, we find that there are no critical points for $0 < p < 1$ since

$$\frac{d}{dp}E\left[c^*\right] = \sqrt{2\sigma^2\ln(R)}\frac{\Gamma(a+b)\Gamma\left(b+\frac{1}{2}\right)}{\Gamma(b)\Gamma\left(a+b+\frac{1}{2}\right)}\frac{d}{dp}p^{\frac{\beta}{2}} \tag{5.66}$$

$$= \sqrt{2\sigma^2\ln(R)}\frac{\Gamma(a+b)\Gamma\left(b+\frac{1}{2}\right)}{\Gamma(b)\Gamma\left(a+b+\frac{1}{2}\right)}\frac{\beta}{2}p^{\frac{\beta}{2}-1} \tag{5.67}$$

$$> 0. \tag{5.68}$$

Therefore, we can conclude that the best resource allocation would be to allocate as many resources as possible to dispersal while still maintaining the persistence condition that $(1-p)^\alpha R > 1$. This would mean that

$$p < 1 - \frac{1}{\sqrt[\alpha]{R}}. \tag{5.69}$$

Therefore, we would want to choose p as close to $1 - \frac{1}{\sqrt[\alpha]{R}}$ as possible without reaching or going over this value. □

5.5.1.0.5 Proof of Theorem 5.3.5

Proof. Assuming that σ is a random variable defined on the real line with probability density function $f_3(\sigma)$, the expected spreading speed is given by

$$E\left[c^*\right] = \int_0^\infty \sqrt{2p^\beta\sigma^2\ln[(1-p)^\alpha R]}f_3(\sigma)\,d\sigma \tag{5.70}$$

$$= \sqrt{2p^\beta\ln[(1-p)^\alpha R]}\int_0^\infty \sigma f_3(\sigma)\,d\sigma \tag{5.71}$$

$$= \sqrt{2p^\beta\ln[(1-p)^\alpha R]}E\left[\sigma\right]. \tag{5.72}$$

Determining the optima resource allocation to dispersal, we find that

$$0 = \frac{d}{dp}E\left[c^*\right] \tag{5.73}$$

$$= E[\sigma]\frac{d}{dp}\sqrt{2p^\beta\ln[(1-p)^\alpha R]} \tag{5.74}$$

$$= E[\sigma]p^\beta\frac{\frac{\ln((1-p)^\alpha R)}{p} - \frac{\alpha}{1-p}}{\sqrt{2p^\beta\ln\left((1-p)^\alpha R\right)}}. \tag{5.75}$$

Hence, we have our critical point when

$$\frac{\ln\left((1-p)^{\alpha}R\right)}{p} = \frac{\alpha}{1-p}. \tag{5.76}$$

□

5.5.1.0.6 Proof of Theorem 5.3.6

Proof. Assuming that $\ln(R)$ is a random variable defined on $(-\alpha\ln(1-p),\infty)$ with probability density function $f_4(\ln(R))$, the expected spreading speed is given by

$$E\left[c^*\right] = \int_{-\alpha\ln(1-p)}^{\infty} \sqrt{2p^{\beta}\sigma^2\ln[(1-p)^{\alpha}R]}f_4(\ln(R))\,d\ln(R) \tag{5.77}$$

$$= \sqrt{2p^{\beta}\sigma^2}\int_{-\alpha\ln(1-p)}^{\infty} \sqrt{\ln[(1-p)^{\alpha}R]}f_4(\ln(R))\,d\ln(R) \tag{5.78}$$

$$= \sqrt{2p^{\beta}\sigma^2}\int_{-\alpha\ln(1-p)}^{\infty} \sqrt{\alpha\ln(1-p)+\ln(R)}f_4(\ln(R))\,d\ln(R) \tag{5.79}$$

$$= \sqrt{2p^{\beta}\sigma^2}E\left[(\ln(R)+\alpha\ln(1-p))^{\frac{1}{2}}\right]. \tag{5.80}$$

Assuming that $\ln(R) \sim \text{Gamma}(a,b)$ on $(-\alpha\ln(1-p),\infty)$, we define $r = \ln(R)+\alpha(1-p)$ and calculate the one halfth moment to be

$$E\left[(\ln(R)+\alpha\ln(1-p))^{\frac{1}{2}}\right] = E\left[r^{\frac{1}{2}}\right] \tag{5.81}$$

$$= \int_{-\alpha\ln(1-p)}^{\infty} r^{\frac{1}{2}}f_4(\ln(R))\,d\ln(R) \tag{5.82}$$

$$= \int_{-\alpha\ln(1-p)}^{\infty} r^{\frac{1}{2}}\frac{1}{\Gamma(a)b^a}r^{a-1}e^{-\frac{r}{b}}\,d\ln(R) \tag{5.83}$$

$$= \frac{1}{\Gamma(a)b^a}\int_{-\alpha\ln(1-p)}^{\infty} r^{a+\frac{1}{2}-1}e^{-\frac{r}{b}}\,d\ln(R) \tag{5.84}$$

$$= \frac{1}{\Gamma(a)b^a}\Gamma\left(a+\frac{1}{2}\right)b^{a+\frac{1}{2}} \tag{5.85}$$

$$= \frac{\Gamma\left(a+\frac{1}{2}\right)b^{\frac{1}{2}}}{\Gamma(a)}. \tag{5.86}$$

Then, using (5.86) the expected spreading speed becomes

$$E\left[c^*\right] = \sqrt{2p^\beta\sigma^2}E\left[\left(\ln(R) + \alpha\ln(1-p)\right)^{\frac{1}{2}}\right] \tag{5.87}$$

$$= \sqrt{2p^\beta\sigma^2}\frac{\Gamma\left(a+\frac{1}{2}\right)b^{\frac{1}{2}}}{\Gamma(a)} \tag{5.88}$$

$$= \sqrt{2p^\beta\sigma^2 b}\frac{\Gamma\left(a+\frac{1}{2}\right)}{\Gamma(a)}. \tag{5.89}$$

Determining the optimal resource allocation to dispersal, we find that

$$\frac{d}{dp}E\left[c^*\right] = \frac{d}{dp}\sqrt{2p^\beta\sigma^2 b}\frac{\Gamma\left(a+\frac{1}{2}\right)}{\Gamma(a)} \tag{5.90}$$

$$= \sqrt{2\sigma^2 b}\frac{\Gamma\left(a+\frac{1}{2}\right)}{\Gamma(a)}\frac{\beta}{2}p^{\frac{\beta}{2}-1} \tag{5.91}$$

$$> 0. \tag{5.92}$$

Therefore, we can conclude that the best resource allocation would be to allocate as many resources as possible to dispersal while still maintaining the persistence condition that $(1-p)^\alpha R > 1$. This would mean that

$$p < 1 - \frac{1}{\sqrt[\alpha]{R}}. \tag{5.93}$$

Therefore, we would want to choose p as close to $1 - \frac{1}{\sqrt[\alpha]{R}}$ as possible without reaching or going over this value. □

References

Barbour, Michael G, Jack H Burk, Wanna D Pitts, Frank S. Gillian, and Schwartz Mark W. (1999). "Allocation and life history patterns." *Terrestrial Plant Ecology*. Ed. by Benjamin Cummings. USA: Adison Wesley Longman, pp. 88–116.

Bateman, Andrew W, Andreas Buttenschön, Kelley D Erickson, and Nathan G Marculis (2017). "Barnacles vs bullies: modelling biocontrol of the invasive European green crab using a castrating barnacle parasite." *Theoretical Ecology* 10.3, pp. 305–318.

Beverton, Raymond JH and Sidney J Holt (2012). *On the Dynamics of Exploited Fish Populations*. Vol. 11. Springer Science & Business Media.

Bonte, Dries et al. (2012). "Costs of dispersal." *Biological Reviews* 87.2, pp. 290–312.

Burton, Olivia J, Ben L Phillips, and Justin M J Travis (2010). "Trade-offs and the evolution of life-histories during range expansion." *Ecology Letters* 13.10, pp. 1210–1220.

Chuang, Angela and Christopher R Peterson (2016). "Expanding population edges: theories, traits, and trade-offs." *Global Change Biology* 22.2, pp. 494–512.

Clark, James S, Mark Lewis, and Lajos Horvath (2001). "Invasion by extremes: population spread with variation in dispersal and reproduction." *The American Naturalist* 157.5, pp. 537–554.

Cody, Martin L (1966). "A general theory of clutch size." *Evolution*, pp. 174–184.

Cotto, Olivier, Manuel Massot, Ophélie Ronce, and Jean Clobert (2015). "Dispersal as a source of variation in age-specific reproductive strategies in a wild population of lizards." *Proceedings of the Royal Society B: Biological Sciences* 282.1820, p. 20151741.

Cox, Robert M and Ryan Calsbeek (2010). "Severe costs of reproduction persist in Anolis lizards despite the evolution of a single-egg clutch." *Evolution: International Journal of Organic Evolution* 64.5, pp. 1321–1330.

Cressler, Clayton E, Aaron A King, and Earl E Werner (2010). "Interactions between behavioral and life-history trade-offs in the evolution of integrated predator-defense plasticity." *The American Naturalist* 176.3, pp. 276–288.

Dewhirst, Sebastian and Frithjof Lutscher (2009). "Dispersal in heterogeneous habitats: thresholds, spatial scales, and approximate rates of spread." *Ecology* 90.5, pp. 1338–1345.

Dockery, Jack, Vivian Hutson, Konstantin Mischaikow, and Mark Pernarowski (1998). "The evolution of slow dispersal rates: a reaction diffusion model." *Journal of Mathematical Biology* 37.1, pp. 61–83.

Duthie, A Bradley, Karen C Abbott, and John D Nason (2014). "Trade-offs and coexistence: a lottery model applied to fig wasp communities." *The American Naturalist* 183.6, pp. 826–841.

Elliott, Christina G and Maya L Evenden (2012). "The effect of flight on reproduction in an outbreaking forest lepidopteran." *Physiological Entomology* 37.3, pp. 219–226.

Ellner, Stephen P and Sebastian J Schreiber (2012). "Temporally variable dispersal and demography can accelerate the spread of invading species." *Theoretical Population Biology* 82.4, pp. 283–298.

Freedman, Herbert I and Peter Moson (1990). "Persistence definitions and their connections." *Proceedings of the American Mathematical Society* 109.4, pp. 1025–1033.

Geritz, Stefan AH (1995). "Evolutionarily stable seed polymorphism and small-scale spatial variation in seedling density." *The American Naturalist* 146.5, pp. 685–707.

Ghalambor, Cameron K, David N Reznick, and Jeffrey A Walker (2004). "Constraints on adaptive evolution: the functional trade-off between reproduction and fast-start swimming performance in the Trinidadian guppy (Poecilia reticulata)." *The American Naturalist* 164.1, pp. 38–50.

Gharouni, Ali, Myriam A Barbeau, Andrea Locke, Lin Wang, and James Watmough (2015). "Sensitivity of invasion speed to dispersal and demography: an application of spreading speed theory to the green crab invasion on the northwest Atlantic coast." *Marine Ecology Progress Series* 541, pp. 135–150.

Gibbs, Melanie and Hans Van Dyck (2010). "Butterfly flight activity affects reproductive performance and longevity relative to landscape structure." *Oecologia* 163.2, pp. 341–350.

Gill, Frank B (2006). *Ornithology*. W.H. Freeman.

Greene, David F and Edward A Johnson (1993). "Seed mass and dispersal capacity in wind-dispersed diapores." *Oikos* 67.1, pp. 69–74.

Guerra, Patrick A (2011). "Evaluating the life-history trade-off between dispersal capability and reproduction in wing dimorphic insects: a meta-analysis." *Biological Reviews* 86.4, pp. 813–835.

Haefner, James W (2005). *Modeling Biological Systems: Principles and Applications*. Springer Science & Business Media.

Hanski, Ilkka, Marjo Saastamoinen, and Otso Ovaskainen (2006). "Dispersal-related life-history trade-offs in a butterfly metapopulation." *Journal of Animal Ecology* 75.1, pp. 91–100.

Harrison, Richard G (1980). "Dispersal polymorphisms in insects." *Annual Review of Ecology and Systematics* 11.1, pp. 95–118.

Hastings, Alan (1983). "Can spatial variation alone lead to selection for dispersal?" *Theoretical Population Biology* 24.3, pp. 244–251.

Hoyle, Andrew, Roger G Bowers, Andrew White, and Michael Boots (2008). "The influence of trade-off shape on evolutionary behaviour in classical ecological scenarios." *Journal of Theoretical Biology* 250.3, pp. 498–511.

Hughes, Clare L, Jane K Hill, and Calvin Dytham (2003). "Evolutionary trade-offs between reproduction and dispersal in populations at expanding range boundaries." *Proceedings of the Royal Society of London B: Biological Sciences* 270.Suppl 2, S147–S150.

Jones, Laura E and Stephen P Ellner (2004). "Evolutionary tradeoff and equilibrium in an aquatic predator-prey system." *Bulletin of Mathematical Biology* 66.6, pp. 1547–1573.

Kawasaki, Kohkichi and Nakako Shigesada (2007). "An integrodifference model for biological invasions in a periodically fragmented environment." *Japan Journal of Industrial and Applied Mathematics* 24.1, pp. 3–15.

Kot, Mark (1992). "Discrete-time travelling waves: ecological examples." *Journal of Mathematical Biology* 30.4, pp. 413–436.

Kot, Mark, Mark A Lewis, and Pauline van den Driessche (1996). "Dispersal data and the spread of invading organisms." *Ecology* 77.7, pp. 2027–2042.

Kot, Mark and William M Schaffer (1986). "Discrete-time growth-dispersal models." *Mathematical Biosciences* 80.1, pp. 109–136.

Latore, J, P Gould, and AM Mortimer (1999). "Effects of habitat heterogeneity and dispersal strategies on population persistence in annual plants." *Ecological Modelling* 123.2-3, pp. 127–139.

Lewis, Mark A and Stephen Pacala (2000). "Modeling and analysis of stochastic invasion processes." *Journal of Mathematical Biology* 41.5, pp. 387–429.

Link, William A and Paul F Doherty Jr (2002). "Scaling in sensitivity analysis." *Ecology* 83.12, pp. 3299–3305.

Miles, Donald B, Barry Sinervo, and W Anthony Frankino (2000). "Reproductive burden, locomotor performance, and the cost of reproduction in free ranging lizards." *Evolution* 54.4, pp. 1386–1395.

Mole, Simon and Anthony J Zera (1994). "Differential resource consumption obviates a potential flight–fecundity trade-off in the sand cricket (Gryllus firmus)." *Functional Ecology* 8, pp. 573–580.

Mollison, Denis (1991). "Dependence of epidemic and population velocities on basic parameters." *Mathematical Biosciences* 107.2, pp. 255–287.

Neubert, Michael G and Hal Caswell (2000). "Demography and dispersal: calculation and sensitivity analysis of invasion speed for structured populations." *Ecology* 81.6, pp. 1613–1628.

Proctor, Noble S and Patrick J Lynch (1993). *Manual of ornithology: avian structure & function*. Yale University Press.

Prop, Jouke, Jeffrey M Black, and Paul Shimmings (2003). "Travel schedules to the high arctic: barnacle geese trade-off the timing of migration with accumulation of fat deposits." *Oikos* 103.2, pp. 403–414.

Récapet, Charlotte, Pierre Bize, and Blandine Doligez (2017). "Food availability modulates differences in parental effort between dispersing and philopatric birds." *Behavioral Ecology* 28.3, pp. 688–697.

Roff, Derek A (1984). "The cost of being able to fly: a study of wing polymorphism in two species of crickets." *Oecologia* 63.1, pp. 30–37.

— (1990). "The evolution of flightlessness in insects." *Ecological Monographs* 60.4, pp. 389–421.

— (1995). "Antagonistic and reinforcing pleiotropy: a study of differences in development time in wing dimorphic insects." *Journal of Evolutionary Biology* 8.4, pp. 405–419.

Sappington, Thomas W and William B Showers (1992). "Reproductive maturity, mating status, and long-duration flight behavior of Agrotis ipsilon(Lepidoptera: Noctuidae) and the conceptual misuse of the oogenesis-flight syndrome by entomologists." *Environmental Entomology* 21.4, pp. 677–688.

Schmidt-Wellenburg, Carola A, G Henk Visser, Brigitte Biebach, Kaspar Delhey, Martina Oltrogge, Andrea Wittenzellner, Herbert Biebach, and Bart Kempenaers (2008). "Trade-off between migration and reproduction: does a high workload affect body condition and reproductive state?" *Behavioral Ecology* 19.6, pp. 1351–1360.

Seigel, Richard A, M M Huggins, and Neil B Ford (1987). "Reduction in locomotor ability as a cost of reproduction in gravid snakes." *Oecologia* 73.4, pp. 481–485.

Siggins, Howard W (1933). "Distribution and rate of fall of conifer seeds." *Journal of Agricultural Research* 47, pp. 119–128.

Snyder, Robin E (2003). "How demographic stochasticity can slow biological invasions." *Ecology* 84.5, pp. 1333–1339.

Stevens, David J, Michael H Hansell, and Pat Monaghan (2000). "Developmental trade–offs and life histories: strategic allocation of resources in caddis

flies." *Proceedings of the Royal Society of London B: Biological Sciences* 267.1452, pp. 1511–1515.

Therry, Lieven, Dries Bonte, and Robby Stoks (2015). "Higher investment in flight morphology does not trade off with fecundity estimates in a poleward range-expanding damselfly." *Ecological Entomology* 40.2, pp. 133–142.

Thompson, Ken, Louise C Rickard, Dunmail J Hodkinson, and Mark Rees (2002). "Seed dispersal: the search for trade-offs." *Dispersal ecology*. Blackwell Oxford, UK. Chap. 8, pp. 152–172.

Tigreros, Natasha and Goggy Davidowitz (2019). "Flight-fecundity tradeoffs in wing-monomorphic insects." *Advances in Insect Physiology* 56, p. 1.

Van Dyck, Hans and Michel Baguette (2005). "Dispersal behaviour in fragmented landscapes: routine or special movements?" *Basic and Applied Ecology* 6.6, pp. 535–545.

Van Kirk, Rob W and Mark A Lewis (1997). "Integrodifference models for persistence in fragmented habitats." *Bulletin of Mathematical Biology* 59.1, pp. 107–137.

Vasilyeva, Olga, Frithjof Lutscher, and Mark A Lewis (2016). "Analysis of spread and persistence for stream insects with winged adult stages." *Journal of Mathematical Biology* 72.4, pp. 851–875.

Verdolin, Jennifer L (2006). "Meta-analysis of foraging and predation risk trade-offs in terrestrial systems." *Behavioral Ecology and Sociobiology* 60.4, pp. 457–464.

Weinberger, Hans F (1982). "Long-time behavior of a class of biological models." *SIAM Journal on Mathematical Analysis* 13.3, pp. 353–396.

Yoshida, Takehito, Nelson G Hairston Jr, and Stephen P Ellner (2004). "Evolutionary trade–off between defence against grazing and competitive ability in a simple unicellular alga, Chlorella vulgaris." *Proceedings of the Royal Society of London. Series B: Biological Sciences* 271.1551, pp. 1947–1953.

Zera, Anthony J and Robert F Denno (1997). "Physiology and ecology of dispersal polymorphism in insects." *Annual Review of Entomology* 42.1, pp. 207–230.

Zera, Anthony J and Lawrence G Harshman (2001). "The physiology of life history trade-offs in animals." *Annual Review of Ecology and Systematics* 32.1, pp. 95–126.

Zhao, Zhangwu and Anthony J Zera (2002). "Differential lipid biosynthesis underlies a tradeoff between reproduction and flight capability in a wing-

polymorphic cricket." *Proceedings of the National Academy of Sciences* 99.26, pp. 16829–16834.

Ziv, Yaron and Goggy Davidowitz (2019). "When Landscape Ecology Meets Physiology: Effects of Habitat Fragmentation on Resource Allocation Trade-Offs." *Frontiers in Ecology and Evolution* 7, p. 137.

Chapter 6

Conclusion

In this thesis, I use integrodifference equations as a modeling tool to study complex ecological processes. In particular, there were two overarching themes; in the first I use integrodifference equations to understand how range expansions influence the spatial patterns of genetic spread and the second concerning the role that dispersal-reproduction trade-offs have on the spreading speed of the population. The neutral genetic patterns formed by spatial spread was studied in Chapters 2-4, and the trade-off effect was considered in Chapter 5. In this conclusion, I put our work in context for how it fits into the current mathematical and ecological literature. For the remainder of this section, I will summarize our results, reference how they fit into the literature, discuss some shortcomings, and point to some suggestions for future work.

In Chapters 2-4, we studied the effect that range expansions have on the neutral genetic patterns of a spreading population. The analysis performed in this section is dubbed "inside dynamics" because we am concerned the dynamics of the inside structure of the population. The term inside dynamics was coined by Garnier et al. (2012) in their seminal study. The primary assumption in this kind of analysis is that the dispersal and reproduction are the same for all individuals. This allows us to partition the population into distinct subgroups that only differ by label and location. Thus, the inside

dynamics of the population, can be directly applied to understand how neutral genetic components of a population spread through space.

In Chapter 2, we use a scalar integrodifference equation to determine the spatial patterns of genetic spread. Our motivation is driven by the previous work on this topic for continuous-time models (Bonnefon et al., 2014, 2013; Garnier et al., 2012; Roques et al., 2012). In this study, we consider three different types of growth functions. In the first case, we begin with the classic monotone growth function, with the maximal growth rate at zero. We prove that if the dispersal kernel is thin-tailed, then the population spread is dominated by the individuals that are initially present at the leading edge of the population. This case is equivalent to the concept of pulled fronts because the spread of the population is pulled by those individuals at low density in the leading edge (Stokes, 1976). This pattern can be interpreted as an extreme version of the founder effect (Mayr, 1940).

The second growth function we consider is one with overcompensation. That is, at high density, reproduction becomes suppressed by crowding and depletion of resources. We are the first in the inside dynamics literature to study this growth function because overcompensation cannot be modeled by a scalar continuous-time model. In the case of the Ricker growth function, if the dispersal kernel is thin-tailed, then we find that overcompensation does not impact the genetic patterns of spread and the solution is a pulled front where the population is driven by individuals initially at the leading edge. This suggests with our simplistic model that the high level density dependence of the growth function is not a critical factor for determining the genetic patterns of population spread. However, previous work has found that survival of beneficial mutations increases with stronger overcompensation (Münkemüller et al., 2011). Thus, with some form of selection and mutation on the neutral genes, overcompensation has shown to play an important role.

The final growth function we study in Chapter 2 is one with a strong Allee effect. Recall that a population exhibiting a strong Allee effect will have a critical population density under which the population growth rate becomes negative. With a Gaussian dispersal kernel, we were able to prove that each neutral component converges to a proportion of the traveling wave solution. Moreover, we derive an explicit formula for the proportion that depends on the initial spatial distribution of neutral fractions, the traveling wave solution, the dispersal parameters, and the spreading speed. This result is consistent with its counterpart that was previously shown for reaction-diffusion equations (Garnier et al., 2012). However, our result allows for dispersal to not only be a diffusive process but also includes advection since we allow for the mean in the Gaussian dispersal kernel to be non-zero. While the Allee effect is generally thought to have a negative impact on expanding populations due to the capability of the population to die out at low density levels, our results show that the strong Allee effect promotes genetic diversity in spreading populations. One draw back of this result is the restriction of the dispersal kernel to be Gaussian. We conjecture that a result similar to this should be possible for other thin-tailed dispersal kernels and leave this for future directions of this work.

To expand on the work presented in Chapter 2, we extend our study from a scalar model to a stage-structure integrodifference equation in Chapter 3. In this chapter, we shift our focus from understanding how the different growth functions influence the genetic patterns of population spread into understanding how the structure of the population influences these patterns. Previous work has shown that the inclusion of a juvenile class into the population dynamics has shown a decrease in the founder effect (Austerlitz et al., 2000). This provides us with motivation for adding the complexity of stage-structure into our model. In the inside dynamics literature, there is only one study to

our knowledge that considers a system of equations (Roques et al., 2015). The study by Roques et al. (2015) considered a diffusive Lotka-Volterra competition system. Our analysis is quite different from the work by Roques et al. (2015) because the stage-structured integrodifference equation is a cooperative not competitive system.

Our results in Chapter 3 illustrate how the structure of the population and the spatial distribution of individuals alter the neutral genetic patterns of spread. In particular, we prove that if a neutral fraction is present at the leading edge of the population, then it approaches a proportion of the population density. Moreover, this proportion is dependent on the right and left eigenvectors of the population projection matrix evaluated at zero and the initial distribution of neutral fractions. Thus, our results are consistent with those concluded by Austerlitz et al. (2000) that including structure in the population dynamics reduces the strength of the founder effect in a spreading population. This is due to the ability for multiple stages to each have a different neutral fraction present at the leading edge which in turn increases the genetic heterogeneity of the expanding population.

In Chapter 4, we consider one more complexity in the inside dynamics analysis by including mutation between neutral fractions into the model. This is motivated by recent work that has shown spatial patterns in neutral mutations can occur even in homogeneous landscapes (Edmonds et al., 2004; Klopfstein et al., 2006). These patterns are said to occur due to the propagation of low-frequency alleles on the wave front of a population's range expansion. This phenomena is commonly referred to as mutation surfing and has been demonstrated in laboratory experiments using florescently labeled strains of *Escherichia coli* (Hallatschek et al., 2007). There are two primary drivers for this process: first, low population density at the leading edge of the expansion is believed to result in reduced competition pressure, and second, because

of limited dispersal, the offspring of colonizers of the last generation dominate the population dynamics, resulting in the acceleration of genetic drift (Münkemüller et al., 2011).

Our primary findings in Chapter 4 show how the neutral mutations influence the spatial patterns of genetic spread. In particular, we show that the mutation structure of the population and the initial distribution of neutral fractions are the two important pieces of information needed to determine the long-time dynamics of the neutral fractions. We show that if a neutral fraction at the leading edge belongs to a particular mutation class, then asymptotically each neutral fraction in this mutation class approaches a proportion of the population density. Moreover, this proportion is simply given by the right eigenvector of the mutation matrix for said mutation class. Thus, our model demonstrates how spatial patterns can form from neutral mutations in homogeneous landscapes. This agrees with the previous studies that have also found this same behavior (Edmonds et al., 2004; Klopfstein et al., 2006).

There are still many avenues left to explore for the inside dynamics analysis of integrodifference equations. One that is immediately evident is to determine the role that long-distance dispersal plays in the neutral genetic patterns formed by range expansions. This process is generally modeled by fat-tailed dispersal kernels, or in other words dispersal kernels whose tails are not exponentially bounded. A previous study using integro-differential equations proved that the solution of an accelerating wave is a pushed front showing that all neutral fractions contribute to the population spread at the leading edge (Bonnefon et al., 2014), thereby reducing the founder effect in spreading populations. The complexity with studying this problem is that we are no longer able to analyze traveling wave solutions that spread at a constant speed, but must instead consider accelerating waves whose speed increases over time.

Another natural extension would be to test how environmental heterogene-

ity affects the inside dynamics of the population. It is well known that high levels of environmental heterogeneity is positively correlated with species diversity (Stein et al., 2014). In the context of climate change, this has been studied in reaction-diffusion equations (Garnier and Lewis, 2016) and integrodifference equations (Lewis et al., 2018) by assuming a finite habitat size that shifts in space over time. In these studies, it is shown how the size and speed of the shifting habitat influence the genetic diversity of the population. More general environmental configurations such as periodic habitats have yet to be studied, but there are many mathematical results that could be directly applied to an inside dynamics model with a periodic habitat (Kawasaki and Shigesada, 2007).

The inherent limitation with the inside dynamics analysis is that the genes are assumed to be neutral. However in reality, there are many genes that are chosen for under selection that influence population level dynamics (Saccheri and Hanski, 2006). While the role of neutral genes can inform us about many important processes such as genetic drift, gene flow, and migration; by considering non-neutral genes we can learn more about the evolutionary potential of individuals. The mathematical complexity with studying non-neutral genes is that the system of equations becomes a competition model. While many results pertaining to the case with two different strategies can be applied (Lewis et al., 2002), understanding in higher dimensions is still an open question.

In Chapter 5, we construct a model using integrodifference equations for the dispersal-reproduction trade-off. To model the trade-off, we use the principle of allocation that which states the energy allocation to one function reduces the amount of energy available to all other functions (Cody, 1966). As done in previous studies of trade-off effects (Cressler et al., 2010; Jones and Ellner, 2004), the trade-off is modeled using power functions for the amount of resources invested to dispersal and reproduction. This work is motivated by the

empirical evidence reported for a variety of insects (Duthie et al., 2014; Elliott and Evenden, 2012; Hanski et al., 2006; Hughes et al., 2003; Stevens et al., 2000; Z. Zhao and Zera, 2002). In particular, we are motivated to understand how the spreading speed of the population is altered by this trade-off. For simplicity in our analysis, we assume that the dispersal kernel is Gaussian and the growth is modeled by a Beverton-Holt function. This, allows us to write down an explicit formula for the spreading speed.

The first step in our analysis is to perform a sensitivity analysis on the spreading speed with respect to the trade-off parameters and the dispersal and reproduction parameters. While other studies have have determined the sensitivity of the invasion speed with respect to the dispersal and reproduction parameters (Gharouni et al., 2015; Neubert and Caswell, 2000), we expand on these ideas to incorporate a dispersal-reproduction trade-off into the model. The first conclusion we make is that the sensitivity of the spreading speed with respect to the trade-off shape parameters is always negative. This means that as the trade-off becomes more pronounced, then the spreading speed decreases. We are able to prove that if the population is persistent, then there is a unique allocation of resources to dispersal and reproduction that allow for the largest value for the spreading speed. Unfortunately, it is not possible to derive an explicit form for this resource allocation, but we can write the condition as a transcendental equation. Next, we prove that if the population is at its optimal resource allocation and the resources are split equally between dispersal and reproduction, then the shape parameters for the reproduction and dispersal trade-off curves are equally sensitive. We also show that if the population is at its optimal resource allocation and more (less) resources are allocated to dispersal than reproduction, then the shape parameter for reproduction is more (less) sensitive than the shape parameter for dispersal.

For the dispersal and reproduction parameters, we find that the sensitivity

of the spreading speed with respect to the standard deviation in dispersal distance is equal to one because it is a scaling parameter in the formula for the spreading speed, and the sensitivity of the the spreading speed with respect to the population growth rate per generation is always positive when the population is persistent. Comparing these two, we find that the population growth rate per generation is more sensitive than the standard deviation in dispersal distance when the population is close to extinction, but if the population is not at risk of extinction, then the sensitivity switches.

After the sensitivity analysis, we move on to test how parameter uncertainty affects the spreading speed for the population and calculate the expected spreading speed for the population. Previous studies have determined how periodic and stochastic environments impact the spreading speed (Neubert et al., 2000; Weinberger et al., 2008). The terms uncertainty and stochasticity should not be misunderstood. When we say uncertainty, we mean that that parameter value of interest is known up to some distribution whereas the stochastic studies have time dependent parameter values. In the stochastic studies, the formula for the spreading speed is written in terms of the geometric mean and because the geometric mean is less than the arithmetic mean the stochastic invasion process eventually spreads slower than the expected population spread as calculated in our work. This problem has been studied before for linear models where the emphasis is on how stochasticity can influence the spreading speed (Mollison, 1991) and more complicated nonlinear models (Lewis and Pacala, 2000).

Our first uncertainty result pertains to when the dispersal trade-off shape parameter. In this case, we assume that the parameter is distributed as a gamma random variable and write the expected spreading speed in terms of the moment generating function. Moreover, we show that the optimal resource allocation to dispersal to maximize the spreading speed can be expressed in

terms of the mean and variable of the random variable. The important conclusion to draw from this result is that when the variance increases, the value for the optimal resource allocation to dispersal decreases. That is, if there is a lot of variation in the shape of the dispersal trade-off curve, then it is a better strategy to invest more resources into reproduction. We can also conclude that as the expected value of increases, the optimal resource allocation to dispersal increases.

When the standard deviation in the dispersal distance is uncertain, we can express the expected value for the spreading speed in terms of the expected value of the standard deviation in the dispersal distance because it is a scaling parameter. Thus, the optimal resource allocation to dispersal when the standard deviation in the dispersal distance is uncertain is the same for when all parameter values are known.

In the cases when we assume that the reproduction parameter and the shape of the reproduction trade-off curve are uncertain, we can express the expected value of the spreading speed in terms of Gamma functions that depend on the distribution parameters. Moreover, we find that the optimal strategy is to invest as many resources into dispersal as possible while still maintaining the persistence criteria. This is an artifact of the assumption that the population is persistent. Recall from the sensitivity analysis earlier that we showed if the population is not in risk of extinction, then the standard deviation in dispersal distance is more sensitive than the growth rate per generation. We were required to make this assumption because in its absence, there is no formula for the spreading speed of the population.

While our model reveals some interesting dynamics in the trade-off between dispersal and reproduction, it is also limited in its applicability. A shortcoming in the model is the assumption that the life history strategies do not evolve over time. This assumption is only biological reasonable if the time scale of

the model is much shorter than the time it takes for the life history to change which, in many cases, is not feasible. For example, it has been empirically shown in the literature that strategies for resource allocation to different processes can have seasonal fluctuations (Barbour et al., 1999) or evolve due to genetic mutations in offspring (Burton et al., 2010). Typical annual plants, that complete their life cycle within one year and then die, devote a majority of resources to growth in the early part of the growing season with a small amount of resources for maintenance, and then late in the growing season a majority of the resources are devoted to reproduction. Where as stress-tolerant plants such as shrubs in subarctic or dessert region must allocate most of its resources to maintenance and only allocate a small amount to growth. Only during good years, where resources are plentiful, can they devote resources to reproduction (Barbour et al., 1999). Thus, resource allocation is highly dependent on the particular species of interest and has shown to be time-dependent in many cases. It has also been shown that time-dependent variation in reproduction and dispersal can accelerate the spread of invading species (Ellner and Schreiber, 2012), something not seen in our results. Including time-dependent trade-offs would be a natural extension to the work we presented in Chapter 5 that could produce interesting dynamics.

Another drawback of the modeling techniques presented is that there is no spatial heterogeneity in the resource allocation. As shown by Burton et al. (2010) we know that resource allocation is highly dependent on the location of the individuals in the population. In their study, they found that individuals in the core of the population should allocate more resources on growth than dispersal while individuals at the front of the population will allocate more resources to dispersal than growth. Understanding the consequences of species colonizing new habitats can also be explored by incorporating spatial heterogeneity in the resource allocation.

References

Arenas, Miguel (2015). "Trends in substitution models of molecular evolution." *Frontiers in Genetics* 6, p. 319.

Austerlitz, Frédéric and Pauline Hélène Garnier-Géré (2003). "Modelling the impact of colonisation on genetic diversity and differentiation of forest trees: interaction of life cycle, pollen flow and seed long-distance dispersal." *Heredity* 90.4, p. 282.

Austerlitz, Frédéric, Stéphanie Mariette, Nathalie Machon, Pierre-Henri Gouyon, and Bernard Godelle (2000). "Effects of colonization processes on genetic diversity: differences between annual plants and tree species." *Genetics* 154.3, pp. 1309–1321.

Bapat, Ravi B and Tirukkannamangai ES Raghavan (1997). *Nonnegative matrices and applications*. Vol. 64. Cambridge university press.

Barbour, Michael G, Jack H Burk, Wanna D Pitts, Frank S. Gillian, and Schwartz Mark W. (1999). "Allocation and life history patterns." *Terrestrial Plant Ecology*. Ed. by Benjamin Cummings. USA: Adison Wesley Longman, pp. 88–116.

Bataillon, Thomas M, Jacques L David, and Daniel J Schoen (1996). "Neutral genetic markers and conservation genetics: simulated germplasm collections." *Genetics* 144.1, pp. 409–417.

Bateman, Andrew W, Andreas Buttenschön, Kelley D Erickson, and Nathan G Marculis (2017). "Barnacles vs bullies: modelling biocontrol of the invasive European green crab using a castrating barnacle parasite." *Theoretical Ecology* 10.3, pp. 305–318.

Beverton, Raymond JH and Sidney J Holt (2012). *On the Dynamics of Exploited Fish Populations*. Vol. 11. Springer Science & Business Media.

Birkhoff, Garrett (1957). "Extensions of Jentzsch's theorem." *Transactions of the American Mathematical Society* 85.1, pp. 219–227.

Bonnefon, Olivier, Jérôme Coville, Jimmy Garnier, and Lionel Roques (2014). "Inside dynamics of solutions of integro-differential equations." *Discrete and Continuous Dynamical Systems-Series B* 19.10, pp. 3057–3085.

Bonnefon, Olivier, Jimmy Garnier, François Hamel, and Lionel Roques (2013). "Inside dynamics of delayed traveling waves." *Mathematical Modelling of Natural Phenomena* 8.3, pp. 42–59.

Bonte, Dries et al. (2012). "Costs of dispersal." *Biological Reviews* 87.2, pp. 290–312.

Bramson, Maury (1983). *Convergence of solutions of the Kolmogorov equation to travelling waves*. Vol. 285. American Mathematical Society.

Bromham, Lindell and David Penny (2003). "The modern molecular clock." *Nature Reviews Genetics* 4.3, p. 216.

Burton, Olivia J, Ben L Phillips, and Justin M J Travis (2010). "Trade-offs and the evolution of life-histories during range expansion." *Ecology Letters* 13.10, pp. 1210–1220.

Casella, George and Roger L Berger (2002). *Statistical inference*. Vol. 2. Duxbury Pacific Grove, CA.

Chuang, Angela and Christopher R Peterson (2016). "Expanding population edges: theories, traits, and trade-offs." *Global Change Biology* 22.2, pp. 494–512.

Clark, James S, Mark Lewis, and Lajos Horvath (2001). "Invasion by extremes: population spread with variation in dispersal and reproduction." *The American Naturalist* 157.5, pp. 537–554.

Cody, Martin L (1966). "A general theory of clutch size." *Evolution*, pp. 174–184.

Cooley, James W and John W Tukey (1965). "An algorithm for the machine calculation of complex Fourier series." *Mathematics of Computation* 19.90, pp. 297–301.

Cotto, Olivier, Manuel Massot, Ophélie Ronce, and Jean Clobert (2015). "Dispersal as a source of variation in age-specific reproductive strategies in a wild population of lizards." *Proceedings of the Royal Society B: Biological Sciences* 282.1820, p. 20151741.

Cox, Robert M and Ryan Calsbeek (2010). "Severe costs of reproduction persist in Anolis lizards despite the evolution of a single-egg clutch." *Evolution: International Journal of Organic Evolution* 64.5, pp. 1321–1330.

Cressler, Clayton E, Aaron A King, and Earl E Werner (2010). "Interactions between behavioral and life-history trade-offs in the evolution of integrated predator-defense plasticity." *The American Naturalist* 176.3, pp. 276–288.

Crouse, Deborah T, Larry B Crowder, and Hal Caswell (1987). "A stage-based population model for loggerhead sea turtles and implications for conservation." *Ecology* 68.5, pp. 1412–1423.

Cullingham, Catherine I, Janice EK Cooke, Sophie Dang, Corey S Davis, Barry J Cooke, and David W Coltman (2011). "Mountain pine beetle host-range expansion threatens the boreal forest." *Molecular Ecology* 20.10, pp. 2157–2171.

Davis, Margaret B and Ruth G Shaw (2001). "Range shifts and adaptive responses to Quaternary climate change." *Science* 292.5517, pp. 673–679.

Dewhirst, Sebastian and Frithjof Lutscher (2009). "Dispersal in heterogeneous habitats: thresholds, spatial scales, and approximate rates of spread." *Ecology* 90.5, pp. 1338–1345.

Dlugosch, Katrina M and Ingrid M Parker (2008). "Founding events in species invasions: genetic variation, adaptive evolution, and the role of multiple introductions." *Molecular Ecology* 17.1, pp. 431–449.

Dockery, Jack, Vivian Hutson, Konstantin Mischaikow, and Mark Pernarowski (1998). "The evolution of slow dispersal rates: a reaction diffusion model." *Journal of Mathematical Biology* 37.1, pp. 61–83.

Duret, Laurent (2008). "Neutral theory: the null hypothesis of molecular evolution." *Nature Education* 1, pp. 803–806.

Duthie, A Bradley, Karen C Abbott, and John D Nason (2014). "Trade-offs and coexistence: a lottery model applied to fig wasp communities." *The American Naturalist* 183.6, pp. 826–841.

Easterling, Michael R, Stephen P Ellner, and Philip M Dixon (2000). "Size-specific sensitivity: applying a new structured population model." *Ecology* 81.3, pp. 694–708.

Edmonds, Christopher A, Anita S Lillie, and L Luca Cavalli-Sforza (2004). "Mutations arising in the wave front of an expanding population." *Proceedes of the National Academy of Sciences* 101.4, pp. 975–979.

Elliott, Christina G and Maya L Evenden (2012). "The effect of flight on reproduction in an outbreaking forest lepidopteran." *Physiological Entomology* 37.3, pp. 219–226.

Ellner, Stephen P and John Guckenheimer (2011). *Dynamic models in biology*. Princeton University Press.

Ellner, Stephen P and Sebastian J Schreiber (2012). "Temporally variable dispersal and demography can accelerate the spread of invading species." *Theoretical Population Biology* 82.4, pp. 283–298.

Excoffier, Laurent (2004). "Patterns of DNA sequence diversity and genetic structure after a range expansion: lessons from the infinite-island model." *Molecular Ecology* 13.4, pp. 853–864.

Excoffier, Laurent, Matthieu Foll, and Rémy J Petit (2009). "Genetic consequences of range expansions." *Annual Review of Ecology, Evolution, and Systematics* 40, pp. 481–501.

Excoffier, Laurent and Nicolas Ray (2008). "Surfing during population expansions promotes genetic revolutions and structuration." *Trends in Ecology & Evolution* 23.7, pp. 347–351.

Fang, Jian and Xiao-Qiang Zhao (2015). "Bistable traveling waves for monotone semiflows with applications." *Journal of the European Mathematical Society* 17.9, pp. 2243–2288.

Felsenstein, Joseph (1981). "Evolutionary trees from DNA sequences: a maximum likelihood approach." *Journal of Molecular Evolution* 17.6, pp. 368–376.

Freedman, Herbert I and Peter Moson (1990). "Persistence definitions and their connections." *Proceedings of the American Mathematical Society* 109.4, pp. 1025–1033.

Gantmakher, Feliks Ruvimovich (1998). *The theory of matrices*. Vol. 131. American Mathematical Society.

Garnier, Jimmy, Thomas Giletti, François Hamel, and Lionel Roques (2012). "Inside dynamics of pulled and pushed fronts." *Journal de Mathématiques Pures et Appliquées* 98.4, pp. 428–449.

Garnier, Jimmy and Mark A Lewis (2016). "Expansion under climate change: the genetic consequences." *Bulletin of Mathematical Biology* 78.11, pp. 2165–2185.

Geritz, Stefan AH (1995). "Evolutionarily stable seed polymorphism and small-scale spatial variation in seedling density." *The American Naturalist* 146.5, pp. 685–707.

Ghalambor, Cameron K, David N Reznick, and Jeffrey A Walker (2004). "Constraints on adaptive evolution: the functional trade-off between reproduc-

tion and fast-start swimming performance in the Trinidadian guppy (Poecilia reticulata)." *The American Naturalist* 164.1, pp. 38–50.

Gharouni, Ali, Myriam A Barbeau, Andrea Locke, Lin Wang, and James Watmough (2015). "Sensitivity of invasion speed to dispersal and demography: an application of spreading speed theory to the green crab invasion on the northwest Atlantic coast." *Marine Ecology Progress Series* 541, pp. 135–150.

Gibbs, Melanie and Hans Van Dyck (2010). "Butterfly flight activity affects reproductive performance and longevity relative to landscape structure." *Oecologia* 163.2, pp. 341–350.

Gill, Frank B (2006). *Ornithology*. W.H. Freeman.

Greene, David F and Edward A Johnson (1993). "Seed mass and dispersal capacity in wind-dispersed diapores." *Oikos* 67.1, pp. 69–74.

Guerra, Patrick A (2011). "Evaluating the life-history trade-off between dispersal capability and reproduction in wing dimorphic insects: a meta-analysis." *Biological Reviews* 86.4, pp. 813–835.

Haefner, James W (2005). *Modeling Biological Systems: Principles and Applications*. Springer Science & Business Media.

Hallatschek, Oskar, Pascal Hersen, Sharad Ramanathan, and David R Nelson (2007). "Genetic drift at expanding frontiers promotes gene segregation." *Proceedings of the National Academy of Sciences* 104.50, pp. 19926–19930.

Hallatschek, Oskar and David R Nelson (2008). "Gene surfing in expanding populations." *Theoretical Population Biology* 73.1, pp. 158–170.

Hanski, Ilkka, Marjo Saastamoinen, and Otso Ovaskainen (2006). "Dispersal-related life-history trade-offs in a butterfly metapopulation." *Journal of Animal Ecology* 75.1, pp. 91–100.

Harrison, Richard G (1980). "Dispersal polymorphisms in insects." *Annual Review of Ecology and Systematics* 11.1, pp. 95–118.

Hastings, Alan (1983). "Can spatial variation alone lead to selection for dispersal?" *Theoretical Population Biology* 24.3, pp. 244–251.

Hastings, Alan, Kim Cuddington, Kendi F Davies, Christopher J Dugaw, Sarah Elmendorf, Amy Freestone, Susan Harrison, Matthew Holland, John Lambrinos, Urmila Malvadkar, Brett A Melbourne, Kara Moore, Caz Taylor, and Diane Thomson (2005). "The spatial spread of invasions: new developments in theory and evidence." *Ecology Letters* 8.1, pp. 91–101.

Hewitt, Godfrey M (1996). "Some genetic consequences of ice ages, and their role in divergence and speciation." *Biological Journal of the Linnean Society* 58.3, pp. 247–276.

— (2000). "The genetic legacy of the Quaternary ice ages." *Nature* 405.6789, pp. 907–913.

Ho, Simon (2008). "The molecular clock and estimating species divergence." *Nature Education* 1.1, pp. 1–2.

Holderegger, Rolf, Urs Kamm, and Felix Gugerli (2006). "Adaptive vs. neutral genetic diversity: implications for landscape genetics." *Landscape Ecology* 21.6, pp. 797–807.

Holmes, Elizabeth E, Mark A Lewis, John E Banks, and Richard R Veit (1994). "Partial differential equations in ecology: spatial interactions and population dynamics." *Ecology* 75.1, pp. 17–29.

Howe, Henry F and Judith Smallwood (1982). "Ecology of seed dispersal." *Annual Review of Ecology and Systematics* 13.1, pp. 201–228.

Hoyle, Andrew, Roger G Bowers, Andrew White, and Michael Boots (2008). "The influence of trade-off shape on evolutionary behaviour in classical ecological scenarios." *Journal of Theoretical Biology* 250.3, pp. 498–511.

Hughes, Clare L, Jane K Hill, and Calvin Dytham (2003). "Evolutionary trade-offs between reproduction and dispersal in populations at expanding range boundaries." *Proceedings of the Royal Society of London B: Biological Sciences* 270.Suppl 2, S147–S150.

Ibrahim, Kamal M, Richard A Nichols, and Godfrey M Hewitt (1996). "Spatial patterns of genetic variation generated by different forms of dispersal." *Heredity* 77, pp. 282–291.

Jones, Laura E and Stephen P Ellner (2004). "Evolutionary tradeoff and equilibrium in an aquatic predator-prey system." *Bulletin of Mathematical Biology* 66.6, pp. 1547–1573.

Jukes, Thomas H and Charles R Cantor (1969). *Evolution of protein molecules. In 'Mammalian Protein Metabolism'.(Ed. HN Munro.) pp. 21–132.*

Kawasaki, Kohkichi and Nakako Shigesada (2007). "An integrodifference model for biological invasions in a periodically fragmented environment." *Japan Journal of Industrial and Applied Mathematics* 24.1, pp. 3–15.

Kimura, Motoo (1980). "A simple method for estimating evolutionary rates of base substitutions through comparative studies of nucleotide sequences." *Journal of Molecular Evolution* 16.2, pp. 111–120.

Kimura, Motoo (1991). "The neutral theory of molecular evolution: a review of recent evidence." *The Japanese Journal of Genetics* 66.4, pp. 367–386.

Klopfstein, Seraina, Mathias Currat, and Laurent Excoffier (2006). "The fate of mutations surfing on the wave of a range expansion." *Molecular Biology and Evolution* 23.3, pp. 482–490.

Kot, Mark (1992). "Discrete-time travelling waves: ecological examples." *Journal of Mathematical Biology* 30.4, pp. 413–436.

Kot, Mark, Mark A Lewis, and Pauline van den Driessche (1996). "Dispersal data and the spread of invading organisms." *Ecology* 77.7, pp. 2027–2042.

Kot, Mark and William M Schaffer (1986). "Discrete-time growth-dispersal models." *Mathematical Biosciences* 80.1, pp. 109–136.

Krasnosel'skii, Mark A and Petr P Zabreiko (1984). *Geometrical methods of nonlinear analysis*.

Krkošek, Martin, Jean-Sébastien Lauzon-Guay, and Mark A Lewis (2007). "Relating dispersal and range expansion of California sea otters." *Theoretical Population Biology* 71.4, pp. 401–407.

Lande, Russell and Susan Shannon (1996). "The role of genetic variation in adaptation and population persistence in a changing environment." *Evolution* 50.1, pp. 434–437.

Latore, J, P Gould, and AM Mortimer (1999). "Effects of habitat heterogeneity and dispersal strategies on population persistence in annual plants." *Ecological Modelling* 123.2-3, pp. 127–139.

Lefkovitch, LP (1965). "The study of population growth in organisms grouped by stages." *Biometrics*, pp. 1–18.

Lehe, Rémi, Oskar Hallatschek, and Luca Peliti (2012). "The rate of beneficial mutations surfing on the wave of a range expansion." *PLoS Computational Biology* 8.3, e1002447.

Leslie, Patrick H (1945). "On the use of matrices in certain population mathematics." *Biometrika* 33.3, pp. 183–212.

— (1948). "Some further notes on the use of matrices in population mathematics." *Biometrika* 35.3/4, pp. 213–245.

Levin, Lisa A (2006). "Recent progress in understanding larval dispersal: new directions and digressions." *Integrative and Comparative Biology* 46.3, pp. 282–297.

Lewis, Mark A, Bingtuan Li, and Hans F Weinberger (2002). "Spreading speed and linear determinacy for two-species competition models." *Journal of Mathematical Biology* 45.3, pp. 219–233.

Lewis, Mark A, Nathan G Marculis, and Zhongwei Shen (2018). "Integrodifference equations in the presence of climate change: persistence criterion, travelling waves and inside dynamics." *Journal of Mathematical Biology* 77.6-7, pp. 1649–1687.

Lewis, Mark A and Stephen Pacala (2000). "Modeling and analysis of stochastic invasion processes." *Journal of Mathematical Biology* 41.5, pp. 387–429.

Lewis, Mark A, Sergei V Petrovskii, and Jonathan R Potts (2016). *The Mathematics Behind Biological Invasions*. Vol. 44. Springer.

Li, Bingtuan, Mark A Lewis, and Hans F Weinberger (2009). "Existence of traveling waves for integral recursions with nonmonotone growth functions." *Journal of Mathematical Biology* 58.3, pp. 323–338.

Li, Bingtuan, Hans F Weinberger, and Mark A Lewis (2005). "Spreading speeds as slowest wave speeds for cooperative systems." *Mathematical Biosciences* 196.1, pp. 82–98.

Liebhold, Andrew M, Joel A Halverson, and Gregory A Elmes (1992). "Gypsy moth invasion in North America: a quantitative analysis." *Journal of Biogeography*, pp. 513–520.

Link, William A and Paul F Doherty Jr (2002). "Scaling in sensitivity analysis." *Ecology* 83.12, pp. 3299–3305.

Lubina, John A and Simon A Levin (1988). "The spread of a reinvading species: range expansion in the California sea otter." *The American Naturalist* 131.4, pp. 526–543.

Lui, Roger (1982a). "A nonlinear integral operator arising from a model in population genetics I. Monotone initial data." *SIAM Journal of Mathematical Analysis* 13.6, pp. 913–937.

— (1982b). "A nonlinear integral operator arising from a model in population genetics II. Initial data with compact support." *SIAM Journal of Mathematical Analysis* 13.6, pp. 938–953.

— (1983). "Existence and stability of travelling wave solutions of a nonlinear integral operator." *Journal of Mathematical Biology* 16.3, pp. 199–220.

— (1985). "A Nonlinear Integral Operator Arising from a Model in Population Genetics III. Heterozygote Inferior Case." *SIAM Journal of Mathematical Analysis* 16.6, pp. 1180–1206.

Lui, Roger (1986). "A nonlinear integral operator arising from a model in population genetics IV. Clines." *SIAM Journal of Mathematical Analysis* 17.1, pp. 152–168.

— (1989a). "Biological growth and spread modeled by systems of recursions. I. Mathematical theory." *Mathematical Biosciences* 93.2, pp. 269–295.

— (1989b). "Biological growth and spread modeled by systems of recursions. II. Biological theory." *Mathematical Biosciences* 93.2, pp. 297–311.

Lutscher, Frithjof (2008). "Density-dependent dispersal in integrodifference equations." *Journal of Mathematical Biology* 56.4, pp. 499–524.

Lutscher, Frithjof and Mark A Lewis (2004). "Spatially-explicit matrix models." *Journal of Mathematical Biology* 48.3, pp. 293–324.

Lutscher, Frithjof, Elizaveta Pachepsky, and Mark A Lewis (2005). "The effect of dispersal patterns on stream populations." *SIAM Review* 47.4, pp. 749–772.

Lutscher, Frithjof and Nguyen Van Minh (2013). "Traveling waves in discrete models of biological populations with sessile stages." *Nonlinear Analysis: Real World Applications* 14.1, pp. 495–506.

Marculis, Nathan G, Jimmy Garnier, Roger Lui, and Mark A Lewis (2019). "Inside dynamics for stage-structured integrodifference equations." *Journal of Mathematical Biology* In Press.

Marculis, Nathan G and Roger Lui (2016). "Modelling the biological invasion of Carcinus maenas (the European green crab)." *Journal of Biological Dynamics* 10.1, pp. 140–163.

Marculis, Nathan G, Roger Lui, and Mark A Lewis (2017). "Neutral Genetic Patterns for Expanding Populations with Nonoverlapping Generations." *Bulletin of Mathematical Biology* 79.4, pp. 828–852.

Mayr, Ernst (1940). "Speciation phenomena in birds." *The American Naturalist* 74.752, pp. 249–278.

— (1942). *Systematics and the origin of species, from the viewpoint of a zoologist*. Harvard University Press.

Miles, Donald B, Barry Sinervo, and W Anthony Frankino (2000). "Reproductive burden, locomotor performance, and the cost of reproduction in free ranging lizards." *Evolution* 54.4, pp. 1386–1395.

Mole, Simon and Anthony J Zera (1994). "Differential resource consumption obviates a potential flight–fecundity trade-off in the sand cricket (Gryllus firmus)." *Functional Ecology* 8, pp. 573–580.

Mollison, Denis (1991). "Dependence of epidemic and population velocities on basic parameters." *Mathematical Biosciences* 107.2, pp. 255–287.

Moloney, Kirk A (1986). "A generalized algorithm for determining category size." *Oecologia* 69.2, pp. 176–180.

Morin, Phillip A, Gordon Luikart, and Robert K Wayne (2004). "SNPs in ecology, evolution and conservation." *Trends in Ecology & Evolution* 19.4, pp. 208–216.

Müller, Melanie JI, Beverly I Neugeboren, David R Nelson, and Andrew W Murray (2014). "Genetic drift opposes mutualism during spatial population expansion." *Proceedings of the National Academy of Sciences* 111.3, pp. 1037–1042.

Münkemüller, Tamara, Justin MJ Travis, Olivia J Burton, Katja Schiffers, and Karin Johst (2011). "Density-regulated population dynamics and conditional dispersal alter the fate of mutations occurring at the front of an expanding population." *Heredity* 106.4, pp. 678–689.

Neubert, Michael G and Hal Caswell (2000). "Demography and dispersal: calculation and sensitivity analysis of invasion speed for structured populations." *Ecology* 81.6, pp. 1613–1628.

Neubert, Michael G, Mark Kot, and Mark A Lewis (2000). "Invasion speeds in fluctuating environments." *Proceedings of the Royal Society of London. Series B: Biological Sciences* 267.1453, pp. 1603–1610.

Petit, Rémy J, Abdelhamid El Mousadik, and Odile Pons (1998). "Identifying populations for conservation on the basis of genetic markers." *Conservation Biology* 12.4, pp. 844–855.

Pluess, Andrea R (2011). "Pursuing glacier retreat: genetic structure of a rapidly expanding Larix decidua population." *Molecular Ecology* 20.3, pp. 473–485.

Proctor, Noble S and Patrick J Lynch (1993). *Manual of ornithology: avian structure & function*. Yale University Press.

Prop, Jouke, Jeffrey M Black, and Paul Shimmings (2003). "Travel schedules to the high arctic: barnacle geese trade-off the timing of migration with accumulation of fat deposits." *Oikos* 103.2, pp. 403–414.

Récapet, Charlotte, Pierre Bize, and Blandine Doligez (2017). "Food availability modulates differences in parental effort between dispersing and philopatric birds." *Behavioral Ecology* 28.3, pp. 688–697.

Reimer, Jody R, Michael B Bonsall, and Philip K Maini (2016). "Approximating the critical domain size of integrodifference equations." *Bulletin of Mathematical Biology* 78.1, pp. 72–109.

Ricker, William E (1954). "Stock and recruitment." *Journal of the Fisheries Board of Canada* 11.5, pp. 559–623.

Roff, Derek A (1984). "The cost of being able to fly: a study of wing polymorphism in two species of crickets." *Oecologia* 63.1, pp. 30–37.

— (1990). "The evolution of flightlessness in insects." *Ecological Monographs* 60.4, pp. 389–421.

— (1995). "Antagonistic and reinforcing pleiotropy: a study of differences in development time in wing dimorphic insects." *Journal of Evolutionary Biology* 8.4, pp. 405–419.

Roques, Lionel, Jimmy Garnier, François Hamel, and Etienne K Klein (2012). "Allee effect promotes diversity in traveling waves of colonization." *Proceedings of the National Academy of Sciences* 109.23, pp. 8828–8833.

Roques, Lionel, Yuzo Hosono, Olivier Bonnefon, and Thomas Boivin (2015). "The effect of competition on the neutral intraspecific diversity of invasive species." *Journal of Mathematical Biology* 71.2, pp. 465–489.

Rothe, Franz (1981). "Convergence to pushed fronts." *Rocky Mountain Journal of Mathematics* 11.4.

Saccheri, Ilik and Ilkka Hanski (2006). "Natural selection and population dynamics." *Trends in Ecology & Evolution* 21.6, pp. 341–347.

Sappington, Thomas W and William B Showers (1992). "Reproductive maturity, mating status, and long-duration flight behavior of Agrotis ipsilon(Lepidoptera: Noctuidae) and the conceptual misuse of the oogenesis-flight syndrome by entomologists." *Environmental Entomology* 21.4, pp. 677–688.

Schaffer, William M (1974). "Selection for optimal life histories: the effects of age structure." *Ecology* 55.2, pp. 291–303.

Schmidt-Wellenburg, Carola A, G Henk Visser, Brigitte Biebach, Kaspar Delhey, Martina Oltrogge, Andrea Wittenzellner, Herbert Biebach, and Bart Kempenaers (2008). "Trade-off between migration and reproduction: does a high workload affect body condition and reproductive state?" *Behavioral Ecology* 19.6, pp. 1351–1360.

Seigel, Richard A, M M Huggins, and Neil B Ford (1987). "Reduction in locomotor ability as a cost of reproduction in gravid snakes." *Oecologia* 73.4, pp. 481–485.

Selkoe, Kimberly A and Robert J Toonen (2006). "Microsatellites for ecologists: a practical guide to using and evaluating microsatellite markers." *Ecology Letters* 9.5, pp. 615–629.

Siggins, Howard W (1933). "Distribution and rate of fall of conifer seeds." *Journal of Agricultural Research* 47, pp. 119–128.

Slatkin, Montgomery and Laurent Excoffier (2012). "Serial founder effects during range expansion: a spatial analog of genetic drift." *Genetics* 191.1, pp. 171–181.

Snyder, Robin E (2003). "How demographic stochasticity can slow biological invasions." *Ecology* 84.5, pp. 1333–1339.

Stearns, Steven C (1989). "Trade-offs in life-history evolution." *Functional Ecology* 3.3, pp. 259–268.

Stein, Anke, Katharina Gerstner, and Holger Kreft (2014). "Environmental heterogeneity as a universal driver of species richness across taxa, biomes and spatial scales." *Ecology Letters* 17.7, pp. 866–880.

Stevens, David J, Michael H Hansell, and Pat Monaghan (2000). "Developmental trade–offs and life histories: strategic allocation of resources in caddis flies." *Proceedings of the Royal Society of London B: Biological Sciences* 267.1452, pp. 1511–1515.

Stokes, AN (1976). "On two types of moving front in quasilinear diffusion." *Mathematical Biosciences* 31.3-4, pp. 307–315.

Therry, Lieven, Dries Bonte, and Robby Stoks (2015). "Higher investment in flight morphology does not trade off with fecundity estimates in a poleward range-expanding damselfly." *Ecological Entomology* 40.2, pp. 133–142.

Thomas, Chris D, EJ Bodsworth, Robert J Wilson, Adam D Simmons, Zoe G Davies, Martin Musche, and Larissa Conradt (2001). "Ecological and evolutionary processes at expanding range margins." *Nature* 411.6837, pp. 577–581.

Thompson, Grant G (1993). "A proposal for a threshold stock size and maximum fishing mortality rate." *Canadian Special Publication of Fisheries and Aquatic Sciences*, pp. 303–320.

Thompson, Ken, Louise C Rickard, Dunmail J Hodkinson, and Mark Rees (2002). "Seed dispersal: the search for trade-offs." *Dispersal ecology*. Blackwell Oxford, UK. Chap. 8, pp. 152–172.

Tigreros, Natasha and Goggy Davidowitz (2019). "Flight-fecundity tradeoffs in wing-monomorphic insects." *Advances in Insect Physiology* 56, p. 1.

Van Dyck, Hans and Michel Baguette (2005). "Dispersal behaviour in fragmented landscapes: routine or special movements?" *Basic and Applied Ecology* 6.6, pp. 535–545.

Van Kirk, Rob W and Mark A Lewis (1997a). "Integrodifference models for persistence in fragmented habitats." *Bulletin of Mathematical Biology* 59.1, p. 107.

— (1997b). "Integrodifference models for persistence in fragmented habitats." *Bulletin of Mathematical Biology* 59.1, pp. 107–137.

Vandermeer, John (1978). "Choosing category size in a stage projection matrix." *Oecologia* 32.1, pp. 79–84.

Vasilyeva, Olga, Frithjof Lutscher, and Mark A Lewis (2016). "Analysis of spread and persistence for stream insects with winged adult stages." *Journal of Mathematical Biology* 72.4, pp. 851–875.

Veit, Richard R and Mark A Lewis (1996). "Dispersal, population growth, and the Allee effect: dynamics of the house finch invasion of eastern North America." *The American Naturalist* 148.2, pp. 255–274.

Verdolin, Jennifer L (2006). "Meta-analysis of foraging and predation risk trade-offs in terrestrial systems." *Behavioral Ecology and Sociobiology* 60.4, pp. 457–464.

Vladimirov, Vasilij Sergeevič (1971). *Equations of mathematical physics (Uravneniia matematicheskoĭ fiziki)*. Marcel Dekker, New York.

Volkov, Darko and Roger Lui (2007). "Spreading speed and travelling wave solutions of a partially sedentary population." *IMA Journal of Applied Mathematics* 72.6, pp. 801–816.

Wang, Mei-Hui, Mark Kot, and Michael G Neubert (2002). "Integrodifference equations, Allee effects, and invasions." *Journal of Mathematical Biology* 44.2, pp. 150–168.

Weinberger, Hans F (1978). "Asymptotic behavior of a model in population genetics." *Nonlinear Partial Differential Equations and Applications*. Springer, pp. 47–96.

— (1982). "Long-time behavior of a class of biological models." *SIAM Journal on Mathematical Analysis* 13.3, pp. 353–396.

Weinberger, Hans F, Kohkichi Kawasaki, and Nanako Shigesada (2008). "Spreading speeds of spatially periodic integro-difference models for populations with nonmonotone recruitment functions." *Journal of Mathematical Biology* 57.3, pp. 387–411.

Yoshida, Takehito, Nelson G Hairston Jr, and Stephen P Ellner (2004). "Evolutionary trade–off between defence against grazing and competitive ability in a simple unicellular alga, Chlorella vulgaris." *Proceedings of the Royal Society of London. Series B: Biological Sciences* 271.1551, pp. 1947–1953.

Zemanian, Armen H (1968). *Generalized integral transformations*. Vol. 140. Interscience Publishers New York.

Zera, Anthony J and Robert F Denno (1997). "Physiology and ecology of dispersal polymorphism in insects." *Annual Review of Entomology* 42.1, pp. 207–230.

Zera, Anthony J and Lawrence G Harshman (2001). "The physiology of life history trade-offs in animals." *Annual Review of Ecology and Systematics* 32.1, pp. 95–126.

Zhao, Zhangwu and Anthony J Zera (2002). "Differential lipid biosynthesis underlies a tradeoff between reproduction and flight capability in a wing-polymorphic cricket." *Proceedings of the National Academy of Sciences* 99.26, pp. 16829–16834.

Zhou, Ying and Mark Kot (2011). "Discrete-time growth-dispersal models with shifting species ranges." *Theoretical Ecology* 4.1, pp. 13–25.

Ziv, Yaron and Goggy Davidowitz (2019). "When Landscape Ecology Meets Physiology: Effects of Habitat Fragmentation on Resource Allocation Trade-Offs." *Frontiers in Ecology and Evolution* 7, p. 137.